K. F. Dunker F. W. Klaiber F. K. Daoud W. E. Wiley W. W. Sanders, Jr.
July 1987

Strengthening of Existing Continuous Composite Bridges

Sponsored by the Highway Division, Iowa Department of Transportation,
and the Iowa Highway Research Board

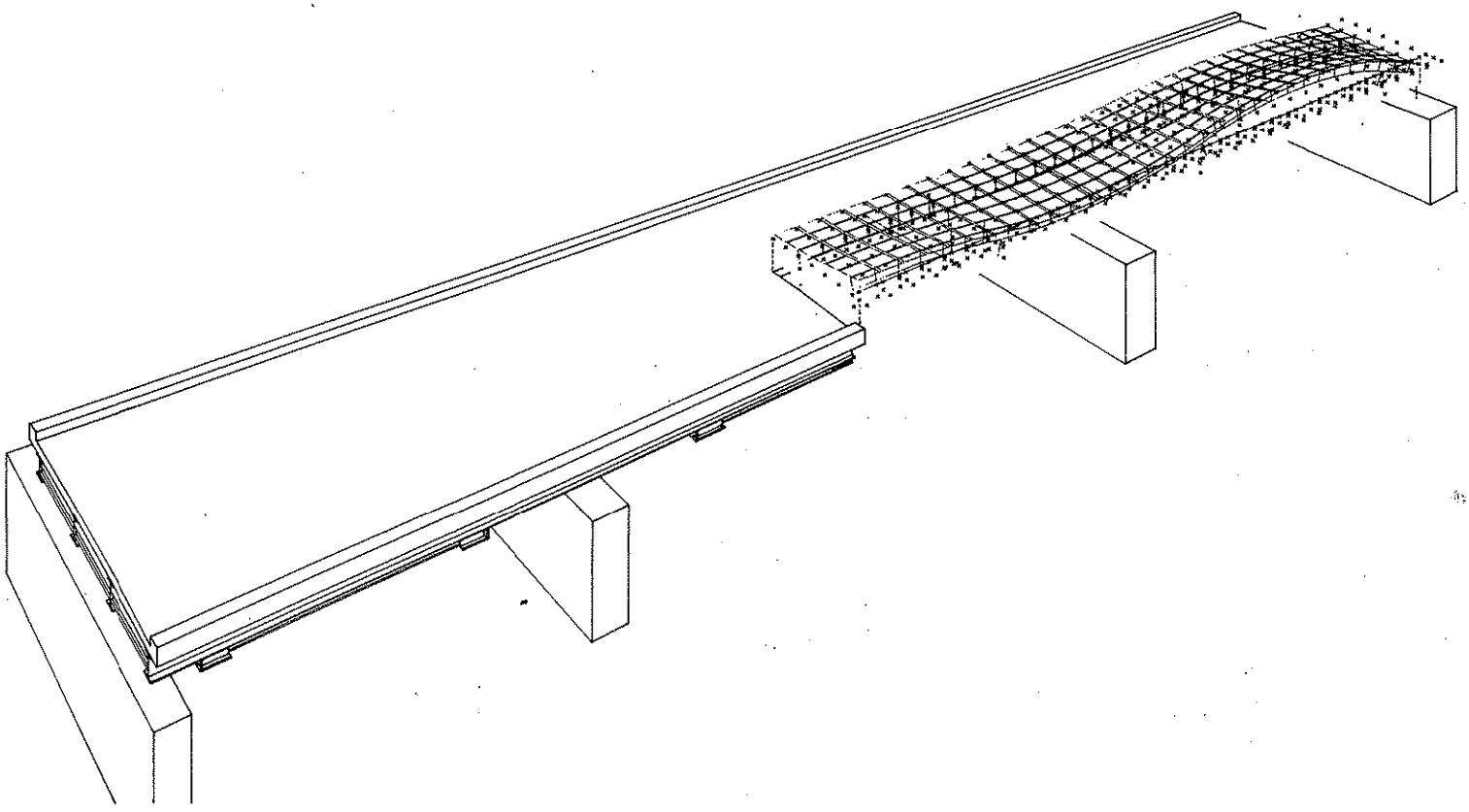

engineering research institute
iowa state university

Iowa Department of Transportation

The procedures and recommendations expressed in this report are those of the authors and not necessarily those of the Highway Division of the Iowa Department of Transportation.

Final Report

K. F. Dunker F. W. Klaiber F. K. Daoud W. E. Wiley W. W. Sanders, Jr.

July 1987

Strengthening of Existing Continuous Composite Bridges

Sponsored by the Highway Division,
Iowa Department of Transportation
and the Iowa Highway Research Board
Iowa DOT Project HR-287
ERI Project 1846
ISU-ERI-Ames-88007

Engineering Research Institute
Iowa State University
Iowa Department of Transportation

TABLE OF CONTENTS

LIST OF FIGURES

LIST OF TABLES

ABSTRACT

The need for upgrading a large number of understrength and obsolete bridges in the United States is well known, and Iowa has many of the bridges that require upgrading. Iowa began designing and constructing continuous span, composite bridges earlier than other states, and consequently, there are many such bridges in Iowa. Because of changes in bridge design standards and increases in truck loads, a considerable number of the continuous, composite bridges in Iowa require posting for reduced loads.

The posted bridges, if in otherwise good condition, often can be strengthened at a cost considerably less than replacement cost. Because strengthening should be based on adequate testing and design information, the research described in this report was conducted to investigate the potential of strengthening continuous bridges by post-tensioning.

The research program conducted and described in this report included the following: a literature review, selection and rating of a prototype continuous composite bridge, tests of a one-third-scale continuous composite bridge model, finite element analysis of the bridge model, and tests of a full-scale composite beam mockup for a negative moment region.

The research program indicated that the strengthening of continuous, composite bridges is feasible. The primary objective in applying the post-tensioning should be to provide moments opposite to those produced by live and dead loads. Longitudinal distribution of that post-tensioning always must be considered if only exterior or only interior

beams are post-tensioned. Testing and finite element analysis showed that post-tensioning of positive moment regions with straight tendons was more effective than post-tensioning negative moment regions with straight tendons. Changes in tension in tendons may be either beneficial or detrimental when live loads are applied to a strengthened bridge and thus must be carefully considered in design.

1. INTRODUCTION

1.1. Background

Nearly half of the approximately 600,000 highway bridges in the United States were built before 1940. The majority of those bridges were designed for lower traffic volumes, smaller vehicles, slower speeds, and lighter loads than they experience today. To compound the problem further, maintenance has not been adequate for many of these older bridges. Almost 40% of the nation's bridges are classified as deficient and thus in need of rehabilitation or replacement according to the Federal Highway Administration. The deficiency in some of these bridges is their inability to carry current legal live loads. Rather than posting these bridges for reduced loads or replacing them, strengthening has been found to be a cost-effective alternative in many cases.

Many different methods exist for increasing the live load carrying capacity of the various types of bridges. Through Iowa Department of Transportation (Iowa DOT) Projects HR-214 [19] and HR-238 [9,10,18], the concept of strengthening simple span, composite steel beam and concrete deck bridges by post-tensioning was developed. These projects took the concept from the feasibility phase through the implementation and design methodology phase. Two simple span bridges (one 2.2 miles north of Terril on N 14 and the other just south of the Greene-Webster County line on I-144) were strengthened by post-tensioning during the summer of 1982 and retested during the summer of 1984. Results of these tests verified that strengthening of the simple span bridges by post-tensioning is a viable, economical strengthening technique. The design methodology

developed by Dunker et al. [10] provided a procedure by which the required post-tensioning force could be determined relatively easily. This design methodology has since been used successfully by the Iowa DOT and other agencies for strengthening of simple span composite bridges.

As a result of the previous success, that is strengthening of simple span bridges by post-tensioning, this study was undertaken to extend the method to continuous span bridges. Because Iowa began designing and constructing continuous, composite steel beam and concrete deck bridges earlier than most states, Iowa has a considerable inventory of those bridges in need of rehabilitation or replacement. This study parallels the feasibility study completed for simple span bridges, and it is anticipated that this study will be extended to an implementation phase, in order to field test concepts developed in this report.

1.2. Objectives and Scope

Iowa has a considerable inventory of continuous span, composite bridges that are structurally inadequate according to current AASHTO Standards and Iowa legal loads. On the basis of experience from previous Iowa DOT simple span strengthening projects (HR-214 and HR-238), it appeared that post-tensioning also could be implemented to strengthen continuous bridges. The primary objective of this study, then, was to determine the feasibility of strengthening continuous composite bridges by post-tensioning. More specific objectives were

- to determine the best tendon configurations: intermittent straight, continuous straight, intermittent harped, or con-

tinuous harped tendons for post-tensioning positive or negative moment regions or both.

- to determine the best method for attaching tendons in negative moment regions.
- to determine the distribution of post-tensioning forces and moments longitudinally and transversely within the bridge for various post-tensioning schemes.
- to determine whether the deck contributes to and/or could be made to contribute to the composite section in negative moment regions.

These objectives were pursued by the research team through undertaking a comprehensive literature review, testing a one-third scale bridge model in the Iowa State University (ISU) Structural Engineering Research Laboratory, testing of a full-scale mockup of a composite bridge beam in the laboratory, and conducting a finite element analysis of the laboratory bridge model for various combinations of post-tensioning forces and vertical loads.

1.3. Research Program

The research program consisted of the distinct parts outlined above but with an emphasis on laboratory testing. Initially a comprehensive literature review was performed, which extended beyond the earlier literature reviews for simple span structures [9,18,19]. The review made use of the many international references obtained in the National Cooperative Highway Research Program (NCHRP) Project "Methods of Strengthening Existing Highways Bridges" [20].

In order to begin the laboratory testing program, the researchers consulted with the Iowa DOT Office of Bridge Design and obtained plans

for standard continuous, composite bridges. From the various sets of plans the V12(1957) series of composite, three-span bridges was selected, and from that series, a 125-ft-long prototype bridge was chosen. The prototype bridge was rated for bending stress in order to determine amounts and locations of overstress.

From the prototype bridge plans, a one-third scale model was designed and constructed in the ISU Structural Engineering Research Laboratory. The steel beams for the model were built up from steel strip and plate because no wide flange sections were available that would accurately model the prototype bridge beams at one-third scale. The beams were fitted with steel tabs which served as attachments for brackets for straight tendons in all negative moment regions and in positive moment regions for the exterior beams. The steel frame for the model was instrumented with strain gages, and the concrete deck was poured on top of the frame. The model was subjected to a variety of post-tensioning, vertical load, and combined load schemes. During all load tests, strains and deflections were monitored.

Also from the plans for the V12(1957) series of bridges, a full-size mockup was constructed for a typical bridge beam above an interior support. The mockup consisted of a salvaged wide flange bridge beam on which a concrete deck was poured. Two tendon configurations were tested on the mockup: straight, threadbar tendons and harped, cable tendons. Along with the tendons, strengthening angles were added to the lower region of the mockup for some of the tests. The various load schemes in the testing program included post-tensioning and vertical loads. During all tests, strains and deflections were monitored.

Several of the preprocessing and postprocessing computer programs from earlier research projects [9,10] were adapted for use with continuous bridges such as the three-span prototype bridge. Those programs were utilized with SAP IV [3], a well-known finite element program in order to analyze the laboratory model bridge. For the finite element analysis, a series of post-tensioning schemes were analyzed, which included some of the schemes tested in the laboratory.

The results from the various parts of the research program are summarized in this report. The literature review and rating of the prototype are given in Sections 1.4 and 1.5, respectively. Chapters 2 and 3 describe the bridge model and mockup tested in the laboratory as well as the test procedures employed. The results from the laboratory testing program and the finite element analysis schemes are summarized in Chapter 4. Following the results are the summary and conclusions in Chapter 5.

1.4. Literature Review

Since the 1950s there have been numerous examples of prestressing of continuous span, composite structures. The examples include both new structures and existing structures that required strengthening. There also has been a certain amount of laboratory testing of prestressed continuous structures, development of analysis methods, and development of catalogs of tendon configurations. In addition to the summary of literature which is given below, there are literature reviews in Reference [19] for simple span structures and in Klaiber et al. [20] for simple and continuous span structures.

The literature review which follows is a summary of the examples of actual structures, laboratory testing, and catalogs of tendon configurations available on the subject of prestressing continuous structures. The examples have been arranged in chronological order and have been selected to show the variety of concepts, the application of the concepts, and the successes and problems when some of the concepts were applied. Although the emphasis is on composite bridges, reinforced concrete and prestressed concrete bridge structures and steel and composite building structures are included when necessary to illustrate a full range of concepts. Many of the concepts have been explored during the testing and analysis portions of this project, as described in Chapters 2 through 4.

One of the first modern examples of a continuous, prestressed steel structure was the aircraft hangar designed in the early 1950s by G. Magnel and constructed in Melsbroeck, Belgium [12]. The two-span truss which supports the roof near the open wall of the hangar is illustrated in Fig. 1.1. Each span of the truss is prestressed with two cables in a harped configuration. The tendon configuration provides a negative moment in the positive moment regions of each span and also a positive moment in the negative moment regions near the central support. Because the negative moment near the central support is larger than the positive moment on each span, the tendons were overlapped so that there were four tendons above the central support. The ends of the tendons were then anchored at truss panels with double diagonals. The tendon configuration chosen by Magnel was optimal for the two-span steel truss.

In 1964, Tachibana et al. [25] published a paper on experimental work with two-span composite beams that simulate a two-girder bridge. Two beams were constructed with the tendon configuration as shown in Fig. 1.2. One beam was prestressed before the deck was poured, and one beam was prestressed after the deck had cured. The latter is equivalent to a strengthening condition. During the prestressing, it was evident that there was a certain amount of prestress loss even with lubricated saddles and jacking from each end of the cable. Each beam was loaded to failure with concentrated loads placed at four-tenths of the span length from the beam ends. The beam which had been prestressed before the deck was poured had a relatively low deck-cracking load above the central support but had essentially the same ultimate load as the beam prestressed after the deck had cured.

A surprising result of the tests was that the plastic hinges at the concentrated loads and the central support formed at essentially the same load. This would indicate that the concrete deck had the same effect in both compression and tension. The authors attributed this behavior to several causes:

- Even though the deck had cracked, the reinforcing continued to carry the deck tension and thus delayed the increase in tension strain in the steel beams
- The reduction in moment of inertia for the cracked section at the interior support caused moment to be shifted to the beam spans.

In the 1960s, Hoadley developed analysis methods for prestressed composite beams. Hoadley made the suggestion that for a typical three-span bridge beam, only the center, longest span need be prestressed [13]. This concept was applied in the design of a three-span floor

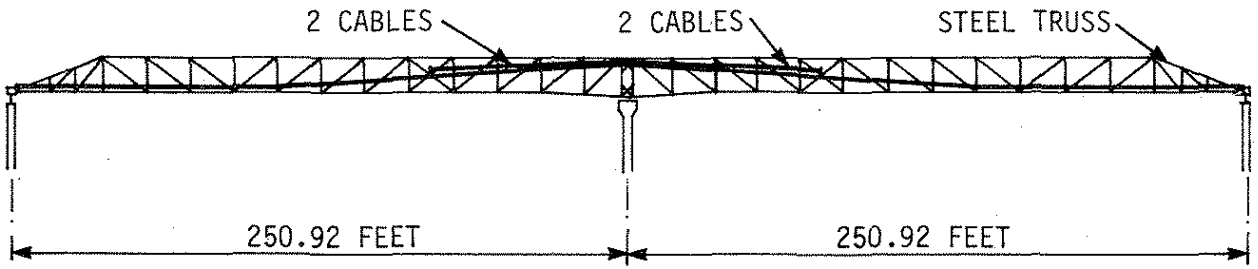

Fig. 1.1. Two-span, prestressed steel truss for an aircraft hangar in Melsbroeck, Belgium, circa 1953.

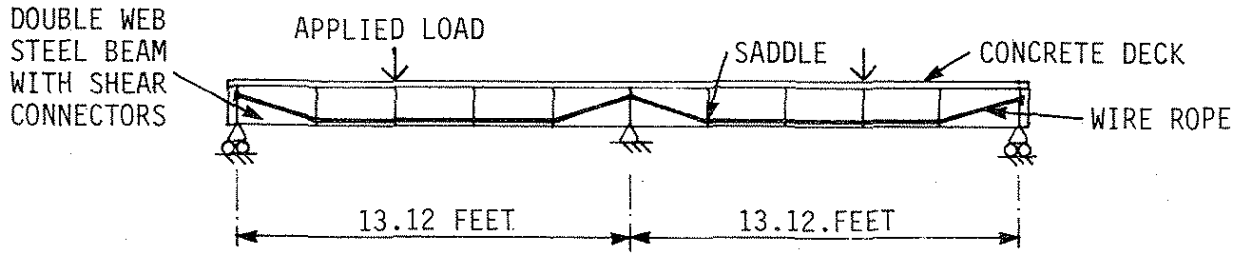

Fig. 1.2. Experimental two-span, prestressed composite beam, circa 1964.

structure for an apartment building, as shown in Fig. 1.3. The straight tendons over the central region of the center beam span were tensioned so as to reduce the tension in the composite concrete deck over the supports and thus to minimize cracking. Because of longitudinal distribution, the moments generated by the eccentric tendons also reduced the stresses in the bottom flange of the beam over the center span and over the interior supports.

In 1968 Kandall [16] pointed out the differences between the purpose for prestressing concrete and the purpose for prestressing steel beams. For concrete the purpose is to overcome the tension weakness of concrete; whereas for steel the purpose is to reverse the effect of the applied loads. The prestressing method which Kandall suggested for strengthening a two-span steel beam, which is illustrated in Fig. 1.4, actually involves attaching supplementary load-carrying mechanisms to the beam. The existing steel beam provides lateral support for new, free-to-slide compression members and attachment for tendon brackets for the harped tendons. By adding the compression members, the undesirable effect of the axial force caused by the post-tensioning does not affect the beam. By placing the compression member near the top of the steel beam and anchoring tendons near the bottom of the steel beam, a larger eccentricity is utilized to reduce the required tendon force. If a tendon is simply applied near the flange of a steel beam, the eccentricity will be only half as large as that achieved by Kandall's mechanism.

Several Polish authors prepared an analysis reference for pre-stressed steel structures, which was then translated and published in

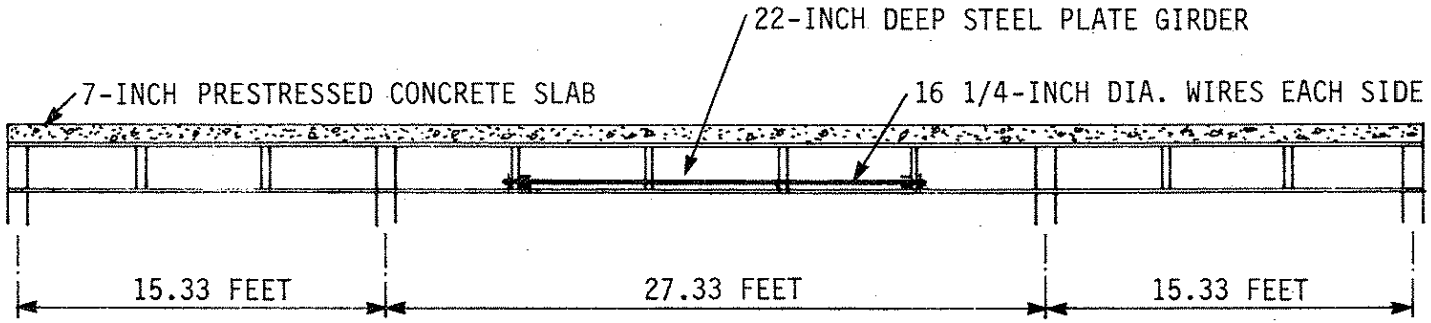

Fig. 1.3. Three-span, prestressed composite girder for an Oakland, California apartment building, circa 1967.

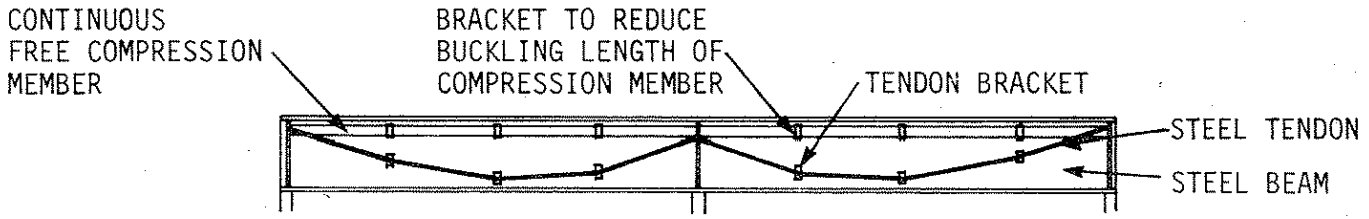

Fig. 1.4. Concept for strengthening of a two-span steel beam by post-tensioning, circa 1968.

German in 1968 [5]. The reference includes a variety of straight and harped tendon configurations for simple and continuous span structures. The configuration illustrated for a two-span steel beam in Fig. 1.5 is one of the configurations. The tendon configuration is similar to that utilized earlier by Magnel and bears a strong resemblance to a bent-bar pattern for a two-span reinforced concrete beam.

One of the alternatives for strengthening an existing simple span structure is to post-tension the structure in such a way so as to make it a continuous structure. This alternative was utilized by Vernigora et al. [28] in strengthening a six-span, reinforced concrete tee beam bridge over the Welland Canal in Ontario, Canada. The harped cable configuration, shown for a typical span in Fig. 1.6, was employed over the entire length of the bridge in order to provide the continuity. The harped cable minimized the tendon force by providing maximum eccentricity at critical moment locations and minimized the axial force component which would cause axial shortening. Even with the reduced axial shortening, it was necessary to replace most of the bridge bearings with new, relatively friction-free bearings. In order to eliminate the expansion joints between the spans and provide better lateral load transfer, ends of beams were cut away, and new diaphragms were cast and post-tensioned. Because the lateral distribution of the post-tensioning was unknown, all tendons were jacked in two stages, and thus approximately equal tendon forces were obtained.

The strengthening mechanism shown in Fig. 1.4, which Kandall published in 1968 [16], was applied to a bridge in Aarwangen, Switzerland in 1969 [23]. The mechanism was used in order to strengthen the bridge

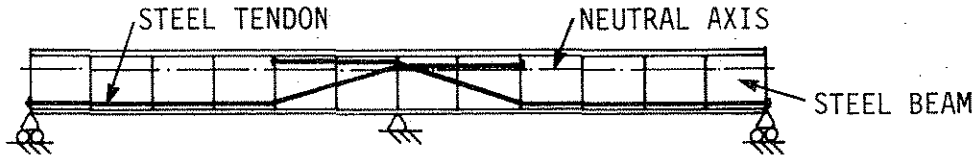

Fig. 1.5. Concept for a two-span, prestressed steel beam, circa 1968.

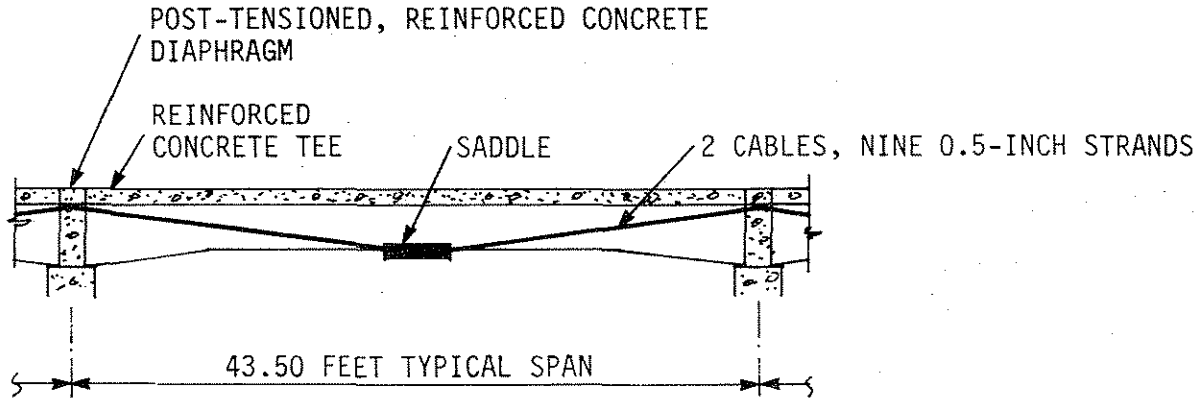

Fig. 1.6. Six-span Welland Canal Bridge, Canada, strengthened by post tensioning, 1968.

for heavier loads and to prevent excessive deflections. The two-span wrought iron truss bridge with compression member and tendons is illustrated in Fig. 1.7. The compression member was attached to the top chord of each bridge truss with connections that permitted the member to slide longitudinally, except at the central pylon. Cables were harped at the quarter points of each truss span and tensioned against the compression member. Even with carefully designed saddles and reinforcing at the quarter points, friction forces were high, and there was need for repairs during post-tensioning. The truss was monitored with strain gages before and after post-tensioning. Measured strains generally were 3% to 20% less than computed strains, and after nine months, only 5% to 7% of the initial tendon forces had been lost.

Brodka and Klobukowski described a variety of concepts and applications for prestressed steel structures in their reference work which was translated from Polish and published in German in 1969 [6]. One of the concepts for a four-span, prestressed steel beam is shown in Fig. 1.8. The alternating bottom and top tendons in positive and negative bending moment regions is similar to the straight bar pattern commonly used for reinforcing concrete beams.

Another concept for prestressing steel beams is shown in Fig. 1.9. The harped tendon is placed only at the central support of a two-span beam in such a way so as to provide prestressing for the negative moment region where bending moment is maximum. The concept is one of many included in the work by Ferjencik and Tochacek [12]. The work is written in German but from a Czechoslovakian viewpoint.

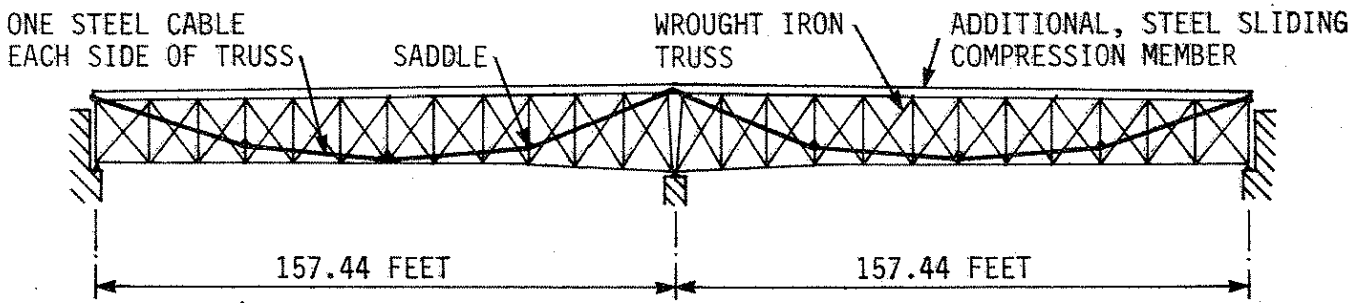

Fig. 1.7. Two-span, wrought iron truss bridge in Aarwangen, Switzerland, strengthened by post-tensioning, circa 1969.

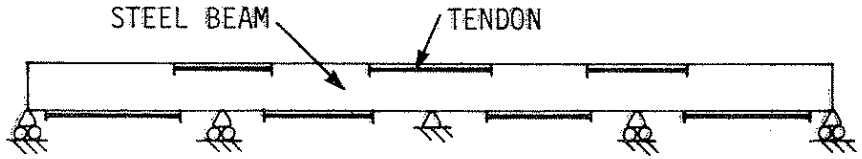

Fig. 1.8. Concept for a four-span, prestressed steel beam, circa 1969.

The early prestressed concrete bridges constructed in France by means of successive cantilevering often developed problems caused by insufficient prestress. The initial prestressing forces did not adequately account for losses caused by concrete creep, temperature movements, and cable friction. Virlogeux [29] briefly described the strengthening of a six-span, double-tee bridge over the Rhone River, which is illustrated in Fig. 1.10. Twelve cables, extremely long, were tensioned and anchored at the ends of the bridge in order to provide the prestress required to replace the unexpected losses. The tendons were placed a small distance below the deck and supported at regular intervals to prevent excessive sag.

In the mid 1970s, design standards for box girder bridges were revised in the United Kingdom and thus made it necessary to strengthen many long span bridges. The Erskine Bridge over the Clyde River near Glasgow, Scotland was one of the bridges that required strengthening to satisfy the then new Merrison requirements [24]. The harped tendon arrangement illustrated in Fig. 1.11 was utilized at the approach span piers to provide a part of the required strengthening. Anchoring the threadbar tendons at diaphragms within the steel box section required that the diaphragms be strengthened.

During the last decade California has strengthened many steel and composite bridges by means of post-tensioning [22]. One of the earliest strengthening projects was the Pit River Bridge, which was framed with trusses, floor beams, and multiple-span stringers. When the bridge was widened and brought up to then-current standards in 1979, it was necessary to strengthen the wide-flange stringers in negative moment

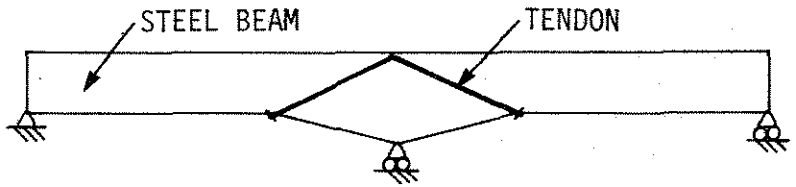

Fig. 1.9. Concept for a two-span, prestressed steel beam, circa 1975.

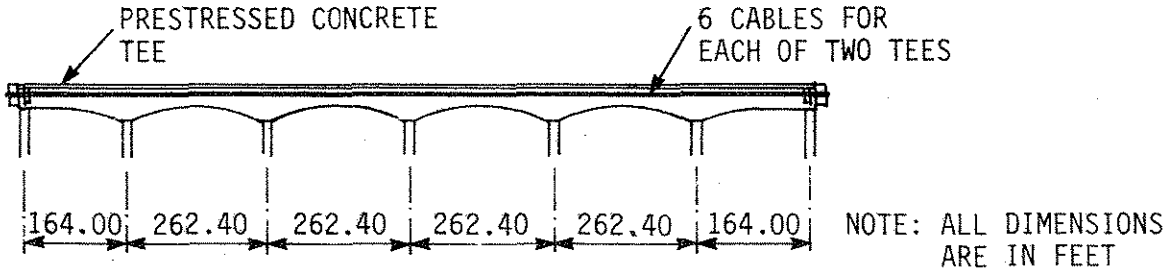

Fig. 1.10. Six-span bridge over the Rhone River, France, strengthened by post-tensioning, 1975-76.

regions, as shown in Fig. 1.12. Because the post-tensioning cables would add compression stress to the already overstressed bottom flanges, steel bars were bolted to the bottom flanges of each stringer in the negative moment region. The steel bars lowered the neutral axis of the stringer and thus provided additional eccentricity and moment from the tendons. The bars therefore served a dual purpose: to increase the post-tensioning moment and to carry a portion of the post-tensioning axial force in the compression region of the stringer.

The earlier Welland Canal Bridge example made use of post-tensioning to create a continuous span bridge from a series of simple spans. Jungwirth and Kern [15] present a similar example for a series of simple spans for a composite steel beam and concrete deck bridge. Figure 1.13 illustrates the two basic components: new reinforced concrete diaphragms over the support and straight tendons in the negative moment region. The purpose of the post-tensioning was simply to reduce deflections on the spans and eliminate problems with expansion joints at the supports. No compression bars were required for the bottom flanges because in a series of simple spans before the post-tensioning is applied, the bottom flanges have very minimal tension stresses.

A series of prestressed concrete bridges constructed over the Netekanaal in Belgium in 1955 developed problems because of inadequate initial prestress and apparent loss of prestress. DeBuck et al. [8] outlined the problems as water damage, incomplete grouting and subsequent corrosion of prestressing cables, and inadequate prestress due to underestimates of the effects of creep and overestimates of the

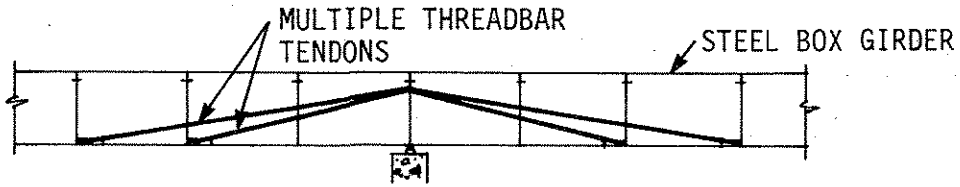

Fig. 1.11. Multiple-span, Erskine Bridge over Clyde River, Scotland, strengthened by post-tensioning, 1976.

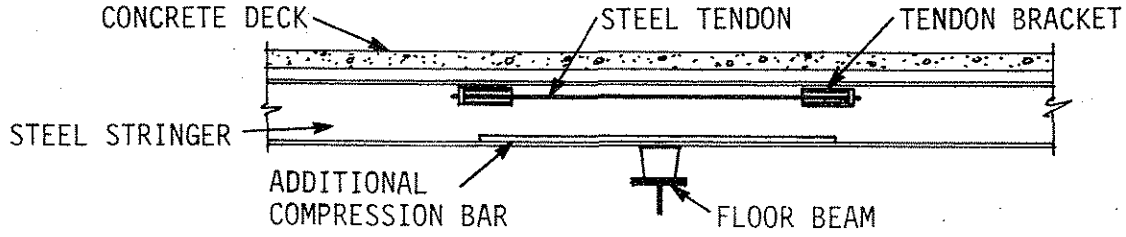

Fig. 1.12. Steel stringers in Pit River Bridge, California, strengthened by post-tensioning, 1979.

modulus of elasticity of the concrete. The tee beam bridge was strengthened with additional harped cable prestressing shown in Fig. 1.14. The cables were harped in the vertical direction as shown in the figure and also in the horizontal direction in order to pass the cables through openings in cross frames. Cables were anchored at new steel cross beams attached in the end spans. In the regions where the steel beams were attached to the existing prestressed concrete webs, steel plates were epoxy-bonded to the concrete webs in order to carry the additional local stress of the post-tensioning. Along the bottom surface of the beams in the center span, steel plates were epoxy-bonded in order to prevent potential tension overstress if a certain amount of the original prestress had been lost.

The Pont du Givors over the Rhone River in France was strengthened by post-tensioning in 1981 [21]. The bridge was a five-span, prestressed concrete, double box girder, as shown in Fig. 1.15. The bridge had water leakage into the boxes and cracks caused by inadequate initial prestress and loss of prestress. The harped cable pattern chosen for strengthening essentially reversed a part of the moment caused by applied loads. In order to provide the change in direction for the tendons near the centers of the long spans, new reinforced concrete diaphragms were cast in the box sections. Before the post-tensioning was applied, all cracks were injected with epoxy.

One of the lingering questions regarding composite action in continuous span bridges has been the effect of the deck and shear connectors in the negative moment regions. Without evidence of dependable composite action, most bridge engineers when computing section properties for

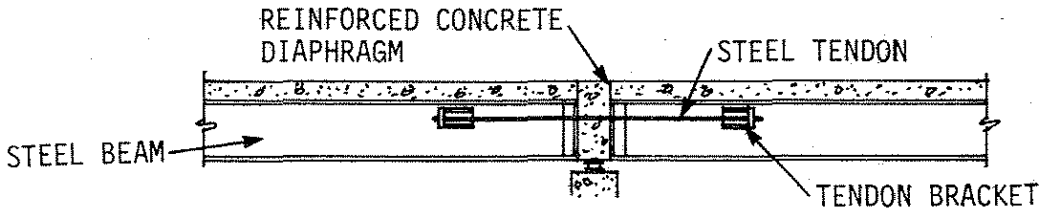

Fig. 1.13 Concept for reduction of deflection in simple span bridges. West Germany, circa 1980.

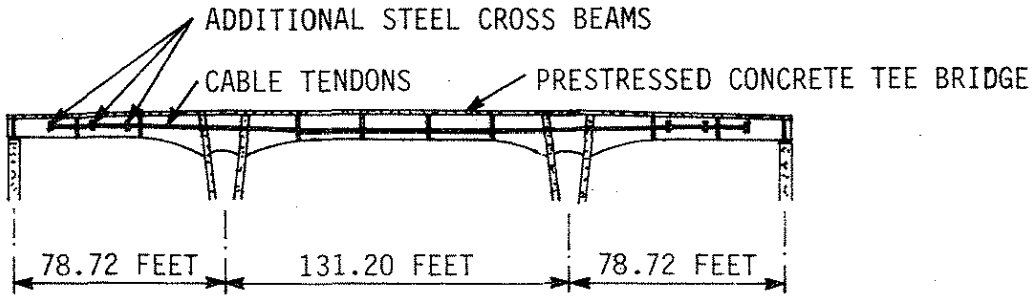

Fig. 1.14. Three-span bridge over the Netekanaal, Belgium, strengthened by post-tensioning, 1981.

bridge beams, neglect the concrete deck in negative moment regions. Lack of composite action causes early cracking of the concrete deck and loss of stiffness, as indicated by the tests conducted by Tachibana et al. [25].

One potential method for obtaining dependable composite action in negative moment regions is to prestress the deck above supports so that it remains in compression under all service loading conditions. That method was analyzed and tested by Kennedy and Grace [17] for a two-span bridge model. Two five-beam bridge models were constructed at one-eighth horizontal scale and one-third vertical scale: one model without prestressing and one model with longitudinal deck prestressing above the interior support. A longitudinal section through the prestressed model is given in Fig. 1.16. The deck in the model without prestressing cracked above the central support at a relatively low load; however the deck in the model with prestressing did not crack until a much larger load was applied. The model without prestressing had deflections and strains approximately 15% larger than the model with prestressing. The distribution pattern of those deflections, from beam to beam across the bridge model, did not vary significantly between models, however. Thus the deck prestressing eliminated cracking, maintained composite action, and maintained the stiffness of the bridge model under what could be considered to be service loading conditions.

Many of the prestressed concrete bridges constructed by cantilever construction in West Germany in the 1960s and early 1970s developed severe cracking near the construction joints a few years after construction. The nine-span bridge described by Holzapfel et al. in Reference 14 is one of the bridges with construction joint problems. For

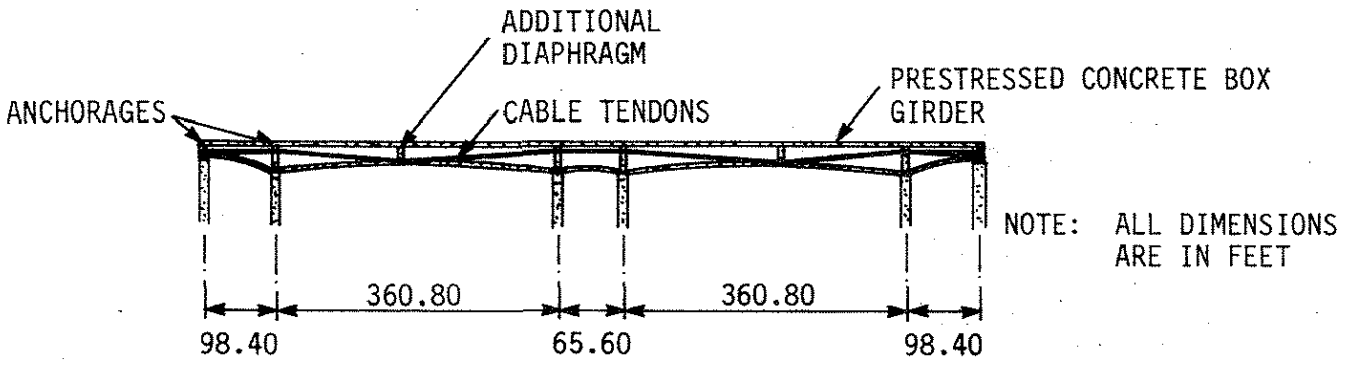

Fig. 1.15. Five-span bridge over Rhone River, France, strengthened by post-tensioning, 1981.

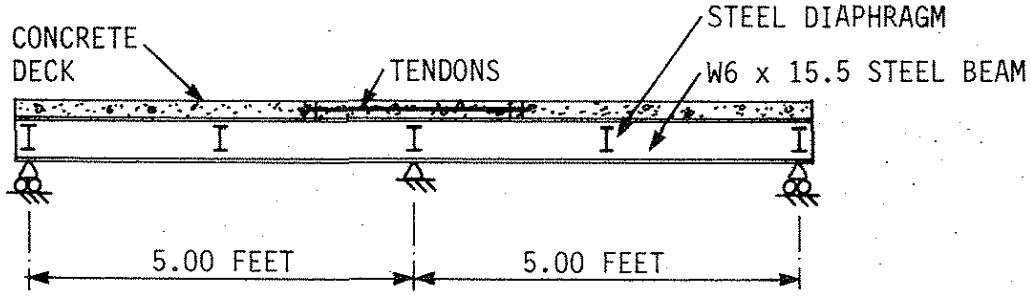

Fig. 1.16. Experimental, two-span, prestressed composite bridge model, circa 1982.

the bridge it was determined that the causes of the cracking were: minimal prestressing near the construction joints, inadequate provisions for temperature and shrinkage, and minimal reinforcement for tension stresses near the construction joints. The bridge was strengthened with harped cables, and the harped configuration was achieved by adding a steel diaphragm between the prestressed concrete beam webs at each construction joint as shown in Fig. 1.17. The harped configuration was chosen because it minimized the required cable force and thus minimized the elastic shortening of the relatively long bridge. In order to further adjust stress conditions in the bridge, the bridge was jacked to slightly higher elevations at three of the supports after post-tensioning.

Another West German bridge with a different problem was strengthened with a harped tendon arrangement similar to the arrangement described in the previous example. The Autobahn bridge reported by Engelbach [11] had corrosion and loss of prestress in the tendons for one of the four prestressed beams within the bridge. In order to avoid the unknown distribution effects if only the deficient beam were post-tensioned for strengthening, all of the beams were post-tensioned equally by using the harped tendon scheme illustrated in Fig. 1.18.

In order to provide a haul road for several relatively large and heavy preassembled industrial equipment parts, a series of bridges was strengthened in New Zealand. The Waiwaka Terrace Bridge described by Blakeley et al. [4] was strengthened by partial length cable tendons as illustrated in Fig. 1.19. The tendons were placed on both sides of each of the six beam webs and tensioned by depressing them at the saddles

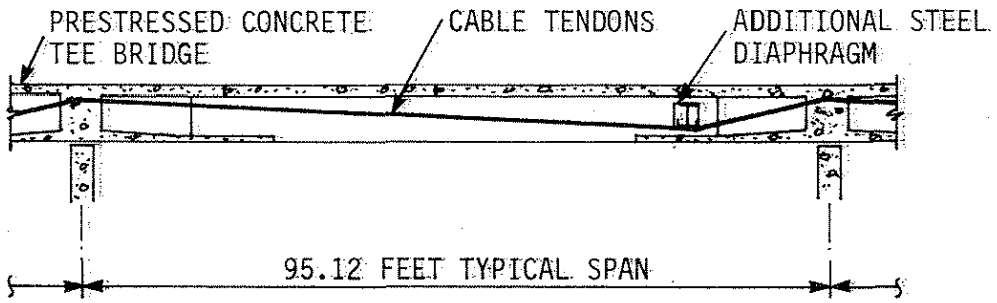

Fig. 1.17. Nine-span bridge over Highway L284, West Germany, strengthened by post-tensioning, circa 1983.

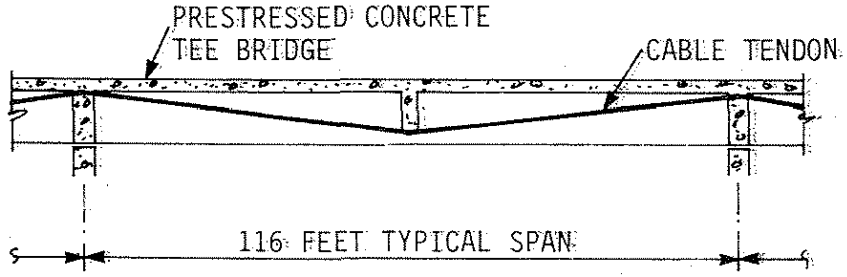

Fig. 1.18. Multiple-span Autobahn bridge, West Germany, strengthened by post-tensioning, 1984.

rather than by longitudinal jacking. The tendons, by means of the harped configuration and longitudinal distribution of the forces and moments applied by the tendons, strengthened the bridge the required amount without running the entire length of the bridge. The axial force applied by the tendons apparently would have overstressed the compression zones at the bottoms of the haunches, and thus it was necessary to bolt and epoxy-bond steel plates to those haunches for compression strengthening. In concept, this compression strengthening is similar to that used for the Pit River Bridge [22].

On the ten-span Bonners Ferry Bridge, constructed recently in Boundary County, Idaho, both the steel girders and the concrete deck were prestressed in negative moment regions above the piers [27]. The prestressing was applied in two stages by straight tendons located as shown in Fig. 1.20. In the first stage, tendons attached to the girders reduced the dead load tension stresses in the top flanges to an allowable level. In the second stage the tendons, placed in the deck and tensioned after the deck had cured, eliminated the tension in the deck under full service live load. Thus, the second stage of prestressing made use of the concept analyzed and tested by Kennedy and Grace [17] and assured full composite action throughout the bridge, even in the negative moment regions. The full composite action reduced deflections and improved the fatigue strength of the bridge. Use of the prestressing also provided enhanced redundancy through the multiple load path network.

A recent experimental research program at Concordia University in Montreal, Canada explored prestressing of continuous steel bridges

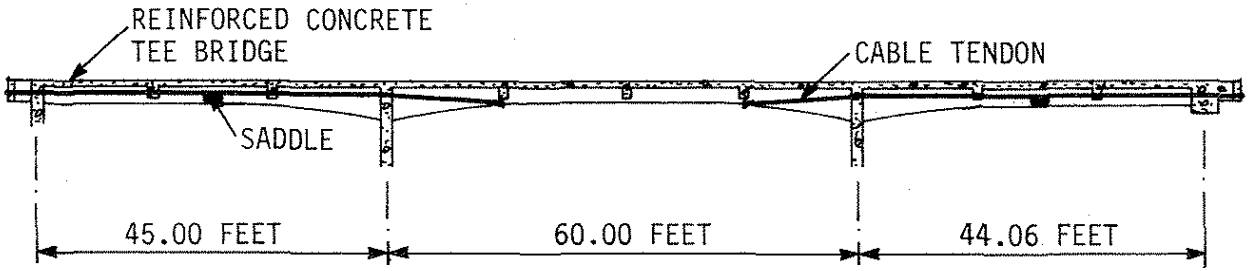

Fig. 1.19. Three-span Waiwaka Terrace Bridge, New Zealand, strengthened by post-tensioning, 1985.

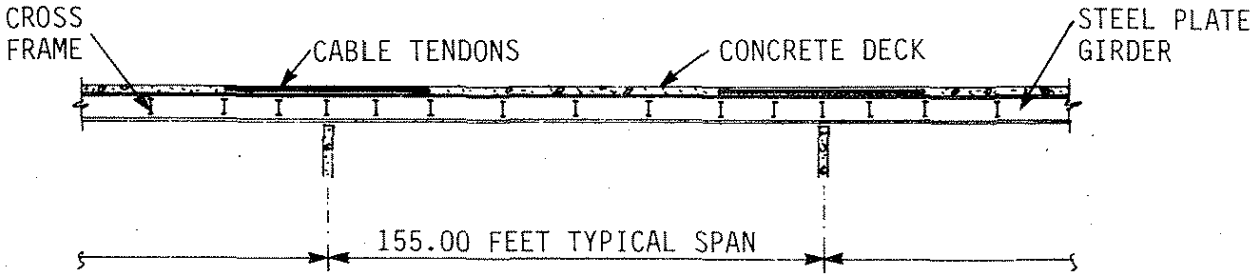

Fig. 1.20. Ten-span, prestressed composite girder, Bonners Ferry Bridge, Idaho, circa 1985.

[26]. A scale model of a two-span, two-web plate girder bridge with an orthotropic steel deck was constructed of plexiglass. The model was tested and analyzed with six different tendon configurations, one of which is shown in Fig. 1.21. The authors were unable to reach any strong conclusions regarding the different tendon configurations. They did point out, however, that the tendon configuration shown in Fig. 1.21 would be reasonably optimal if the design of the two-span bridge were governed by negative dead load moment.

The prestressing examples reviewed above either specifically state or imply that prestressing steel structures or post-tensioning existing structures for strengthening purposes is different from prestressing new concrete structures. Post-tensioning for strengthening continuous bridges generally must be conceived in such a way as to reverse the moments caused by dead and live loads rather than to overcome a tension weakness in the structure. One exception is the case of continuous composite structures. In this case, if the post-tensioning can be applied in such a way as to eliminate tension in the deck above supports, full composite action can be achieved throughout the structure rather than only in positive moment regions.

The examples illustrate a variety of tendon configurations: straight, harped, and harped with an additional compression member. Straight tendons are the simplest to use; however straight tendons require larger forces because of minimal eccentricity. In negative moment regions of composite structures, it may be difficult to achieve any eccentricity, and in that case, straight tendons apply only an axial force. In many cases straight tendons applied to negative moment

regions require additional compression reinforcing for the applied compression forces. Harped tendons can more nearly reverse the applied dead and live load moments and, therefore, require smaller tendon forces to strengthen a given bridge. The reduced force becomes especially important when relatively long bridges are post-tensioned and there is concern for axial shortening. When harped tendons are used with separate compression members, the mechanism created is more efficient than a simple harped tendon. With the additional compression member, the eccentricity of the tendon is increased; the increased eccentricity can be used to provide more strengthening capacity or to reduce the required tendon force.

The behavior of the entire continuous bridge must be considered when the bridge is strengthened by post-tensioning. Post-tensioning is distributed longitudinally within a continuous structure; there are several examples where the engineer has made use of post-tensioning at one or more locations and not only strengthened these regions but also strengthened all critical stress regions. None of the examples cited above, however, deal with transverse distribution of post-tensioning. In fact there are several examples where the engineer post-tensioned all beams or applied the post-tensioning in stages in order to avoid the unknown effects of lateral distribution.

The literature review shows that continuous composite bridges can be strengthened by post-tensioning. For existing continuous bridges, post-tensioning can be used to reverse the moments caused by applied dead and live loads and may be able to overcome the tension weakness in the concrete deck over supports and achieve full composite action throughout a bridge.

1.5. Selection and Rating of Prototype Bridge

Iowa began designing and constructing continuous span steel stringer bridges relatively early in comparison with other states, and for that reason, Iowa has a considerable inventory of those bridges. The Office of Bridge Design at the Iowa DOT provided the researchers with plans for six standard series of continuous span bridges from the period 1939 to 1960, which might be candidates for a prototype bridge.

In selecting a standard series for a prototype bridge, the researchers considered the following factors. The bridge series must have a roadway wide enough for two standard 12-ft traffic lanes. A considerable number of bridges should have been constructed in Iowa from the standard plans so that if strengthening is applied to a bridge as part of another phase of this research, a suitable bridge will be available in central Iowa. The shortest bridge in the standard series, at a scale no less than one-third full size, must fit space available in the ISU Structural Engineering Research Laboratory.

Considering these factors and the advice of the Office of Bridge Design, the V12(1957) series of bridges was selected for the prototype. This series was in effect for approximately eight years, and a search of the Iowa DOT records indicated that 100 to 150 bridges were constructed from the standard plans for that series. In order to minimize the size of the laboratory model, the shortest V12(1957) bridge, 125 ft, was selected. A transverse section of that bridge is given in Fig. 1.22a, and a longitudinal section is given in Fig. 1.22b.

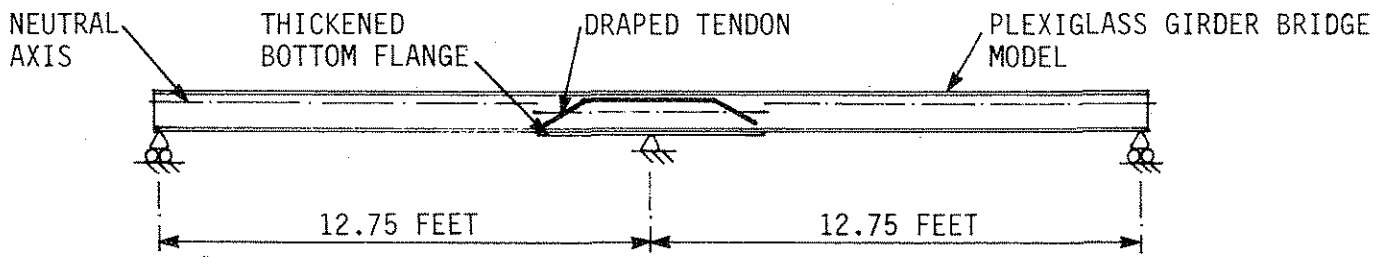

Fig. 1.21. Experimental, two-span bridge model, circa 1986.

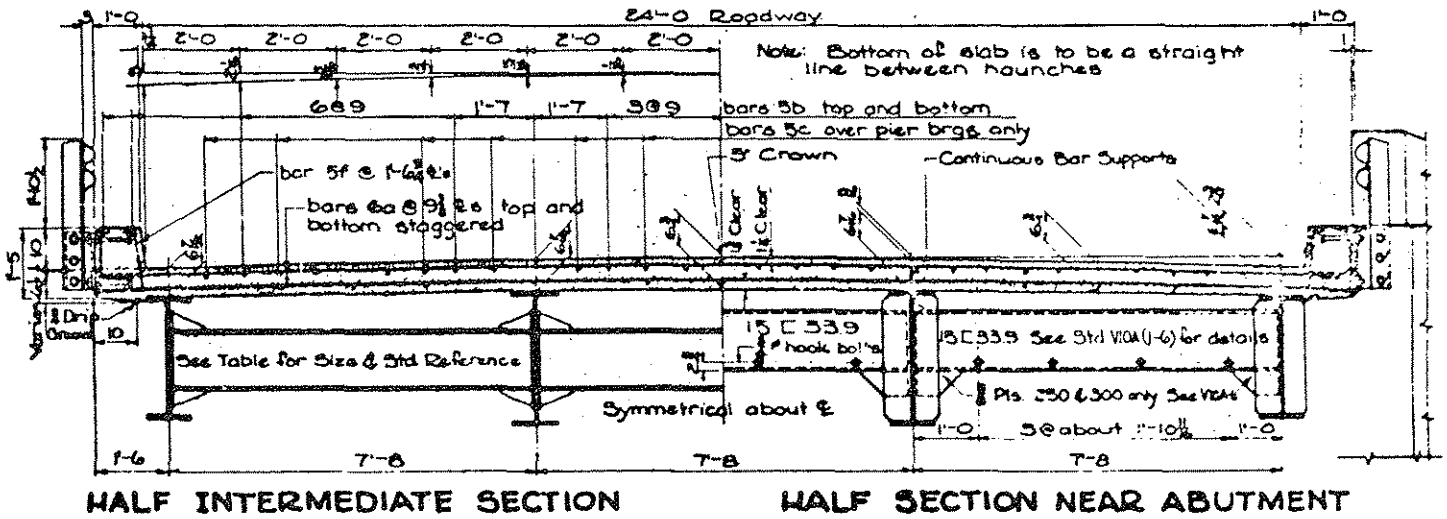

a. TRANSVERSE SECTION

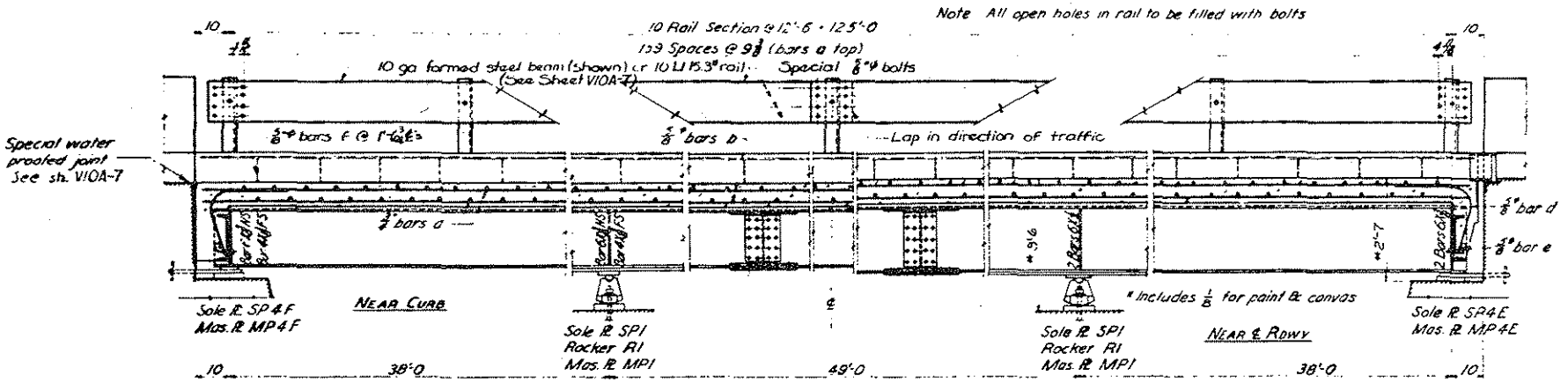

b. LONGITUDINAL SECTION

Fig. 1.22. Prototype V12 (1957) series bridge, 125-ft length.

Figure 1.22a shows the bridge to have a 24-ft wide roadway with low, integral curbs and four steel beams made composite with the concrete deck. Because the bridge was designed before the change in AASHO bridge design specifications that required a large increase in wheel load fraction for exterior beams, the exterior beams are smaller than the interior beams.

Figure 1.22b shows the bridge to have three spans. The two end spans are 38 ft long, and the center span is 49 ft long. The longitudinal section shows the steel beams to be coverplated on both top and bottom near the piers. The section also shows that there were two beam splices within the center span and that those splices consisted of both flange and web splice plates in order to achieve shear and moment continuity.

According to the Office of Bridge Design, there are two typical problems with continuous, composite steel beam-concrete deck bridges: the bridges often have coverplates over the piers that are not long enough, and the compression flange of the steel beams at the piers often is overstressed. The bending stress checks given later in this section indicate that the prototype bridge has both problems described above and additional overstresses at other locations.

On the basis of Iowa DOT records, and with the assistance of nine county engineers' offices, the researchers located two of the V12(1957) bridges in central Iowa. Two of the researchers briefly inspected one of the bridges on old US 30 in Greene County.

Under current AASHTO specifications [1,2], Iowa DOT policies, and Iowa legal truck loads, a V12(1957), 125-ft long bridge requires a

minor load restriction because bending stresses in steel beams exceed the allowable operating stress of 24.75 ksi for A7 steel. With the assistance of the Office of Bridge Design, the researchers performed a partial rating for bending stress for the prototype bridge in order to determine the magnitudes and locations of overstress. The bending stress checks were conducted with the current AASHTO Bridge Design Specifications [2] and supplemented with usual Iowa DOT practice and Iowa legal truck loads as noted below:

- Truck loads were taken to be Iowa legal loads: Type 3 and Type 4 straight trucks, Type 3S2(A), Type 3S2(B), and Type 3S3 trucks and semi-trailers, and Type 3-3 truck and trailer.
- Only one truck per lane was placed on the bridge.
- Curbs and steel bridge rails were considered to be long-term dead load.
- A future wearing surface of 19 psf was included in the long-term dead load.
- Moments along the bridge were based on moments of inertia which changed as follows. For positive moment regions, composite beam moments of inertia were computed with integral curbs for exterior beams and concrete decks with deducted wearing surfaces for both interior and exterior beams. For negative moment regions over the piers, beams and coverplated beams were considered to be noncomposite; the deck and reinforcing were neglected.

On the basis of standard V12(1957) plans and Iowa DOT specifications, the steel for the prototype bridge was taken to be A7 with a yield stress of 33 ksi, and the concrete deck and curb were assumed to have a 28-day strength of 3000 psi.

Results of the bending stress checks are given in Table 1.1. Figure 1.23 supplements the table in showing the assumptions for live load moments of inertia and the sections at which stresses were checked.

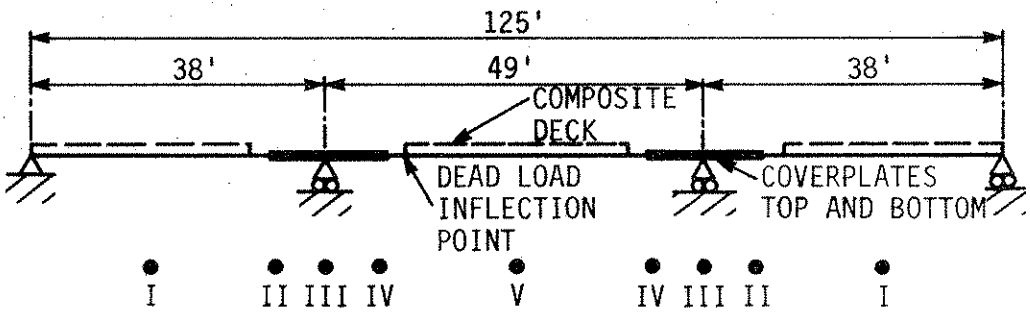

I = SECTION FOR MAXIMUM POSITIVE MOMENT AT 0.4L FROM ABUTMENT, END SPAN

II = SECTION AT THEORETICAL COVERPLATE CUTOFF, END SPAN

III = SECTION FOR MAXIMUM NEGATIVE MOMENT, PIER

IV = SECTION AT THEORETICAL COVERPLATE CUTOFF, CENTER SPAN

V = SECTION FOR MAXIMUM POSITIVE MOMENT AT 0.5L FROM PIER, CENTER SPAN

Fig. 1.23. Critical stress locations and beam stiffness assumptions, prototype V12 (1957) series bridge.

Table 1.1. Overstress with respect to allowable inventory stress, prototype V12 (1957) series bridge.

		OVERSTRESS, ksi				
SECTION		I	II	III	IV	V
EXTERIOR BEAM	TOP FLANGE	-	+4.41	+6.13	+0.84	-
	BOTTOM FLANGE	+5.16	-6.02	-6.13	-2.45	+7.65
INTERIOR BEAM	TOP FLANGE	-	+1.42	+2.45	-	-
	BOTTOM FLANGE	+6.27	-2.76	-2.45	-0.46	+7.71

NOTE: - INDICATES COMPRESSION OVERSTRESS

+ INDICATES TENSION OVERSTRESS

The table shows the largest overstresses that would require load restriction (posting) at Section V on the center span for both exterior and interior beams. There are also relatively large overstresses at Section I on the end spans for both exterior and interior beams and at Sections II and III on the exterior beams. The majority of the critical stress locations show overstresses with respect to the allowable inventory stress of 18 ksi.

On the basis of the bending stress checks, it is apparent that all critical positive and negative moment sections in both exterior and interior beams are overstressed. Strengthening of the prototype bridge by post-tensioning, therefore, would require stress relief in all of those regions, in order to keep bending stresses within the allowable inventory stresses.

CHAPTER 2. DESCRIPTION OF TEST SPECIMENS

This chapter outlines the details of the model and mockup used in this investigation. The instrumentation employed, procedures followed, and the actual tests performed are presented in Chapter 3. Discussion and analysis of results as well as behavior characteristics noted during testing are presented in Chapter 4. This chapter, as well as the next two chapters of this report, has been subdivided into two sections; the first section pertains to the bridge model, while the second section pertains to the full-scale negative moment region mockup.

2.1. Model Bridge

2.1.1. Description

The model bridge (Figs. 2.1 and 2.2) was constructed to be, as nearly as possible, a one-third-scale replica of the three span V12(1957) bridge (illustrated in Fig. 1.22). The scale was selected to make the model as large as possible, yet to fit within the confines of the Structural Engineering Laboratory.

As shown in Fig. 2.1, the steel frame is composed of four longitudinal beams connected transversely by 24 diaphragms; for additional information on the framing and structural steel details, see Appendix A. Note that the exterior stringers are 1 in. shallower than the interior stringers which correctly models the 3 in. difference in stringer height found in the prototype. Plan view dimensions shown in Figs. 2.1 and A.1 are one third of the values given on the original V12(1957) plans. Thus the bridge model follows the principles of similitude and will respond to loadings essentially the same as the prototype.

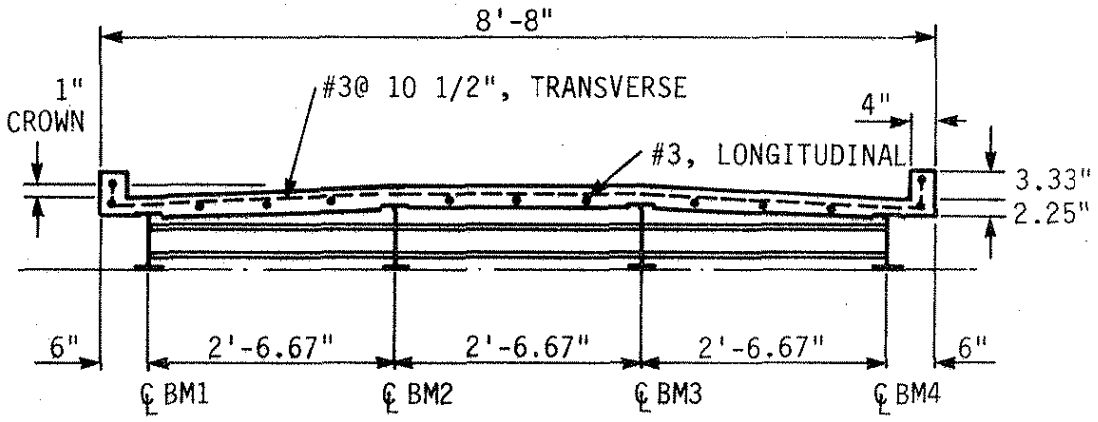

a. CROSS SECTION AT MID-SPAN (SEC A-A)

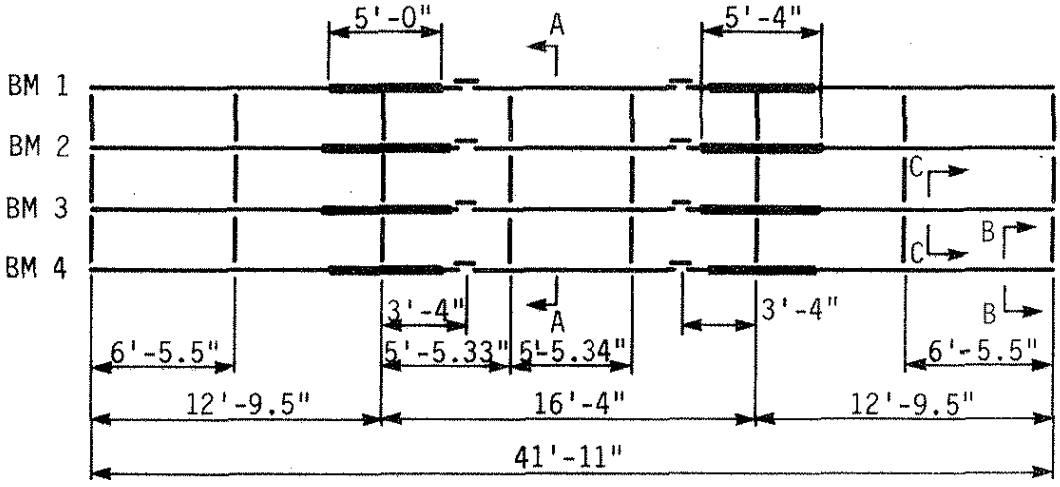

b. PLAN VIEW

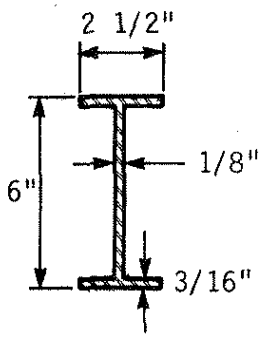

c. SECTION B-B

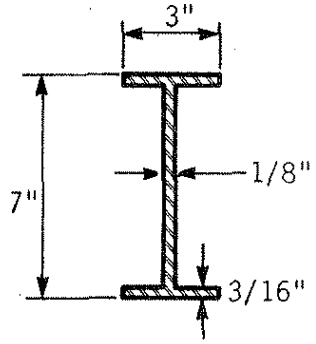

d. SECTION C-C

Fig. 2.1. Model bridge.

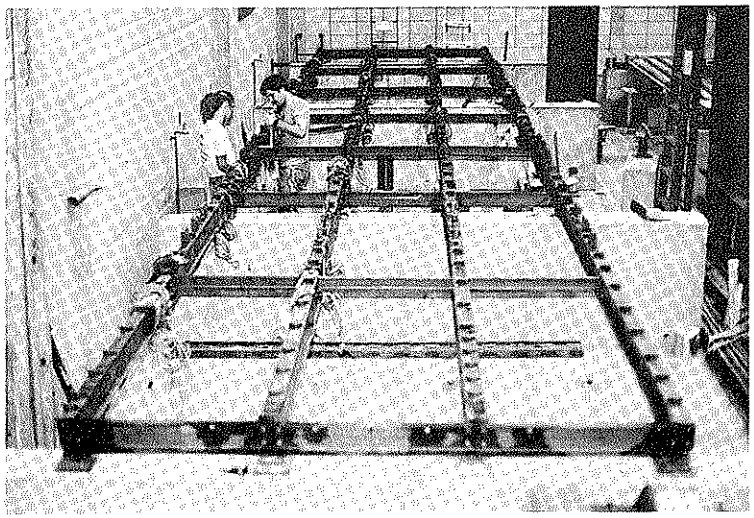

a. STEEL FRAME

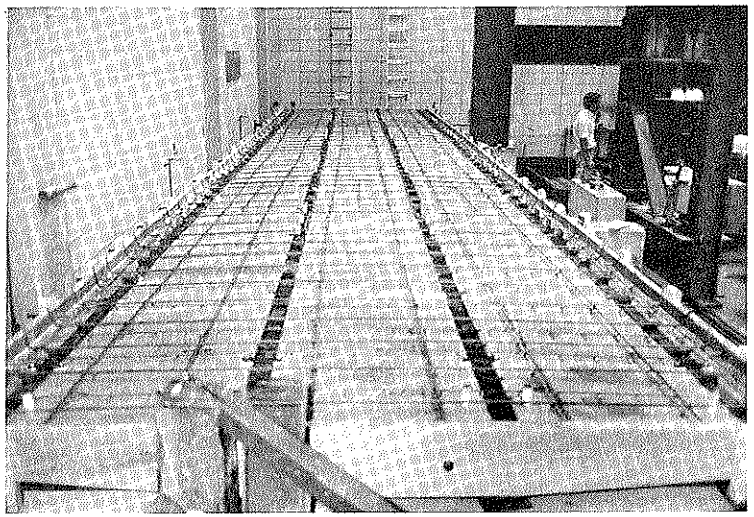

b. FORMWORK AND REINFORCING

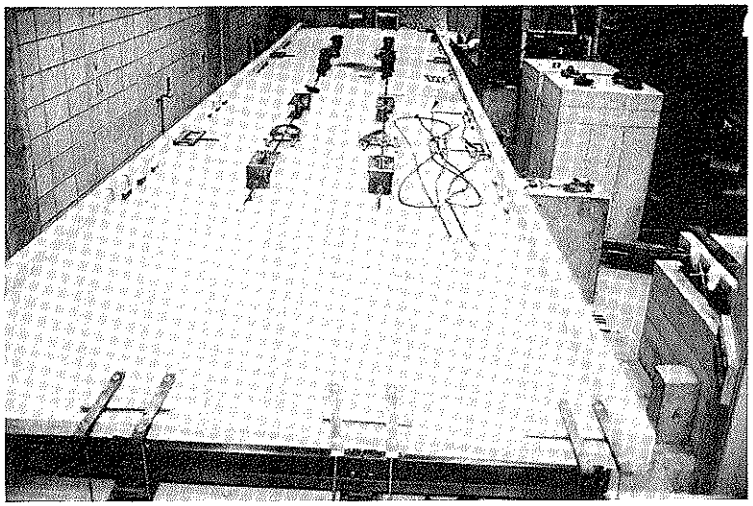

c. DECK WITH CURBS

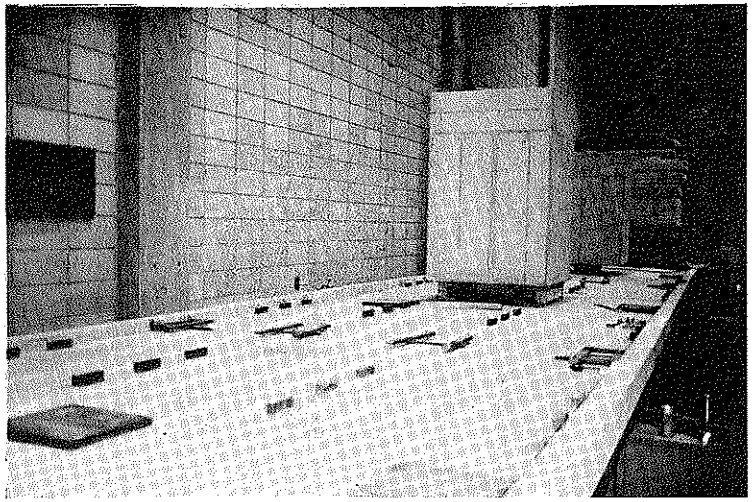

d. TWO VERTICAL LOADS

Fig. 2.2. Photographs of model bridge.

Each steel stringer consists of three lengths that are bolted together to make the 41-ft 11-in. continuous stringer. As illustrated in Fig. A.8, each connection consists of six flexural plates and two shear plates; twenty-two 1/2-in.-diameter, high-strength bolts (8 per flange and 6 per web) were used in each connection. For composite action between the concrete deck and the steel stringers, angle-plus-bar shear connectors were welded to the top flanges of the stringers. Figure A.5 illustrates the size of the connectors while the spacing utilized is given in Fig. A.4.

Because of the size limitations of the steel stringers, the post-tensioning brackets had to be placed on top of the slab in the negative moment regions and under the lower stringer flanges in the positive moment regions. Also, because of the eccentricities resulting from the brackets in these locations, the resulting ratio of post-tensioning moment to force was significantly larger than the ratio that would result in the field when post-tensioning brackets are positioned below the upper flange and above the lower flange in the negative and positive regions, respectively.

Tabs for attaching post-tensioning brackets were welded to the top flanges in all eight negative moment regions and to the bottom flanges in all the positive moment regions of the exterior beams (see Figs. A.9 and A.10). Preliminary analysis of a three-span continuous beam indicated that the moment produced by post-tensioning is a function of the distance between the brackets. Two tabs are required to connect one bracket; however, three tabs were welded on each side of the eight negative moment regions so that two different lengths of post-tensioning

tendons could be tested (ℓ_1 = 123 in. and ℓ_2 = 99 in. in Fig. 2.3). The locations of the negative tabs, the interior positive tabs (see Fig. A.9), and the beam splices are approximately where the inflection points would occur if a uniformly distributed load were applied to the three-span bridge model. The distance between the brackets (post-tensioning lengths of ℓ_3 = 95 in. for end spans and ℓ_4 = 111 in. for middle spans as illustrated in Fig. 2.3) in the positive moment regions and negative moment regions are also shown in Fig. A.9. Also shown in Fig. 2.3 are the coordinates of the supports, coverplates, splices, diaphragms, and anchorages.

Figure A.11 shows that there are two types of diaphragms: intermediate diaphragms and pier or abutment diaphragms. The intermediate diaphragms are channels with steel plates welded on the ends. These channels are connected to the webs of the longitudinal girders by bolts through the end plates as shown in Fig. A.11. The abutment diaphragms are also channels; however, they are attached by bolting through their webs to stiffeners that were welded to the webs of the longitudinal stringers as shown in Fig. A.6.

The model bridge is supported on four reinforced concrete walls, 10 in. wide, 3 ft high and 12 ft 6 in. long. At each abutment or pier, each longitudinal girder is supported on a roller that is placed on a 1/2-in. steel plate that was grouted on the abutment or pier as shown in Fig. A.12. A transit was utilized for leveling the abutments and piers to make sure that they were at the same elevation.

After the steel stringers and diaphragms were assembled (see Fig. 2.2a), formwork was constructed (see Fig. 2.2b) and the concrete

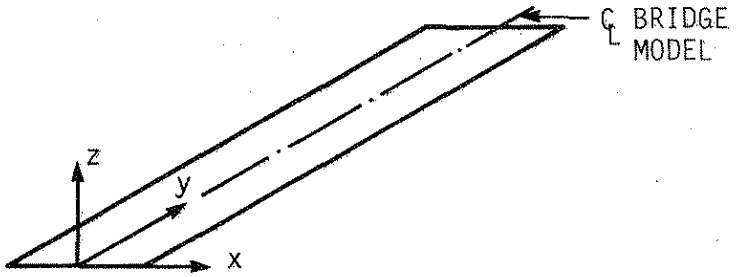

a. COORDINATE AXES

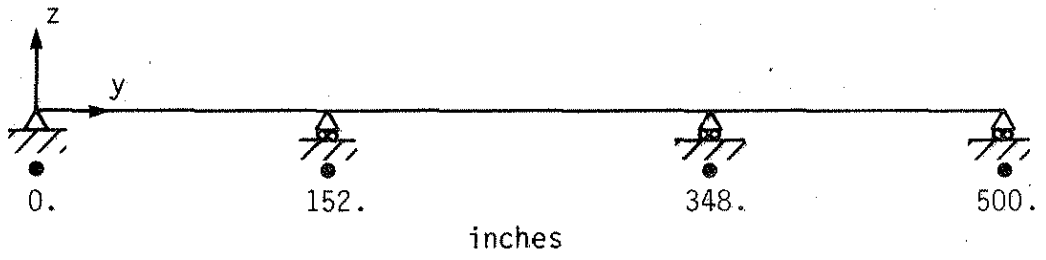

b. y-COORDINATES FOR SUPPORTS

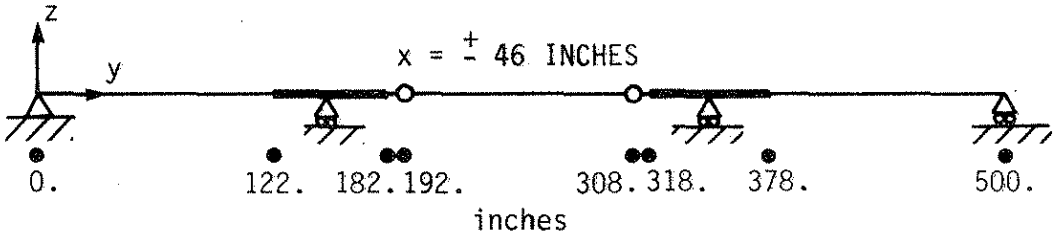

c. y-COORDINATES FOR EXTERIOR BEAM

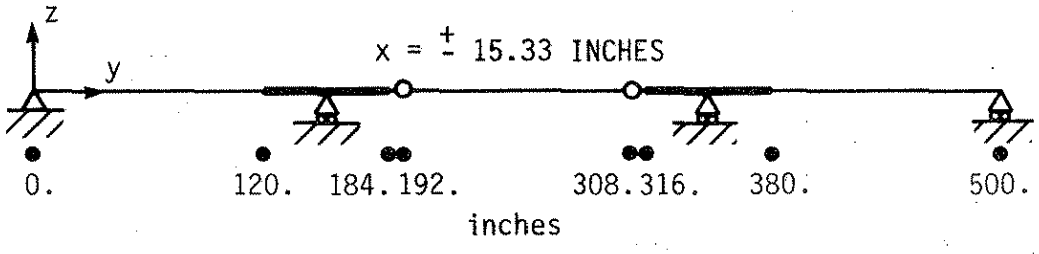

d. y-COORDINATES FOR INTERIOR BEAM

Fig. 2.3. Model bridge coordinates.

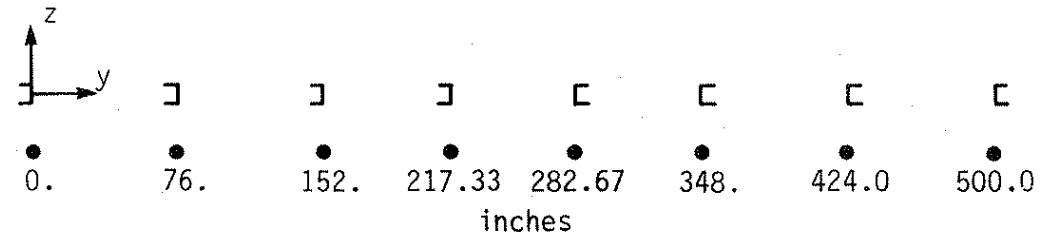

e. y-COORDINATES FOR DIAPHRAGMS

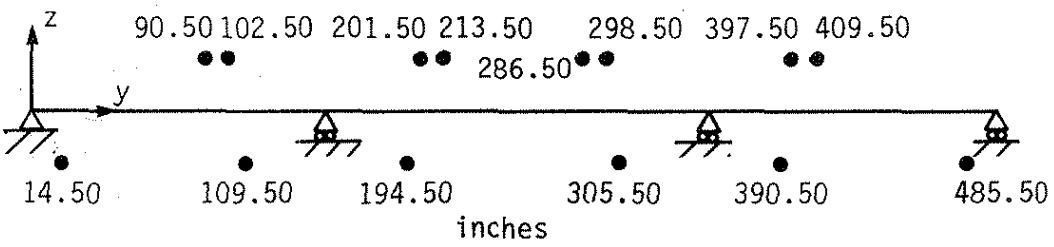

f. y-COORDINATES FOR ANCHORAGES

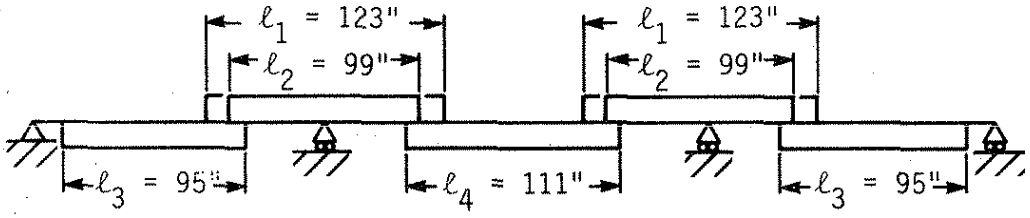

g. TENDON LENGTHS

Fig. 2.3. Continued.

deck was placed as shown in Fig. 2.2c. Note that Fig. 2.2c also shows the curbs that were cast in place two weeks after the deck. The positive moment regions of the concrete slabs were placed before the negative moment regions. Figure 2.4 shows the casting sequence of the concrete deck. The model deck thickness of 2.25 in. (1/3 that of the prototype) precluded the placement of reinforcement in two layers as would be the case in the prototype bridge. Reinforcement (#3 at 10.5 in. transverse and #3 at 14 in. longitudinal) was placed at mid-depth in the deck; additional #3 reinforcement was placed longitudinally in the negative moment regions.

The concrete deck has a crown (see Fig. 2.1a) caused by the change in depth between the exterior and interior beams. The average deck thickness is 2.65 in., which is slightly larger than one-third of the deck thickness of the prototype bridge (2.25 in.). This deck thickness is the average of 48 measurements taken at different locations on the bridge. The curb was placed two weeks after the concrete deck. As shown in Fig. 2.1a, the desired width and total depth (deck + curb height) are 4 in. and 5.58 in., respectively. The average measured curb width was 3.88 in., while the average curb height was 5.50 in. The curb dimensions were obtained by averaging 16 measurements taken at different locations along the curb.

In order to prevent uplift of the model bridge caused by various post-tensioning and vertical loading conditions, tie downs were fabricated and placed at each stringer support (see Fig. 2.5). These tie downs were designed to prevent vertical uplift, but to permit horizontal movements.

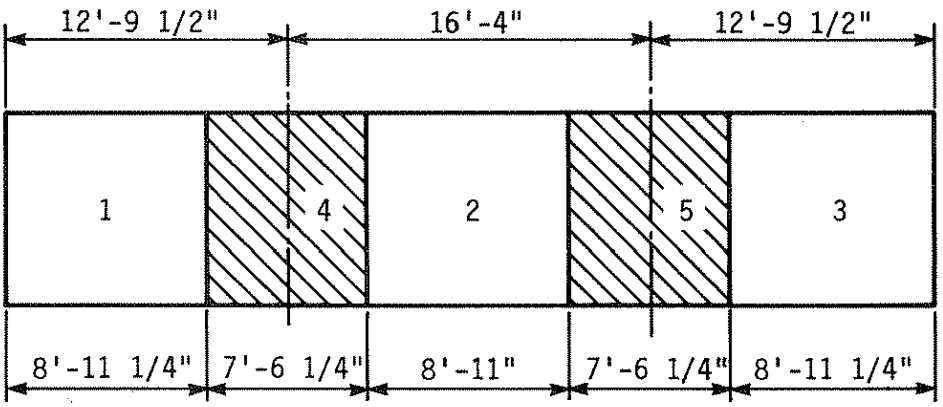

a. POUR SEQUENCE

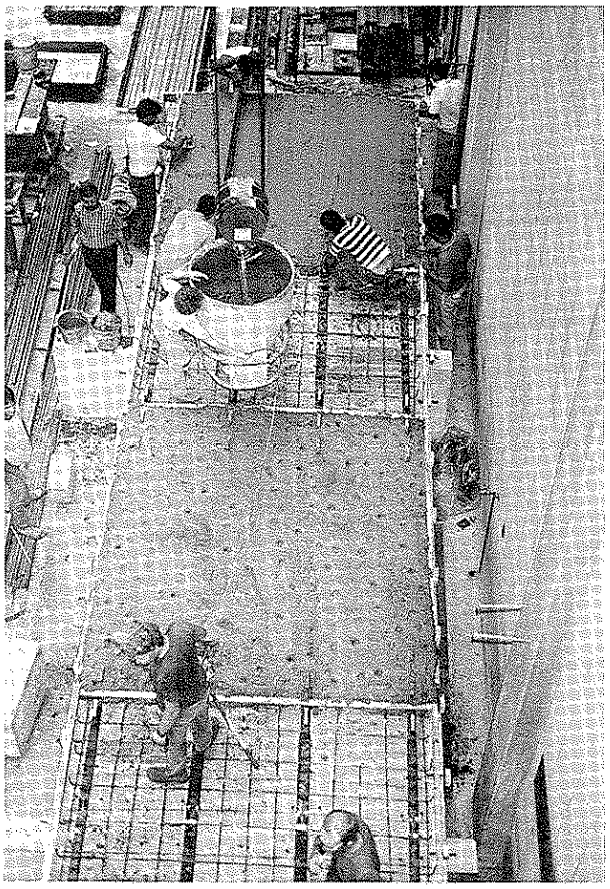

b. PHOTOGRAPH OF POURING BRIDGE DECK

Fig. 2.4. Pouring of concrete deck for model bridge.

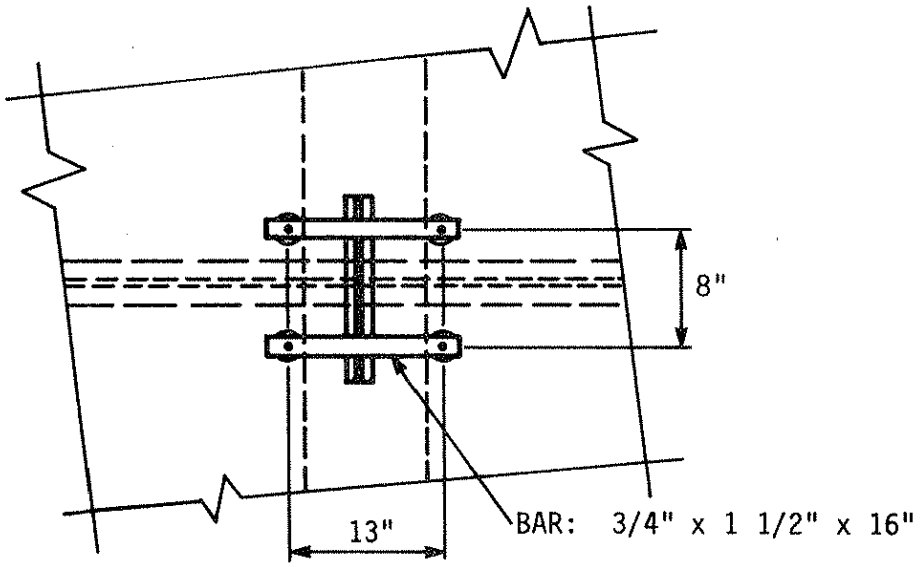

a) PLAN VIEW

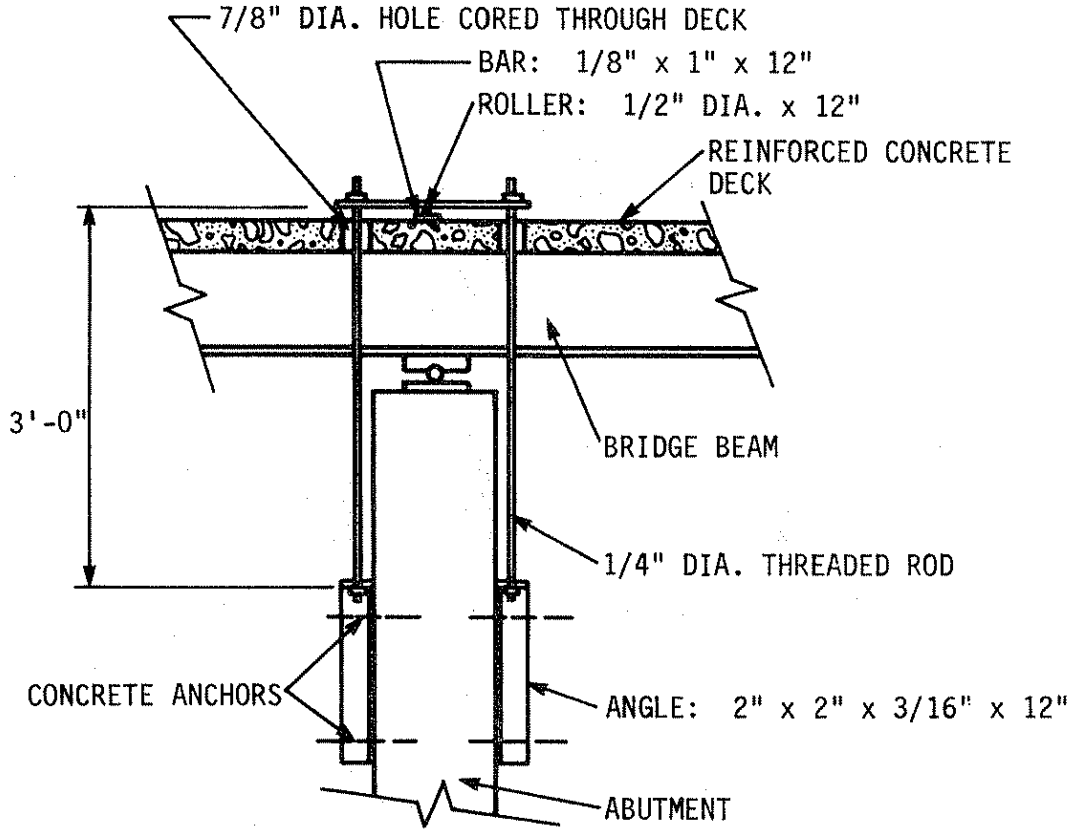

b) SECTION

Fig. 2.5. Support tie-down system.

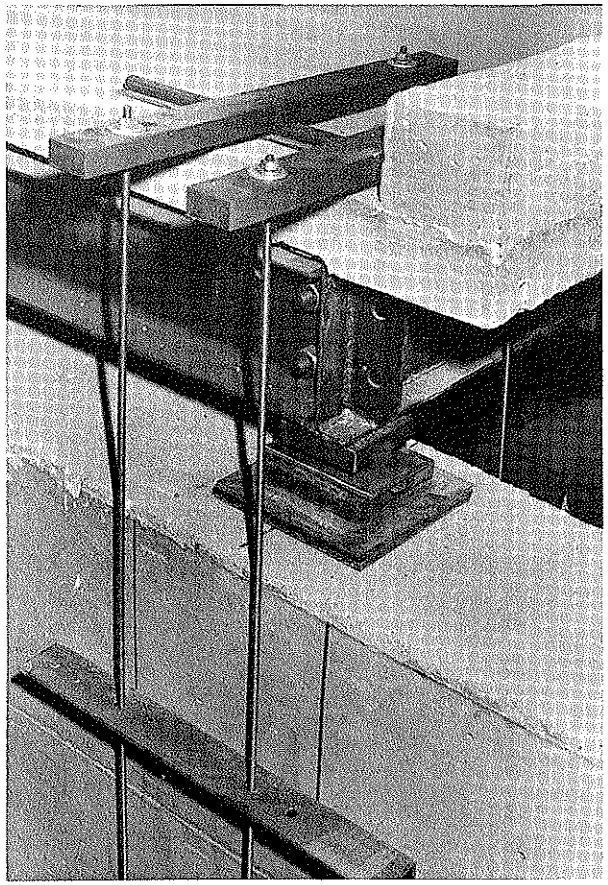

c. TIE DOWN AT ABUTMENT

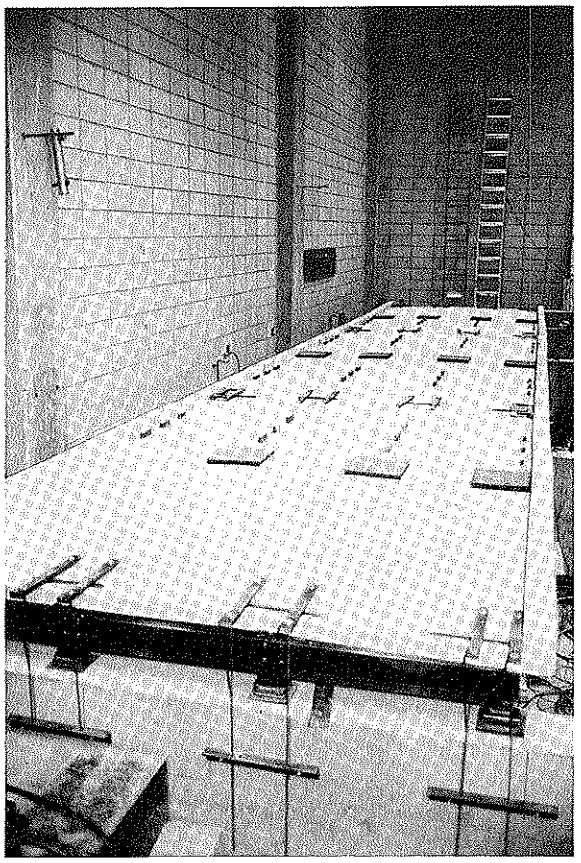

d. MODEL BRIDGE WITH TIE-DOWN SYSTEM

Fig. 2.5. continued

The dead load stresses in the model were approximately 1/9 the dead load stresses in the prototype. As the purpose of the model was to determine its response to live loads and post-tensioning, no attempt was made to add dead load to the model to simulate the actual dead load in the prototype.

To produce live load stresses in the prototype bridge, two 6-kip concrete weights were constructed in the laboratory. Live load stresses in the model resulting from one of the 6-kip weights, as a result of the principles of similitude, duplicate the stresses in the prototypes resulting from a 54-kip weight. Each 6-kip vertical load is a 3-ft x 3-ft x 4-ft 8-in. concrete block that has a 1-ft x 1-ft x 4-in. concrete block integral with its base to approximate a concentrated load and which simplifies placing the weight on the bridge (see Fig. 2.6). Although the actual weights of the blocks were 6020 lbs and 6010 lbs, they will be referred to as 6-kip loads in the remainder of this report.

2.1.2. Physical Properties

2.1.2.1. Concrete

Twelve standard cylinders (6 in. diameter x 12 in. long) and two beams (6 in. x 6 in. x 30 in.) were made during the placing of both the concrete deck and curbs. The maximum aggregate size used in both concrete mixes was 3/8 in. These cylinders and beams were subjected to the same curing conditions as the slab and the curb. Table 2.1 presents the slump, unit weight, compressive strength, and modulus of rupture of the concrete slab and curb. Each modulus of rupture value given is the average of four tests, while each compressive strength value given is the average of three tests for either the slab or the curb. The

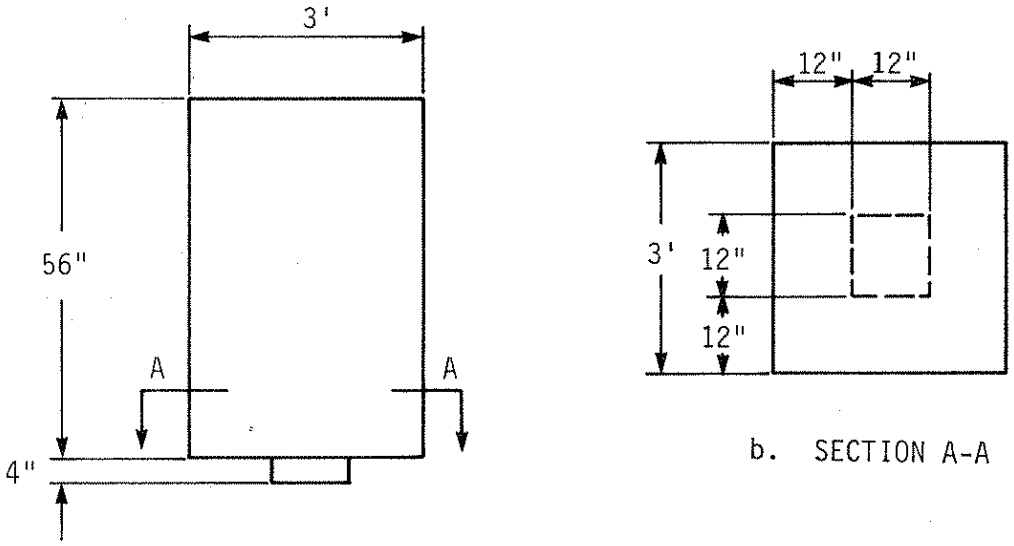

a. ELEVATION VIEW

b. SECTION A-A

Fig. 2.6. Concrete dead weight.

Table 2.1. Physical properties of concrete.

	Slump (in.)	Unit Weight (lb/ft^3)	f'_c (psi)	f'_r (psi)
Deck	2.75	140	3450	447
Curb	4.25	142	3355	445

compressive strength of the concrete in the bridge model was slightly higher than the specified concrete compressive strength in the prototype bridge. However, the concrete compressive strength in the prototype bridge is most likely higher than that specified; thus the concrete compressive strength in the model and prototype are probably very close.

2.1.2.2. Steel

Because the steel strength was not one of the variables being studied in the investigation and because the bridge was tested within the steel elastic stress range, no tension tests were conducted on any of the steels utilized in this testing program. In the analysis presented in Chapter 4, nominal values of the modulus of elasticity of the steel beams and Dywidag tendons were assumed to be 29,000 ksi and 24,000 ksi, respectively. These assumed values were based on steel tension tests made in other research projects.

2.2. Full-scale Negative Moment Region Mockup

As previously noted, the size of the stringers in the bridge model forced placement of the post-tensioning tendons above the deck in the negative moment region and below the bottom flange in the positive moment region. In order to investigate the effect of post-tensioning below the deck and also to investigate other post-tensioning schemes in the negative moment region, a full-scale model of a negative moment region within a continuous bridge was constructed. This full-scale model of the negative moment region in a continuous bridge will henceforth simply be referred to as the mockup.

2.2.1. Description

Figure 2.7 illustrates how the mockup simulates the negative moment region in a continuous bridge. (Compare the bridge moment diagram shown in Fig. 2.7b to the mockup moment diagram shown in Fig. 2.7d.)

The mockup was constructed to replicate the negative moment region of the V12(1957) bridge series. General dimensions of the mockup are given in Fig. 2.8, whereas photographs of the mockup are given in Fig. 2.9. Detailed drawings and structural steel details are presented in Appendix B. Review of plans for the V12(1957) bridge series indicated that the beam and coverplate for an interior stringer of a given length bridge are approximately the same size as those of an exterior stringer of the next longer length bridge. Interior stringers can be idealized as symmetrical tee beams; an exterior stringer can be thought of as an unsymmetrical tee beam because of the unequal flange widths on each side of the beam and the presence of the integral curb. As a result of the shape of the composite exterior beam, post-tensioning stress distribution may differ somewhat between an interior and an exterior stringer. In the present investigation, it was intended to only test a mockup of an interior stringer. However, the mockup was constructed with stirrups in the concrete slab (see Fig. 2.8b) so that curbs could be added and portions of the slab removed if desired in the future. Such changes could transform the mockup of an interior stringer into the configuration of an exterior stringer.

For the V12(1957) series, inflection points are located at approximately 11, 13.25, and 16 ft on each side of an interior pier support for bridges of 125, 150, and 175 ft, respectively. Space limitations

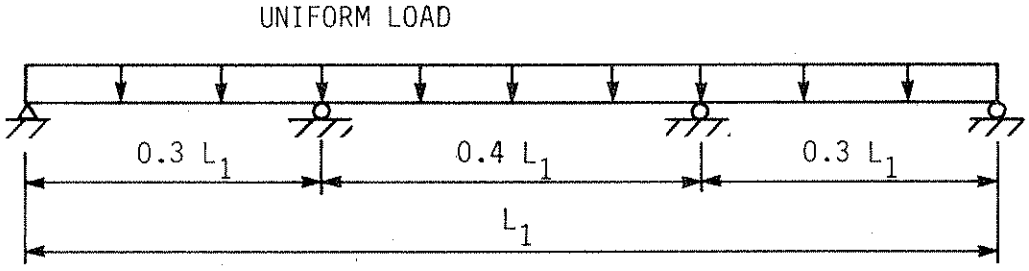

a. SPANS FOR V12 (1957) BRIDGE SERIES

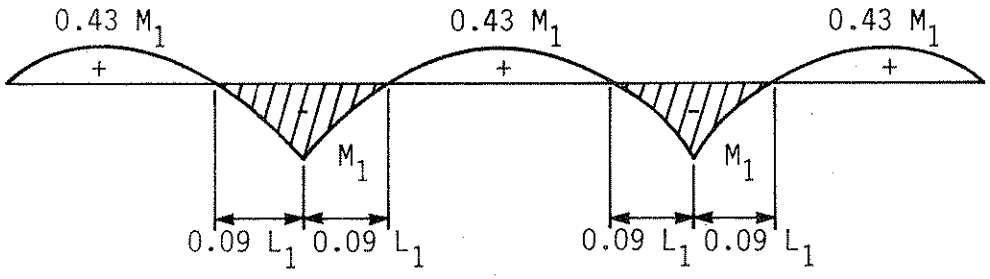

b. MOMENT DIAGRAM FOR V12 (1957) BRIDGES WITH UNIFORM LOAD

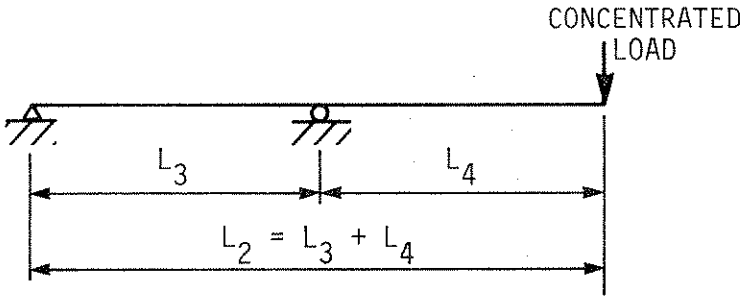

c. MOCKUP SPANS

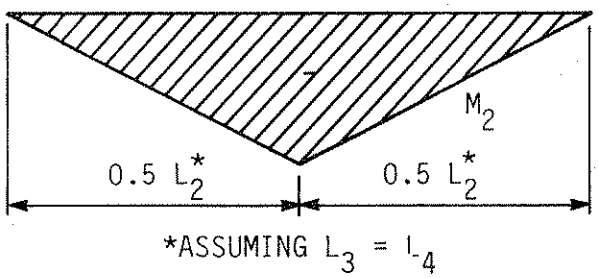

d. MOMENT DIAGRAM FOR MOCKUP

Fig. 2.7. Correlation between full-scale mockup and prototype.

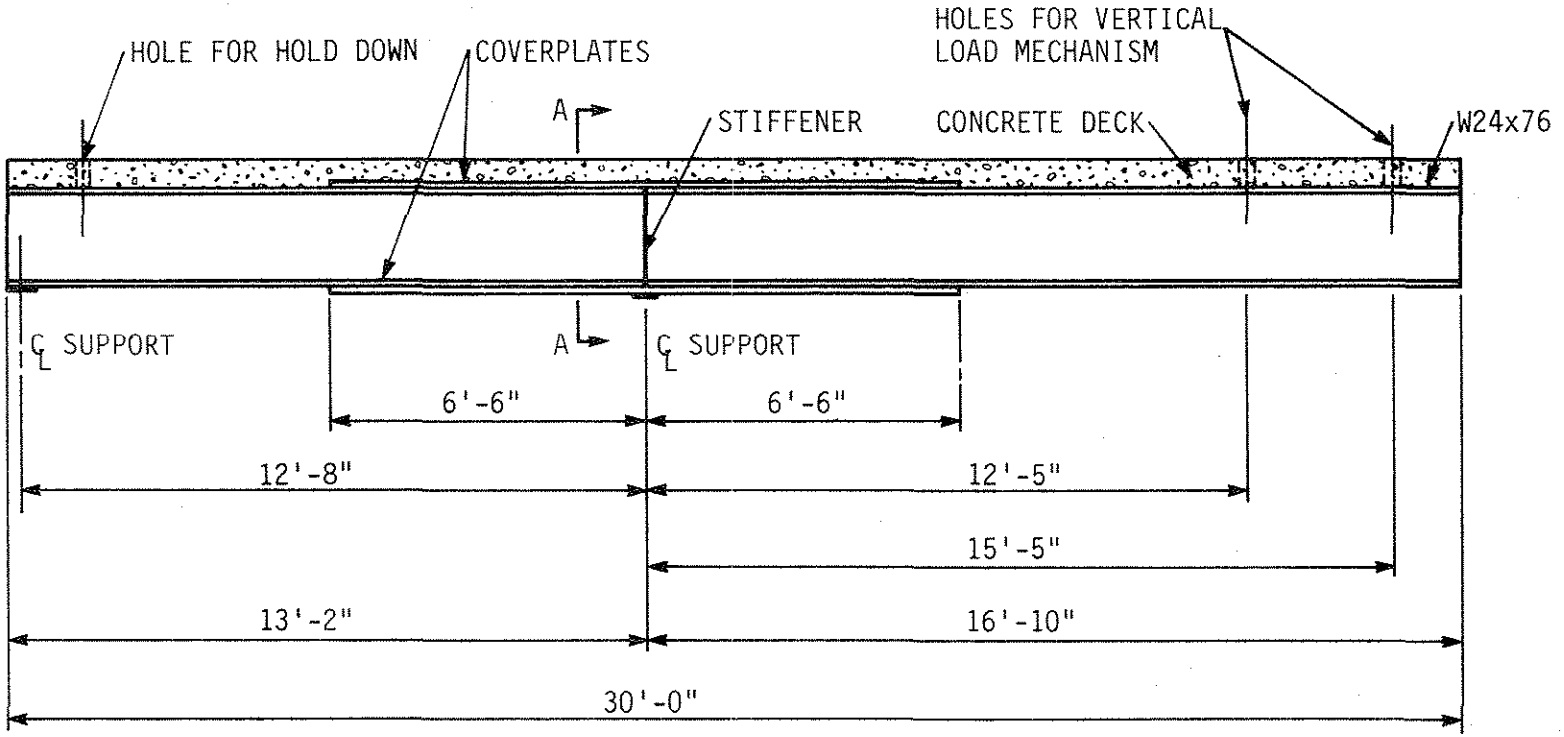

a. ELEVATION

Fig. 2.8. Full-scale mockup.

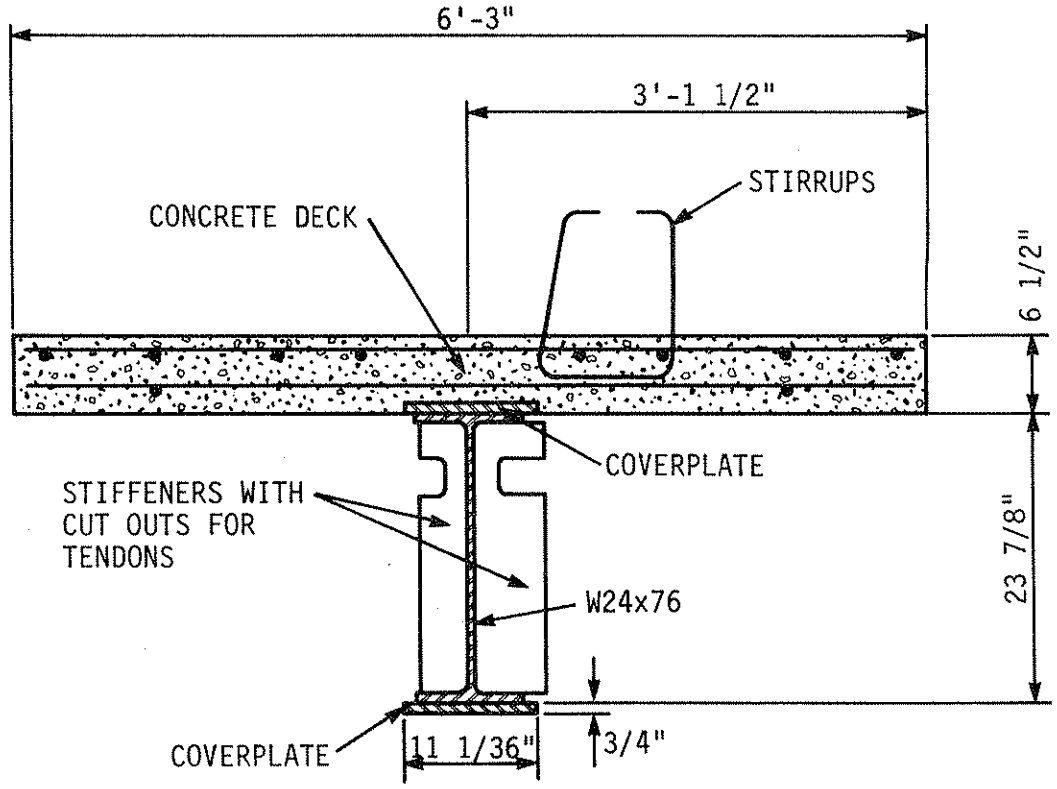

b. CROSS-SECTION A-A

Fig. 2.8. Continued.

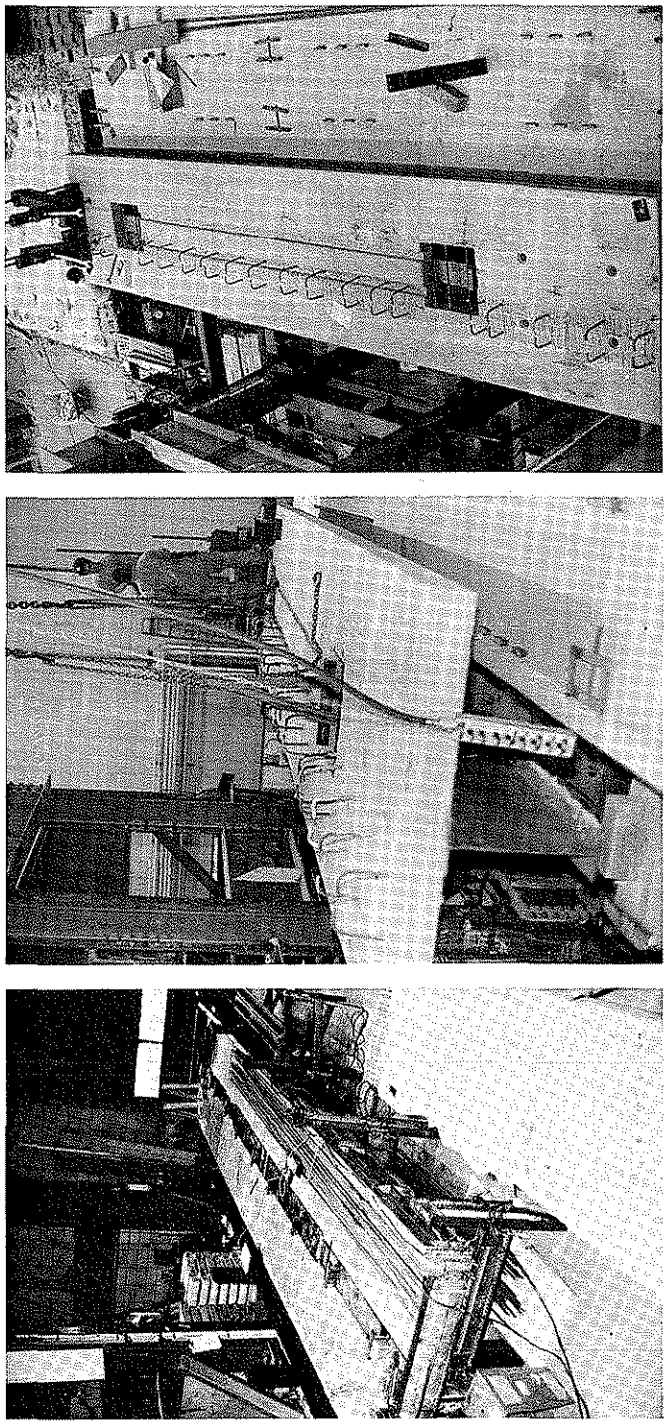

a. COMPLETED FORMWORK b. INSTALLATION OF HOLD DOWN c. DECK BLOCKOUTS AND CABLE GROOVES

Fig. 2.9. Photographs of mockup.

within the Structural Engineering Laboratory limited the overall length of the mockup to 30 ft and also required that the abutments already in place for the bridge model be used in testing the mockup. Thus dimension L_3 in Fig. 2.7c was required to be 12.67 ft.

In reviewing the Iowa DOT list of surplus beams, the authors determined that a W24 x 76 x 34-ft long beam, was available. As this is the size of an interior stringer in a 150-ft V12(1957) series bridge, this beam was obtained and cut to the 30 ft length required for the mockup.

Although coverplates on a 150-ft V12(1957) bridge extend 9.5 ft on each side of a pier support center line, the mockup's coverplates were limited to a shorter length. Jacking clearances for the harped cable post-tensioning scheme allowed the coverplates to extend only 6.5 ft on each side of the support (see Figs. 2.8a and B.1a). Coverplate thickness and width were chosen to match the depth and moment of inertia of the prototype.

The bearing stiffeners, sole plate, roller, and bearing plate were chosen to reflect typical components on the prototype. Shear connectors were the angle-plus-bar type. Their size and spacing were duplicated from those on the prototype (see Fig. B.4).

Applying the AASHTO effective width requirements for an interior stringer of the prototype, it was determined that the mockup required a concrete slab 6 ft 3 in. wide (see Figs. 2.8b and Fig. B.5). Also shown in these figures is the slab thickness of 6.5 in., which duplicates the thickness of V12(1957) bridge decks. Figure B.7 illustrates the location of the blockouts and holes that were formed in the slab. The

holes (formed with 3-in. diameter PVC pipe) were for the hold downs and loading hardware to pass through. The two larger blockouts shown in Fig. B.7 were provided to allow use of through deck post-tensioning cables at a later date if desired. Transverse deck reinforcing, both bar size and spacing, was duplicated from the prototype (see Figs. B.5 and B.6). Longitudinal reinforcing (see Figs. B.5 and B.6) was the same bar size as in the prototype and was spaced as for an interior beam with slight modification so that it would also work for an exterior beam if the curb were added later.

2.2.2. Physical Properties

2.2.2.1. Concrete

Fifteen standard cylinders (6 in. diameter x 12 in. long) and two modulus of rupture beams (6 in. x 6 in. x 30 in.) were made during the pouring of the concrete deck. All cylinders and rupture beams were subject to the same curing conditions as the deck. Cylinders were broken at seven days to determine if formwork could be removed. Cylinders were also broken at 14 and 28 days. The 28-day compressive strength, f_c', was 6700 psi and modulus of rupture, f_r', was 477 psi. Unit weight was 144.5 pcf. This compressive strength is considerably higher than that found in the prototype bridge. However since the testing program employed (see Secs. 3.2.2 through 3.2.4) involved elastic tests rather than ultimate strength tests, this greater concrete strength was of no great concern.

2.2.2.2. Steel

As was the case in the model bridge, no tension tests were conducted on the steels utilized in this portion of the testing program.

The steel beam (W24x76) was assumed to be A7 structural steel because of its age. All new steel used (coverplates, sole plates, bearing stiffeners, and strengthening angles) was A36 steel. Since all testing was performed in the elastic range, variations in yield strengths and/or ultimate strengths of the various structural steel elements has essentially no effect on the results. A modulus of elasticity of 29,000 ksi was assumed for all structural steel.

Straight tendons were 1 1/4-in. diameter Grade 150 Dywidag threadbars. Cable tendons were 7/16-in. diameter Grade 270 seven wire stress-relieved, ℓo/ℓax prestressing strand. Since all testing was done in the elastic range and both the Dywidag threadbars and prestressing strand were instrumented and calibrated, it was not necessary to determine the actual moduli of elasticity, yield strengths, or other material properties.

3. TESTS AND TEST PROCEDURES

This chapter outlines the details of the specific tests and events that occurred in conducting of the laboratory tests. Each test program (for example, bridge model tests and mockup tests) consisted of several individual tests. In the following sections, only test setups, instrumentation and procedures will be outlined; discussion and analysis of results obtained as well as the behavior will be presented in Chapter 4.

The instrumentation for all tests consisted of electrical-resistance strain gages (strain gages) and direct current displacement transducers (DCDTs). The strain gages were temperature compensated and were attached to the specimens with recommended surface preparation and adhesive. Three-wire leads were used to minimize the effect of the long lead wires and any temperature changes. All strain gages were water-proofed with a minimum of two layers of protective coatings. Strain gages and DCDTs on the bridge model and mockup were read and recorded with a computerized data acquisition system (DAS). A switch and balance unit and strain indicator were used to read the strain gages on the threadbars and strands; these data were recorded by hand in all tests.

3.1. Model Bridge Instrumentation and Tests

3.1.1. Instrumentation

A total of 64 strain gages were mounted on the four beams in the bridge model. Figure 3.1 indicates the location of the strain gages; at each of the 16 sections instrumented, four strain gages were oriented with their axes parallel to the axis of the beam. Two of the four

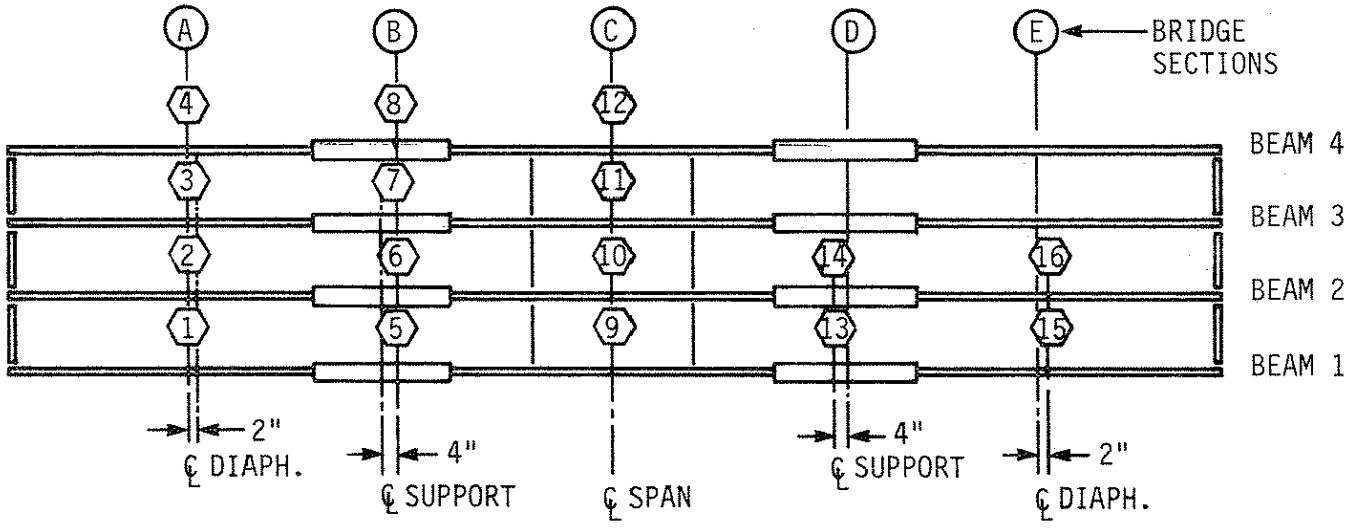

Fig. 3.1. Locations of strain-gage sections.

gages were on the top flange of the beam and two were on the bottom flange. All strain gages were placed at a distance equal to one-sixth the flange width in from the flange edge. This distance was approximately 1/2 in. and ranged from a minimum of 0.41 in. for the exterior beams to a maximum of 0.58 in. for the coverplated regions of the interior beams. As may be seen in Fig. 3.1, the majority of the instrumentation was on Beams 1 and 2; however, sufficient instrumentation was placed on Beams 3 and 4 (Sections 3, 4, 7, 8, 11 and 12) so that symmetry could be verified.

Two strain gages were also mounted on each threadbar with their axes parallel with the longitudinal axis of the bar. Two compensating strain gages mounted on a steel plate were connected to the active strain gages on the threadbars in a full bridge arrangement. In this arrangement, the strain gages on the threadbars read the actual value of the axial force in threadbar as bending strains were cancelled.

Twelve DCDTs were utilized to measure the vertical displacements of the beams. These DCDTs were placed at the center of each beam in each span.

When a uniform load is applied to a three-span beam, it generates regions of positive and negative moments. Regions in the vicinity of Sections A, C, and E shown in Fig. 3.1 are referred to as positive moment regions; regions in the vicinity of Sections B and D are referred to as the negative moment regions.

The longitudinal beams of this bridge were identified as 1 through 4 (see Fig. 3.1). A particular region of a given beam can thus be identified by beam number and section. For instance, the positive

moment regions of Beam 4 shown in Fig. 3.1 are identified as 4-A, 4-C, and 4-E, while the negative moment regions are identified as 4-B and 4-D.

For clarity, the bridge testing program will be described in five phases: post-tensioning the positive moment regions, post-tensioning the negative moment regions, post-tensioning both the positive and negative moment regions, vertical loading, and combination of vertical loading and post-tensioning.

The following procedures were used in each of the testing programs:

- Record "zero" strain readings and "zero" deflection readings with the data acquisition system.
- Apply predetermined increment of force at desired location.
- Take strain gage and DCDT readings as in Step 1. Record any behavioral changes.
- Remove force from tendon(s) and take second "zero" strain and deflection readings as in Step 1.
- Repeat Steps 1 and 2 if post-tensioning scheme requires post-tensioning to be applied to several locations on the bridge.

3.1.2. Post-tensioning Tests--Positive Moment Regions

Post-tensioning a positive moment region refers to the case when a tendon was placed in a positive moment region and a specified force was applied to it. As can be seen in parts a and c of Fig. 3.2, tendons were placed well below the neutral axis of the composite beam to generate a negative moment and a compressive force in this particular region.

Preliminary analysis indicated that the overstresses in the exterior beams of the prototype bridge could be eliminated by post-tensioning all the exterior positive moment regions with a force of 60 kips. Thus, a force of 60/9 (6.67 kips) would be required in all the tendons

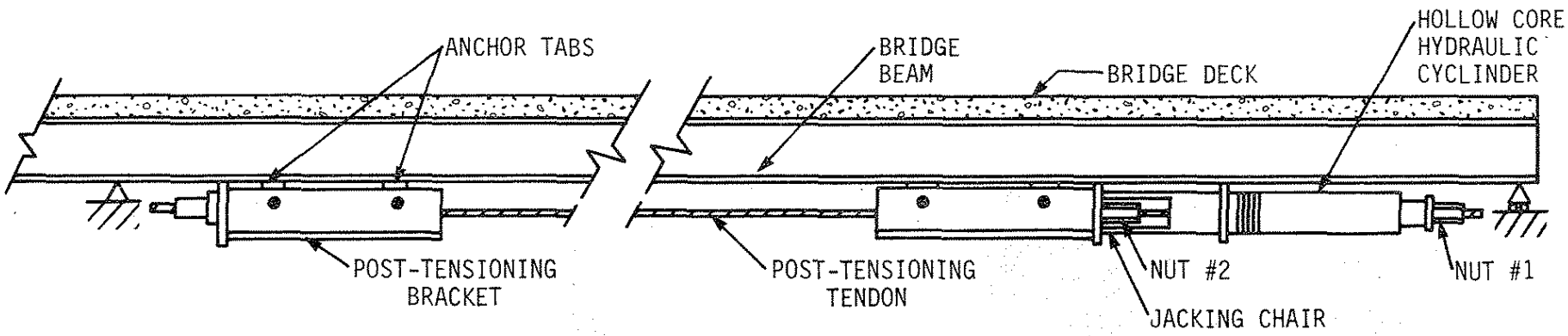

a. POSITIVE MOMENT REGION

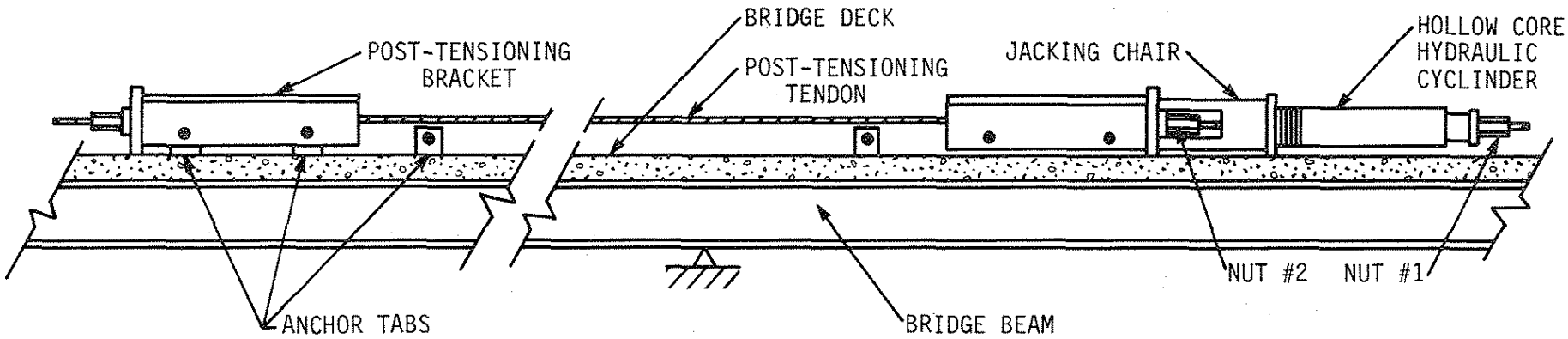

b. NEGATIVE MOMENT REGION

Fig. 3.2. Location of post-tensioning system in positive and negative moment regions.

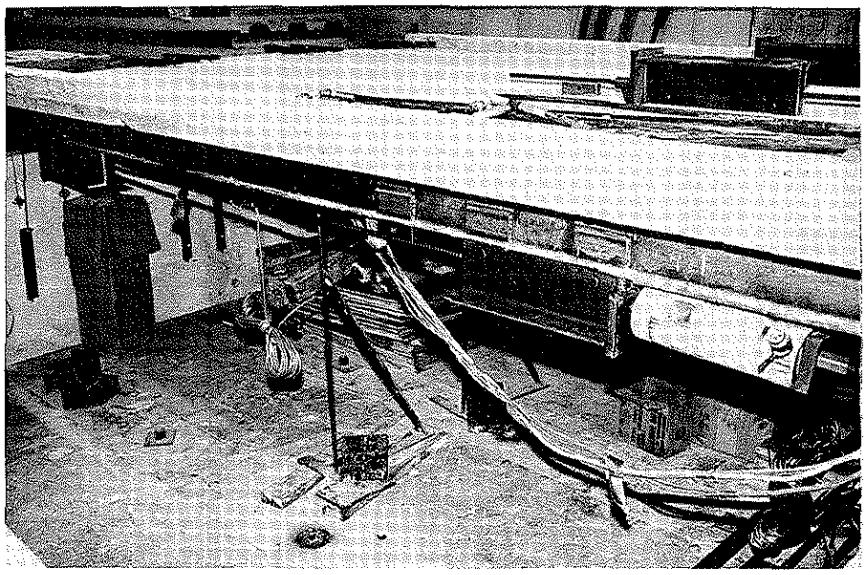

c. TENDONS IN POSITIVE MOMENT REGION

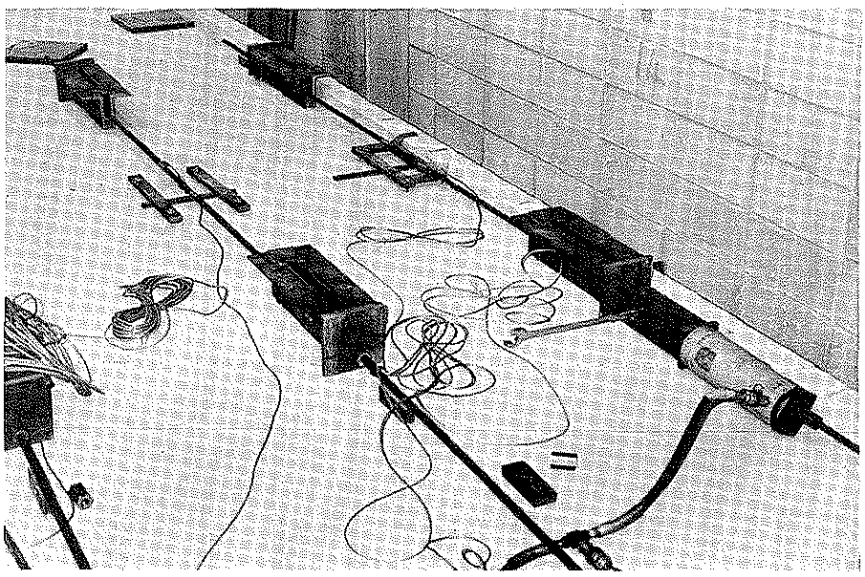

d. TENDONS IN NEGATIVE MOMENT REGIONS

Fig. 3.2. continued

in the exterior positive moment regions of the model to produce the desired stress reduction. However to obtain strains of a magnitude that could be measured accurately, this force was increased to 20 kips.

Tests involving post-tensioning the exterior positive moment regions are shown in Fig. 3.3. Nine different arrangements were investigated and represented by post-tensioning schemes 1 through 9, henceforth referred to as PTS-1, PTS-2, etc. The number assigned to the various post-tensioning schemes was also used as the test number; for example, Test No. 1 was PTS-1.

The following loading procedures were used in PTS-1 through PTS-9. In PTS-1 through PTS-6, a 20-kip force was applied to the tendons in increments of 5 kips; see Fig. 3.3 a through f for the location of post-tensioning in each scheme. In PTS-7, a 10-kip force was applied to the tendons in regions 4-A, 4-E, 1-A and 1-E simultaneously (see Fig. 3.3g). This test was repeated with a 20-kip force applied to the same regions.

In PTS-8, a 10-kip force was applied to the tendons in regions 4-C and 1-C simultaneously (see Fig. 3.3h). This test was repeated with a 20-kip force applied to the same regions.

In PTS-9, a force of 10 kips was first locked in the tendons in regions 4-C and 1-C simultaneously. Next a force of 10 kips was applied to the tendons in regions 4-A, 4-E, 1-A and 1-E simultaneously (see Fig. 3.3i). This test was repeated with a force of 20 kips applied to the same regions and following the same steps. The numbers beside the post-tensioning regions in parts i, u and v of Fig. 3.3 indicate the order in which the post-tensioning was applied.

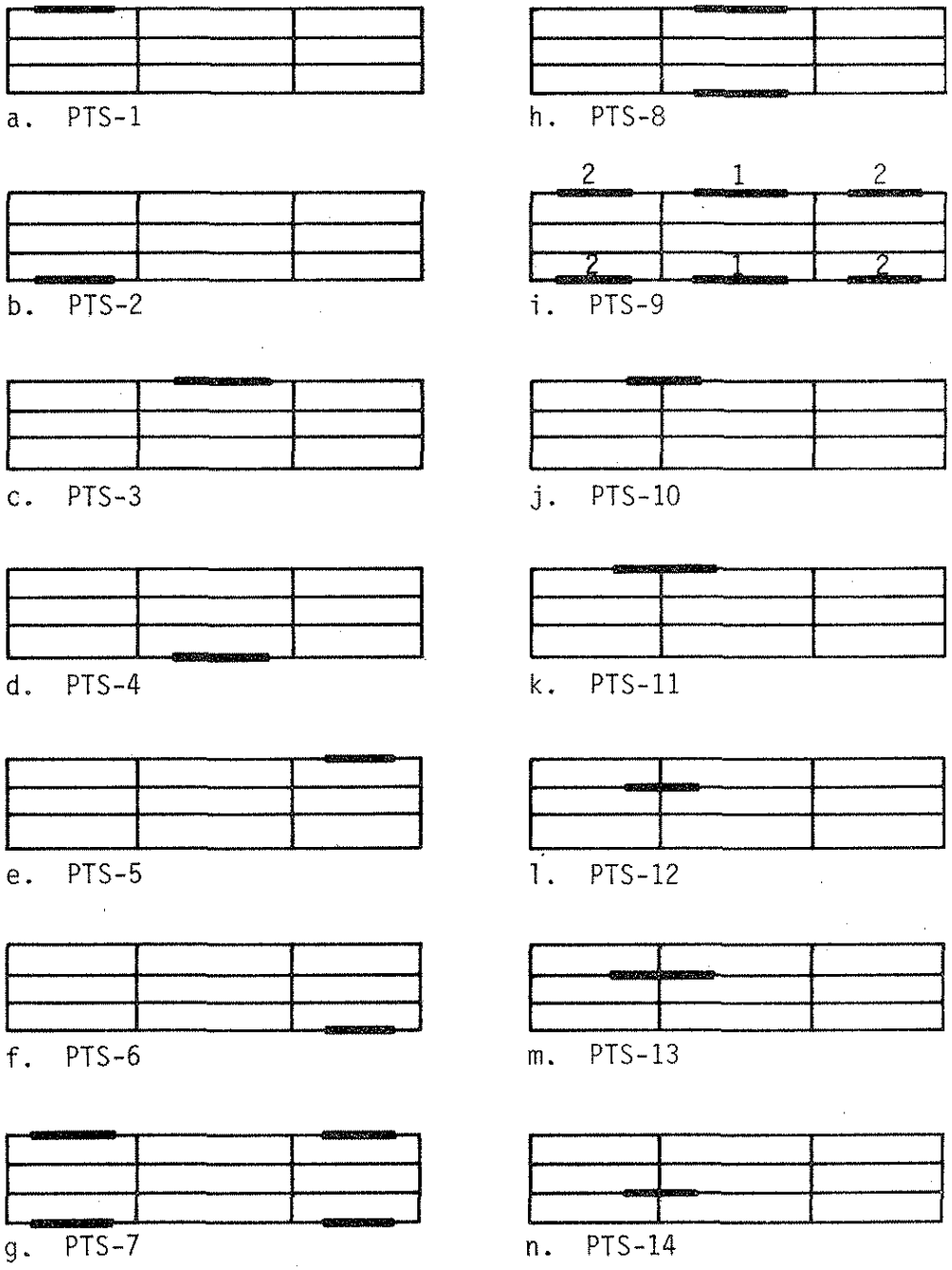

Fig. 3.3. Post-tensioning schemes (PTS) employed on bridge model.

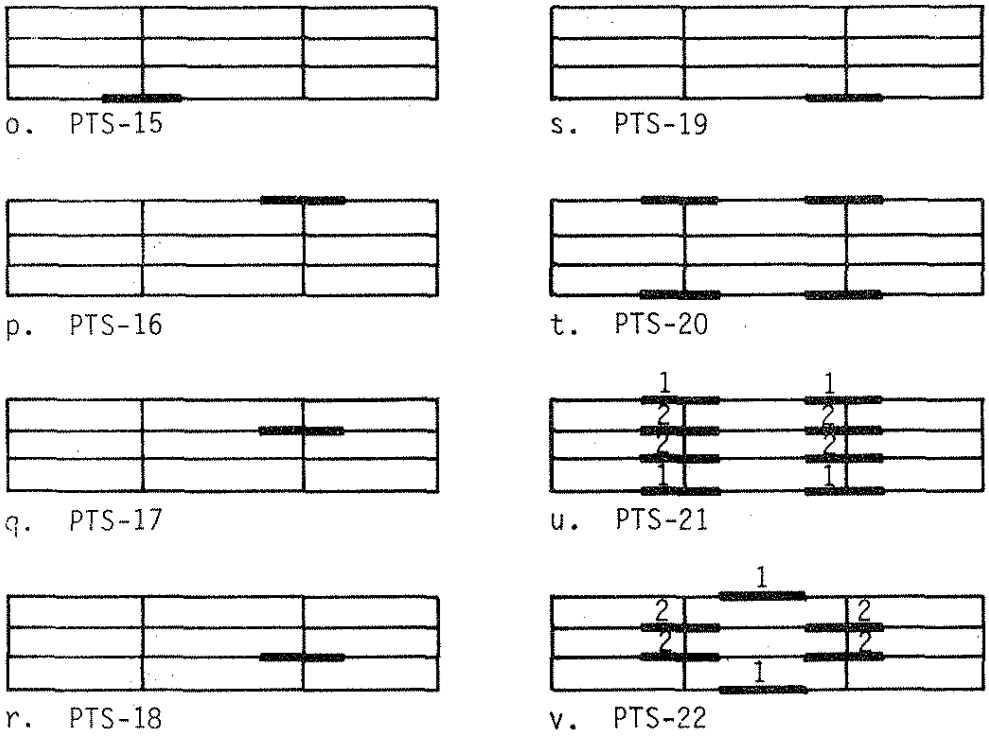

Fig. 3.3. Continued.

3.1.3. Post-tensioning Tests--Negative Moment Regions

Post-tensioning a negative moment region refers to the case when a tendon was placed in a negative moment region and a specified force was applied to it. Tendons were placed above the neutral axis of the composite beam (see parts b and d of Fig. 3.2) in order to produce a positive moment and a compression force at this particular region.

As previously noted, tabs were positioned so that all eight negative moment regions could be post-tensioned. Tests involving post-tensioning the negative moment regions, PTS-10 through PTS-21, are shown in parts j through u of Fig. 3.3.

The following loading procedures were used in each of these post-tensioning schemes. In PTS-10 through PTS-13 a 20-kip force was applied to the tendons in increments of 5 kips; see parts j through m of Fig. 3.3 for the location of post-tensioning in each scheme. As may be seen in parts j and k of Fig. 3.3, the only difference between PTS-10 and PTS-11 is the bracket location. In PTS-10, the interior tabs were used for mounting the brackets; thus 99 in. of the beam was subjected to post-tensioning (see Fig. 2.3). The exterior tabs were used in PTS-11; thus 123 in. of the beam was subjected to post-tensioning. There is a similar difference between PTS-12 and PTS-13.

In PTS-14 through PTS-19, a 20-kip force was applied to the tendons; see parts n through s of Fig. 3.3 for the location of post-tensioning in each scheme.

In PTS-20, a 20-kip force was applied in increments of 5 kips to the tendons in regions of 4-B, 1-B, 4-D and 1-D simultaneously (see Fig. 3.3t).

In PTS-21 (see Fig. 3.3u), a 10-kip force was first locked in the tendons in regions 4-B, 1-B, 4-D and 1-D simultaneously. Next, a force of 10 kips was applied to the tendons in regions 3-B, 2-B, 3-D and 2-D simultaneously. This test was repeated with a 20-kip force applied in the same regions.

3.1.4. Post-tensioning Tests--Positive and Negative Moment Regions

PTS-22 was the only scheme that involved post-tensioning both the negative and positive regions together as shown in Fig. 3.3v. The following loading procedure was used. A 20-kip force was first locked in the tendons in regions 3-B, 2-B, 3-D and 2-D simultaneously. Next a 20-kip force was applied to the tendons in regions 4-C and 1-C simultaneously. As previously noted, the number beside the post-tensioned regions in Fig. 3.3v indicates the order of post-tensioning.

Four 60-kip capacity, hollow core, hydraulic cylinders were used to apply the required force to the 5/8-in. diameter tendons in all the previously described tests. Figure 3.2d illustrates one of the jacks in position. When it was desired to post-tension beams and collect data at various post-tensioning load levels, such as in PTS-1 through PTS-6, and PTS-10 through PTS-13, the procedure was to apply the desired force with the hydraulic cylinders, collect the desired data and release the force. However, for some load cases, such as PTS-9, PTS-21, and PTS-22, the force had to be locked on some of the beams before post-tensioning the remaining beams.

Locking the force in a given beam was accomplished as follows. First the desired force was applied to the tendons by the hydraulic cylinder acting against the jacking chair (see parts a and b of Fig. 3.2).

Nut 2, identified in this figure, was then tightened so that a force slightly higher than desired was in the tendon to offset seating losses. The hydraulic cylinders were then released, and the force was locked in the tendon (and thus the beam) by Nut 2 seated against the post-tensioning bracket. All post-tensioning tendon forces were determined by measuring the axial strain in the tendon.

3.1.5. Vertical Load Tests

Tests involving vertical loading are represented in Table 3.1 as Tests 23 through 26. In Table 3.1, the numbers from 1 to 21 listed under the vertical loading heading represent 21 different positions at which concentrated loading could be applied; location of the 21 points are given in Fig. 3.4. Depending upon the test, one or both of the previously described concrete dead weights were positioned on the bridge. The concrete weights were placed on 9-in. x 9-in. x 1-in. neoprene pads to approximate a concentrated load. Figure 2.2d is a photograph of the two 6-kip loads being applied to the bridge simultaneously.

Test 23 involved placing one 6-kip load at the various loading points. As indicated in Table 3.1, the load was not applied at load points 7, 14, and 21, all on Beam 1 since the crane was unable to reach these points because of their close proximity to the laboratory wall. Test 24 involved placing two 6-kip loads simultaneously at various loading points on the bridge; the various combinations tested are given in Table 3.1.

The test procedure outlined in Section 3.1.1 was again used with the only difference being the type and location of the loading applied.

Table 3.1. Vertical load tests.

Test Number	PTS	Vertical Loading Points*																			
		1	2	3	4	5	6	7	8	9	10	11	12	13	14	15	16	17	18	19	20	21
23	None	●	●	●	●	●	●		●	●	●	●	●	●		●	●	●	●	●	●	
24	None	●														●						
			●							●							●					
				●							●							●				
				●	●							●							●			
					●	●							●							●		
						●	●							●							●	
25	21		●																			
				●	●																	
						●	●					●										
													●	●								
																			●			
																					●	
26	9		●																			
				●	●																	
						●	●					●										
													●	●								
																			●			
																					●	

● = loaded.
* See Fig. 3.4 for location.

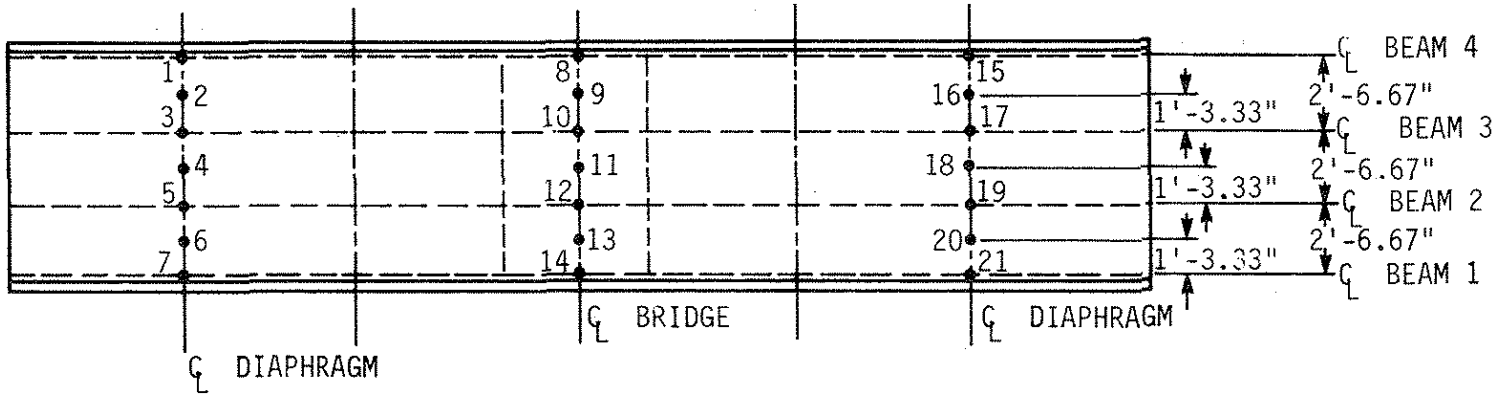

Fig. 3.4. Locations of vertical load points.

3.1.6. Combination Tests--Vertical Load Plus Post-tensioning

Tests involving a combination of a vertical load and post-tensioning are designated in Table 3.1 as Tests 25 and 26. These tests involved both post-tensioning forces and vertical loading. As Table 3.1 indicates, only two post-tensioning schemes were used--namely, PTS-9, where a 20-kip force was locked in all exterior positive moment regions, and PTS-21, where a 20-kip force was locked in all negative moment regions.

Loading procedures, data collection procedures, and so forth were the same as those previously presented. In each of the tests (25 and 26) the post-tensioning forces were applied and locked in prior to the addition of vertical loading. Previously described instrumentation of the tendons permitted measurement of force changes in the tendons as the position of the vertical force(s) was changed.

3.2. Instrumentation and Tests for the Full-Scale Negative Moment Region Mockup

This section outlines the details of the specific tests and procedures used in testing the mockup. Some of the tests performed on the mockup consisted of several steps. The various tests performed on the mockup are summarized in Table 3.2. Note that test number does not indicate order of completion.

3.2.1. Instrumentation and Vertical Load Mechanism

Instrumentation for all tests conducted on the mockup consisted of strain gages, DCDTs and one load cell. At the beginning of all tests, an initial reading was obtained for all instrumentation with

Table 3.2. Mockup tests.

Test #	Tendon Arrangement	Strengthening Angles Used?	Partial Load Applied Before Post-Tensioning?
1	--	no	--
2	--	no	--
3	--	yes	--
4	straight	no	no
5	straight	no	yes
6	straight	yes	no
7	straight	yes	yes
8	harped	no	no
9	harped	yes	no

the DAS. After waiting a few moments, a zero reading was taken. This procedure allowed identification of any instrumentation problems before actual testing began.

The vertical loading mechanism is shown in Fig. 3.5. This figure indicates that the left and right "inflection points" were located 12 ft 8 in. and 12 ft 5 in. respectively, from the "interior support." The left inflection point hold down was preloaded with a 75-kip clamping force to hold the beam on the support when loading was applied to the free end of the beam.

The load cell shown in Fig. 3.5 measured the force exerted by one of the two hollow core hydraulic jacks used. Since the jacks were in parallel, the load cell read one-half the total vertical load. This loading mechanism produced the desired negative moment (see Fig. 2.7d) between the two "inflection points." Photographs in Fig. 3.6 show the hydraulic cylinder in position to apply vertical load and the arrangement of threadbars and structural tubes which were used to vertically restrain the pinned support.

The strengthening angles shown in Fig. 3.7 were present during all tests performed on the mockup. For tests where the angles were to be ineffective (i.e., not carrying an axial force) the angles were supported at two points on the bottom flange of the beam and were held in place by one bolt partially tightened. This arrangement kept the dead load constant for all tests conducted and eliminated the possibility of damaging the instrumentation when the angles in the various tests were intended to be effective or ineffective.

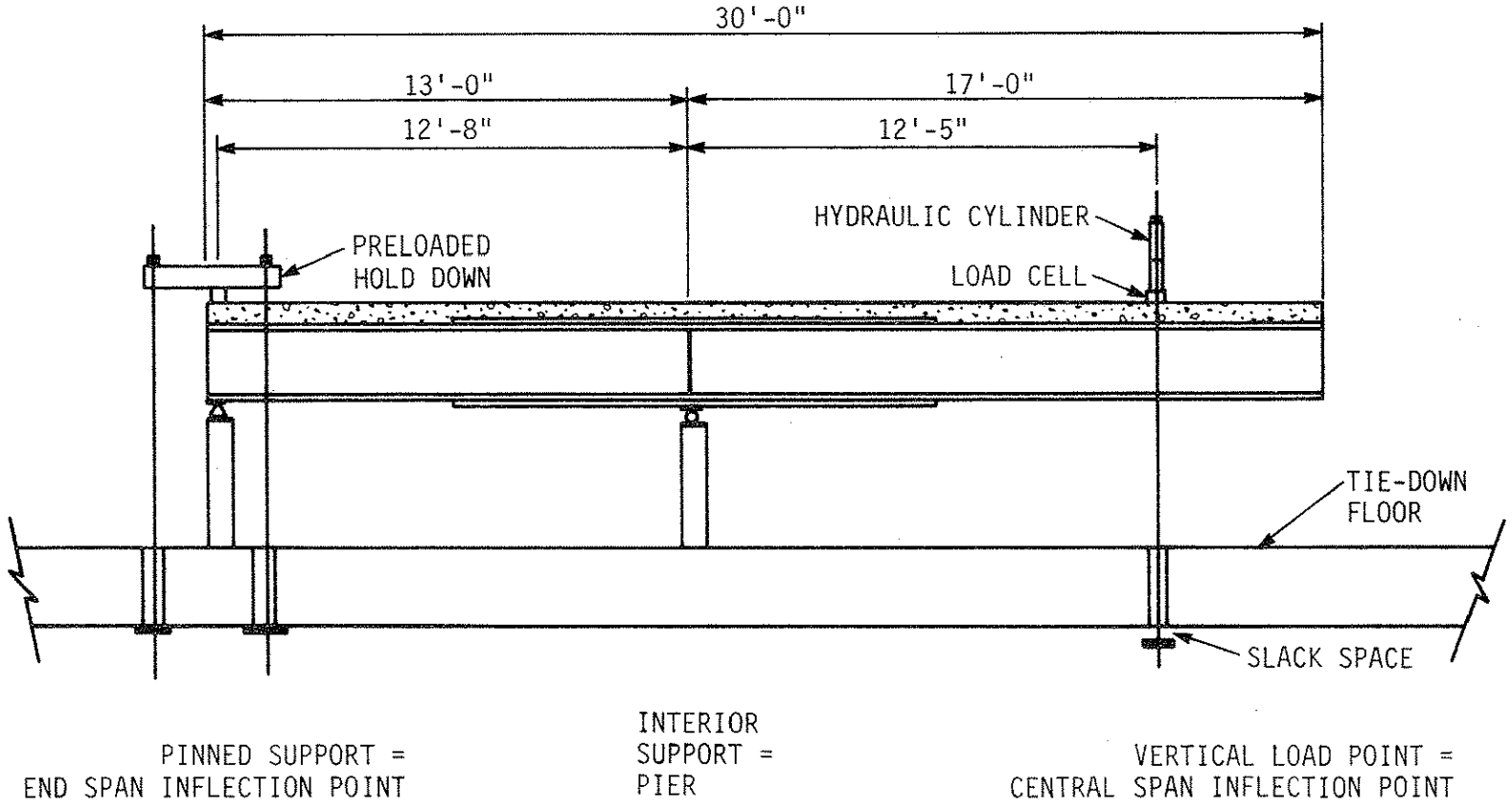

Fig. 3.5. Vertical loading mechanism for full-scale mockup.

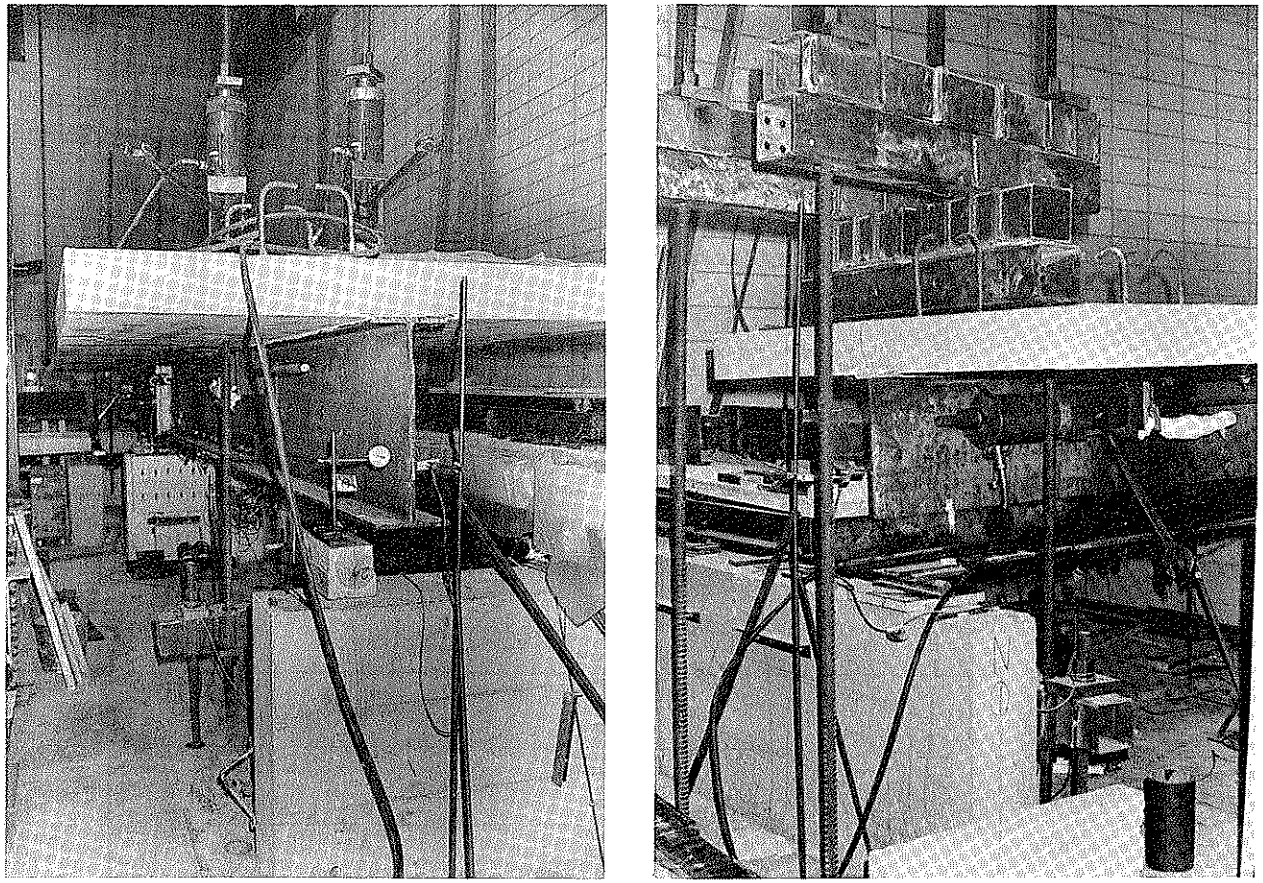

a. FREE END WITH HYDRAULIC CYLINDERS FOR APPLICATION OF VERTICAL LOAD

b. HOLD DOWN END WITH TENSIONED THREAD BARS AND STRUCTURAL TUBE-BEARING FRAME

Fig. 3.6. Photographs of end conditions for the full-scale mockup.

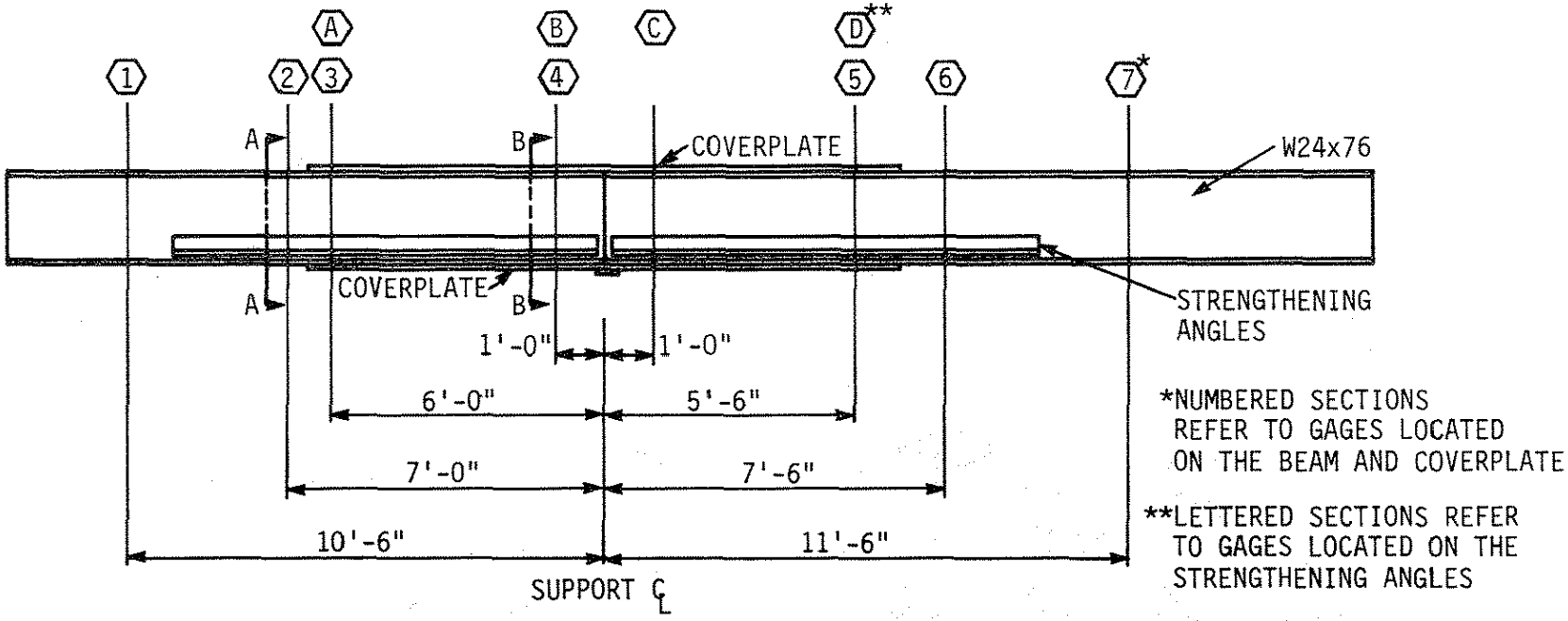

a. LAYOUT

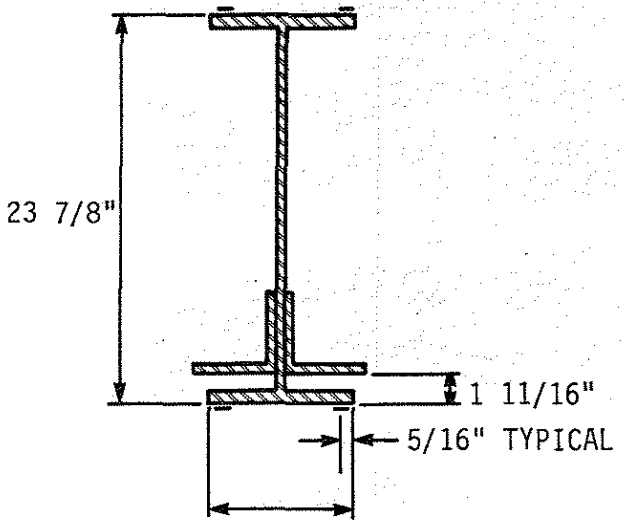

b. SECTION A-A

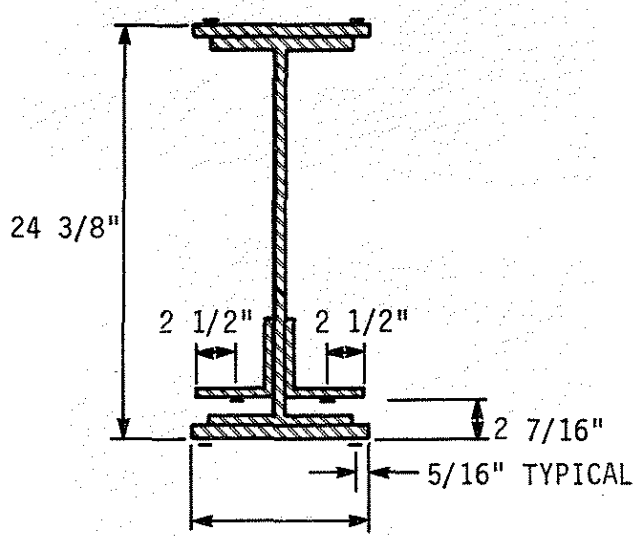

c. SECTION B-B

Fig. 3.7. Strain gage locations for full-scale mockup.

Strain gages were mounted at selected locations on the steel beam, coverplates and strengthening angles as well as on the various tendons. Each strain gage was bonded with its axis parallel to the axis of the beam or the tendon.

Strain gage locations on the beam, coverplates and strengthening angles are shown in Fig. 3.7. Strain gages were offset from the support center line because of the sole plate. They were also offset from the coverplate cutoff points to avoid the high stress gradients at these locations. A total of 28 strain gages were placed on the beam and coverplates, and eight more were placed on the angles. At each of the numbered sections in Fig. 3.7, there were four strain gages on the beam, two on the top beam flange, and two on the bottom beam flange. At each of the lettered sections in Fig. 3.7, there were two strain gages (one on each angle) on the lower surface of the angle. As illustrated in Fig. 3.7 at three locations, the strain gages on the angles are at the same section as strain gages on the beam. Figure 3.8 shows the positions of the DCDTs used for measuring vertical displacements. Positions A and B were used for all tests. Position C was used for the tests without post-tensioning applied and for tests with straight tendons. Position D was used for the tests with the harped cable tendons. When the DCDT was located at position C for the harped tendon tests, it was bumped repeatedly while the jacks and chairs were moved from one tendon to another during the tensioning operation. The DCDT was therefore moved from position C to position D. A total of three DCDTs were used to measure deflections for each test. Although not shown in Fig. 3.8a, a dial gage was positioned to detect any lateral movement of the mockup.

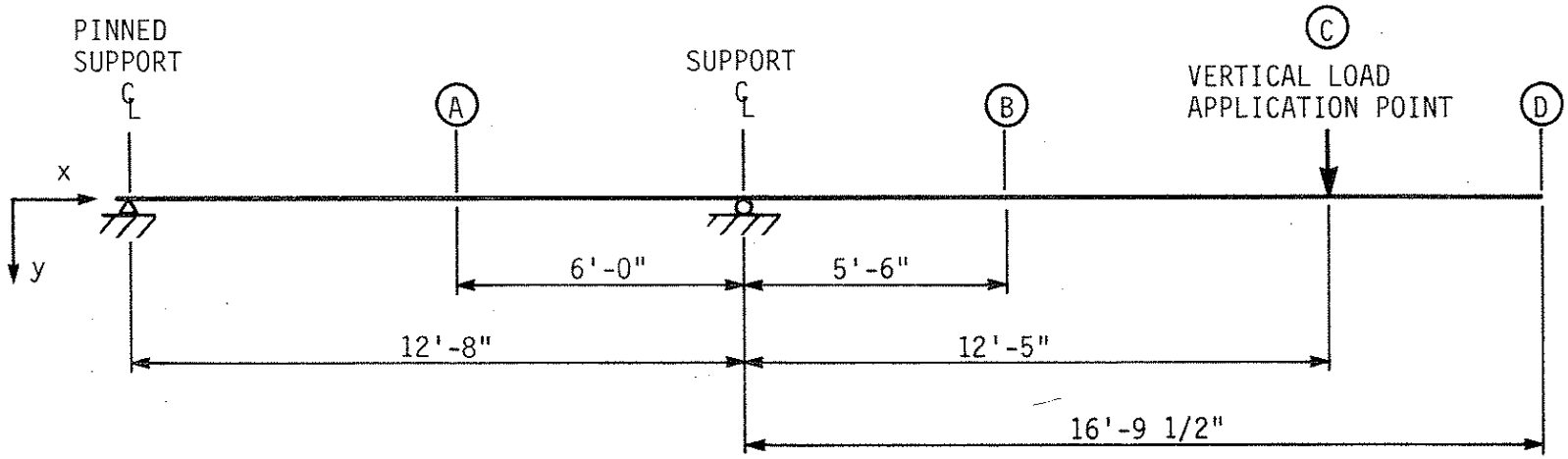

Fig. 3.8. Vertical displacement measurement (DCDT) locations on full-scale mockup.

Both of the 1 1/4-in. ϕ Grade 150 Dywidag threadbar tendons were instrumented with strain gages. One strain gage was placed on each of the "flat" sides of a bar to cancel bending effects. As was done with the tendon used on the bridge model, each threadbar was calibrated by placing it in a universal tension-compression machine and recording strains for various applied tensions. Least squares linear regression was used to provide a calibration factor relating indicated strains to tension loads. Correlation of indicated strain to applied load was excellent with $R^2 > 0.9995$ for each gage.

Grade 270 prestressing strand was used for the harped tendon tests. Each of the six cable tendons was instrumented with strain gages. Because a cable is made up of six strands wrapped around a seventh, placing strain gages on them was somewhat more difficult than placing strain gages on the threadbars. In order to cancel bending effects, strain gages were placed on opposite outer strands at each location. One pair of gages was placed near the middle, and another pair near one of the quarter points on each cable tendon. Therefore a total of four gages were placed on each cable (see Section 3.2.4).

Because of the length and the number of gages on each cable, it was necessary to use a different method for calibration. Two cables were simultaneously tensioned between widely spaced rigid frames. By using identical hollow core jacks attached to the pump in parallel, tension in the cables could be measured with one load cell. Each cable pair was then calibrated by recording strains and tension loads with the DAS. For each strain gage, least squares linear regression was used to provide a calibration factor that related indicated strain to

the tension in the cable. Correlation of indicated strains to applied loads was excellent with $R^2 > 0.998$ for each gage.

3.2.2. Preliminary Vertical Load Tests

Three tests (Tests 1, 2 and 3 in Table 3.2) were performed on the mockup without post-tensioning applied. These tests were: an initial cracking test, a post-cracking test, and a strengthened beam test. During these tests, the straight tendon and associated brackets were in place on the mockup but were not allowed to take load. This was done for convenience and to minimize potential damage to the instrumentation and its wiring.

The initial cracking test (Test 1 in Table 3.2) was performed to determine initial behavior of the beam because of cracking of the concrete and to approximate field conditions on an actual bridge. Since post-tensioning techniques investigated here are intended as rehabilitation measures, they would be applied to a bridge that has been in service for many years. As a result of this service and weathering, the concrete deck would be cracked in the regions of negative moment.

Setup for the initial cracking test was relatively straightforward. No post-tensioning was applied, and the strengthening angles were not effectively attached to the beam. After taking a zero reading with the DAS, vertical load was applied in three cycles with increasing peak loads. For this particular test, smaller increments were used than in the standard vertical load cycles used for all other tests. When a crack occurred, the load after cracking was maintained while data was recorded. Load was then returned to the level obtained just prior to occurrence of the crack whereupon data was again recorded.

Loading was then resumed until another crack occurred. This technique simplified the observation of crack effects.

For the first loading cycle, the top load obtained was about 20 kips or approximately one half the peak load of a standard load cycle. For the second cycle, the top load was about 30 kips or approximately three-fourths of the peak load. For the third cycle, the load was increased to the peak load of 43 kips. After the final load cycle, the mockup was allowed to rest for several minutes before data was taken to determine the final deflections.

After the initial cracking test, Test 2 (see Table 3.2) was performed to determine the basic strength and behavior of the beam. Behavior of other tests will be compared to the results of this test. Although the straight tendons and their brackets were in place, no post-tensioning was applied; as in Test 1, the strengthening angles were also present but were not effectively attached to the beam.

In Test 3, the angles were securely attached to the beam's web to determine their effectiveness as a strengthening measure. For this test, as for the previous two, the threadbar tendon and brackets were in place but no tension was applied.

Vertical loading conformed to a standard load cycle. Three load cycles were applied to the beam in an effort to "seat" the angles on the beam. Even though the bolts securing the angles were tightened by the turn of the net method, some slip between the beam web and the angles occurred. This method of seating the angles was intended to give a better indication of their final effectiveness.

3.2.3. Post-tensioning Tests--Straight Tendons

Four tests (Tests 4 through 7 in Table 3.2) were performed to evaluate the effectiveness of post-tensioning with straight tendons. These tests explored how the mockup responded with and without the addition of the strengthening angles. In addition, post-tensioning was done while a partial vertical load was present. This partial load was removed and reapplied to simulate replacement of a portion of the bridge deck and its effect on tendon tension.

The arrangement of the 1 1/4-in. ϕ Dywidag threadbars used on the mockup is illustrated in Fig. 3.9. One threadbar was mounted on each side of the beam web. Anchorage brackets were positioned with a one-inch clearance between the bracket and the top flange. Details on the brackets are given in Fig. B.8 of Appendix B. The brackets were bolted to the beam web using 7/8-in.-diameter A325 high strength bolts. As shown in Fig. 3.9b, the threadbars were located 19.41 in. above the bottom of the lower coverplate. This position is 6.71 in. above the centroid of the W24x76 plus coverplates but 3.51 in. below the centroid of the completely composite section over the support. Because of the compactness of the brackets, the bearing stiffeners over the support center line had to be notched as was shown in Fig. 2.8b. Threadbar strain gages were located near the midpoint between the anchor brackets. Two 120-kip hollow core jacks connected in parallel were used to tension the threadbars.

The strengthening angles used were 5 in. x 5 in. x 3/8 in.; they extended 9 ft 6 in. on each side of the support center line and were not in contact with the bearing stiffener. Details of their placement

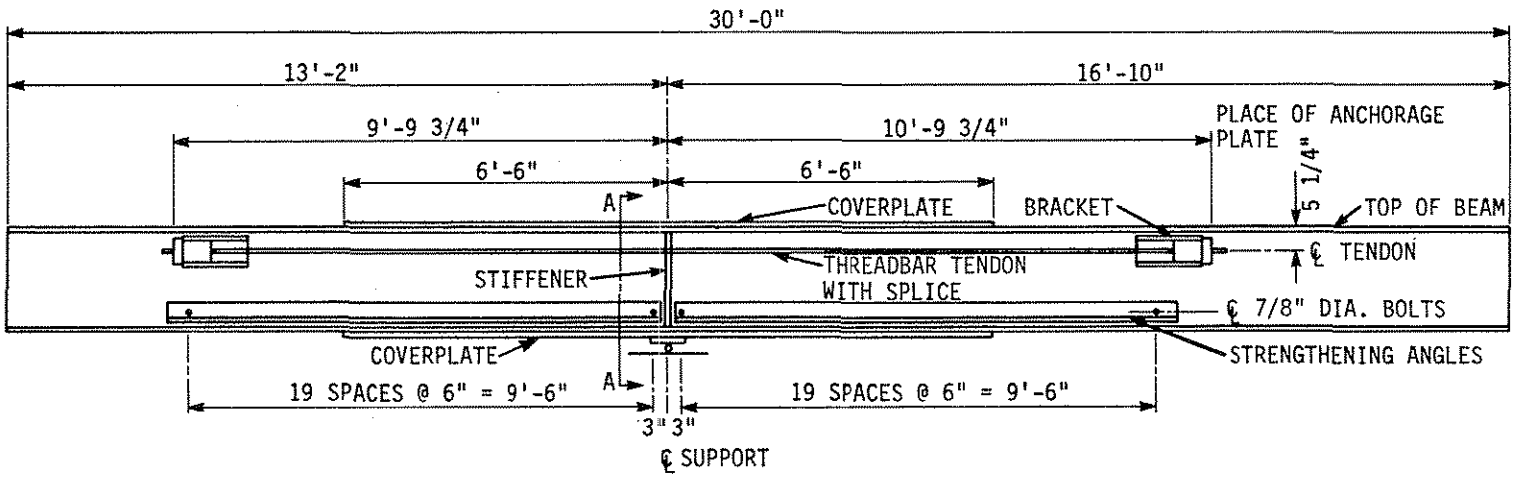

a. THREADBAR TENDON

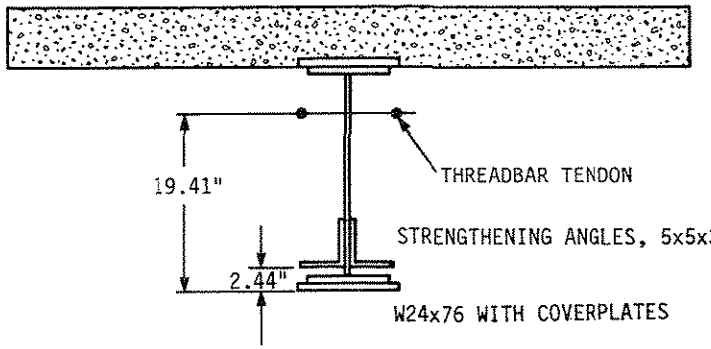

b. SECTION A-A

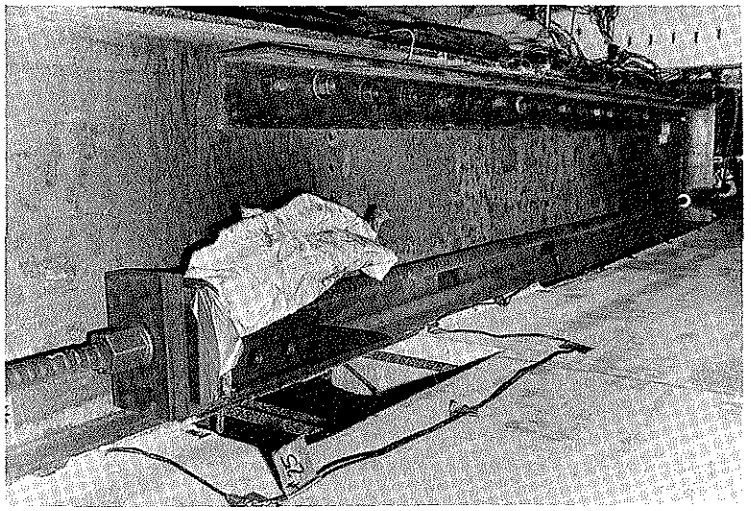

c. PHOTOGRAPH OF STRAIGHT TENDON AND ANCHORAGE BRACKET

Fig. 3.9. Threadbar tendon arrangement.

are shown in Fig. B.9. As shown in this figure, a spacing of 6 in. was used for the 7/8-in.-diameter A325 high-strength bolts. A 1-in. space was maintained between the angle flange and the bottom flange of the beam.

Test 4, the first test, was the most basic of the straight tendon tests since the angles were not effectively attached to the beam web. After zero readings were obtained, the threadbars were tensioned until their total tension was approximately 100 kips, at which time they were locked off and the hydraulic pressure released. Seating losses at lockoff were small, less than 5% of the maximum tension before lockoff. A standard vertical load cycle was then applied after which the threadbar tension was released.

Test 5 was similar to Test 4 except that the threadbars were tensioned while a partial vertical load was present. For this test, as for Test 4, the strengthening angles were not attached to the beam web. After the zero readings were taken, a vertical load of 20 kips, approximately one-half of the peak load, was applied. The threadbars were then tensioned to a total of approximately 100 kips and locked off while the vertical 20-kip load was held constant. Seating losses were again less than 5% of the maximum tension before lockoff. Vertical loading was then resumed until the peak load of 42 kips was obtained. Next the vertical load was completely removed and reapplied as in a standard load cycle. The vertical load was then reduced until approximately 20 kips, or one-half the peak load remained. The threadbar tension was released and the remaining vertical load removed.

For Test 6 the strengthening angles were bolted securely and were thus effective in carrying axial stress. Tensioning of the threadbars and application of vertical load followed the same procedure as for Test 4. However, two vertical load cycles were performed.

For Test 7 as for Test 6, the strengthening angles were bolted securely. The loading and tensioning procedure for this test, however, was identical to that used in Test 5.

3.2.4. Post-tensioning Tests--Harped Tendons

Two tests (Tests 8 and 9 in Table 3.2) were performed to evaluate the effectiveness of post-tensioning with harped cable tendons. These two tests explored how the mockup responded to the cable tendons with and without the addition of the strengthening angles. Because of the difficulty involved in tensioning the cables, tests with a partial vertical load were not performed.

The arrangement of the cable tendons on the mockup is shown in Fig. 3.10. Three cable tendons were placed on each side of the beam web. The harp saddle brackets (see details in Fig. B.11) were mounted as high on the beam web as possible while avoiding the web-flange fillet. The anchorage brackets (see details in Fig. B.10) were mounted as close to the bottom flange as possible but also avoiding the web-flange fillet. The anchorage brackets were positioned so that the axis of the center cable was perpendicular to the tendon-bearing faces of the bracket. As may be seen by comparing the dimensions given in Fig. 3.9a and Fig. 3.10a, the anchorage brackets were located almost directly below where the straight tendon anchorages had been.

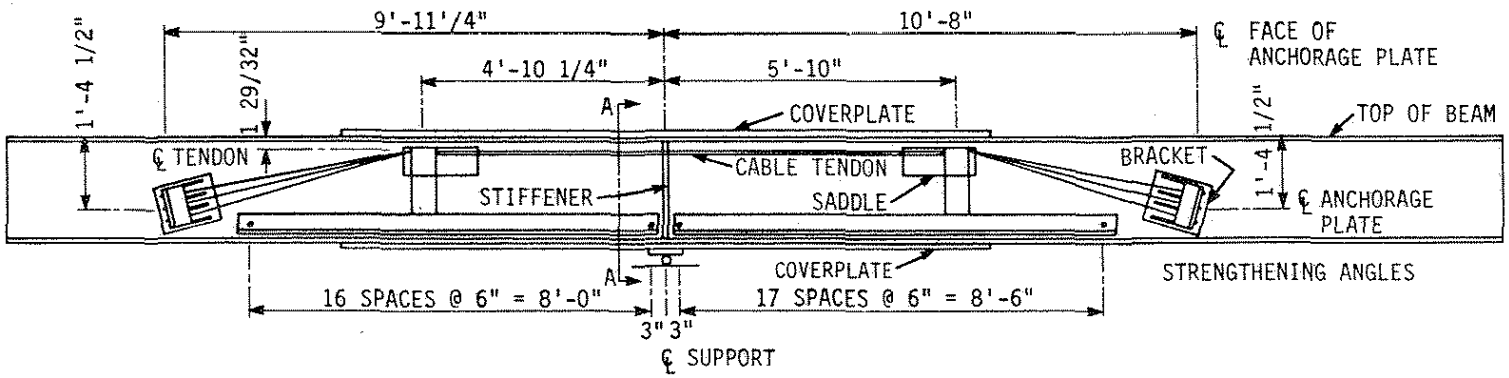

a. CABLE TENDONS

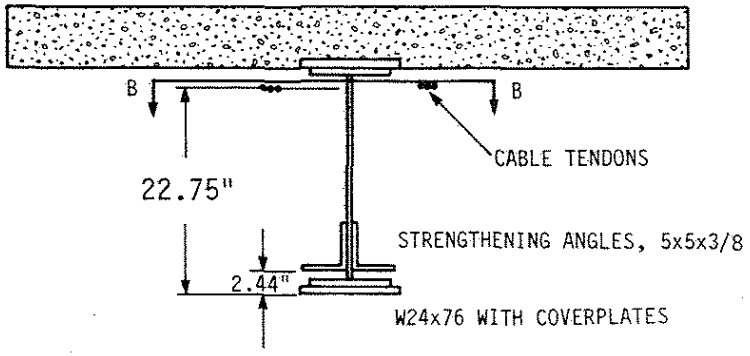

b. SECTION A-A

Fig. 3.10. Harped cable arrangement.

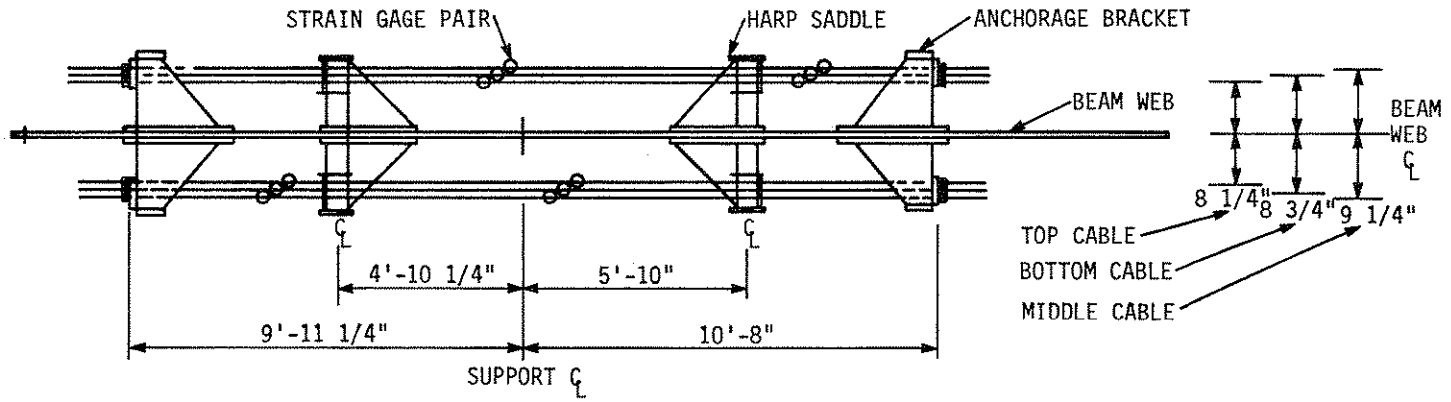

c. SECTION B-B

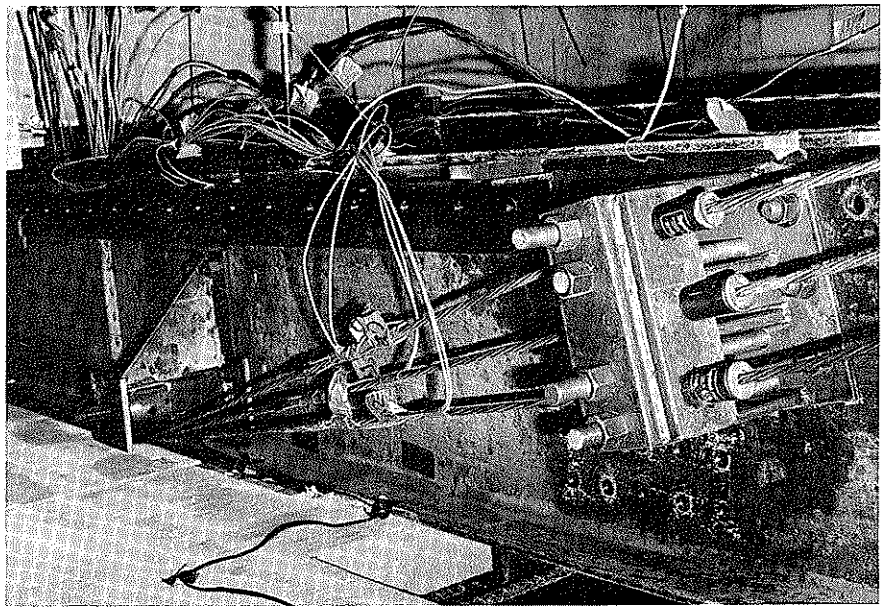

d. PHOTOGRAPH OF HARPED CABLES AND ANCHORAGE SYSTEM

Fig. 3.10. Continued.

Shear loads in both types of brackets were carried by 7/8-in.-diameter A325 high-strength bolts. Loads causing the brackets to "peel" away from the beam web were carried by high-strength threaded bars that passed completely through the brackets to clamp the brackets to the beam web. Gusset plates incorporated into the brackets transferred loads exerted by the cable tendons to the beam web.

As shown in Fig. 3.10b, the cable tendons were located 22.75 in. above the bottom of the lower coverplate. This position is 10 in. above the centroid of the W24x76 plus coverplates and only 0.23 in. below the centroid of the completely composite section over the support. When compared to the threadbar tendons, the cable tendons are 3.34 in. higher on the beam at this cross section. In order to provide clearance past the lower flange for the hydraulic cylinders and jacking chairs used to tension the cables, the cable tendons were placed further from the beam web than the threadbar tendons.

Two 60-kip hollow core hydraulic cylinders were used to tension each pair of cables. Only one pair of tendons was tensioned at a time to reflect probable tensioning operations in the field. When the cables were tensioned (each was tensioned to the same peak load before lockoff), the top pair was done first, then the middle pair, and finally the bottom pair (see Fig. 3.10c). When tension in the cables was released, this order was reversed. Seating losses were quite high, approximately 14% to 18% of the maximum tension before seating. This was primarily due to the type of anchoring chucks employed and the relatively short tendon lengths used.

Cable tendon strain gage placement, shown in Fig. 3.10c, was designed to verify symmetry of tendon tension and to determine friction losses over the harp saddles. To reduce friction losses, the harp saddles were smoothed as much as possible and lubricated with grease. Measured friction losses were 3% or less over the saddles, and therefore the precautions were successful. As previously noted, the DCDT at position C was moved to position D to avoid bumping it during the cable tensioning process.

The first test involving the harped cable tension, Test 8 in Table 3.2, was done without the strengthening angles securely attached to the beam web. After obtaining a zero reading with the DAS, the top cable pair was tensioned and seated, followed by the middle pair and then the bottom cable pair. Two standard vertical load cycles were then applied. Cable tension was then released in the reverse order of application.

In Test 9 the strengthening angles were securely attached to the beam web. Because of the interference with the cable anchorage bracket, the angles had to be shortened as shown in Fig. 3.10a. The same cable-tensioning and vertical-loading procedure was used for this test as in the previous test.

4. ANALYSIS AND TEST RESULTS

As in Chapters 2 and 3, Chapter 4 is divided into two main sections, the first section for the model bridge and the second section for the mockup. Wherever possible in the section for the model bridge, finite element analysis results are plotted with experimental results, in order to provide a complete picture of the behavior of the model bridge and to show the degree of correspondence between theory and experiment. In the section for the mockup, theoretical results based on classical analysis are often presented with the experimental results in order to bracket the experimental data between the theoretical conditions for the mockup with and without composite action.

4.1. Model Bridge Analysis and Test Results

4.1.1. Preliminary Analysis

To determine the desired location of the post-tensioning brackets on the bridge model, the authors conducted a parameter study for moments applied to a three-span beam. The span lengths of the beam used in the study correspond to those of the beams in the model bridge. The beam analyzed had a constant moment of inertia, as opposed to the varying moments of inertia along the actual model bridge beams. As will be noted later, the general trends exhibited in the analyzed beam also occur in the model bridge beams.

Two examples of the parameter study are given here. Both examples are designed to reverse the effects of ordinary service loads applied to the beam. In both examples, moments are applied to the beam which

could be applied in practice by means of straight tendons. For the three-span beam illustrated in Figs. 4.1 and 4.2, there are five regions in which critical service design moments occur. The two regions over the interior supports will be referred to as negative moment regions, and the three remaining regions will be referred to as positive moment regions.

The first example, for applying negative moments to the positive moment regions is given in Fig. 4.1. Figure 4.1a shows the moment diagram for moments applied two feet from the supports, and Fig. 4.1b shows a similar moment diagram for moments applied three feet from the supports. From the two moment diagrams, it is apparent that the application of the moments to the beam spans affects both the service load positive moment regions on the spans and the service load negative moment regions above the interior supports. The amount of moment distributed to the critical design moment locations varies with the position of the applied moments. Applied moments located closer to the interior supports distribute more moment to the support region than applied moments located farther from the interior supports. The moment at the interior supports is 7.05 foot-kips (in Fig. 4.1a), whereas in Fig. 4.1b the moment is 5.71 foot-kips. Conversely, applied moments located farther from the interior supports distribute more moment to the beam spans. In Fig. 4.1a the moment on the center span is -1.27 foot-kips, whereas in Fig. 4.1b the corresponding moment is -2.61 foot-kips.

The second example for applying positive moments to the negative moment regions is given in Fig. 4.2. Figure 4.2 is arranged in the

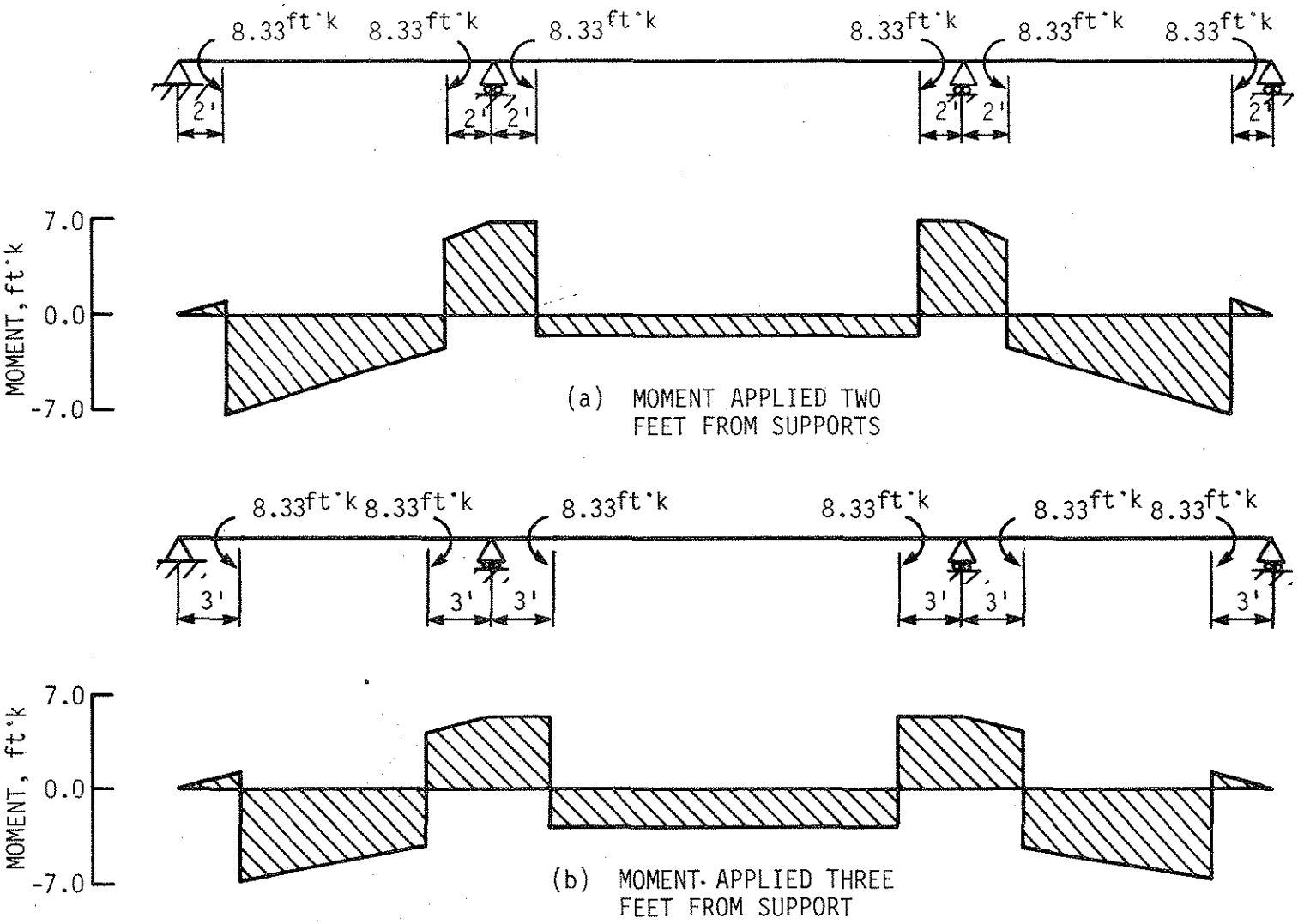

Fig. 4.1. Moment diagrams for three-span beam, negative moments applied to spans.

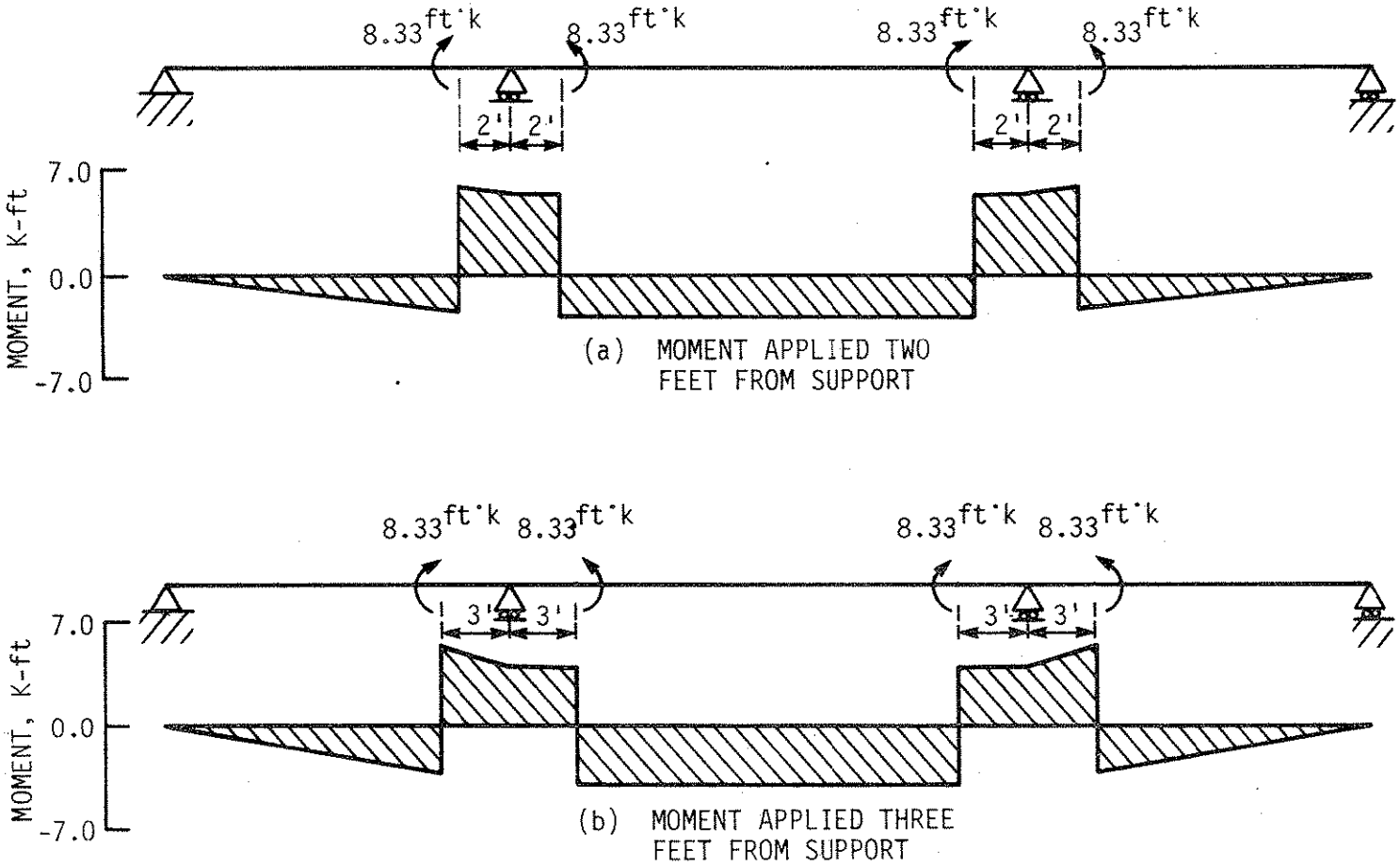

Fig. 4.2. Moment diagrams for three-span beam, positive moments applied near interior support.

same manner as Fig. 4.1, with the moment diagram for applied moments two feet from the supports in Fig. 4.2a and three feet from the supports in Fig. 4.2b. The comments regarding moment distribution made with respect to Fig. 4.1 also apply to Fig. 4.2.

In general, the parameter study showed that design of post-tensioning for strengthening purposes will be more complex for continuous beam bridges than for simple span bridges. Application of post-tensioning moments to one or more regions of a continuous bridge will affect all regions. The continuous bridge will distribute applied moments both longitudinally as demonstrated above and transversely as demonstrated for simple span bridges in References [9,10,18,19].

Because of the longitudinal distribution effects and the changes in the magnitudes of moments depending on the locations at which moments are applied, the tendon bracket locations for the model bridge were set to make provisions for tensioning both positive and negative moment regions and for changing the length of tendons in negative moment regions. Budget limitations prevented placing bracket tabs in all regions and providing tendon length adjustment for all regions on the model bridge. Any significant gaps in the test program for the model bridge were covered by the finite element analysis study.

4.1.2. Finite Element Analysis

The continuous, composite bridge model constructed in the ISU Structural Engineering Laboratory is a variably stiffened orthotropic plate and, therefore, is structurally quite complex. In previous research and development of a design manual for simple span, composite bridges, the authors found finite element theory to be best suited of

several theories for analysis of such bridges [9]. Finite element theory can take into account the complexities of the bridge and also give information on distribution of moments and axial forces.

The finite element model for the laboratory bridge model was developed for use with SAP IV [3], a well-known finite element program available to the authors through the ISU Computation Center. Because of the complexity of the finite element model, a preprocessing program was written to generate the model by using quarter symmetry. Two programs written previously for simple span bridges, which draw a finite element model before and after deformation, were used to verify the model and to draw deflected shapes. A new program was written to plot the strains along top and bottom flanges of each of the beams in the laboratory model bridge.

The basic finite element assembly for the laboratory bridge model is given in Fig. 4.3. Previous experiments with mesh size [9] indicated that reasonable accuracy could be achieved by dividing a full size concrete bridge deck into approximately 30-inch-square shell elements. The fact that the bridge model is at one-third scale suggested that the shell elements be approximately 10 in. square. With consideration of the dimensions of the laboratory bridge model and locations of the steel beams, the elements were made 7.67 in. wide and 8.33 in. long. Between the exterior beam and curb, a row of shell elements, which are narrow and long, were placed to complete the deck.

Deck shell elements were given elastic properties for concrete with the 28-day strength of 3450 psi determined by testing. Deck properties and the finite element model assume that the deck behaves

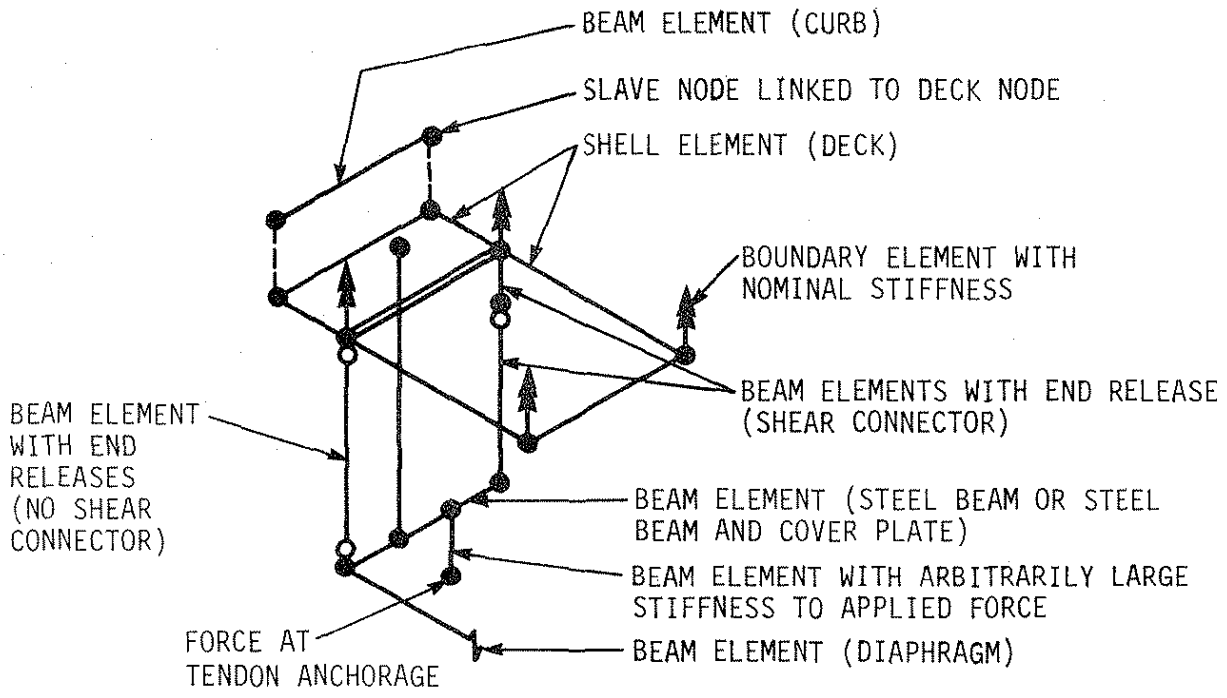

a. ISOMETRIC VIEW

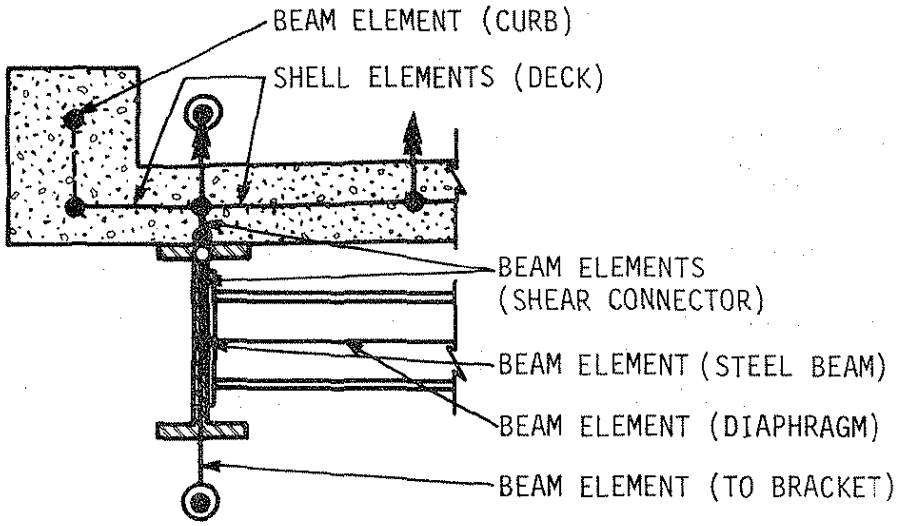

b. SECTION THROUGH EXTERIOR BEAM

Fig. 4.3. SAP IV finite element model.

elastically in both compression and tension and that composite action is achieved in accordance with the input stiffness for the shear connectors. Past research has shown that the treatment of the deck as an elastic material gives accurate results for composite bridge structures loaded within the service load range. In order to avoid numerical problems with the crowned deck, boundary elements with a small and arbitrary rotational stiffness were placed at deck nodes as required.

Curbs integral with the model bridge deck were modeled as beam elements, approximately 8.33 in. long, with elastic properties based on a 28-day concrete strength of 3355 psi. Since there is no significant slip between integral curbs and the bridge deck, curb beam nodes were linked as slave nodes to deck nodes directly below.

Each steel beam was modeled by beam elements having elastic properties as computed for noncomposite beams. Where section properties changed because of change in width and thickness of flanges (to simulate presence or absence of coverplates), beam elements shorter than the 8.33 in. deck node spacing were linked together.

Rather than link the steel beam elements directly to the concrete deck shell elements by means of slave nodes, flexible beam elements were inserted for the connection in order to model shear connector slip and to obtain information regarding the forces on shear connectors. The flexible beam elements were given stiffnesses to approximate the load-slip characteristics of the shear connectors in the laboratory bridge model. When the shear connector location did not match the 8.33 in. mesh, the flexible beam link was placed at the nearest set of beam-deck nodes. Moving the link previously has been shown to have

little effect on the overall finite element model behavior [9]. If no flexible beam link occurred at a set of beam-deck nodes, a spacer link without load-slip characteristics was inserted. Torsional and transverse stiffnesses of the beam web were given to the flexible and spacer beam links in order to correctly model the web behavior [9].

The beam elements used to model diaphragms were attached directly to the main bridge beam elements. For the post-tensioning brackets or arbitrary elevations of applied forces, vertical beam elements with an arbitrarily large stiffness were attached to the bridge beam elements and extended as far above or below the bridge beam elements as necessary. Post-tensioning tendons were not included in the finite element model because inclusion of the tendons adversely affects bandwidth, solution time, and the overall finite element analysis cost.

Right-angle bridges with structural symmetry, which are symmetrically post-tensioned and loaded such as the laboratory bridge model, can be modeled with the quarter symmetry finite element model shown in Fig. 4.4. In order to reduce analysis cost, the finite element analysis was limited to the symmetrical post-tensioning and vertical loading cases shown in Fig. 4.5. Since most of the strengthening requirements in practice are symmetrical, the authors decided that the additional cost and time required for unsymmetrical analyses were not justified. For some unsymmetrical cases, experimental results are given in Section 4.1.4.1; those results give the behavior of the laboratory bridge model under unsymmetrical post-tensioning conditions.

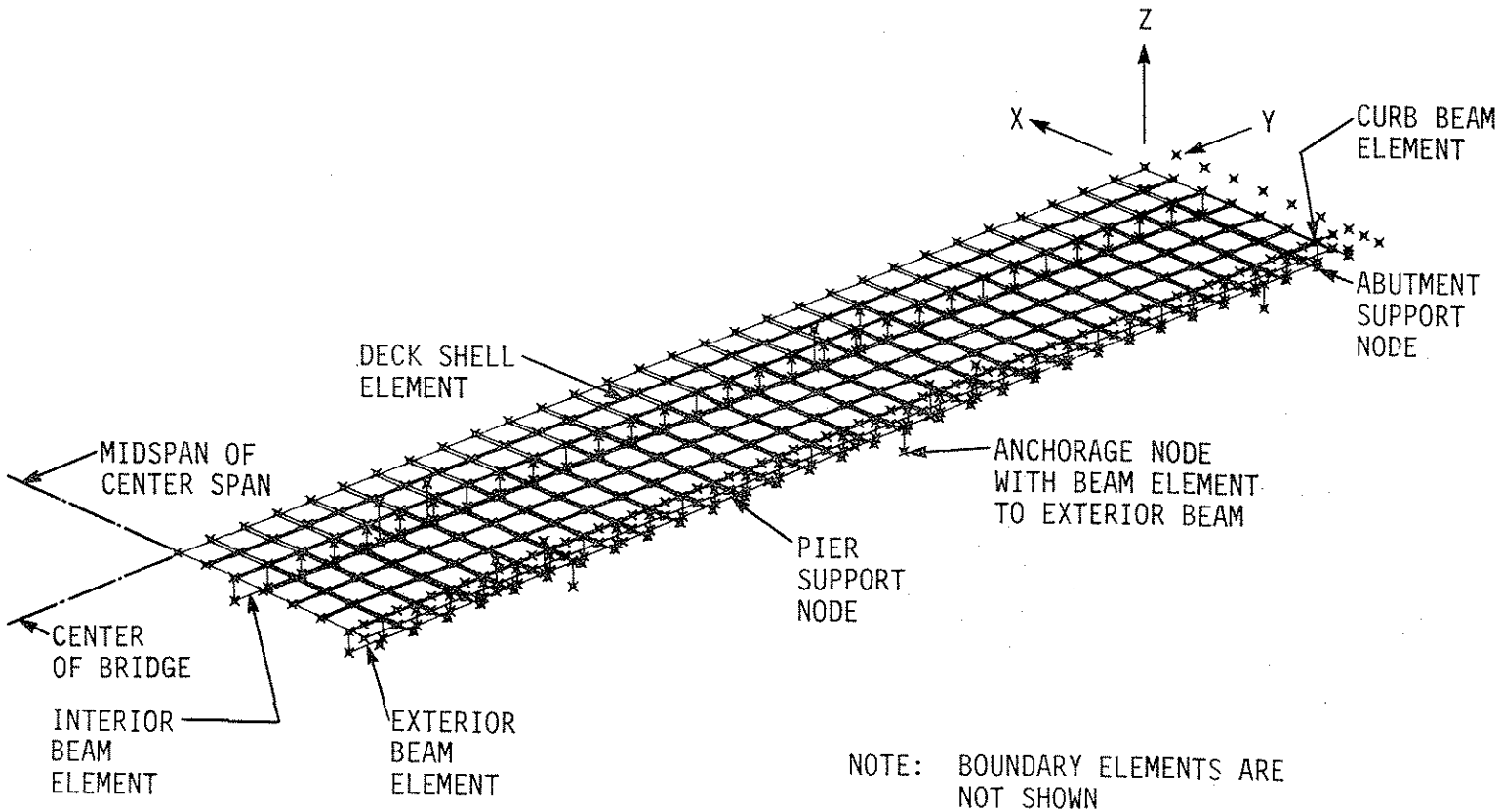

Fig. 4.4 Quarter symmetry finite element model.

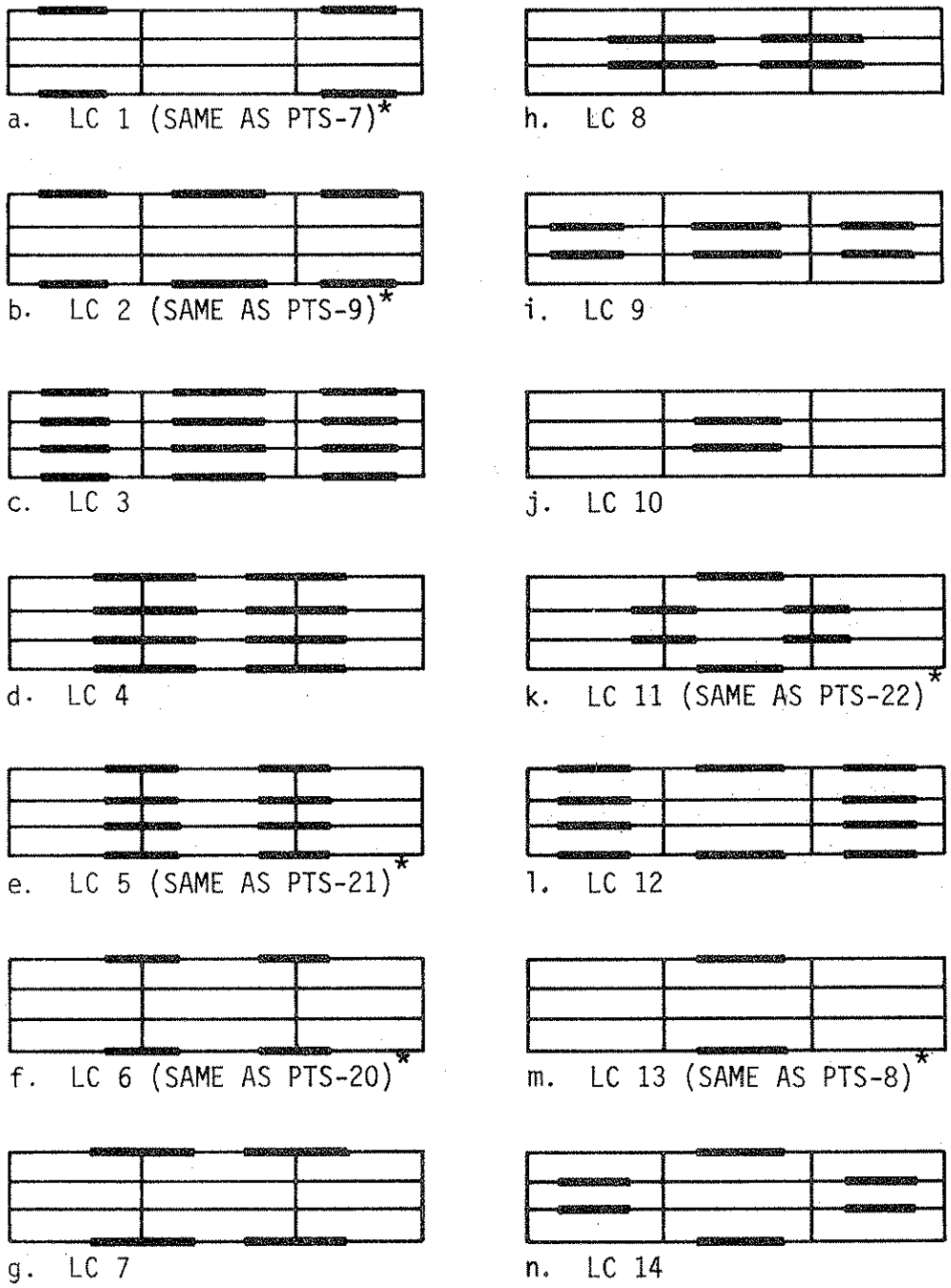

Fig. 4.5. Load cases analyzed with SAP IV finite element model.

o. LC 15

s. LC 19

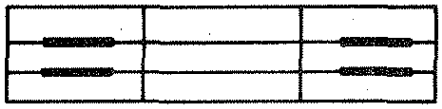

p. LC 16

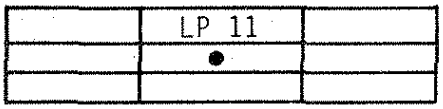

t. LC 20

q. LC 17

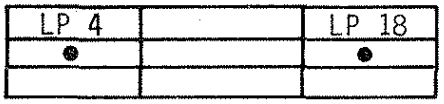

u. LC 21

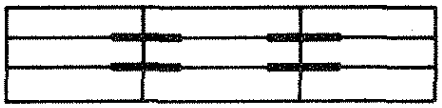

r. LC 18

Fig. 4.5. Continued.

4.1.3. Strain and Deflection Data Interpretation

Considerable quantities of data were gathered during testing of the bridge model. Some of the data, even though redundant, were gathered to provide a check of the bridge model as well as the instrumentation. Because most of the strains measured on the top flanges of the steel beams were very small and thus more subject to instrumentation errors than the larger bottom flange strains, only the bottom flange strains will be reported for most tests. Among the remaining data, only the most significant will be reported.

In order to gain some concept of the magnitude of uncertainties regarding the model construction and instrumentation, the data were systematically compared over the first few months of testing to determine what effect curing and cracking of the concrete deck would have on reliability of the results. Symmetry and superposition also were used as devices to check the reliability of the results. The checks of time effects, symmetry, and superposition are summarized in the following sections.

4.1.3.1. Time Effects

Because the concrete deck was constructed monolithically, the entire length of the bridge was subjected to the effects of shrinkage. The shrinkage was evidenced by bridge beams lifting off of the end supports by amounts ranging from 1/8 to 3/16 in. during the deck-curing period. Before any tests were conducted on the model bridge, all beams were pulled down to their supports. The tie downs (see Fig. 2.5) did not cause any immediate cracking of the deck.

After the deck had cured and the bridge was tied down at the supports, a series of post-tensioning and vertical load tests were conducted. Those tests, including PTS-1, PTS-3, PTS-10, PTS-12, and PTS-20, were then repeated two months later. During the initial two-month testing period, the deck cracked many times and thereby relieved most of the shrinkage stresses. The final crack pattern included cracks at approximately the two-thirds sections on the end spans, the interior support sections, and the quarter sections of the center span.

The second series of tests gave larger strains and deflections. Strains increased by 10%, on the average, and deflections increased by 16%, on the average. The increases are similar to those which occurred (but were not systematically documented) during testing of the simple span, composite bridge model in the ISU Structural Engineering Laboratory [19].

The increases also are very close to the 15% increases in strains and deflections noted by Kennedy and Grace during testing of an unprestressed, two-span, composite bridge model [17]. Kennedy and Grace attributed the increase in strains and deflections to cracks in the deck at the interior support and to subsequent loss of composite action in the negative moment region. They were able to show that with deck prestressing, composite action was maintained; the increase in strains and deflections did not occur.

The increase in strains and deflections noted for the continuous bridge model are probably the result of both deck shrinkage and loss of composite action in the negative moment regions. The simple span model tested earlier at ISU had no negative moment regions, and yet it

exhibited a gain in strains and deflections when deck shrinkage stresses were relieved by cracking. Because no comparable data is available on the actual increase in strains and deflections, the amount of increase caused by shrinkage and the amount of increase caused by loss of composite action in negative moment regions cannot be determined.

4.1.3.2. Symmetry

If loading is symmetrical with respect to an axis of structural symmetry, all displacements, forces, and moments will be symmetrical with respect to the same axis. Because the model bridge has two axes of structural symmetry, symmetrical post-tensioning and vertical loads were applied to the model in order to check the symmetry of the model construction. Data presented in this section are for PTS-9, which is one of the symmetrical post-tensioning schemes.

PTS-9 consists of applying post-tensioning to all of the positive moment regions, A, C, and E, of the exterior beams 1 and 4, as shown in Fig. 4.6. Since only four hydraulic jacking cylinders were available, the tendons were tensioned sequentially, which partially accounts for the 1.5% difference among the final tendon forces. Because the tendons were applied to the positive moment regions of the exterior beams, much of the post-tensioning effect is due to moment rather than axial force; and therefore the strains are larger and more reliable than for other post-tensioning schemes.

Figure 4.6 illustrates the longitudinal symmetry for bottom flange strains for Beam 1, Fig. 4.6a, and for Beam 2, Fig. 4.6b. Transverse symmetry for Sections A, B, and C is shown in Fig. 4.6c, d, and e respectively. Similar numerical comparisons are available in Table 4.1.

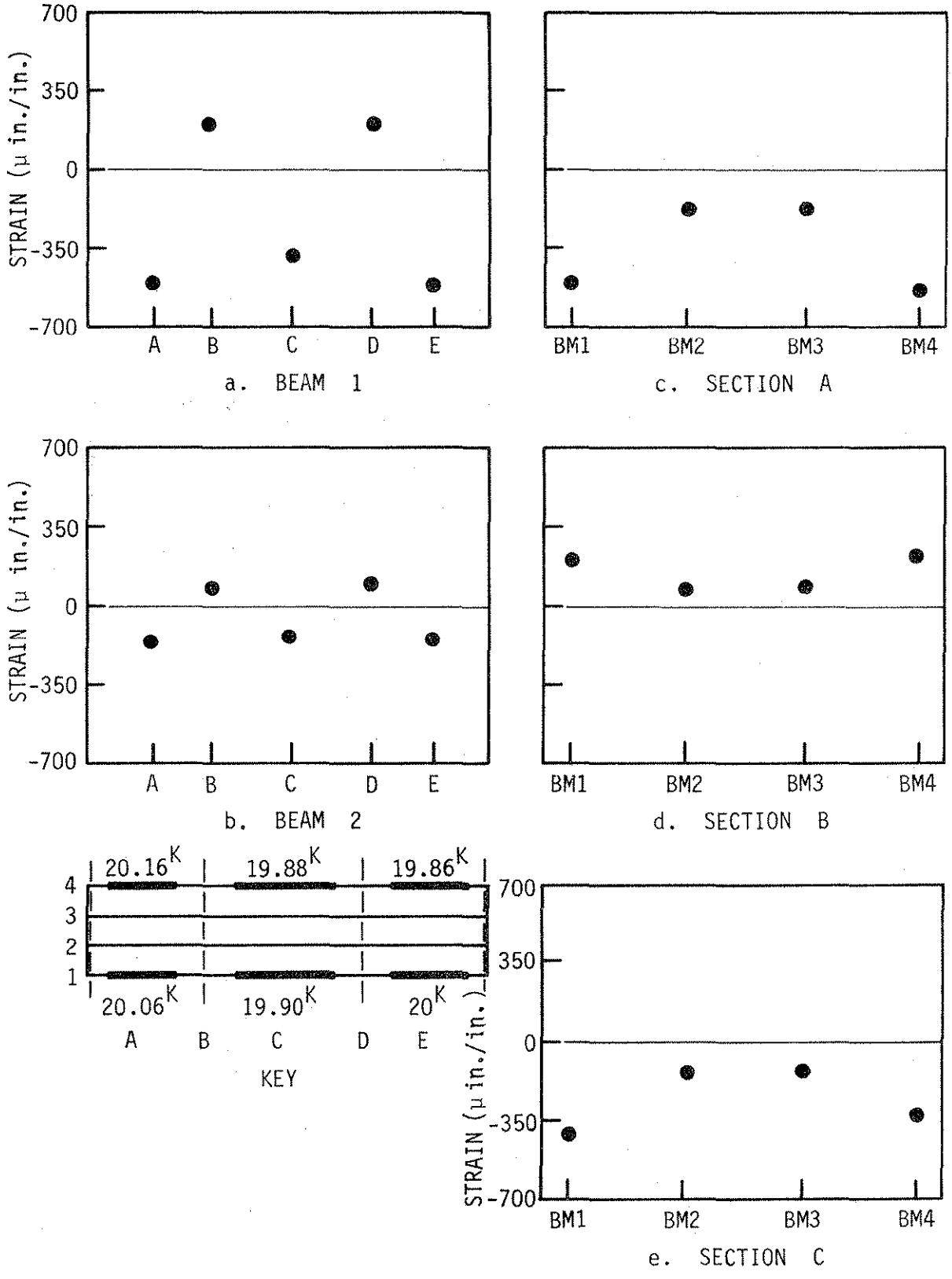

Fig. 4.6. Bottom flange strains for PTS-9.

Table 4.1. Comparisons of bottom flange strains between symmetrical sections for PTS-9.

a. Longitudinal Comparison

	Beam 1				Beam 2			
	Sec. A	Sec. E	Sec. B	Sec. D	Sec. A	Sec. E	Sec. B	Sec. D
Strain	-514	-521	220	242	-174	-160	83	98
Percentage Difference	1.4%		9.5%		8.4%		16.6%	

b. Transverse Comparison

	Section A				Section B				Section C			
	BM 1	BM 4	BM 2	BM 3	BM 1	BM 4	BM 2	BM 3	BM 1	BM 4	BM 2	BM 3
Strain	-514	-533	-174	-168	221	226	83	93	-381	-322	-137	-113
Percentage Difference	3.6%		3.5%		2.2%		11.4%		16.8%		19.2%	

Overall, the magnitude of the differences between symmetrical sections or beams do not vary a great deal; however, the percentage differences vary from a low of 1.4% for a large strain to a high of 19.2% for a moderately low strain. The percentage differences in the table average 9.3, which generally is acceptable for experimental work.

In general, it appears that the largest percentage differences between symmetrical strains are for strains distributed by the bridge. In Table 4.1a, the percentage differences are smaller for the post-tensioned sections A and E than for the unpost-tensioned sections B and D. In Table 4.1b, the post-tensioned beams 1 and 4 usually have smaller percentage differences than the unpost-tensioned beams 2 and 3.

There is a certain amount of error on symmetrical strains, and this error can be attributed to two primary causes: imperfections in the steel beams, concrete deck, and concrete curbs, and imperfections in application of the post-tensioning. Because the bridge model was constructed at one-third scale, ordinary tolerances in beam depth, deck thickness, and curb dimensions have a greater effect than the same differences at full scale. Because the errors which can be attributed to symmetry of the construction are relatively small, no adjustments were made to data in subsequent use and interpretation of the data.

4.1.3.3. Superposition

Another method for checking experimental results is to superpose data taken from separate load tests and compare the superposition data with data taken from a combined load test. In this section, superposition is used with vertical load tests to make such a comparison.

Figure 4.7 shows bottom flange strains plotted for the sum of the strains from individual load tests for 6-kip loads at LP4 and LP18 and for the load test with two 6-kip loads on the model bridge. The solid dots represent the superposition of the two separate tests, and the open dots represent the single test. All of the parts of the figure show little difference between the two conditions, and in some cases, it was difficult to plot the small difference between the two conditions.

Table 4.2 gives the same comparisons as Figure 4.7 but in numerical form. The largest percentage difference between the results from superposition and the individual test is 13%, and the differences average only 6.2%. Since this difference is quite small, it is reasonable to use superposition in interpreting the experimental results.

Differences for superposition were shown to be somewhat larger for post-tensioning schemes [7]. At least part of the increased difference was shown to be caused by secondary effects in tendons. When post-tensioning is applied in stages, the forces in tendons that are locked in place change slightly, and the changes cannot be included in superposition of individual tests. These changes were generally on the order of 3% to 4%.

Table 4.2 also permits a check of symmetry, and on the average, differences are 11.3%. This percentage is very close to the average noted for PTS-9 in Section 4.1.3.2. This average is inflated by two very large percentage differences for small strains in Table 4.2a. If those large percentage differences are neglected, the average is only 4.7%. In general, vertical loading is likely to give more accurate results because the application of the load is not affected by imperfections in the bridge model construction.

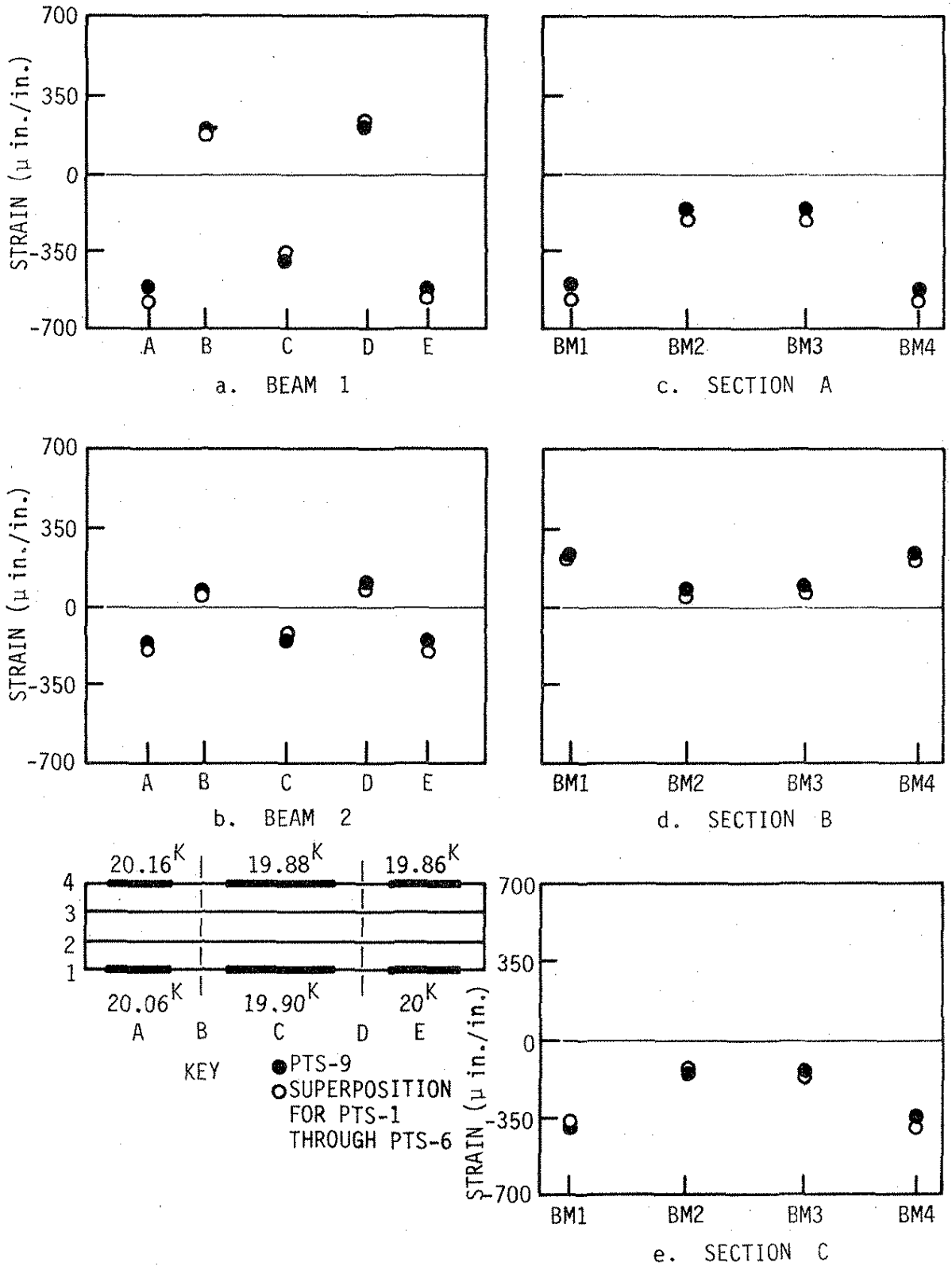

Fig. 4.7. Bottom flange strains for PTS-9 and superposition of PTS-1 through PTS-6.

Table 4.2. Comparisons of bottom flange strains between vertical load load tests with and without superposition.

a. Longitudinal Comparisons

	Beam 1					Beam 2				
	A	B	C	D	E	A	B	C	D	E
Strain for superposition of 6 kips LP 4 + LP 18 acting separately	116	-14	-80	-7	117	264	-71	-86	-79	299
Strain for 6 kips at LP 4 and LP 8 acting simultaneously	125	-15	-76	-7	120	269	-74	-78	-90	296
Percentage Difference	7.5%	6.8%	5.1%	0%	2.5%	1.8%	4.1%	9.7%	13.0%	1.0%

Table 4.2. (Continued)

b. Transverse Comparison

	Section A				Section B				Section C			
	1	2	3	4	1	2	3	4	1	2	3	4
Strain for superposition of 6 kips at LP 4 + LP 18 acting separately	116	264	242	118	-14	-71	-71	-14	-80	-86	-92	-80
Strain for 6 kips at LP 4 and LP 8 acting simultaneously	125	269	269	126	-15	-74	-77	-15	-76	-76	-82	-75
Percentage difference	7.5%	1.8%	10.5%	6.5%	6.8%	4.1%	8.1%	6.8%	5.1%	9.7%	11.5%	6.4%

Checking the experimental data with respect to time and cracking effects, symmetry, and superposition showed relatively small errors; such errors are generally within accepted standards for experimental work. Therefore, in subsequent analysis and presentation of experimental data, the validity of symmetry and superposition will be assumed and used to give a more complete presentation of results.

4.1.4. Effects of Post-tensioning

The laboratory post-tensioning tests were conducted for tendon forces of 10 and 20 kips. Because the larger forces produced larger strains, which were less subject to zero shift and other instrument variations, only data for the 20-kip forces will be presented in the following sections. Because symmetry was validated in Section 4.1.3.2, data from symmetrical tests were utilized to complete data sets for single beam schemes. Data points from symmetrical tests are always noted with separate symbols in the figures so that they may be readily identified.

4.1.4.1. Single Beam Schemes

Post-tensioning of single beams was tested with the objective of determining the feasibility for strengthening a deficient beam or deficient beam region. In practice the deficiency could be caused by damage from localized corrosion or from an overheight vehicle colliding with the bridge. Within the limitations of the bracket tab locations, various service load positive and negative bending moment regions were post-tensioned. The graphs for bottom flange strains presented in this section show the longitudinal and transverse distribution effects for various localized post-tensioning schemes.

The first series of post-tensioning schemes presented involve post-tensioning of positive moment regions. Figure 4.8 gives the bottom flange strains for PTS-1, in which the positive moment region for the end span of one exterior beam was post-tensioned. A force of 20.2 kips was applied to Beam 4 in region A. In the figure, the data set is completed by use of the four data points from PTS-5, which are given with open square symbols.

As could be expected, the largest strains occur on the post-tensioned beam, Beam 4, and the strains gradually decrease for Beams 3, 2, and 1 across the bridge. The far exterior beam, Beam 1, has very small bottom flange strains, but some of which are in the reverse direction from those applied to Beam 4. Those reverse strains would be undesirable from a strengthening viewpoint.

Along Beam 4, the strains decrease gradually from left to right for the sections at which strains were measured. The strains at Sections A and B would be in the correct direction for strengthening, but the strains at Sections C and D would be in the reverse direction for strengthening. The strain at Section E is small but in the correct direction for strengthening. In general for this post-tensioning scheme, the strains decrease in both transverse and longitudinal directions away from the post-tensioned region, and some of the strains are not beneficial with respect to strengthening the bridge.

PTS-3, for which strains are given in Fig. 4.9, is the second in the series of positive moment region post-tensioning schemes. Here the positive moment region for the center span is post-tensioned with a force of 19.71 kips. The maximum strain transmitted to the post-

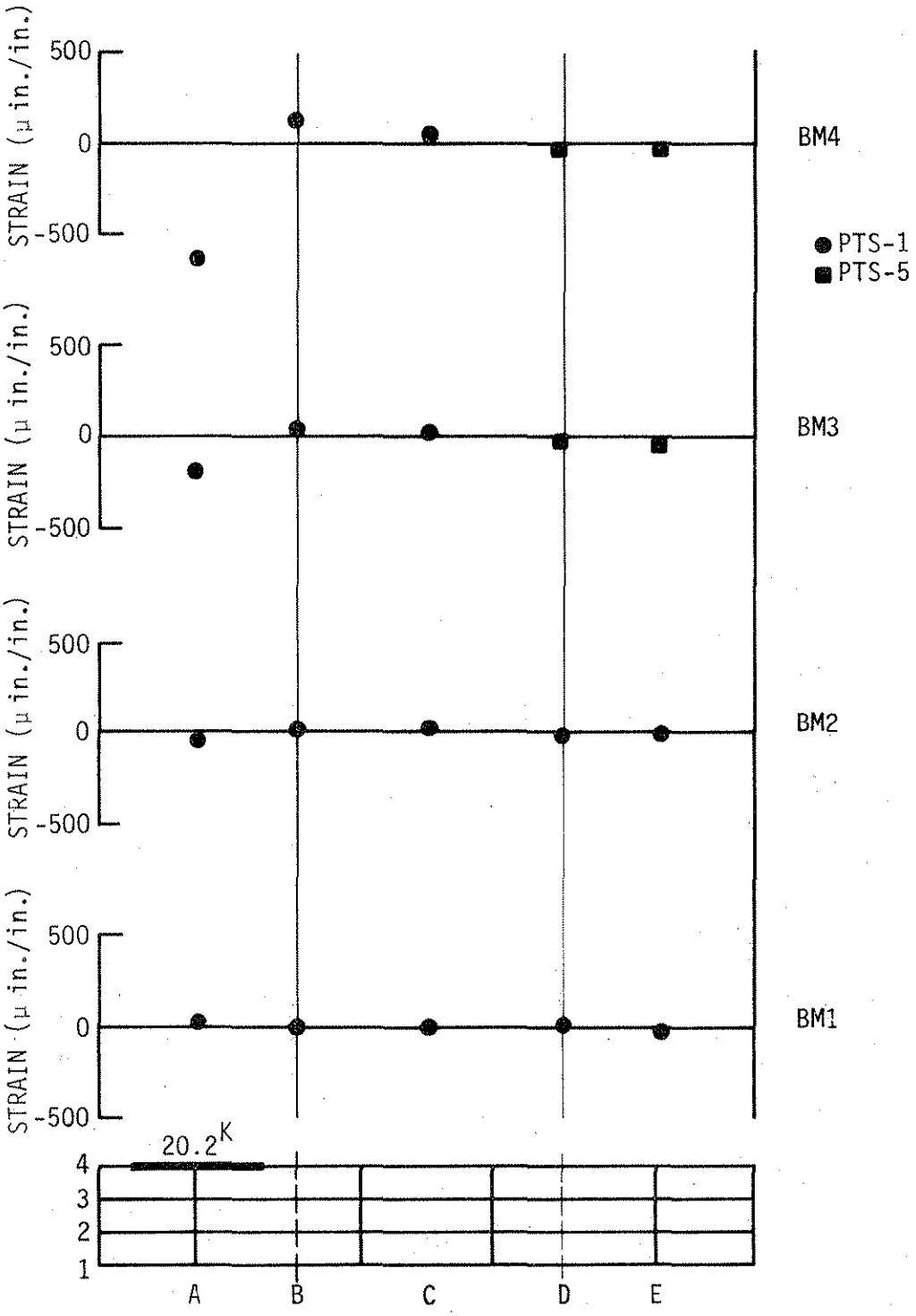

Fig. 4.8. Bottom flange strains for PTS-1.

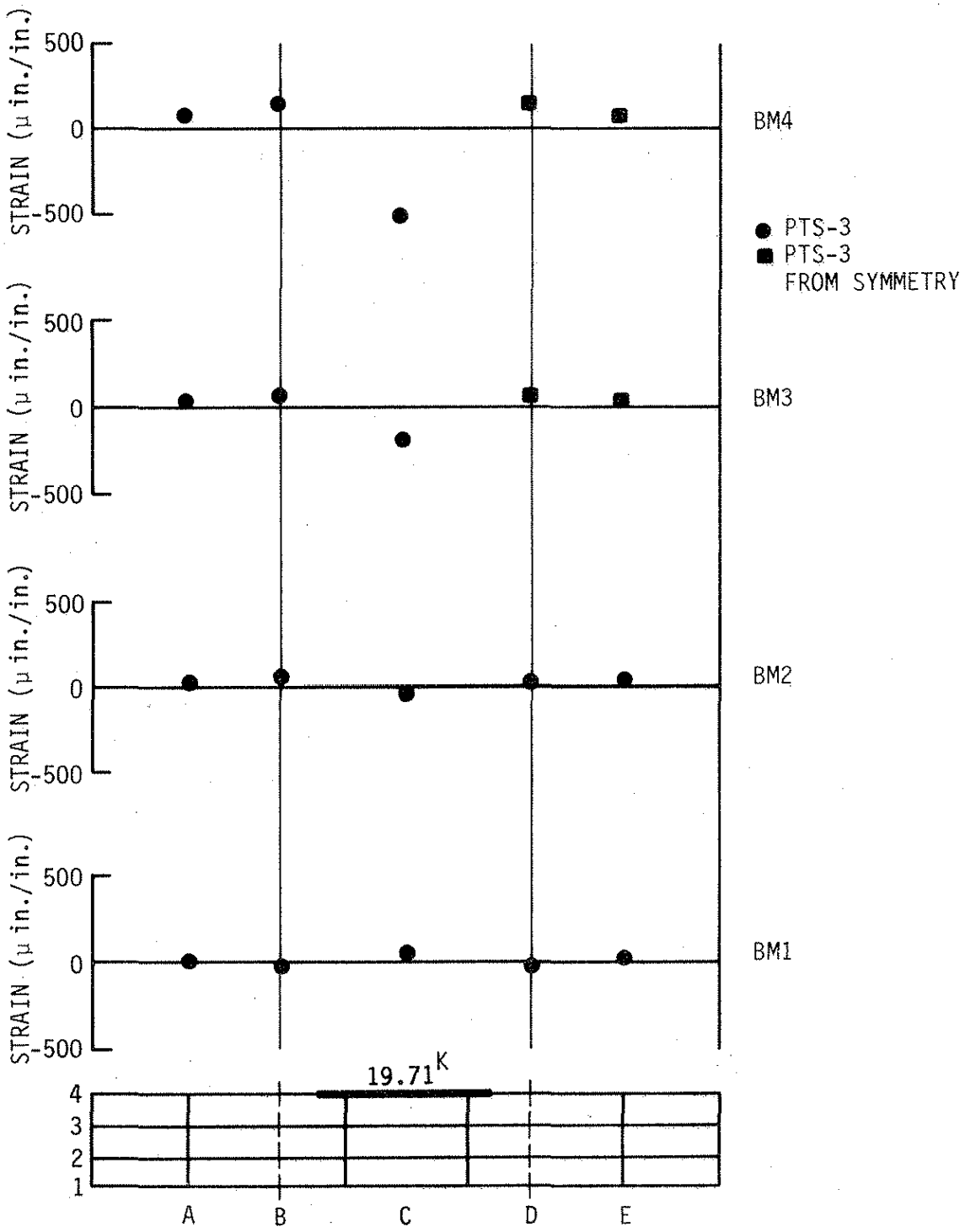

Fig. 4.9. Bottom flange strains for PTS-3.

tensioned beam, Beam 4, is smaller in this scheme than for PTS-1. The probable reason is that the post-tensioning effects are distributed in two directions longitudinally, rather than in one direction. As in PTS-1, the strains decrease in both longitudinal and transverse directions away from the post-tensioned region. Again some of the strains are beneficial and some are not.

For the last positive moment region scheme presented here, which is constructed as the superposition of PTS-1, PTS-3, and PTS-5, all positive moment regions along Beam 4 were post-tensioned. The bottom flange strains shown in Fig. 4.10 indicate that less strain is transmitted to the positive moment region on the center span at Section C than to the positive moment regions on the end spans at Sections A and E. The smaller strain occurs even though the tendon forces are approximately equal and all of the tendons were positioned at the same elevation with respect to the beam and the neutral axis. The smaller strain is due to the larger center span length and, to a lesser extent, to the difference in end conditions between the center span and the end spans.

Strains decrease for the first interior beam, Beam 3, and are essentially zero for the second interior beam, Beam 2. For the far exterior beam, Beam 4, the strains are reversed and would not be beneficial with respect to strengthening the bridge.

Two sets of schemes for post-tensioning negative moment regions are presented next. The first set is for an exterior beam, and the second set is for an interior beam. For all of the negative moment post-tensioning schemes, straight tendons were placed above the deck,

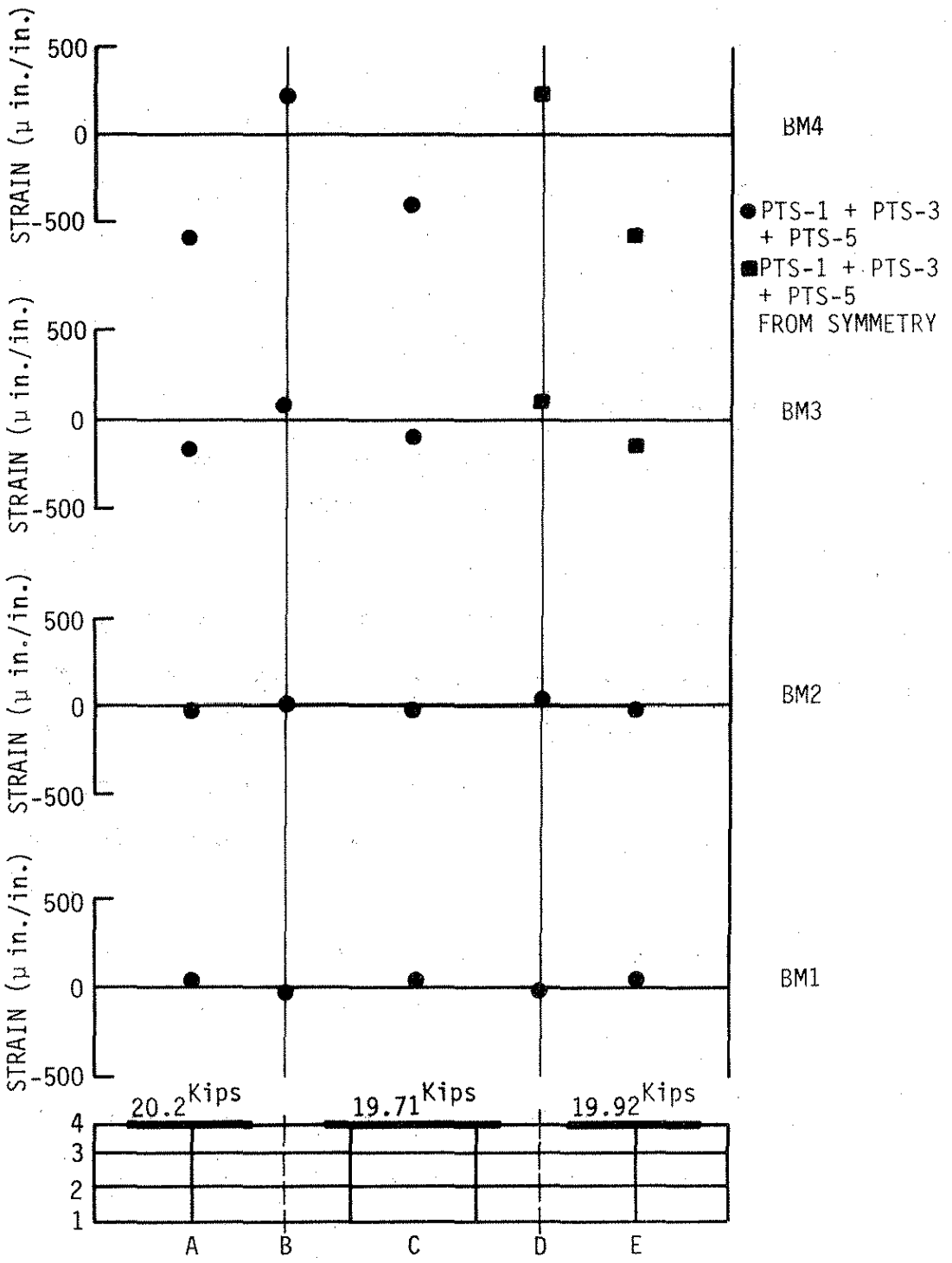

Fig. 4.10. Bottom flange strains for PTS-1 + PTS-3 + PTS-5.

a condition that was necessary because of the scale of the model but which would not be possible in practice. For all of the schemes presented here, the shorter tendon option permitted by location of the bracket tabs was employed because the shorter tendon option gave larger strains in the negative moment regions. Thus the behavior of the bridge was consistent with the behavior described in Section 4.1.1 and illustrated in Fig. 4.2.

PTS-10, for which strains are given in Fig. 4.11, consists of post-tensioning one negative moment region for the exterior beam, Beam 4, through Section B. The maximum strains illustrated in Fig. 4.11 are much smaller than the strains for positive moment region post-tensioning shown in Fig. 4.8 and 4.9. The reason for the smaller strains for the negative moment post-tensioning is primarily the smaller eccentricity. The tendons above the deck had an eccentricity that was only about half that of the tendons below the beams, and therefore, the tendons in positive moment regions applied much larger moments than the tendons in negative moment regions.

Because the strains presented in Fig. 4.11 are small, it is difficult to see the distribution effects. Those effects are similar to those for PTS-1 and PTS-3, however. The strains decrease in both longitudinal and transverse directions away from the post-tensioned region, and not all of the strains are beneficial with respect to strengthening.

In Fig. 4.12, the strains for the superposition of PTS-10 and PTS-16 are given. For this superposition scheme, both negative moment regions along the exterior beam, 4, are post-tensioned. The strains shown for the sections along Beam 4 are similar to, but smaller than, the strains

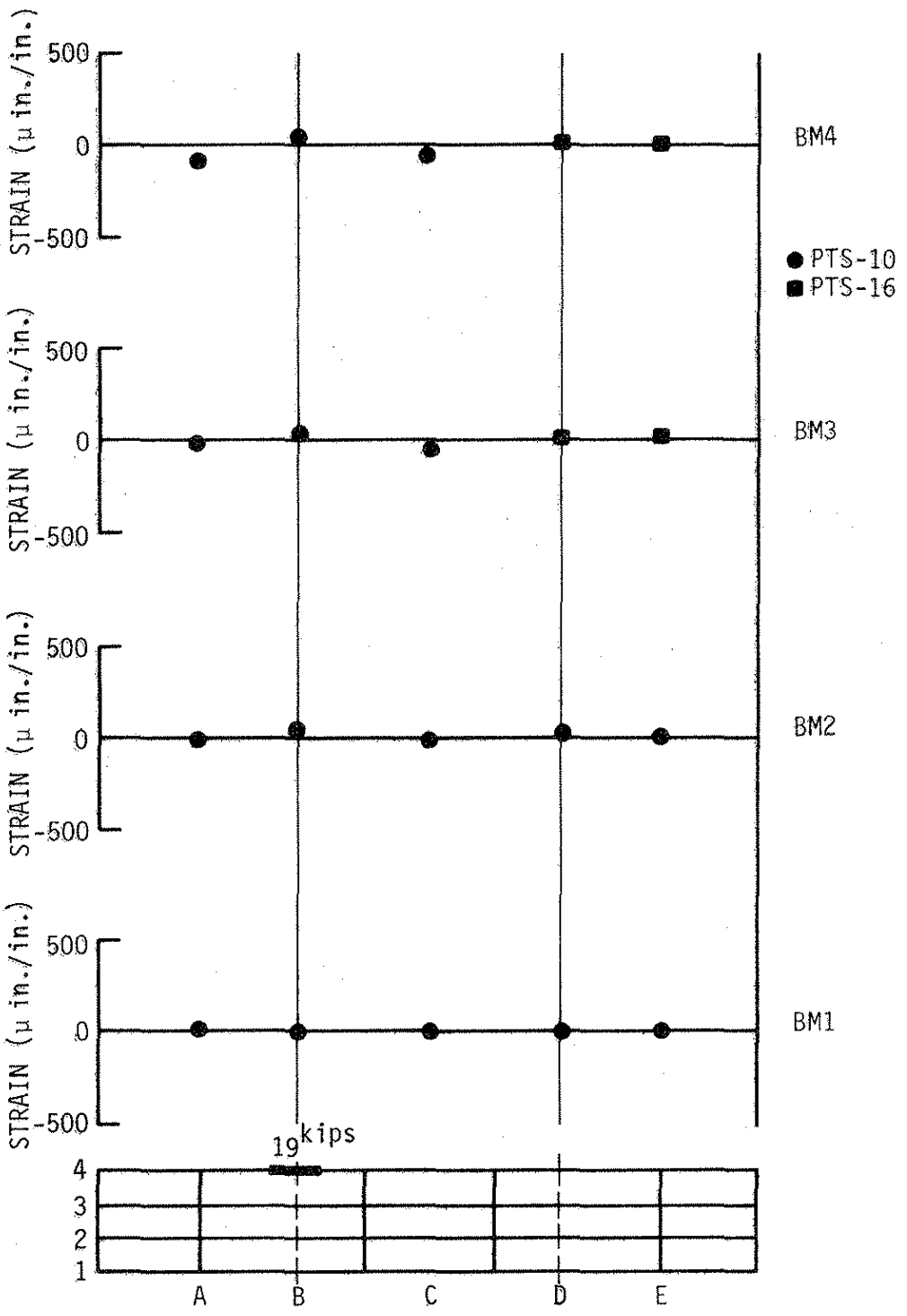

Fig. 4.11. Bottom flange strains for PTS-10.

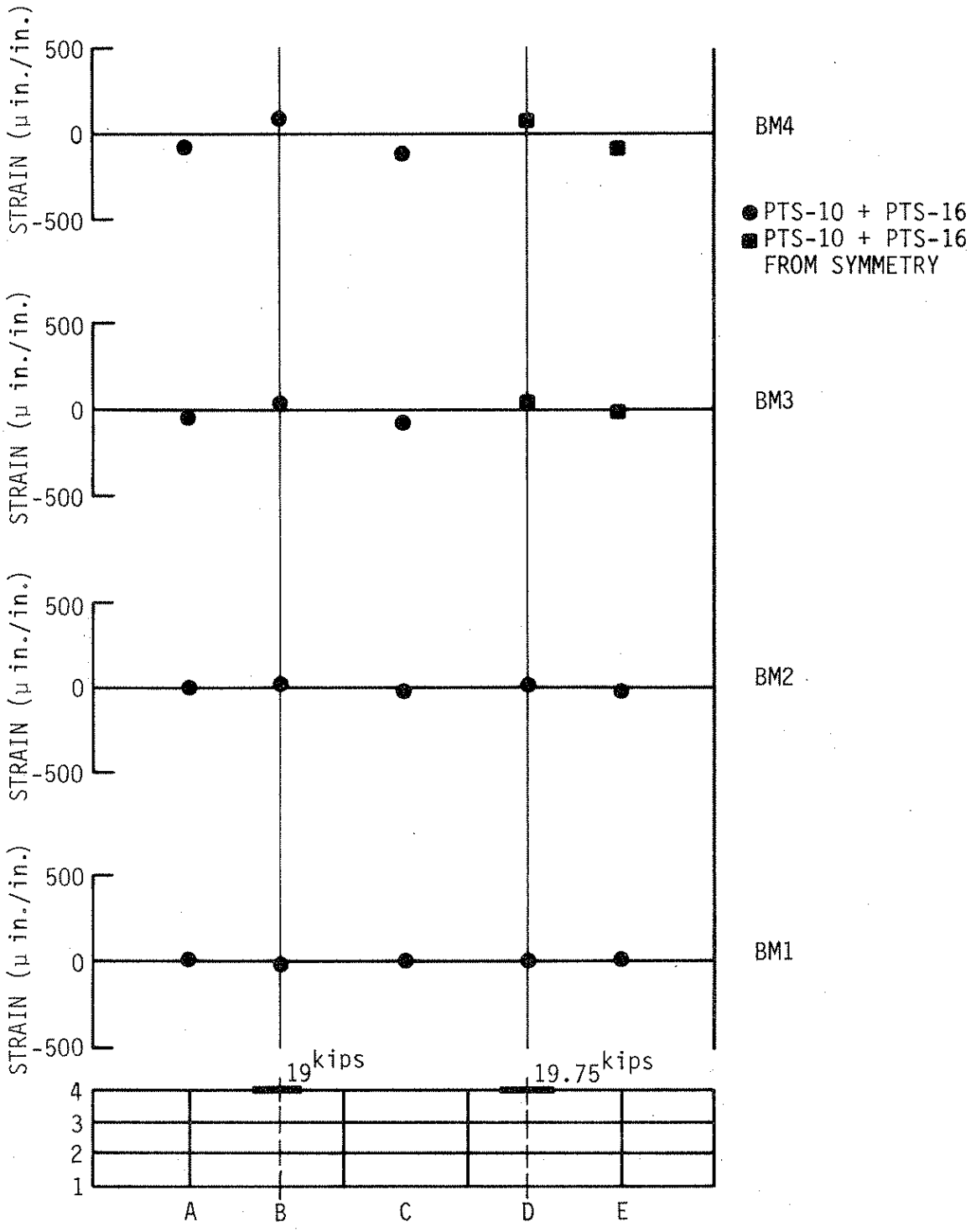

Fig. 4.12. Bottom flange strain distribution for PTS-10 + PTS-16.

for the corresponding positive moment post-tensioning scheme given in Fig. 4.10. The bottom flange strains decrease for Beam 3 and are very near zero for Beam 2. The strains then reverse slightly for the far exterior beam, Beam 1. All of the strains would be beneficial with respect to strengthening except those for Beam 1.

Strains for PTS-12, a negative moment post-tensioning scheme for an interior beam are given in Fig. 4.13. In PTS-12, Beam 3 was post-tensioned at Section B. This particular scheme had the effect of post-tensioning the entire bridge somewhat symmetrically in the transverse direction. The strains for all of the beams are in the same direction as those for the post-tensioned beam, and the strains for Beam 4, which was not post-tensioned, are the largest. All of the strains except those at Section E are beneficial for strengthening. Because of the wide distribution of post-tensioning throughout the bridge, even the maximum strains are very small.

Figure 4.14 shows the strains for the superposition of PTS-12 and PTS-17. In this superposition scheme, both of the negative moment regions along Beam 3 are post-tensioned. All of the strains are in the correct direction for strengthening, and Beams 4, 3, and 2 have approximately equal strains at each of the sections along the bridge, Sections A through E. The strains are relatively small in comparison with the strains caused by positive moment region post-tensioning.

For the single beam schemes, the following should be noted. Not all of the effects of the post-tensioning will be desirable with respect to strengthening. If an exterior beam is post-tensioned, the far exterior beam will be subjected to strains in the same direction as

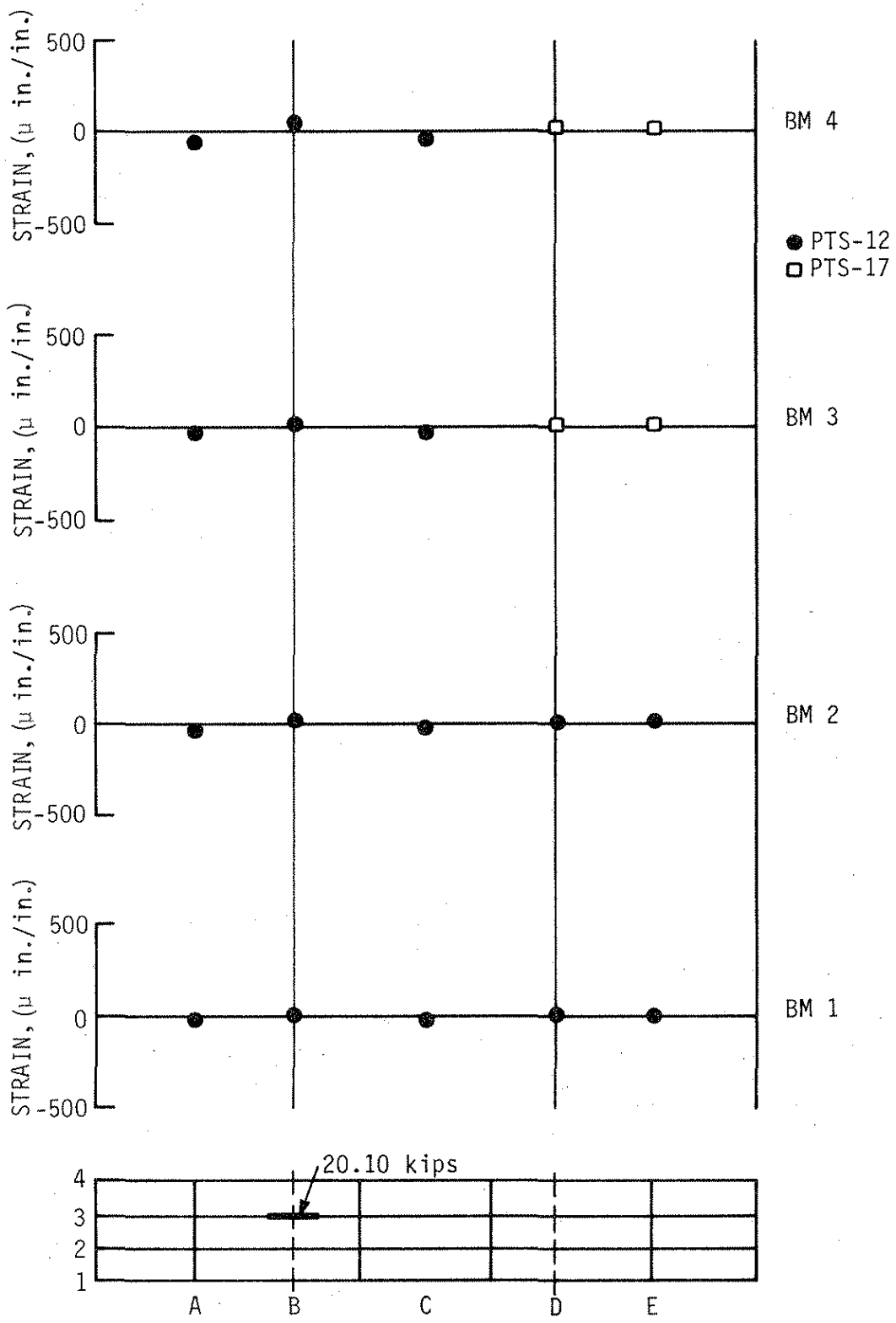

Fig. 4.13. Bottom flange strains for PTS-12.

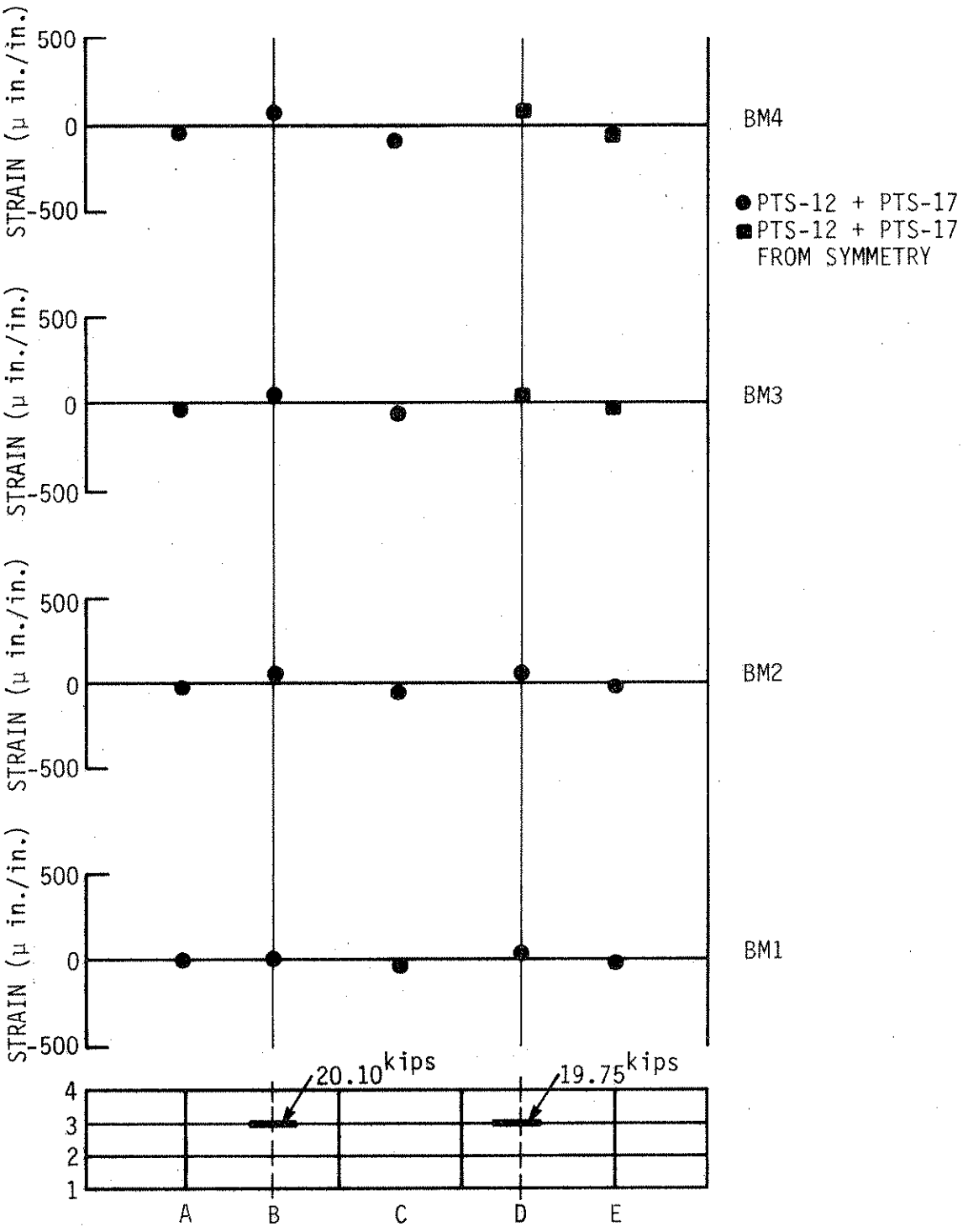

Fig. 4.14. Bottom flange strains for PTS-12 + PTS-17.

service load strains; and those post-tensioning strains are not beneficial. If only one positive or negative moment region along a beam is post-tensioned, other regions of the beam may be subjected to strains that are not beneficial, depending on the position of the post-tensioning and the location of the section in question. Post-tensioning of an interior beam may generate larger strains in the adjacent exterior beam than in the post-tensioned interior beam. Post-tensioning of an interior beam generally distributes post-tensioning throughout the bridge much more uniformly than post-tensioning of an exterior beam.

4.1.4.2. Multiple Beam Schemes

The multiple beam post-tensioning schemes presented in this section are much better suited to strengthening continuous, composite bridges than single beam schemes. The multiple beam schemes are more difficult to handle experimentally than single beam schemes because of the large number of tendons and sequential use of jacking cylinders. The multiple beam schemes, however, are much easier to handle analytically than single beam schemes if the analysis makes use of symmetry. For these reasons much of the presentation in this section is derived from the quarter symmetry finite element model described in Section 4.1.2.

Three types of post-tensioning schemes for the model bridge are presented in this section: a series of positive moment regions, a series for negative moment regions, and a scheme for combined positive and negative moment regions. Figure 4.15, gives beam strains for post-tensioning the three positive moment regions of both exterior beams. For this first figure, both top and bottom flange strains are illustrated in order to demonstrate that the top flange strains are generally

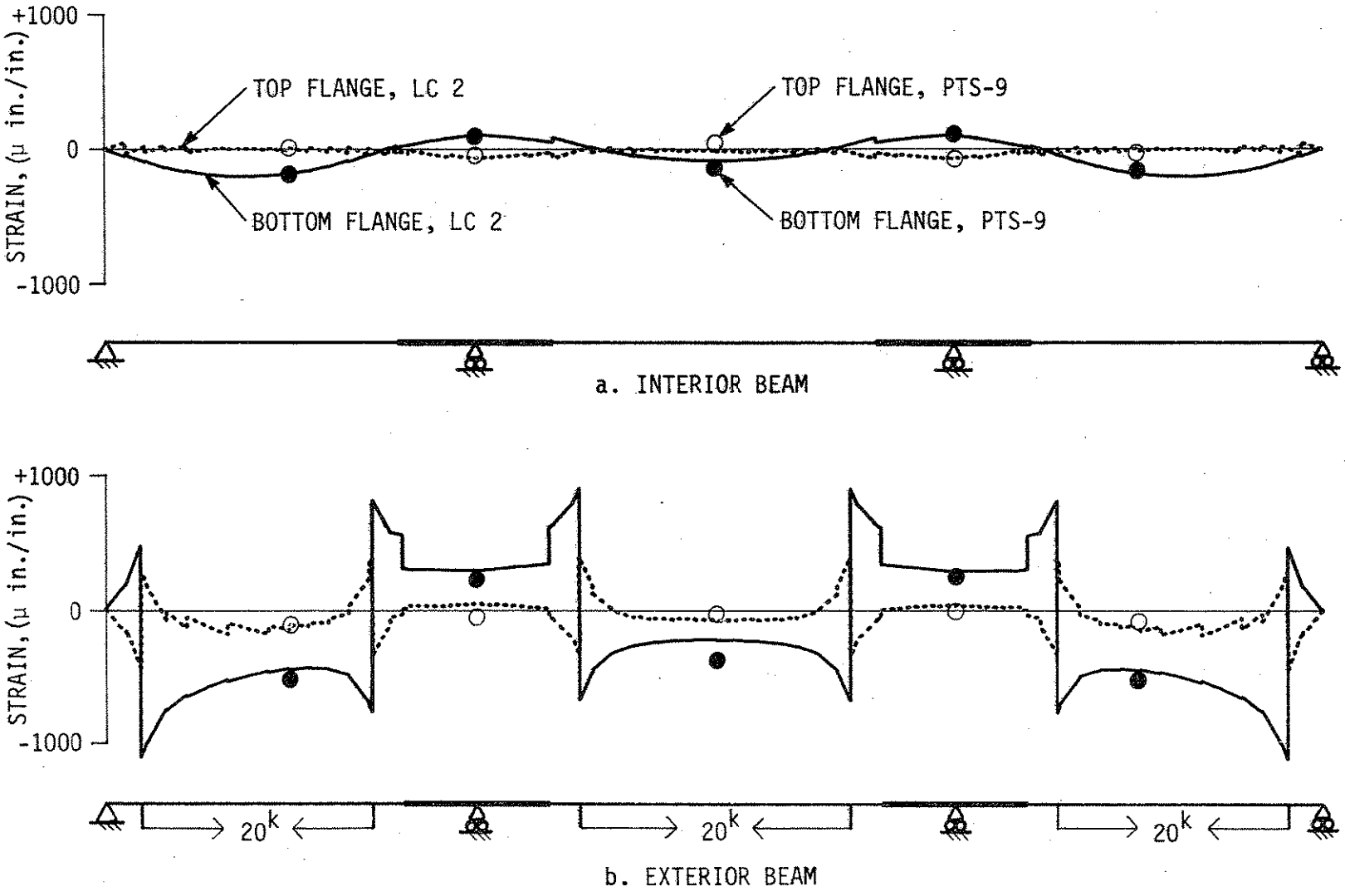

Fig. 4.15. Top and bottom flange strains for LC 2 and PTS-9.

very small and will be of little benefit or harm for strengthening a bridge.

Both the finite element analysis strains for LC2 and the experimental strains for PTS-9 are given in Fig. 4.15. There are some minor differences between the finite element and experimental strains at the various sections along the bridge. The differences are most apparent for the larger strains on the post-tensioned exterior beam. There are several reasons for the differences. The finite element model assumed complete composite action throughout the bridge and also elastic behavior of the concrete deck in both compression and tension, whereas the experimental model was subject to deck shrinkage and subsequent cracking which does not meet the finite element model assumptions. The finite element model also did not account for local variations in steel beam properties, concrete deck thickness, and curb dimensions in the experimental model. There are also some differences between the 20-kip tendon forces assumed for the finite element model and the tendon forces actually applied.

The only noticeable patterns in the differences between the finite element and experimental strains are in Fig. 4.15b. It is apparent that the experimental top flange strains are slightly smaller and that the experimental bottom flange strains are shifted slightly in the direction of compression. The reason for the differences is not obvious, and the differences do not occur for negative moment post-tensioning, as will be noted later. The differences generally are small, however, and the overall correlation between finite element and experimental strains is very good.

For the bottom flange strains from the finite element analysis, there are very large strains on either side of each of the points at which post-tensioning is applied. In practice, such large strains would not exist because a post-tensioning bracket applies moment over a finite length rather than at a point, as is assumed in the finite element analysis. There also are large changes in strain at the points where coverplates begin or end, and those changes are likely to occur in the actual bridge, but perhaps not quite so suddenly.

Figure 4.15 shows that the post-tensioning applied with equal tendon forces transmits the largest bottom flange strains to the positive moment regions of the end spans, less strain to the negative moment regions above the supports, and the least strain to the positive moment region of the center span. The strains could be adjusted by changing the tendon forces, moving the points at which post-tensioning is applied, or both. A comparison of Figures 4.15a and 4.15b shows that the strains distributed to the interior beams are one third to one half of the strains applied to the exterior beams. This distribution is very similar to that determined for the simple span bridge model in previous research [1].

LC9, the scheme illustrated in Fig. 4.16 is for post-tensioning of all positive moment regions of the interior beams. The bottom flange strain pattern is very similar to that shown in Fig. 4.15, except that the exterior and interior beam strains are reversed. When the interior beams are post-tensioned, about one-third to one-half of the post-tensioning transmitted to the interior beams is distributed to the exterior beams.

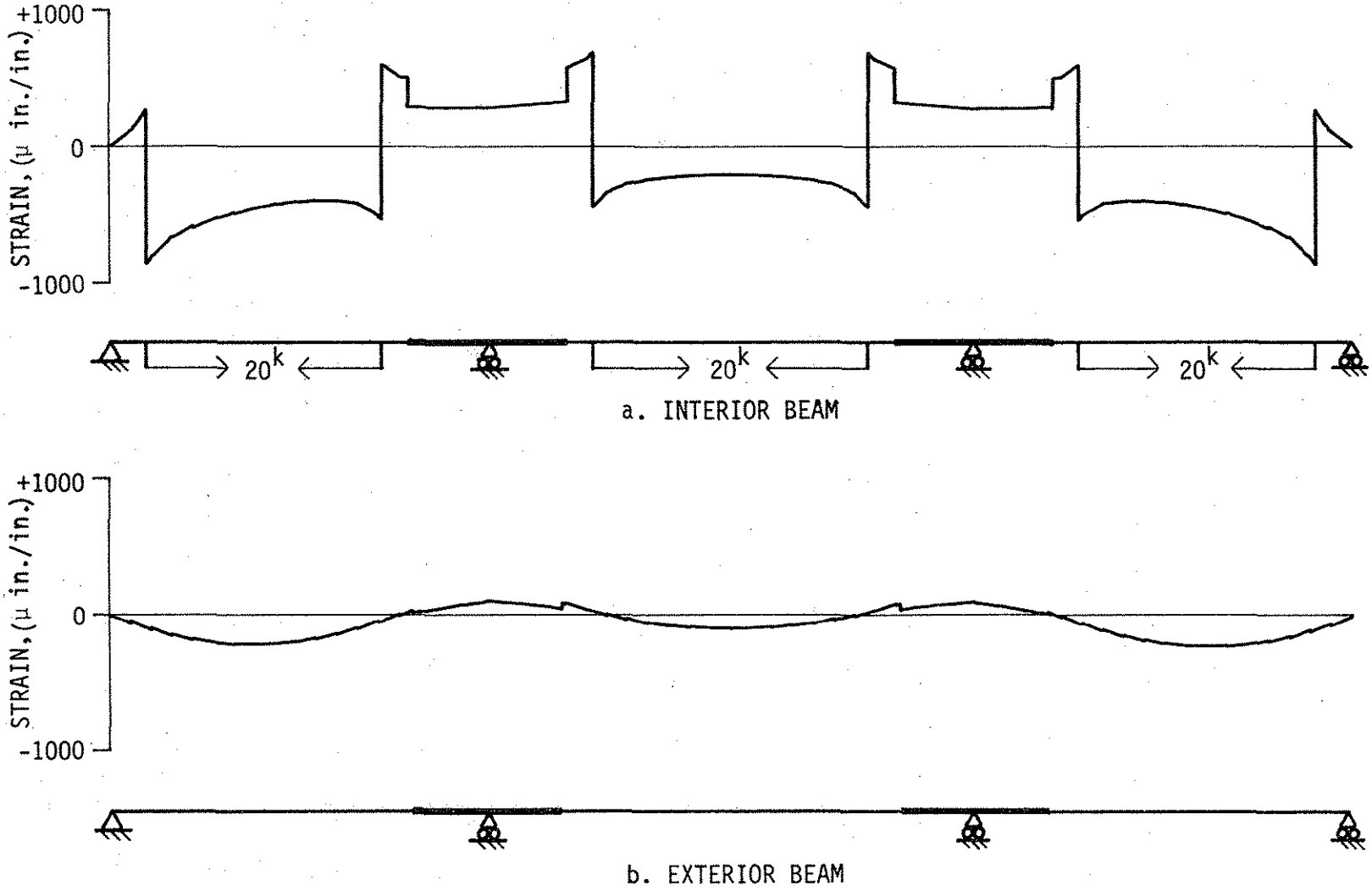

Fig. 4.16. Bottom flange strains for LC 9.

Figure 4.17 gives the bottom flange strains for LC3, in which all positive moment regions in the model bridge are post-tensioned. Both the exterior beam strains illustrated in Fig. 4.17b and the interior beam strains illustrated in Fig. 4.17a have the characteristic shape of the strain diagrams for post-tensioned beams in the two previous figures. Equal tendon forces for all beams cause slightly larger strains in the exterior beams, as can be noted by comparing Figs. 4.17a and 4.17b. The larger strains are caused by the transverse distribution characteristics of the bridge, which from previous research depend on a complex interaction of several factors.

Figure 4.18 begins the series of negative moment region post-tensioning schemes. In Fig. 4.18, the finite element strains are given for LC6 and the experimental strains for PTS-20, both of which are schemes in which the exterior beams were post-tensioned. The tendons for the exterior beams are of the shorter length used in the testing of the model bridge. The only significant strains applied to the model bridge are the finite element strains near the points of post-tensioning application, and those strains would not be realized in practice because of the finite length of the post-tensioning brackets. There is some strain distributed from the post-tensioned exterior beams to the interior beams, but all applied and distributed strains are small and thus difficult to compare. Finite element and experimental strains correlate well, with no obvious pattern of deviations.

Strains for LC18 and Stage 2 of PTS-21 are plotted in Fig. 4.19. For these schemes, post-tensioning was applied to the negative moment regions of the interior beams. Figures 4.19a and 4.19b are very nearly

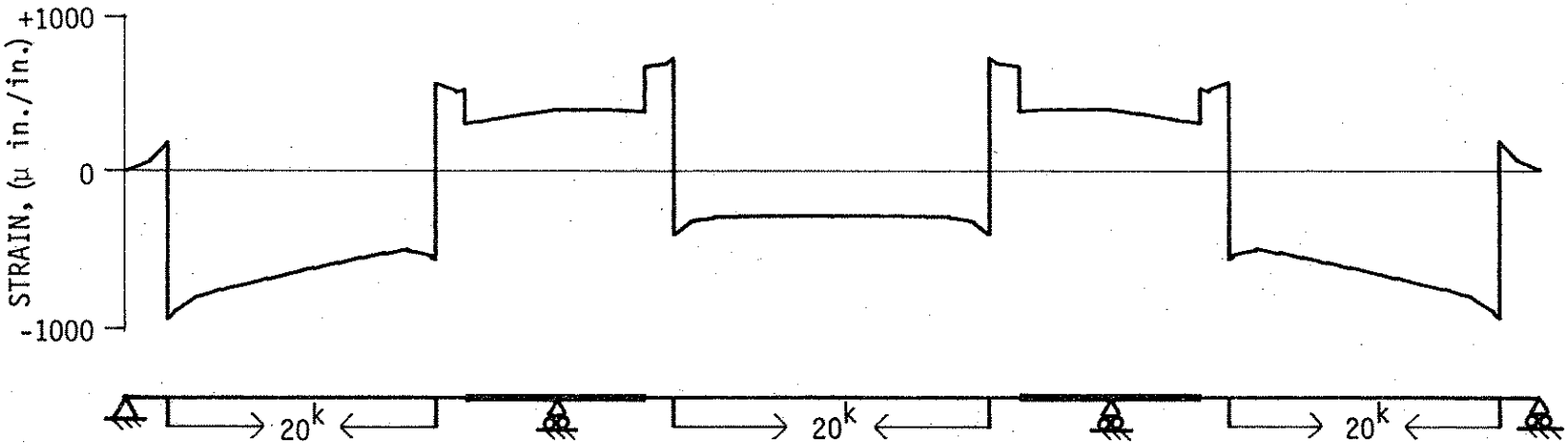

a. INTERIOR BEAM

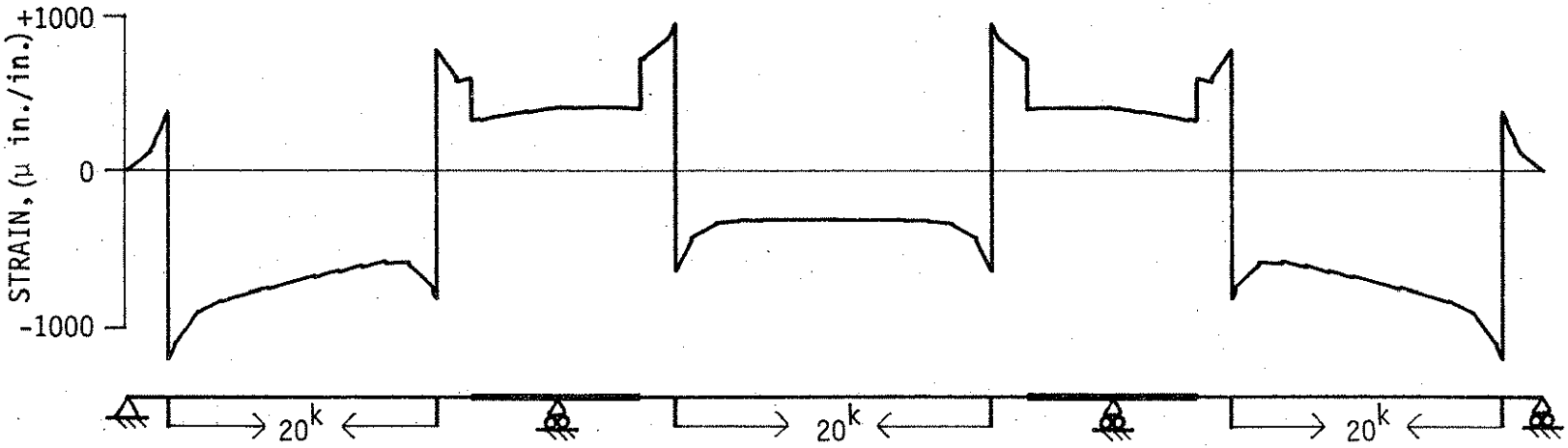

b. EXTERIOR BEAM

Fig. 4.17. Bottom flange strains for LC 3.

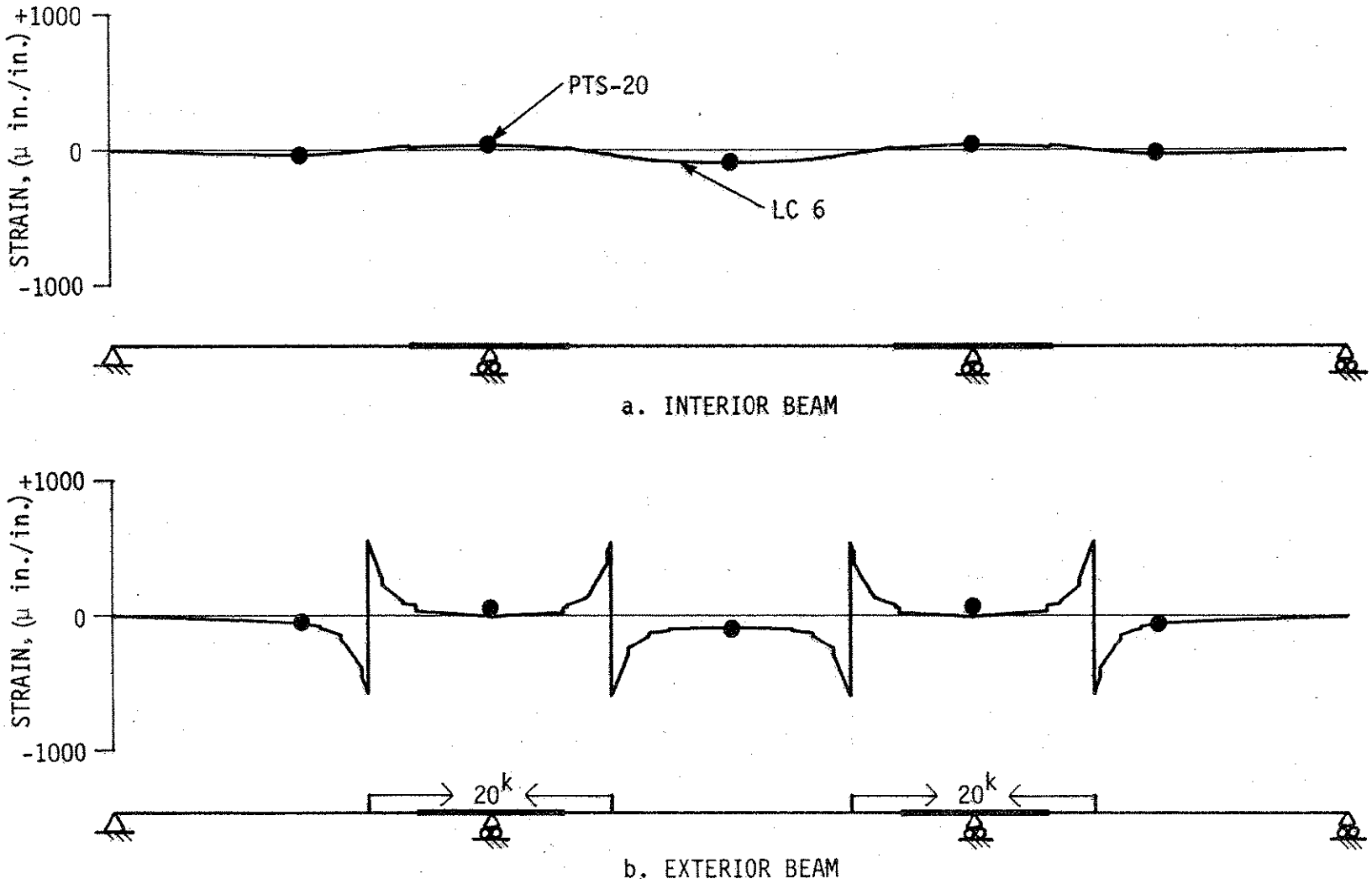

Fig. 4.18. Bottom flange strains for LC 6 and PTS-20.

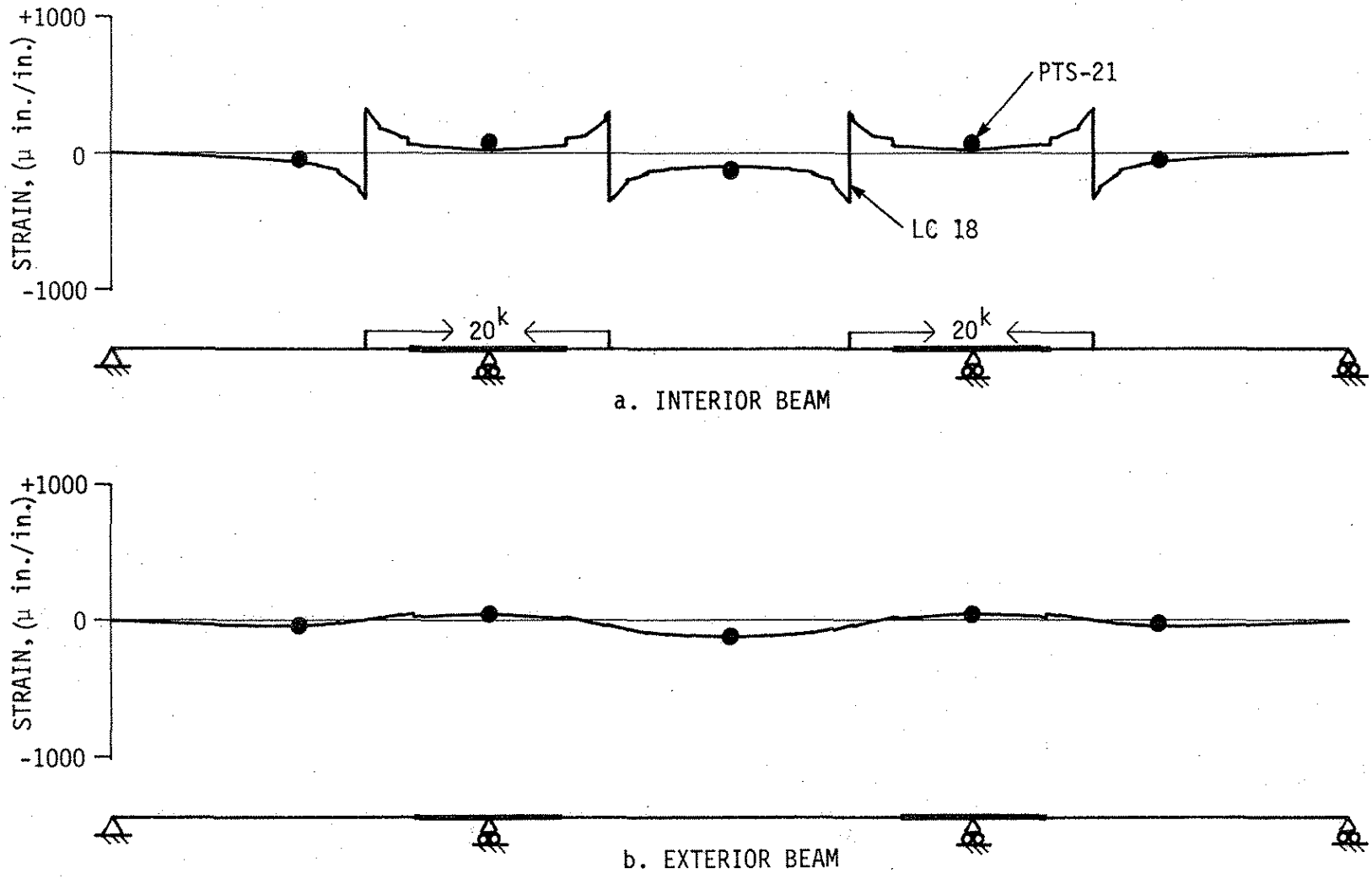

Fig. 4.19. Bottom flange strains for LC 18 and PTS-21, Stage 2.

the reverse of Figs. 4.18a and 4.18b. It appears that slightly more post-tensioning was distributed from the post-tensioned interior beams to the exterior beams, which is consistent with the data from the positive moment post-tensioning schemes described above.

Figure 4.20 completes the series of negative moment region post-tensioning examples. Finite element bottom flange strains from LC5, and experimental strains from PTS-21 show excellent correlation, as they do for the two previous schemes. The point application of post-tensioning to the finite element model creates larger strains near these points for the exterior beams than for the interior beam, but as noted previously, the larger strains are not likely to have any practical meaning. This particular post-tensioning scheme transmits the largest strains to the center spans of the beams, in comparison with the strains transmitted to the other critical stress sections.

In the last scheme presented in this section, all positive and negative moment regions within the bridge were post-tensioned with equal tendon forces. Figure 4.21 illustrates the bottom flange strains for that scheme. As could be expected from the previous schemes, post-tensioning all regions creates the largest strains. The strains and the strain patterns are very similar to those for post-tensioning all the positive moment regions, which is illustrated in Fig. 4.17. There is a slight increase in the bottom flange strains at the interior supports and a more noticeable increase in strains for the center span as a result of the superposition of the negative moment region post-tensioning.

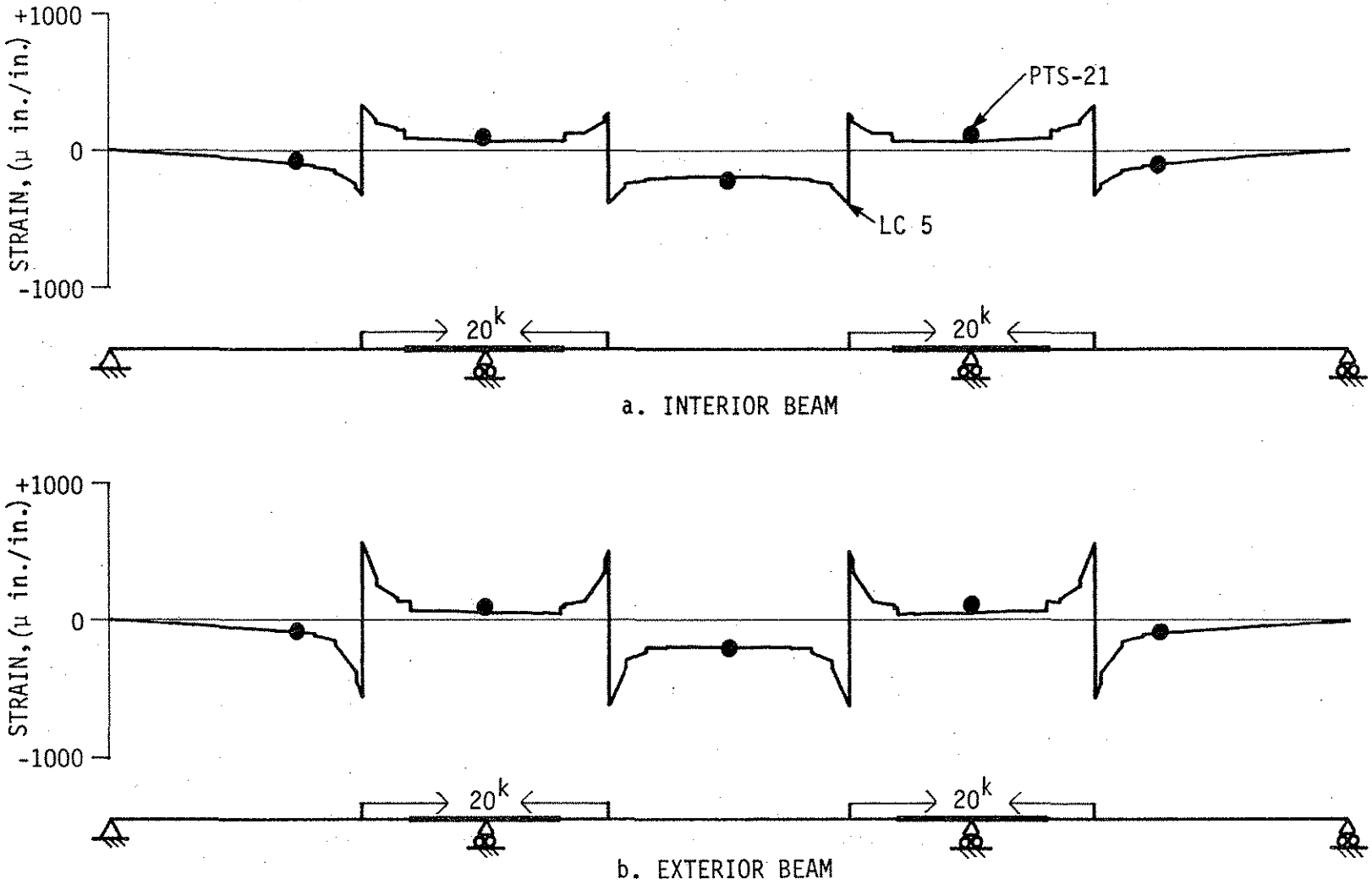

Fig. 4.20. Bottom flange strains for LC 5 and PTS-21.

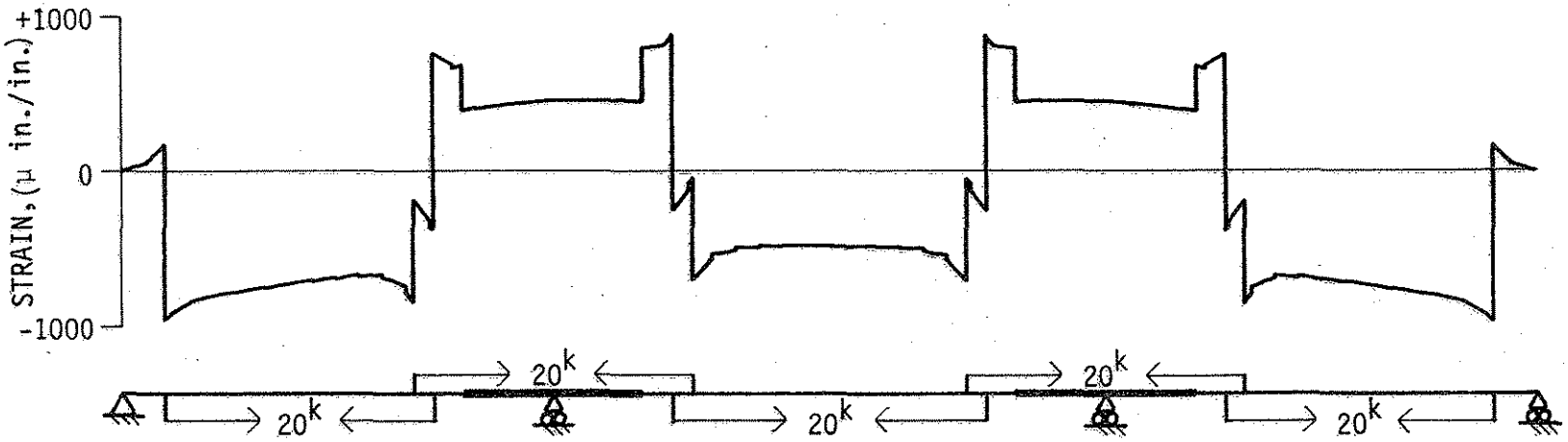

a. INTERIOR BEAM

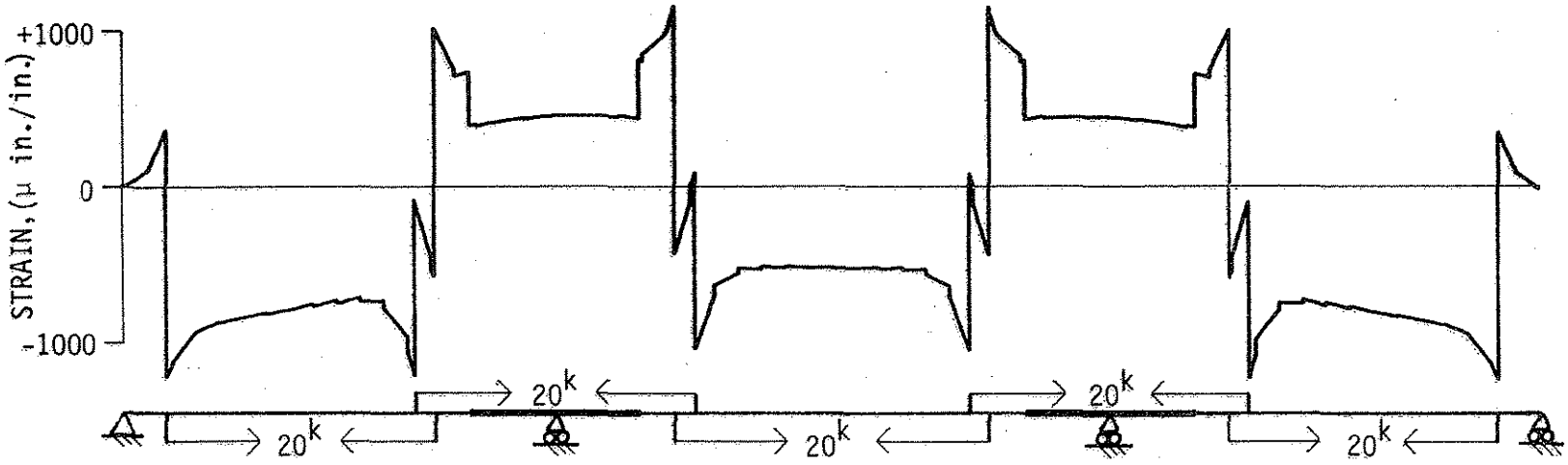

b. EXTERIOR BEAM

Fig. 4.21. Bottom flange strains for LC 19.

The multiple beam schemes presented in this section demonstrate that post-tensioning of the positive moment regions has the largest effect in reversing the service load behavior of the bridge and appears to have greater potential for strengthening than post-tensioning of negative moment regions. Post-tensioning the positive moment regions beneficially affects all critical design sections within the bridge. When all of the positive moment regions were post-tensioned, the resulting strains were approximately 300 to 600 μ inches per inch, which correspond to 9 to 18 ksi. Those stresses are in the range required to strengthen the prototype bridge. The transverse distribution, when only exterior or only interior beams are post-tensioned, appears to be similar to that for simple span bridges; and that distribution will be explored further in the next section.

Although the negative moment region post-tensioning did not appear very promising for reversing the service load behavior of a bridge in either single beam or multiple beam schemes, it may have value for providing dependable composite action throughout the bridge. The possibility of providing composite action will be explored in the second part of this chapter when interpreting the results of the full-size mockup. The post-tensioning schemes applied to the mockup also may provide better reversal of the service load behavior because the neutral axis of the mockup was lowered by the addition of angles bolted to the web near the bottom flanges. The harped tendon configuration also will have a greater moment effect than the straight tendons used in the bridge model tests.

4.1.4.3. Distribution

A continuous bridge will distribute post-tensioning both longitudinally and transversely, as demonstrated in the two sections for single and multiple post-tensioning schemes. The distribution effects can be obtained most accurately by finite element analysis. Although the distribution effects in the two directions may be interrelated, it may be possible to separate the effects for design purposes, if extreme accuracy is not required.

Longitudinal distribution of moments can be determined by treating the post-tensioned beams as individual composite beams with variable stiffnesses as required by coverplated regions and composite action or lack thereof. Many relatively easy-to-use calculator and computer programs are available that can analyze beams with variable moment of inertia and applied moments. By shifting application points for moments longitudinally and experimenting with magnitudes of moments, it should be possible to design a tendon arrangement that provides the required stress relief for individual beams. If all beams are post-tensioned in all positive moment regions, the procedure suggested above may be sufficiently accurate for design.

However, if the strengthening requirements suggest that only exterior or only interior beams be post-tensioned, the strengthening design must consider the transverse distribution because some of the post-tensioning will be distributed away from the post-tensioned beams. Some preliminary study on transverse distribution was conducted by dividing the model bridge into five regions on the basis of dead load inflection point sections. The equations developed for simple span

bridges in Reference 10 were applied to those regions as if they represented simple span bridges and then distribution fractions were computed. Those fractions were compared with force and moment fractions determined from finite element analyses of the model bridge. The fractions determined from the simple span equations were reasonably accurate, but not accurate enough for design purposes.

On the basis of the experimental and finite element work conducted in this study, it appears that longitudinal distribution may be considered accurately through conventional, continuous-beam analysis if all bridge beams are post-tensioned in the same manner. If beams are not post-tensioned in the same manner or if there are significant differences between the stiffnesses of adjacent beams, then the transverse distribution must be considered either through finite element analysis, a similarly accurate analysis method, or a design procedure yet to be developed. Preliminary study indicates that a method for computing transverse distribution fractions, similar to the method for simple span bridges, could be developed for continuous bridges.

4.1.4.4. Tendon Force Changes

Whenever there is a change in deflection of a post-tensioned beam, the forces in eccentric or harped tendons will change. The change in deflection may be caused by application of more post-tensioning or by the application of vertical load. Both of these conditions were tested in the bridge model.

Because only four hydraulic jacking cylinders were available in the laboratory, the more complex post-tensioning schemes required staged jacking. Two or four tendons were tensioned at the first stage,

and then two or four tendons were tensioned at the second stage in order to complete the test.

Table 4.3 lists the gains and losses between the first and second stages of post-tensioning for three schemes. In PTS-9 for post-tensioning the three positive moment regions of the exterior beams, the two tendons on the center spans were tensioned (Stage 1) followed by the tensioning the four tendons on the end spans (Stage 2). As shown in Fig. 4.3a between stages one and two, there were force gains of 3.4% and 4.3% in the center span tendons.

The post-tensioning of all negative moment regions in PTS-21 was staged by tensioning the four tendons for the exterior beams and then tensioning the tendons for the four interior beams. Shown in Table 4.3b are the losses that occurred when the interior beams were tensioned; there were losses of 3.1%, 3.1%, 3.0% and 2.9% in the exterior beam tendons when the second stage post-tensioning was applied.

The third post-tensioning example, in which all interior beam negative moment regions and exterior beam, center span positive moment regions were post-tensioned (shown in Table 4.3c for PTS-22), was staged to apply the negative moment region post-tensioning before the positive moment region post-tensioning. Between the two stages, the tendons above the interior beam supports lost 3.0%, 3.0%, 3.4% and 3.1% of the force applied at the first stage.

All of these examples for staged post-tensioning show relatively small gains or losses in post-tensioning force, in the range of 3% to 4%. The gains and losses are for post-tensioning forces in the range required to relieve stresses in the bridge model approximately equi-

Table 4.3. Variation in tendon force because of applying additional post-tensioning.

a. PTS-9

Post-tensioning Scheme	Stage	Post-tensioning Force Applied to Region					
		1-A	1-C	1-E	4-A	4-C	4-E
PTS-9	1	0	19.3	0	0	19.05	0
	2	20.04	3.4% gain	20	20.14	4.3% gain	19.86

b. PTS-21

Post-tensioning Scheme	Stage	Post-tensioning Force Applied to Region							
		1-B	1-D	2-B	2-D	3-B	3-D	4-B	4-D
PTS-21	1	19.49	19.47	0	0	0	0	18.63	18.66
	2	3.2% loss	3.0% loss	18.38	19.08	18.25	18.72	3.1% loss	2.9% loss

Table 4.3. (Continued)

c. PTS-22

Post-tensioning Scheme	Stage	Post-tensioning Force Applied to Region					
		1-C	4-C	2-B	3-B	2-D	3-D
PTS-22	1	0	0	19.27	19.27	19.11	19.11
	2	19.47	19.55	3.0% loss	3.0% loss	3.4% loss	3.1% loss

valent to those required for the prototype bridge. Although these gains or losses are small they should be included in the design of the strengthening system.

As vertical live loads are applied to a bridge strengthened by post-tensioning, forces will change in the tendons. For a simple span bridge, the tendon forces will always increase when a vertical load is applied unless the load is applied with extreme eccentricity with respect to the center line of the bridge, a condition which is impractical. Thus, in practice, the tendon force increases will provide additional post-tensioning when most needed.

For continuous bridges, the changes in tendon forces will not necessarily be beneficial. Figure 4.22 illustrates the exterior beam and interior beam tendon force changes for PTS-21, a scheme in which all negative moment regions were post-tensioned. In order to present the changes in force changes more clearly, the experimental points have been joined with lines; the lines do not represent a comparison with theory, as in earlier figures. Percentage changes in tendon force are given for nine different positions of a 6-kip vertical load. As the figure shows, most of the force changes are positive; however, there are a few load positions for which the changes are negative, which indicates a decrease in tendon force.

Figure 4.23 for PTS-9, in which all positive moment regions along exterior beams were post-tensioned, shows the tendon force changes for an end span tendon and for a center span tendon. The force changes are for the same 6-kip load and load points as used for constructing

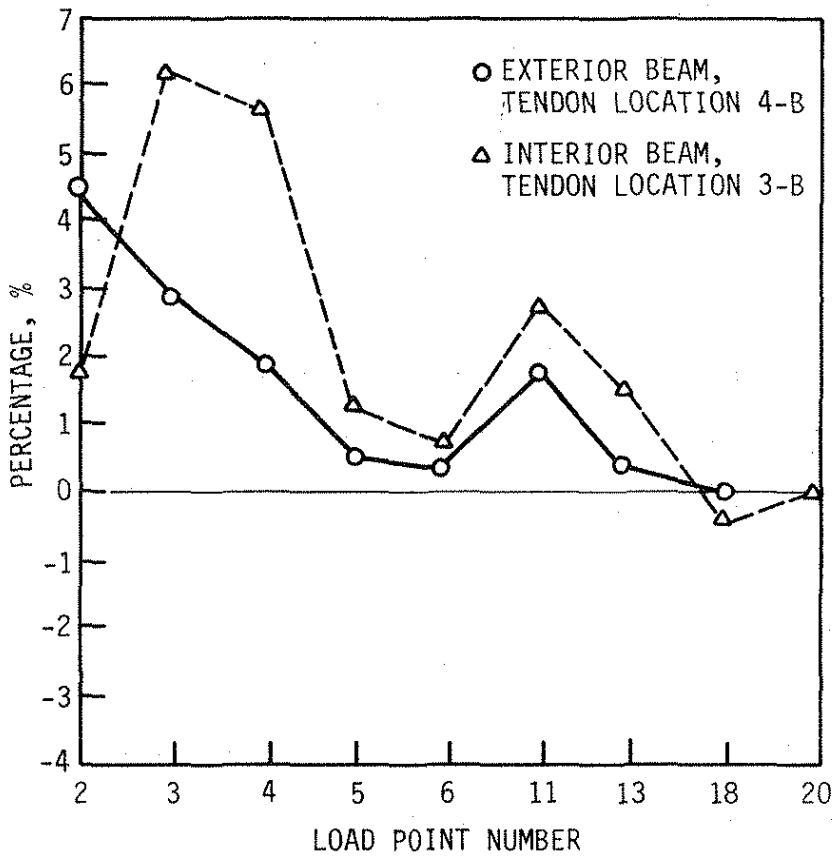

Fig. 4.22. Percent of increase or decrease in the tendon force for PTS-21.

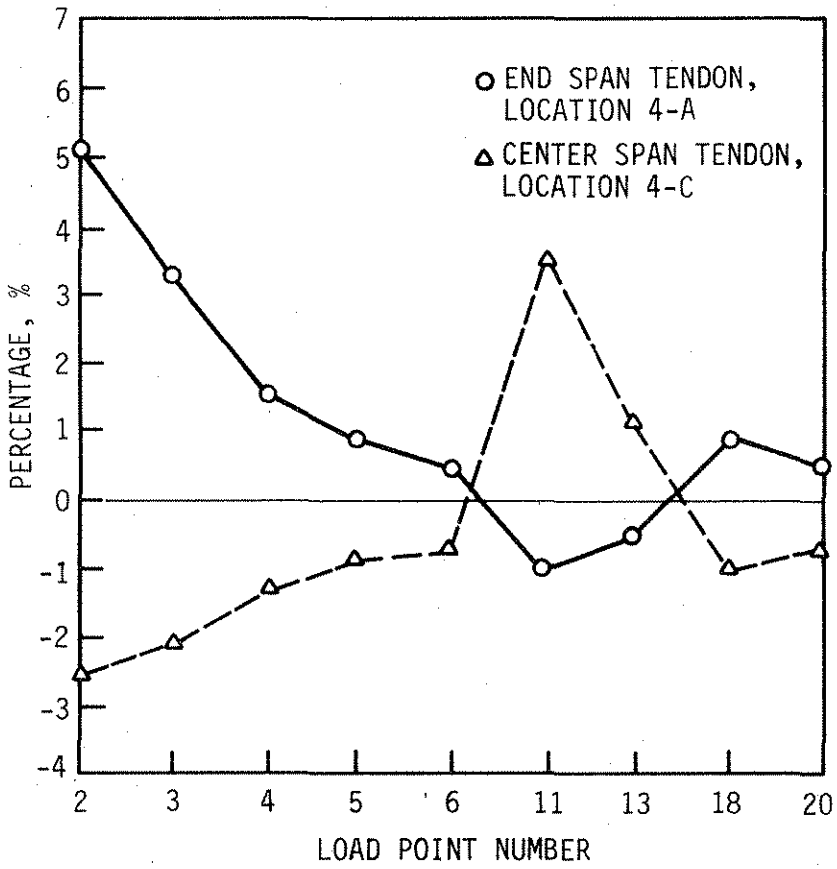

Fig. 4.23. Percent of increase or decrease in the tendon force for PTS-9.

Fig. 4.22. For many of the load points, Fig. 4.23 shows negative tendon force changes or losses in force.

For the continuous bridge model, the total tendon force change from negative to positive is approximately 20% of the applied load. For the simple span bridge model tested during previous research, the maximum tendon gain for a comparable extreme load position was approximately 10% of the applied load [19]. Thus there are larger changes in tendon force for the continuous bridge model. Part of the increased magnitude of the changes in tendon forces comes from locating the positive moment region tendons below the beams. Here they have more eccentricity than the tendons for the simple span bridge model. The remainder of the tendon force change is due to the flexibility of the bridge.

Because the tendon force changes are both positive and negative and the magnitude of the changes may be larger than for a simple span bridge, tendon force changes are an important factor to consider in designing the strengthening of continuous bridges by post-tensioning. Allowable stresses may have to be checked with maximum tendon force gain and maximum tendon force loss in order to provide adequate checks of the post-tensioning design.

4.1.5. Effects of Vertical Loads

In addition to the post-tensioning tests, the continuous bridge model in the ISU Structural Engineering Research Laboratory was subjected to a series of vertical load tests. The vertical load tests used one or two 6-kip vertical loads on the bridge deck at the load points shown in Fig. 3.4. The vertical load tests used one or two 6-

kip vertical loads on the bridge deck at the load points shown in Fig. 3.4. The vertical load tests were, for the most part, unsymmetrical. Only two were comparable to the symmetrical finite element analyses.

Bottom flange strains at Sections A, B, and C for two separate tests, with a single load at one load point in each test, are plotted in each of Figs. 4.24, 4.25, and 4.26. The experimental points in the figures are joined with lines in order to show the pattern of the strains from beam to beam across the bridge. In Fig. 4.24, the strains are plotted for the two loading conditions: a 6-kip load at LP1 and a 6-kip load at LP3. LP1 is located at the center of the end span of Beam 4, an exterior beam; and LP3 is located at the center of the end span of Beam 3, and interior beam. The patterns for the two loading conditions shown in Fig. 4.24a are very similar to those for a simple span bridge [19]. In each loading case the loaded beam has the largest strain, and the same general strain pattern is repeated in parts b and c of Fig. 4.24 for the first interior support and center span sections.

Figure 4.25 presents the strains for 6-kip loads at LP8 and LP10 at the center of the center span. Figure 4.25c for the strains at the loaded section is similar to Fig. 4.25a for the end span loaded section. Parts a and b of Fig. 4.25 are similar to the loaded section in Fig. 4.25c, in that the loaded beam has the largest strain.

Figure 4.26 presents the strains for 6-kip loads at LP15 and LP17 at the center of the second end span. None of the graphs in Fig. 4.26 are for a loaded section. The loaded beam in each of the graphs has the largest strain, as in Figs. 4.24 and 4.25, and Fig. 4.26c is the

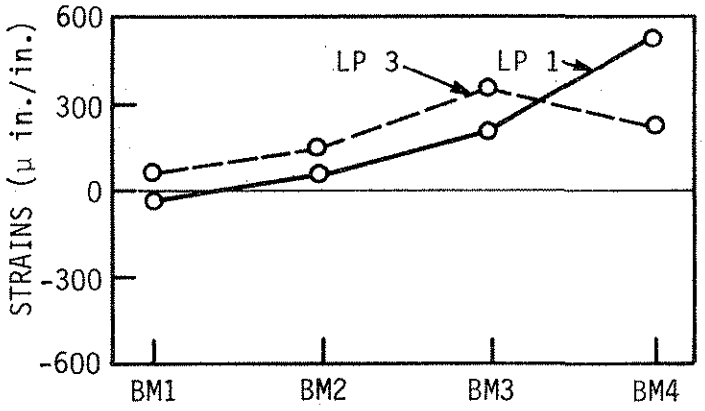

a. SECTION A

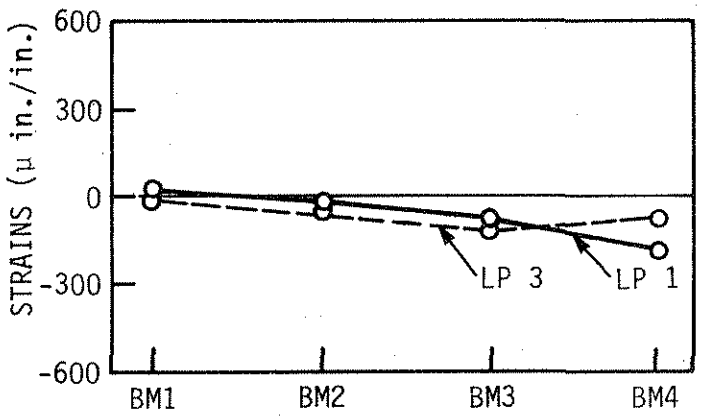

b. SECTION B

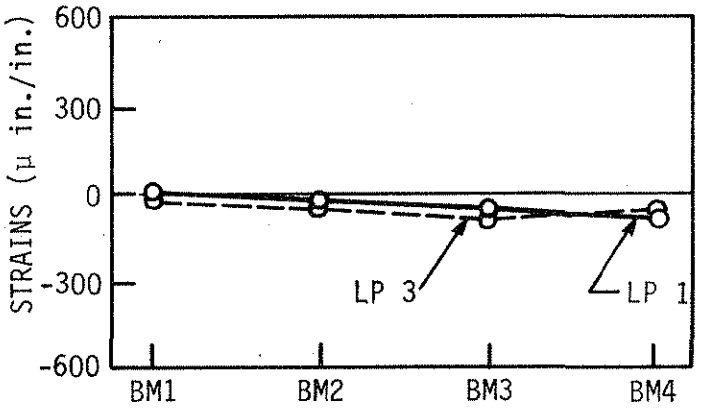

c. SECTION C

Fig. 4.24. Bottom flange strains for 6-kip vertical load at LP 1 and LP 3.

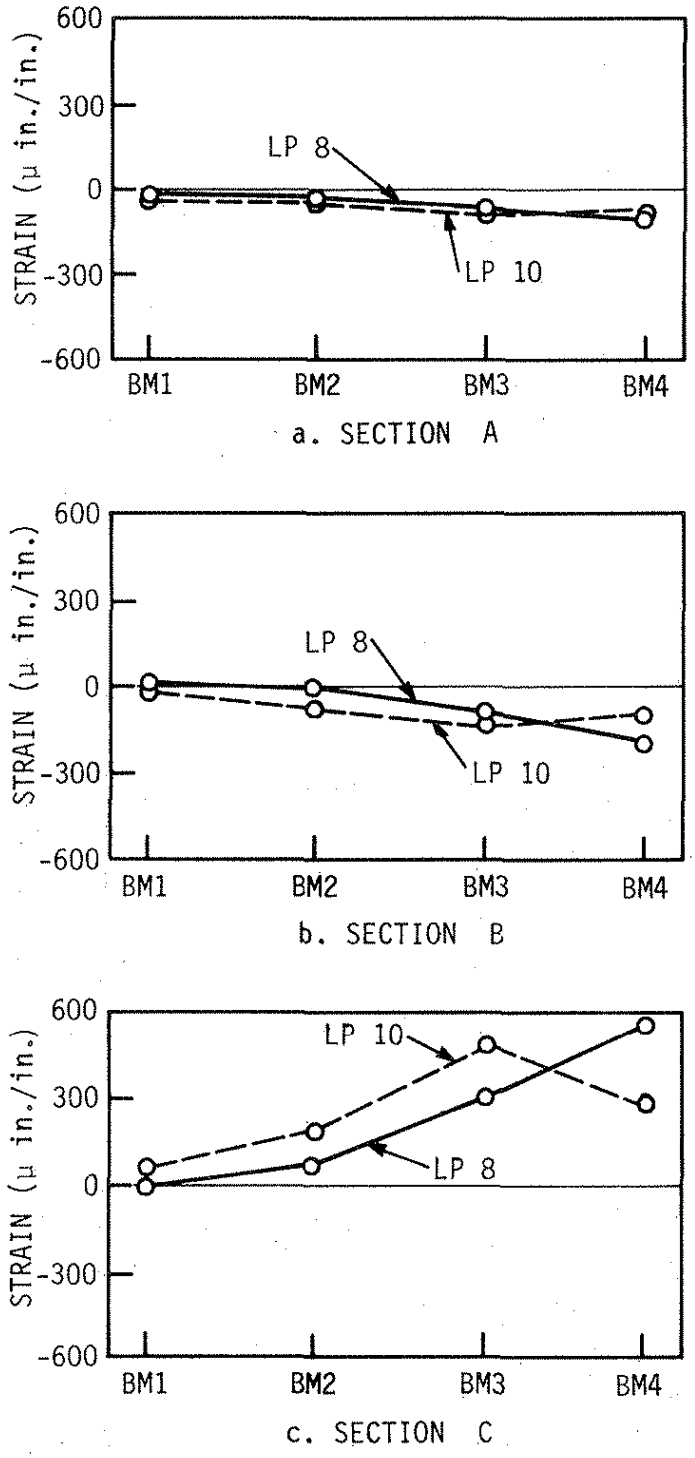

Fig. 4.25. Bottom flange strains for 6-kip vertical load at LP 8 and LP 10.

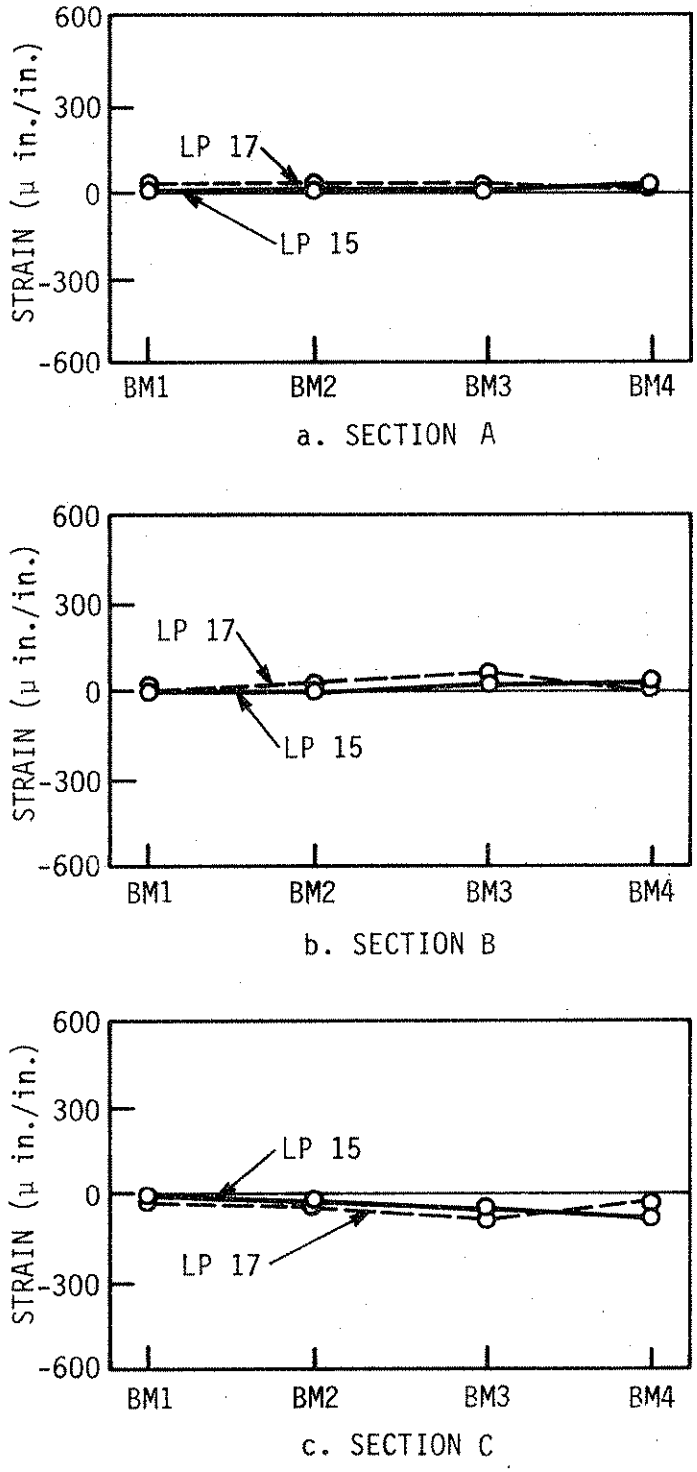

Fig. 4.26. Bottom flange strains for 6-kip vertical load at LP 15 and LP 17.

same as Fig. 4.24c, except for instrumentation errors and differences in distribution effects caused by construction imperfections in the model bridge.

The vertical load tests are quite consistent with similar tests for a simple span bridge model. The loaded beam generally has the highest bottom flange strain. A certain amount of the load is carried by all bridge beams.

4.2. Analysis and Test Results for the Full-scale Negative Moment Region Mockup

This section presents the data obtained from tests of the full-scale composite beam mockup. Three types of data are presented: deflections of the vertical load point or free end of the beam, strain distributions at two mockup sections, and tendon forces. The deflections for Tests 1 and 3 through 7 are taken at the application point of the vertical load, whereas the deflections for Tests 8 and 9 are taken at the free end of the beam. The deflections for Test 2 were taken both at the vertical load and at the free end. Therefore, the deflections for the two groups of tests cannot be compared directly. Strain distributions are shown for Section 4, which is at the support, and at Section 5, which is away from the support but within the coverplated region. The section locations are given in Fig. 3.7. Wherever possible, experimental results are compared with results from separate analyses in order to determine the extent of the composite action. In these cases either a coverplated steel section or a fully composite deck-beam section is assumed.

The maximum applied vertical load for the testing program was chosen to limit stresses in the steel beam and coverplates to 18 ksi compression or tension under the various test conditions. The limitation was chosen to minimize the potential for lateral or torsional buckling of the mockup beam because the beam was not laterally braced at the free end or the central support.

4.2.1. Analysis

Except for some minor practical limitations, the mockup beam was statically determinate until post-tensioning was applied and locked in placed and until the beam was deformed because of application of vertical load or other loads. The mockup was considered to have a hinged support at the hold-down end and a roller support at the central support or pier. The hold-down end support in reality was not a perfect hinge, and strain data indicated that there was a small amount of rotational restraint caused by the hold down. The end near which the vertical load was applied was a free end.

Because of the simplicity of the mockup, analysis was performed with ordinary statics and classical methods, and there was no attempt to analyze the mockup with finite element methods. For composite action, the concrete deck was reduced to an equivalent area of steel by using a modular ratio based on the relative moduli of elasticity of the concrete and steel. Deflection computations took into account the variation of moment of inertia along the beam.

4.2.2. Preliminary Vertical Load Tests

Initially, after the concrete deck was cured, the mockup beam was tested with cycles of vertical load during Test 1. Because the verti-

cal load applied a negative moment to the mockup and thus stressed the concrete deck in tension, the deck cracked at various locations. The effects of the deck cracking are indicated in Fig. 4.27, which contains a load-deflection graph for the first three load cycles.

Figure 4.27a illustrates the theoretical conditions for the test. As shown, the deflection was measured at the point at which the load was applied. The load-deflection curves in Fig. 4.27b clearly distinguish among the first three load cycles. During the first load cycle, the deck cracked directly above the central support at the location of maximum negative moment. Additional cracks occurred during the first load cycle, and each crack caused an immediate increase in beam deflection as well as an abrupt increase in strain in the top flange of the steel beam. After the first load cycle when the vertical load was totally removed, the mockup retained a permanent set. The permanent set increased with each load cycle; the final displacement, after the three cycles and the maximum vertical load had been applied and removed, was 0.28 in.

With each crack there was a transfer of tension stress to the deck reinforcing bars and a partial loss of composite action. The loss of composite action increased deflections as shown in Fig. 4.27b and also altered and increased strains measured in the steel beam. As will be indicated in subsequent figures, the mockup beam tended to behave with a certain amount of composite action that, from separate computations, is slightly larger than the amount predicted by considering the reinforcing bars in the deck to be acting with the steel beam.

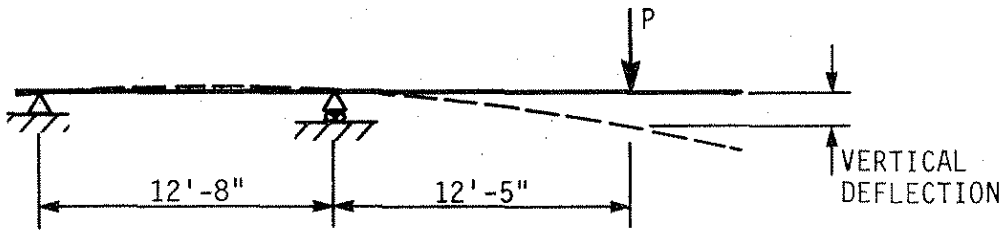

a. TEST SCHEMATIC

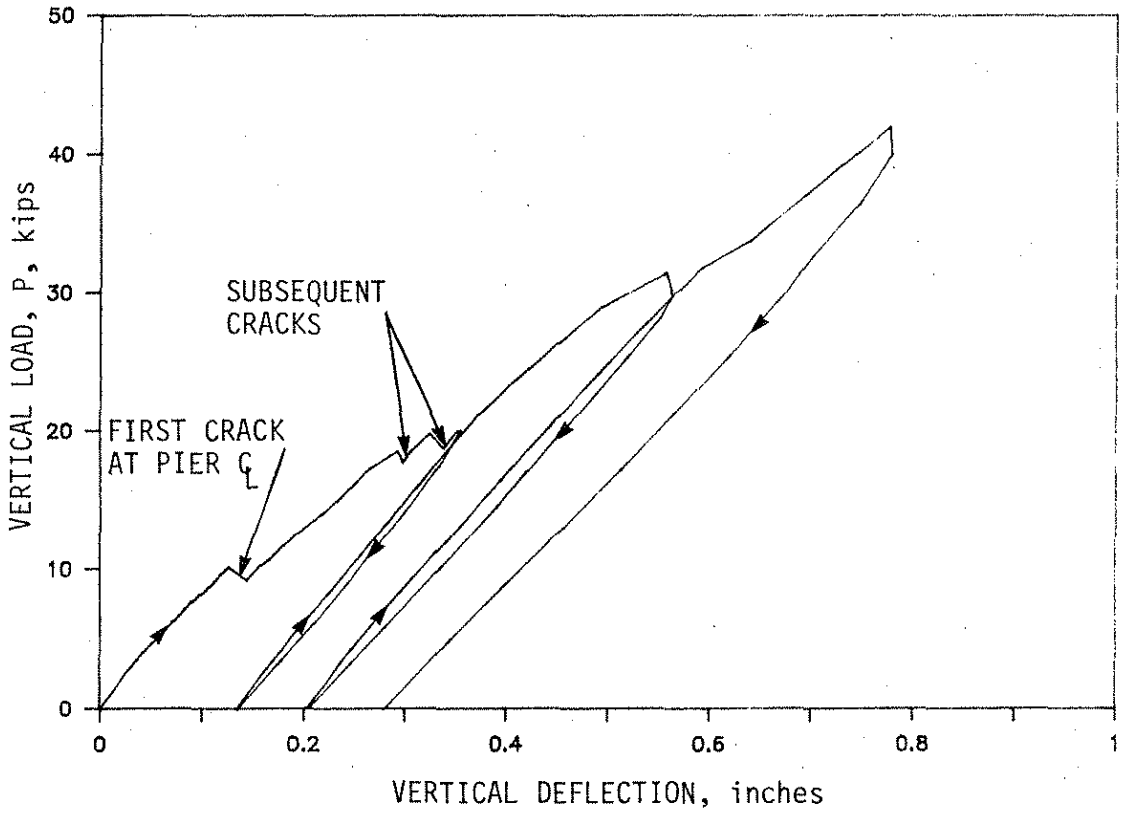

b. LOAD-DEFLECTION CURVES FOR THREE LOAD CYCLES

Fig. 4.27. Load-deflection curves for initial vertical loading, Test 1.

The final deck crack pattern is given in Fig. 4.28. Figure 4.28a gives the plan view of the deck with all of the significant cracks. The transverse cracks across the deck in the central portion of the mockup near maximum negative moment under vertical load are the most closely spaced, as one would expect. A comparison of Fig. 4.28a and 4.28b shows that the cracks generally do not occur at a shear connector. Cracks occur across the deck at the blockouts at which some of the longitudinal deck reinforcing bars are terminated and near which the coverplates are terminated.

There also are a few longitudinal cracks at the hold down and free ends of the mockup beam. The hold-down forces apparently were sufficient to cause radial cracking of the deck and thus indicate that substantial forces were applied with respect to deck strength.

Figure 4.28c (as well as Fig. 3.7) gives the numbered sections at which strain gages were located on the top and bottom flanges of the steel beam. Strain data to be presented later is taken from the gages at Section 4 near the support and at Section 5 which is within the coverplated region but near the coverplate cutoff.

4.2.3. Effects of Post-tensioning

In this section, the effects of post-tensioning will be demonstrated through strain diagrams. In the series of figures in this section, experimental data is plotted along with theory for the coverplated steel beam and the fully composite beam. In the figures, experimental data points are connected with lines to show the pattern of data and not to indicate that theoretical results match experimental results. The first test listed in the key below each graph is for the beam without

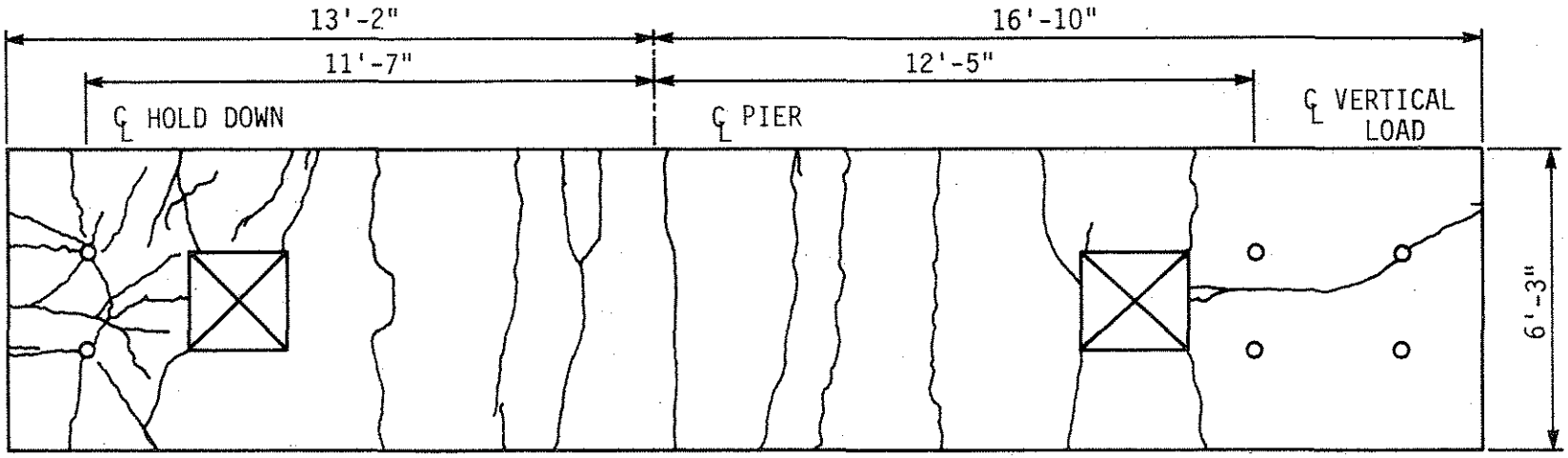

a. DECK CRACK PATTERN

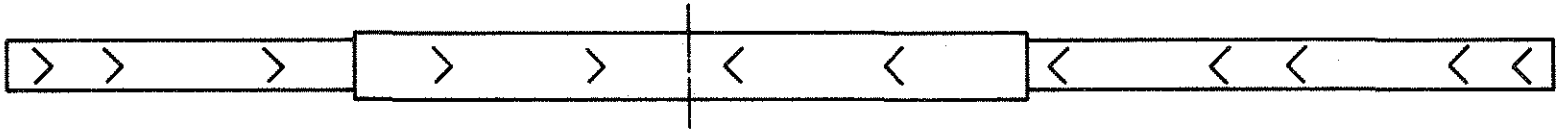

b. SHEAR CONNECTOR LOCATIONS

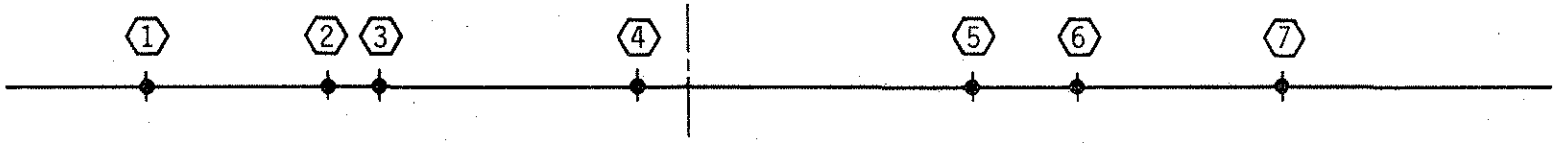

c. STRAIN GAGE SECTIONS

Fig. 4.28. Final crack pattern in full-scale mockup deck.

strengthening angles, and the second test listed is for the beam with strengthening angles.

Figure 4.29a gives the strains at Section 4 for the mockup with the straight tendons, and Fig. 4.29b gives the strains for the mockup with the harped tendons. Both graphs show that the experimental results fall between theoretical results for the coverplated steel beam and the fully composite beam. Both graphs also show that the strengthening angles added near the bottom flange of the mockup had beneficial effects in reducing compression strain on the bottom flange and in increasing compression strain on the top flange. The angles reduce the bottom flange compression strain by providing a larger cross-sectional area and by lowering the neutral axis and thus providing a larger eccentricity for the post-tensioning force. A detailed comparison of Figs. 4.29a for the straight tendon and 4.29b for the harped tendon indicates that the harped tendon provides more beneficial compression strain at the top flange; and even though better than the straight tendon, the harped tendon does add a small amount of compression strain to the bottom flange that is not beneficial.

The strain diagrams in Fig. 4.30 are the same as the strain diagrams in Fig. 4.29, except that those in Fig. 4.30 are for the strains measured at Section 5. The strains are almost the same at both sections, and all of the observations stated above for Fig. 4.29 apply to Fig. 4.30. The largest variations in experimental strains between the two sections are for the top flange strains, which are significantly affected by the cracks in the deck, and therefore some variations should be expected. In general, the experimental strains fall about midway

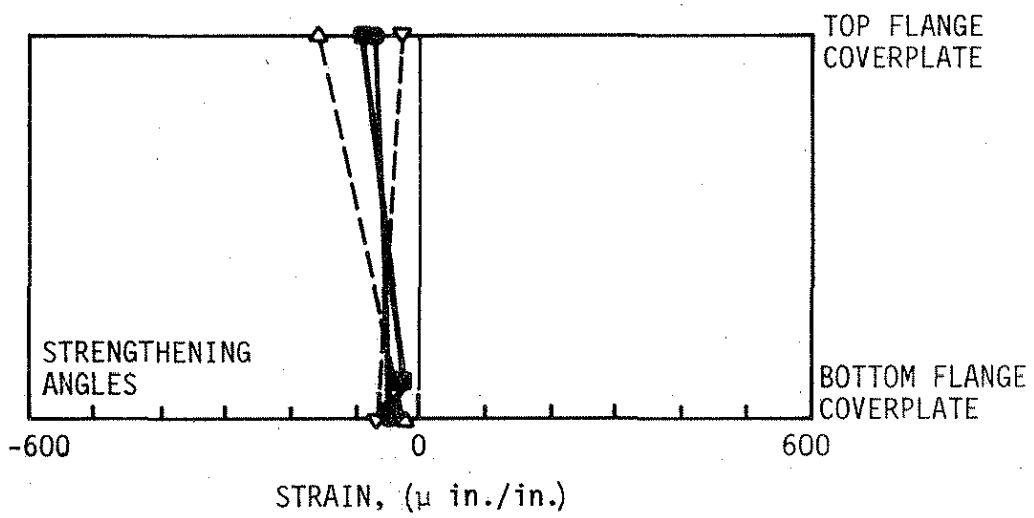

a. STRAIGHT TENDON

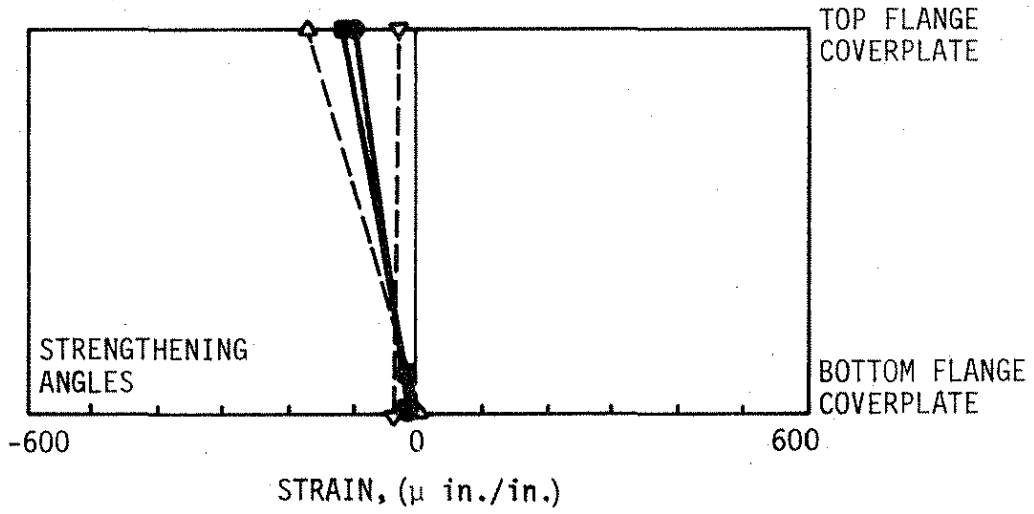

b. HARPED TENDON

Fig. 4.29. Strains at Section 4 for full-scale mockup with post-tensioning.

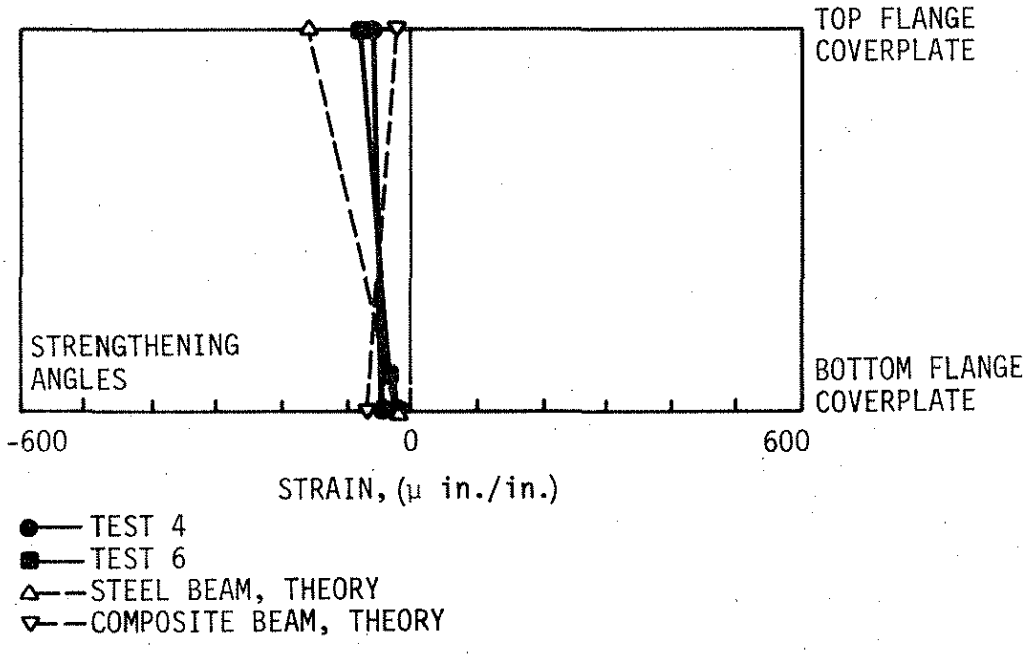

a. STRAIGHT TENDON

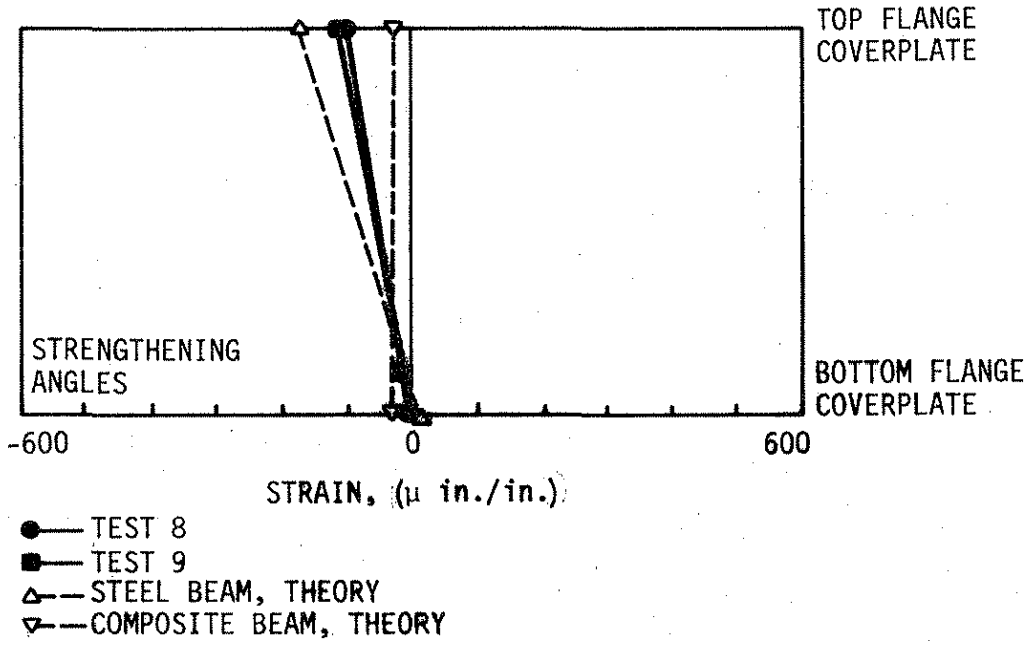

b. HARPED TENDON

Fig. 4.30. Strains at Section 5 for full-scale mockup with post-tensioning.

between the theoretical extremes of coverplated steel beams and fully composite beams. Thus there is only partial composite action in the mockup for the post-tensioning schemes applied.

4.2.4. Effects of Vertical Loads

This section presents the effects of vertical loads both with and without post-tensioning. A series of load-deflection curves are presented first and then a series of strain diagrams. Each of the graphs contains experimental data as well as theoretical results for the mockup beam without and with composite action.

Figure 4.31a illustrates the test conditions for the load-deflection curves given in Fig. 4.31b. For the tests with the straight tendon, the deflection was measured at the point of the applied vertical load.

The lowest curve in Fig. 4.31a gives the theoretical deflections for the steel beam with coverplates that is not post-tensioned, and the uppermost curve gives the theoretical deflections for the fully composite beam that is not post-tensioned. Both of the theoretical curves are for the mockup without the strengthening angles. Because the data for the mockup without strengthening angles and without straight tendon post-tensioning falls between the two theoretical curves, the mockup does have some composite action for vertical load, even with a cracked deck. In the tests without and with post-tensioning, the angles do stiffen the mockup. This is evidenced by the steeper slopes for the curves for the mockup with the angles in Tests 3 and 5, as opposed to Tests 2 and 4, respectively. The post-tensioning does produce a small amount of uplift indicated by the negative deflections. From theoretical computations for the straight tendon, the uplift indicates

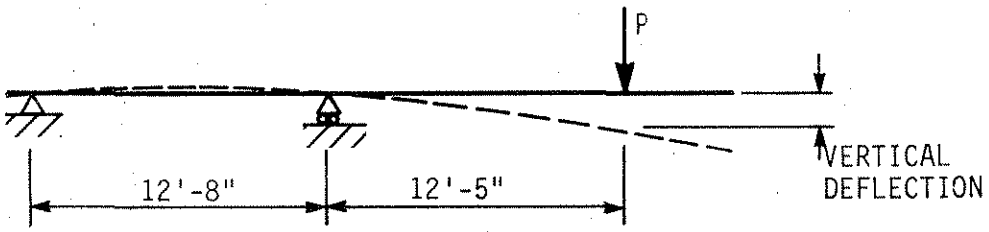

a. TEST SCHEMATIC

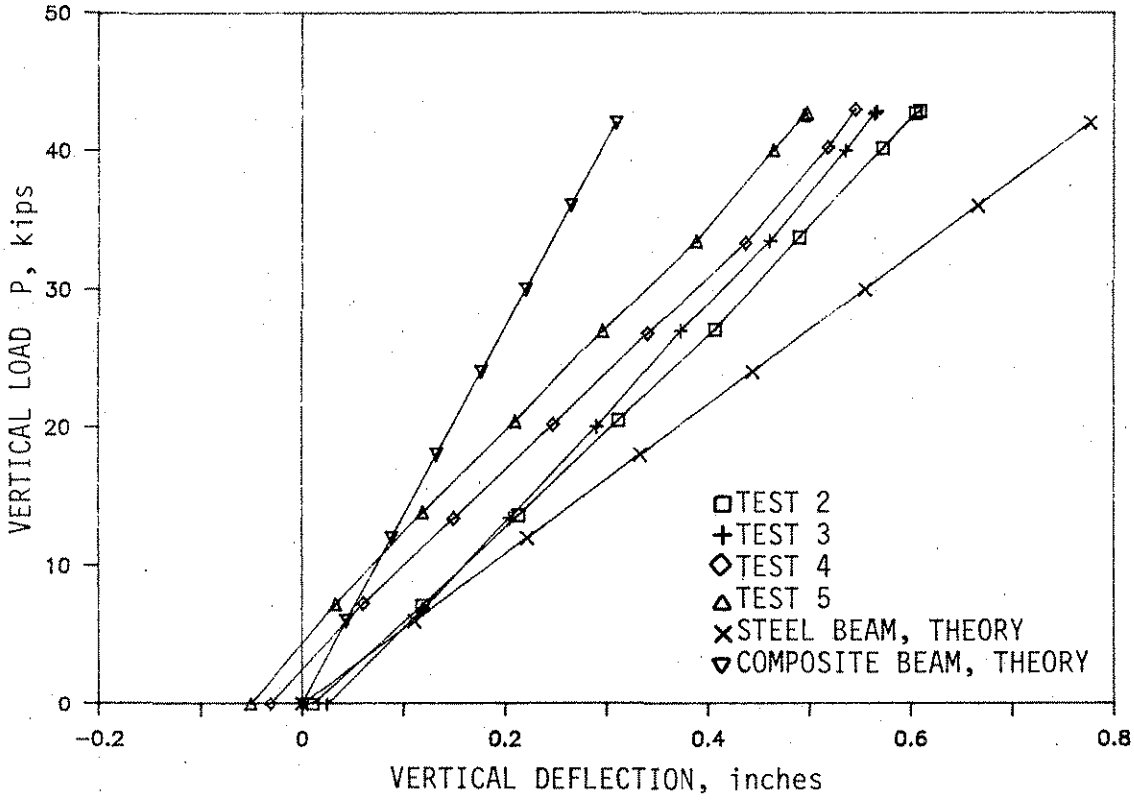

b. LOAD-DEFLECTION CURVES

Fig. 4.31. Load-deflection curves for straight tendon post-tensioning and vertical load.

that the mockup was not behaving as if fully composite because in that condition the mockup would deflect downward. The post-tensioning does not stiffen the mockup, however, because the slopes of the curves for post-tensioning are the same as the curves for the mockup without post-tensioning.

Figure 4.32 presents similar results to those in Fig. 4.31 but for the mockup with the harped tendon. The test schematic in Fig. 4.31a shows that the deflection is measured near the free end of the mockup rather than at the load point, and thus the deflections in Figs. 4.31 and 4.32 cannot be compared directly. The key given in Fig. 4.32b is as follows: Test 2 is for the mockup without post-tensioning; Test 8 is for the mockup with post-tensioning; and Test 9 is for the mockup with post-tensioning and strengthening angles.

The theoretical curves for the mockup (not post-tensioned) with and without composite action are the uppermost and lowest curves, respectively. The experimental curves show that post-tensioning causes uplift but does not stiffen the mockup. The curve for post-tensioning with angles, Test 9, and without angles, Test 8, indicate that the addition of the stiffening angles makes the mockup slightly more flexible. The effect is very small, but the effect seems to have no reasonable explanation.

The next series of figures presents the strain data taken at Sections 4 and 5 for the mockup with vertical load. In Figs. 4.33 and 4.34, the first graph in each figure is for the mockup without post-tensioning; the second graph in the figure is for the mockup with straight tendon post-tensioning; and the third graph in the figure is for the mockup with harped tendon post-tensioning.

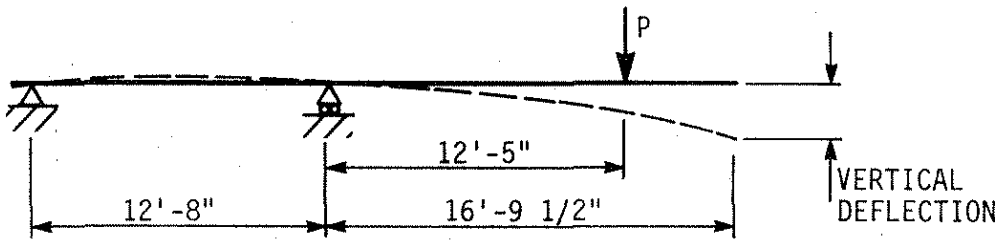

a. TEST SCHEMATIC

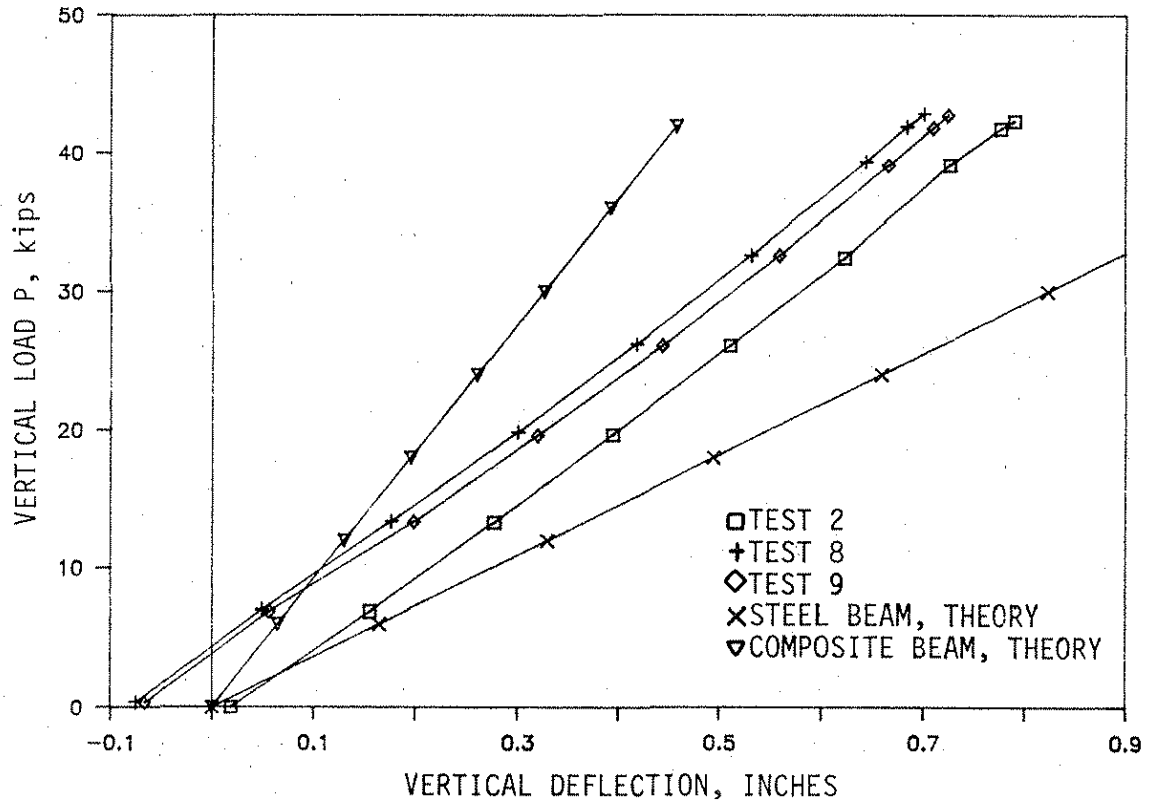

b. LOAD-DEFLECTION CURVES

Fig. 4.32. Load-deflection curves for harped tendon post-tensioning and vertical load.

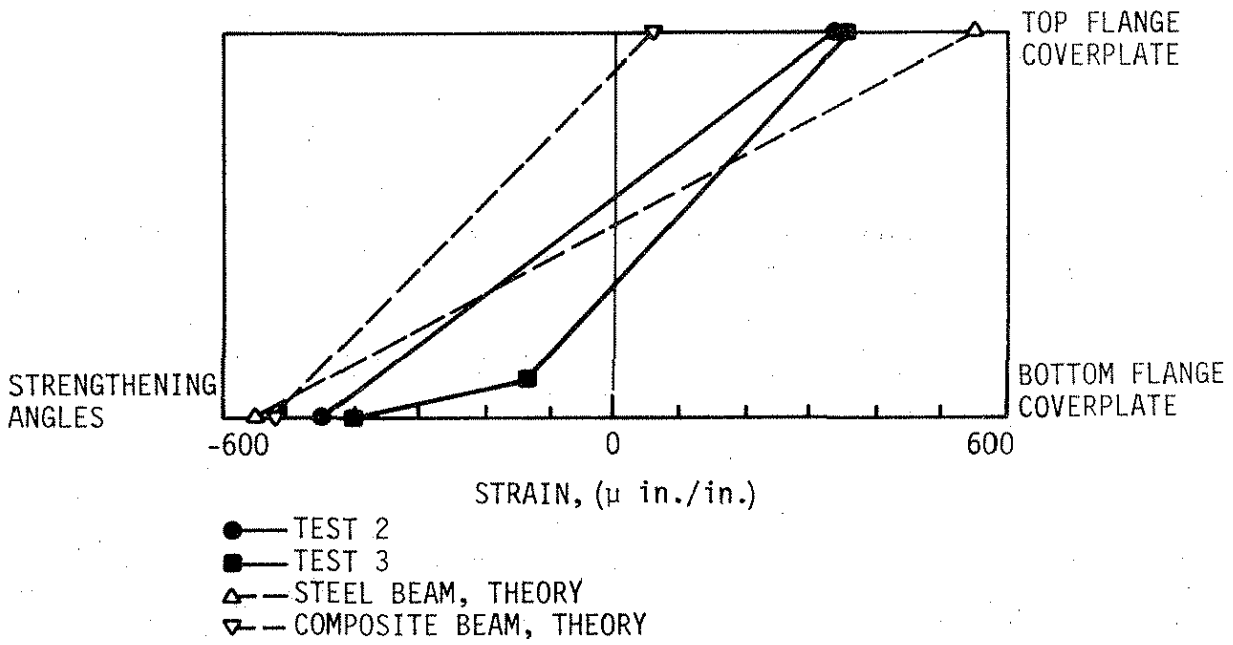

a. VERTICAL LOAD

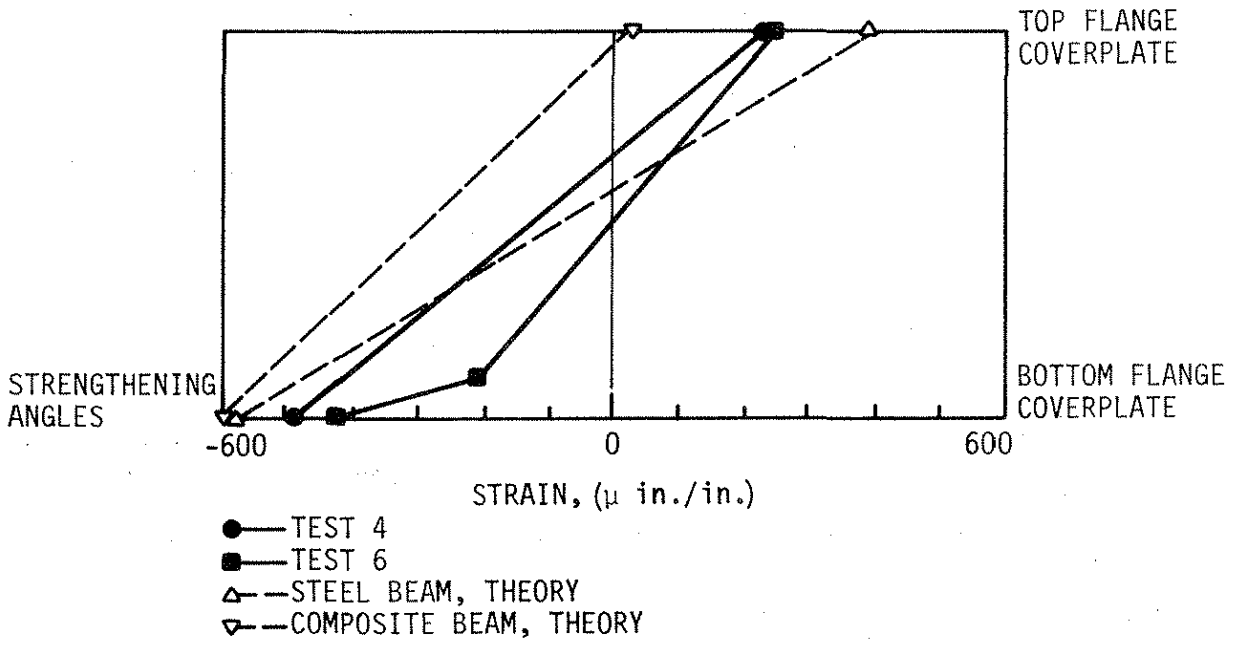

b. VERTICAL LOAD AND STRAIGHT TENDONS

Fig. 4.33. Strains at Section 4 for full-scale mockup with vertical load and post-tensioning.

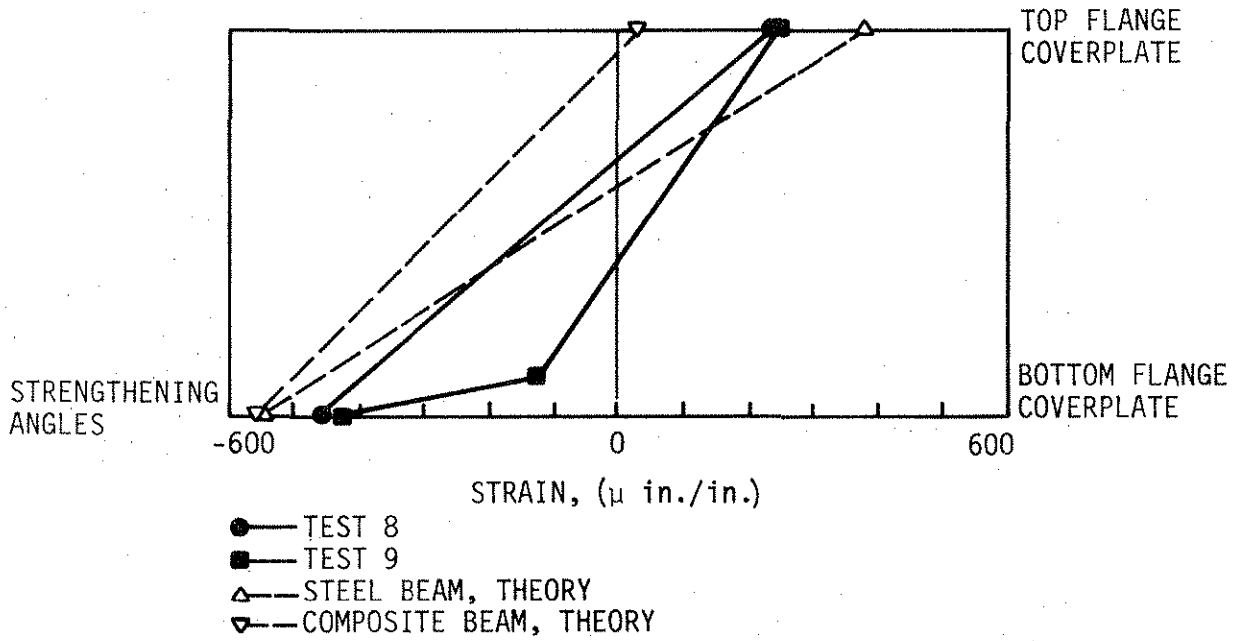

c. VERTICAL LOAD AND HARPED TENDONS

Fig. 4.33. Continued.

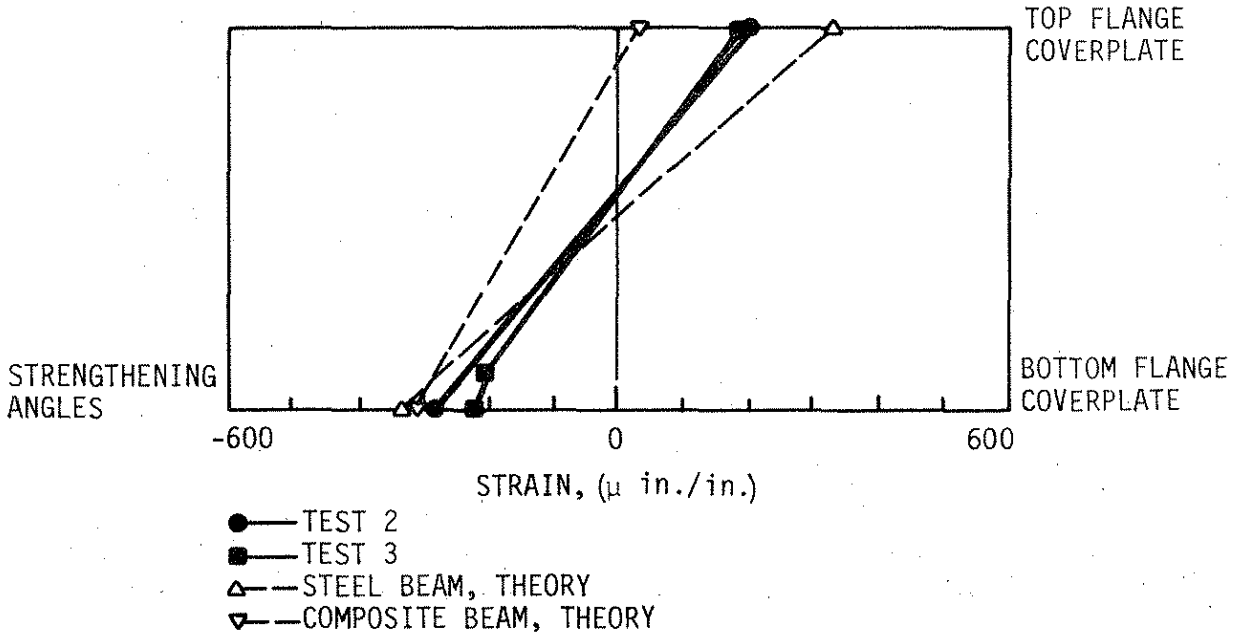

a. VERTICAL LOAD

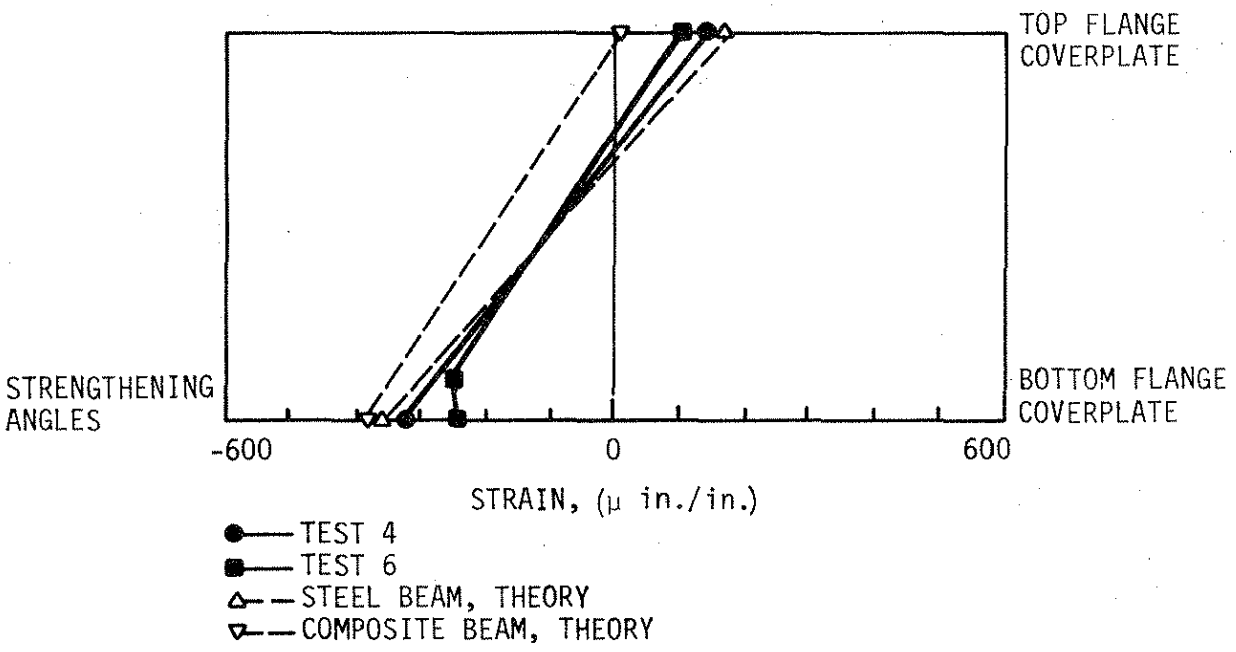

b. VERTICAL LOAD AND STRAIGHT TENDONS

Fig. 4.34. Strains at Section 5 for full-scale mockup with vertical load and post-tensioning.

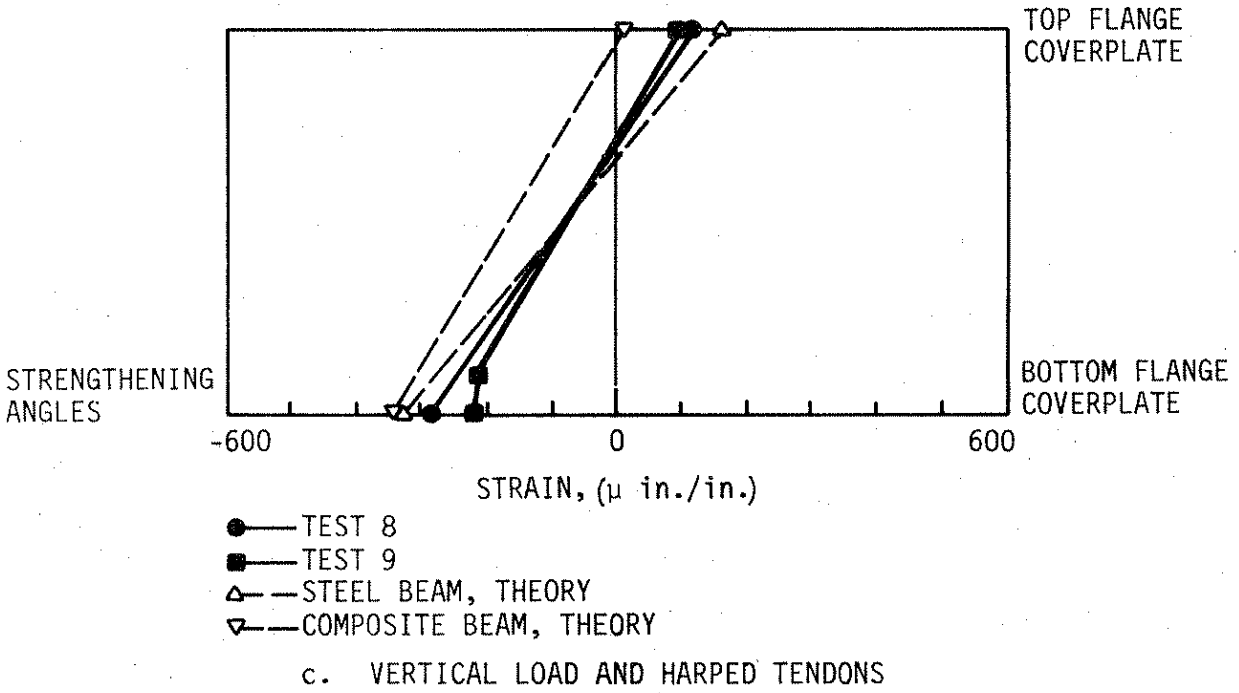

c. VERTICAL LOAD AND HARPED TENDONS

Fig. 4.34. Continued.

In Figs. 4.33a and 4.34a, the diagrams for the mockup with and without the strengthening angles show that the strengthening angles had some effect in reducing compression strain in the bottom flange but little effect in changing the strain at the top flange of the beam. The angles did shift the neutral axis downward on the steel beam.

A comparison of Figs. 4.33 and 4.34 shows that the strains measured in the strengthening angles at Section 4 do not align with strains measured in top and bottom flanges, but the strains measured in the angles at Section 5 very closely align with top and bottom flange strains. The fact that the strains do not align at Section 4 can be attributed to shear lag. Section 4 is very near the ends of the angles, and the stresses from the beam web have not been fully and uniformly distributed to the angles. This indicates that if stresses are critical at the support, it may be advisable to butt the angles to the stiffener and to transfer stresses to the angles through direct bearing.

The straight tendon post-tensioning, for which strain diagrams are given in Figs. 4.33b and 4.34b, increased the compression strains in the bottom flange and decreased the tension strains in the top flange. The same comment applies to the strain diagrams given for harped tendon post-tensioning in Figs. 4.33c and 4.34c. Although the change in strain for the top flange is beneficial, the change in strain for the bottom flange is not. Since 100 μ inches per inch is equivalent to 2.90 ksi, the post-tensioning applied to the mockup is not sufficient to overcome the overstresses in the prototype bridge, and larger tendon forces would be required even without considering longitudinal distribution effects.

Figures 4.33 and 4.34 show the measured top flange strains to fall about halfway between the theoretical conditions, as in Figs. 4.29 and 4.30. The bottom flange strains in Figs. 4.33 and 4.34 fall outside of the theoretical extremes by 15% to 20%, however. There is actually less compression strain for vertical load than computed. This behavior might be explained by the mockup beam having one flange that was heavily corroded or by changing composite action within the mockup as vertical load is increased; however, no definitive reason for the behavior has been determined at this time. Further analysis of the unexplained behavior will be included in Reference 30.

4.2.5. Tendon Force Changes

After post-tensioning has been applied to a beam such as the mockup, any change in deformation of the beam will cause a change in tendon force. The tendon force changes for the mockup under straight tendon and harped tendon post-tensioning are given in Fig. 4.35. In Fig. 4.35a the upper two curves give the change in tendon force for the straight tendons, and the lower two curves give the change in tendon force for the harped tendons. The schematic given in Fig. 4.35b indicates that the upper portion of each curve, showing increase in vertical load, was plotted first; the lower portion, showing decrease in vertical load, was plotted second. The gap between the two portions of each curve at zero load is the seating loss at the anchorages of the tendons.

Tension in the straight tendons increases by about 5% with application of the maximum vertical load; but tension in the harped tendons increases by about 2%. The lower curve for the mockup with straight tendons and strengthening angles rises more steeply than the curve for

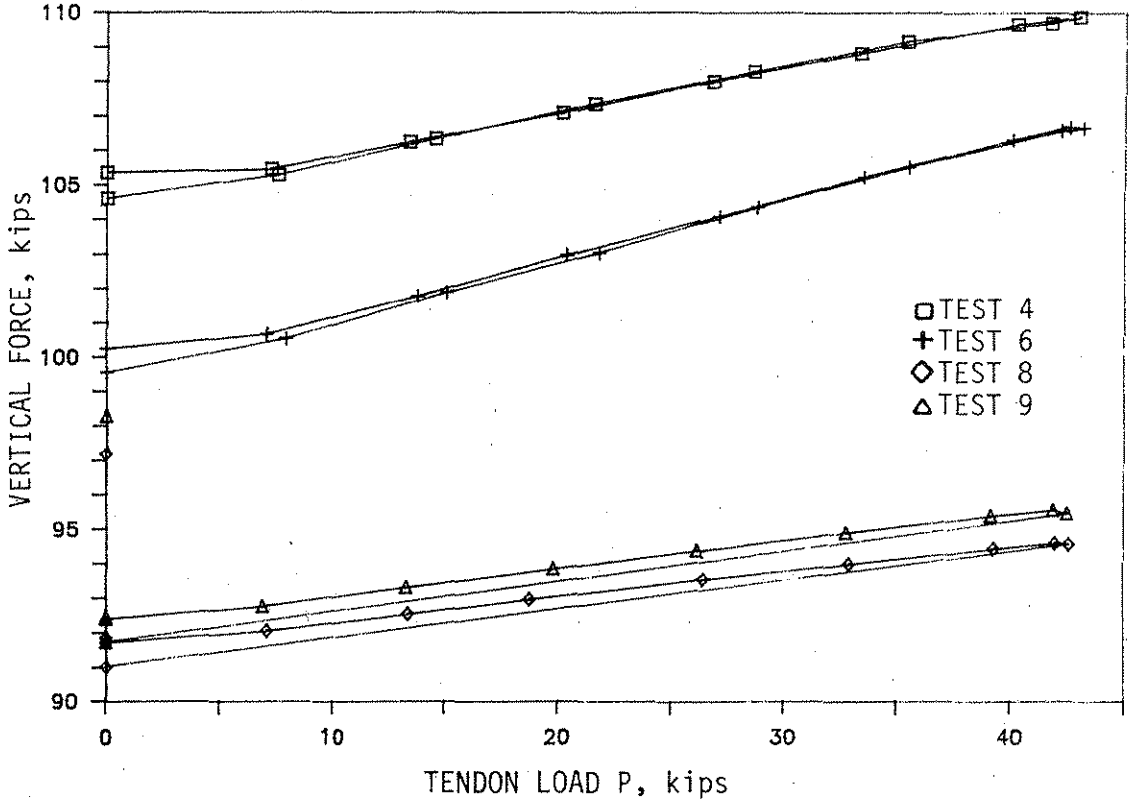

a. TENDON FORCE VS. VERTICAL LOAD

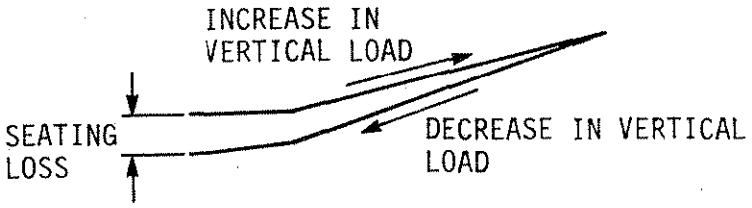

b. PLOT SCHEMATIC

Fig. 4.35. Change in tendon force.

the mockup without the angles. The change in slope is caused by the angles lowering the neutral axis of the mockup and thereby increasing the eccentricity of the tendon and its sensitivity to bending deformations in the mockup. There is a similar change in slope for the harped tendon curves, but those curves are reversed in position with respect to the straight tendon curves.

5. SUMMARY AND CONCLUSIONS

5.1. Summary

This report summarizes the research that has been completed in an initial phase of investigation of strengthening of continuous, composite bridges by post-tensioning. The research program included reviewing the literature, selecting and rating a prototype bridge, constructing and testing a one-third scale model of the prototype, using finite analysis on the scale model, and testing a full-scale mockup of the negative moment region of a bridge beam.

The literature review involved a search of publications from both the United States and foreign countries. Twenty-one examples of post-tensioned structures were reviewed in some detail as typical of the many published concepts and applications of post-tensioning. Although the examples emphasized the use of post-tensioning for strengthening composite structures, examples for new construction and reinforced concrete, prestressed concrete, and steel structures were given in order to cover a wide range of concepts and applications that may be of use for strengthening continuous, composite bridges.

The primary purpose of strengthening continuous bridges by post-tensioning must be to reverse the moments and resulting stresses from service loads. This purpose may be accomplished with a variety of tendon configurations, including straight and harped tendons of full length or partial length with respect to the bridge. When negative moment regions above supports are post-tensioned, it is often necessary to add compression reinforcing to carry the axial force applied by the

post-tensioning. Longitudinal distribution of post-tensioning moments is considered in the usual design process; however, previous to this study, transverse distribution of post-tensioning has been avoided through staged post-tensioning or post-tensioning all bridge beams equally.

A secondary purpose for post-tensioning could be the assurance of dependable composite action throughout a bridge. Some testing of the concept has been completed recently, and at least one bridge has been designed and constructed on the basis of composite action throughout the bridge, including the negative moment regions.

With the assistance of the Office of Bridge Design at the Iowa DOT, a bridge from the V12(1957) series of standard, four-beam, composite bridges was selected as the prototype for the laboratory model. The selected 125-foot long V12(1957) bridge was rated for bending stress. The rating determined that there were overstresses at all critical positive and negative moment sections. Both exterior and interior beams were overstressed, although the overstresses generally were larger for the exterior beams.

On the basis of the 125-foot long prototype, a one-third scale model was constructed and tested in the ISU Structural Engineering Research Laboratory. Beams for the model were built up from plate and strip, in order to achieve an accurate scale representation of the actual bridge beams. The concrete deck was poured in accordance with sequence instructions on the prototype plans. After the deck had cured, the model was vertically restrained at supports to prevent beams from lifting as a result of the low model weight and various cases of applied

loading. The model was fitted with tabs for tendon brackets below the beams in positive moment regions of exterior beams and with tabs for tendon brackets above the deck in all negative moment regions.

The bridge model was tested extensively over several months with both unsymmetrical and symmetrical post-tensioning and vertical loads. Unsymmetrical post-tensioning schemes generally gave desirable strains in post-tensioned regions but undesirable strains in some of the other regions. Most symmetrical post-tensioning schemes gave desirable strains in all regions of the bridge model. Because the neutral axis for the composite sections was very close to the bottom of the deck, the strains generated by post-tensioning were largest at the bottom flanges of the beams.

On the basis of earlier research at ISU for strengthening simple span bridges, a finite element model was developed for symmetrical post-tensioning and loading cases. With the finite element model, it was possible to analyze some post-tensioning schemes that had to be omitted from the model test program due to time and budget limitations. In general, the finite element model gave strains and deflections that closely matched those from the laboratory tests. Most of the symmetrical cases, in which positive moment regions were post-tensioned and which were summarized in this report, would be of use in practical situations for strengthening exterior beams, interior beams, or all of the beams in a given bridge.

For determining the potential for post-tensioning negative moment regions above interior supports, a full-size composite beam mockup was constructed and tested in the laboratory. Two different tendon con-

figurations were tested: a straight tendon placed near the underside of the deck and a harped cable tendon. Both tendons were tested without and with strengthening angles bolted to the beam web near the lower flanges of the beam.

In the research program, the post-tensioning schemes investigated had limited strengthening value. Both the straight and harped tendon schemes added beneficial and significant compression to the top flange of the mockup. Neither scheme significantly reduced the compression in the bottom flange, however. In fact, the post-tensioning actually added a small amount of compression to the bottom flange in most cases. The harped tendon configuration was slightly better than the straight tendon configuration, and the strengthening angles were beneficial for both tendon configurations.

Under both post-tensioning and vertical loading the mockup behaved with partial composite action. The amount of the composite action was approximately halfway between the extremes of no composite action and full composite action. Substantially larger post-tensioning forces than those applied to the beam during testing would be required in order to assure full composite action in negative moment regions.

The brackets utilized with both straight tendons and harped tendons performed well during the mockup testing program. Although the harped tendon brackets performed well, after testing it appeared that some modifications could be made in order to improve construction procedures and to place the tendons closer to the beam web. Those modifications would involve use of the original beam splices at the dead load inflection points.

5.2. Conclusions

The following conclusions were developed as a result of this study:

(1) The primary objective in applying post-tensioning to a composite bridge for strengthening should be to reverse the service load moment effects. In order to achieve this objective, straight tendons must be attached with a significant eccentricity. In practice, in most situations, this would mean placing tendons within positive moment regions on the spans of a continuous bridge.

(2) When post-tensioning is applied, both longitudinal and transverse distribution must be considered. Longitudinal distribution ordinarily will be considered during the analysis of the bridge as a series of individual continuous beams. Moment diagrams for the beams will show that the moments transmitted to the bridge are dependent on the location of post-tensioning brackets with respect to supports and that the moments will be distributed to both positive and negative moment regions. Transverse distribution must be considered only when some of the beams are post-tensioned or when all of the beams are not post-tensioned equally.

(3) Unsymmetrical post-tensioning of a continuous bridge, whether unsymmetrical longitudinally or transversely will cause some undesirable stresses. In many cases the undesirable stresses will be significant.

(4) Post-tensioning of negative moment regions with straight tendons will generally apply primarily an axial force. Although addition of compression strengthening angles or plates may give some eccentricity, the eccentricity will be much smaller than that which can be obtained in the positive moment regions; thus, post-tensioning of negative moment regions with straight tendons is unlikely to be effective.

(5) Post-tensioning of negative moment regions with harped tendons is more effective than post-tensioning with straight tendons, but the difference found in this study was small.

(6) Depending upon the position of the applied vertical loading, the change in the post-tensioning force in the tendons may be a gain or a loss. Thus, this change must be carefully taken into account when a post-tensioning strengthening scheme is designed for a given bridge.

6. RECOMMENDED FURTHER RESEARCH

On the basis of the literature review, model and mockup testing, and finite element analysis, it would be logical to continue this strengthening research as follows:

(1) Strengthening composite bridges of the type investigated in this study by post-tensioning is feasible; the next logical step would be to design and implement post-tensioning for an actual bridge. The strengthening for the bridge should be initially tested and then monitored for a period of several years to insure that no unforseen problems develop.

(2) If one assumes that the implementation phase of the strengthening is successful, there will be need for a design procedure for strengthening continuous composite bridges that is similar to the procedures presented in the manual [10] provided to the Iowa DOT for strengthening simple span composite bridges.

(3) It may be possible to strengthen a composite bridge by post-tensioning all beams in the regions above the interior supports to achieve composite action throughout the bridge. Both analytical work and field testing of this concept would be needed before it could be implemented.

7. ACKNOWLEDGMENTS

The study presented in this report was conducted by the Bridge Engineering Center under the auspices of the Engineering Research Institute of Iowa State University. The research was sponsored by the Highway Division, Iowa Department of Transportation, and the Iowa Highway Research Board under Research Project HR-287.

The authors wish to acknowledge the assistance and donations of prestressing materials from the following persons and organizations:

- Jessie G. Barrido, PE, and Eugene Lamberson, PE, of Dywidag Systems International USA, Inc., Lemont, Illinois
- Greg Gear, PE, of Prestressed Concrete Operations, Iowa Falls, Iowa.

The authors extend sincere appreciation to the engineers of the Iowa DOT for their support, cooperation, and counseling. A special thanks is extended to the following individuals for their help in various phases of the project:

- William A. Lundquist, Bridge Engineer
- John P. Harkin, Bridge Rating Engineer
- Vernon J. Marks, Research Engineer
- Thomas L. Ries, Assistant Resident Engineer

The county engineers' offices in the following counties assisted in locating V12 and other composite, continuous bridges: Benton, Boone, Carroll, Greene, Guthrie, Hamilton, Polk, Story, and Webster.

Special thanks are accorded the following students for their assistance in various phases of the project: graduate student Douglas

L. Wood, and undergraduate students Joann Hansen, Mark Henderson, Darin Johnson, Roger Khoury, and Pamela Pierce.

8. REFERENCES

1. American Association of State Highway and Transportation Officials. Manual of Maintenance Inspection of Bridges 1978. Washington: American Association of State Highway and Transportation Officials, 1979.

2. American Association of State Highway and Transportation Officials. Standard Specifications for Highway Bridges, 13th Edition. Washington: American Association of State Highway and Transportation Officials, 1983.

3. Bathe, K.-J., E. L. Wilson, and F. E. Peterson. SAP IV, A Structural Analysis Program for Static and Dynamic Response of Linear Systems. Berkeley: College of Engineering, University of California, 1974.

4. Blakeley, R. W. G., R. S. Dowsing, R. J. Dunlop, R. J. Preston, and K. J. Thompson. "The Road to Motunui." The Institution of Professional Engineers New Zealand: Transportation, Vol. 12, No. 2/CE, July 1985, pp. 104-119.

5. Brodka, J., K. Jerka-Kulawinska, and M. Kwasniewski. Prestressed Steel Members--Static Computations. (Vorgespannte Stahltraeger--Statische Berechnung.) Koeln-Braunsfeld: Verlagsgesellschaft Rudolf Mueller, 1968 (German).

6. Brodka, J., and J. Klobukowski. Prestressed Steel Construction. (Vorgespannte Stahlkonstruktionen.) Berlin: Wilhelm Ernst & Sohn, 1969 (German).

7. Daoud, F. K. "Experimental Strengthening of a Three-Span Composite Model Bridge by Post-Tensioning." M.S. Thesis, Iowa State University, Ames, Iowa, 1987.

8. DeBuck, J., T. Van Essche, D. Van Gemert, K. Gamski, R. Degeimbre, J. M. Rigo, and J. Wiertz. "Conception, Computation and Test Program for the Repair of Two Prestressed Concrete Bridges." (Konceptie, Berekening en Proefprogramma voor de Herstelling van Twee Bruggen in Voorgespannen Beton.) Tijdschrift der Openbare Werken van Belgie, No. 2, 1981, pp. 1-35 (Flemish and French).

9. Dunker, K. F., F. W. Klaiber, B. L. Beck, and W. W. Sanders, Jr. "Strengthening of Existing Single-Span Steel-Beam and Concrete Deck Bridges. Final Report--Part II." ERI Project 1536, ISU-ERI-Ames-85231. Ames: Engineering Research Institute, Iowa State University, Ames, Iowa, 1985.

10. Dunker, K. F., F. W. Klaiber, and W. W. Sanders, Jr. "Design Manual for Strengthening Single-Span Composite Bridges by Post-tensioning. Final Report--Part III." ERI Project 1536, ISU-ERI-Ames-85229. Ames,: Engineering Research Institute, Iowa State University, 1985.

11. Engelbach. "Report on the Strengthening of the Bridge over the Main River at Hochheim on the Federal Autobahn Wiesbaden-Hochheim." (Erfahrungsbericht ueber die Verstaerkungsarbeiten an der Mainbruecke Hochheim (Vorlandbruecke) im Zuge der Bundesautobahn Wiesbaden-Hochheim (A 671). Wiesbaden: Hessisches Landesamt fuer Strassenbau, 1984 (German).

12. Ferjencik, P., and M. Tochacek. Prestressing in Steel Structures. (Die Vorspannung im Stahlbau.) Berlin: Wilhelm Ernst & Sohn, 1975, (German).

13. Hoadley, P. G. "The Nature of Prestressed Steel Structures." Highway Research Report 200, Highway Research Board, 1967, pp. 11-26.

14. Holzapfel, M. W. Keim, J. Saettele, and A. Strobele. "Origin and Repair of Crack Damage in a Prestressed Concrete Bridge." (Entstehung und Beseitigung von Rissschaden an einer Spannbeton-bruecke.) Beton- und Stahlbetonbau. Vol. 78, No. 6, June 1983, pp. 162-164 (German).

15. Jungwirth, D., and G. Kern. "Long-Term Maintenance of Prestressed Concrete Structures--Prevention, Detection, and Elimination of Defects." (Langzeitverhalten von Spannbeton Konstruktionen--Verhueten, Erkennen und Beheben von Schaden.) Beton- und Stahlbetonbau, Vol. 75, No. 11, November 1980, pp. 262-269 (German).

16. Kandall, C. "Increasing the Load-Carrying Capacity of Existing Steel Structures." Civil Engineering, Vol. 38, No. 10, October 1968, pp. 48-51.

17. Kennedy, J. B., and N. F. Grace. "Prestressed Decks in Continuous Composite Bridges." Journal of the Structural Division ASCE, Vol. 108, No. ST11, November 1982, pp. 2394-2410.

18. Klaiber, F. W., D. J. Dedic, K. F. Dunker, and W. W. Sanders, Jr. "Strengthening of Existing Single Span Steel Beam and Concrete Deck Bridges. Final Report--Part I." ERI Project 1536, ISU-ERI-Ames-83185. Ames: Engineering Research Institute, Iowa State University, 1983.

19. Klaiber, F. W., K. F. Dunker, and W. W. Sanders, Jr. "Feasibility Study of Strengthening Existing Single Span Steel Beam Concrete Deck Bridges." ERI Project 1460, ISU-ERI-Ames-81251. Ames: Engineering Research Institute, Iowa State University, 1981.

20. Klaiber, F. W., K. F. Dunker, T. J. Wipf, and W. W. Sanders, Jr. "Methods of Strengthening Existing Highway Bridges. Preliminary Draft II, Final Report." ERI Project 1809. ISU-ERI-Ames-88040. Ames: Engineering Research Institute, Iowa State University, 1987.

21. Lecroq, P. "Additional Prestressing." (Precontrainte additionelle.) Annales de L'Institute Technique du Batiment et des Travaux Publics, No. 411, January 1983, pp. 96-103 (French).

22. Mancarti, G. D. "Strengthening California's Steel Bridges by Prestressing." Transportation Research Record 950, Transportation Research Board, 1984, pp. 183-187.

23. Mueller, T. "Alteration of the Highway Bridge over the Aare River in Aarwangen." (Umbau der Strassenbruecke ueber die Aare in Aarwangen.) Schweizerische Bauzeitung, Vol. 87, No. 11, March 13, 1969, pp. 199-203 (German).

24. "Sagging Erskine to Get a Rise." New Civil Engineer, No. 182, February 26, 1976, p. 9.

25. Tachibana, Y., K. Kondo, and K. Ito. "Experimental Study on Composite Beams Prestressed with Wire Cables." Final Report, International Association for Bridge and Structural Engineering, 7th Congress, Rio de Janeiro, August 10-16, 1964, pp. 677-683.

26. Troitsky, M. S., Z. A. Zielinski, and M. S. Pimprikar. "Experimental Evaluation of Prestressed Steel Plate Girder Bridges." Experimental Assessment of Performance of Bridges, Proceedings. Boston, Massachusetts, October 27, 1986, pp. 1-16.

27. United States Steel. "Bonners Ferry Bridge, Boundary County, Idaho, USS Bridge Report." Pittsburgh: United States Steel, 1985.

28. Vernigora, E., J. R. M. Marcil, W. M. Slater, and R. V. Aiken. "Bridge Rehabilitation and Strengthening by Continuous Post-Tensioning." Journal of the Prestressed Concrete Institute, Vol. 14, No. 2, April 1969, pp. 88-104.

29. Virlogeux, M. "External Prestressing." (La precontrainte exterieure.) Annales de L'Institut Technique du Batiment et des Travaux, No. 420, December 1983, pp. 115-124 (French).

30. Wiley, William E. "Post-tensioning of Composite T-beams Subject to Negative Bending." M.S. Thesis in preparation, Iowa State University, Ames, Iowa, 1987.

APPENDIX A: FRAMING PLANS AND DETAILS FOR THE MODEL BRIDGE

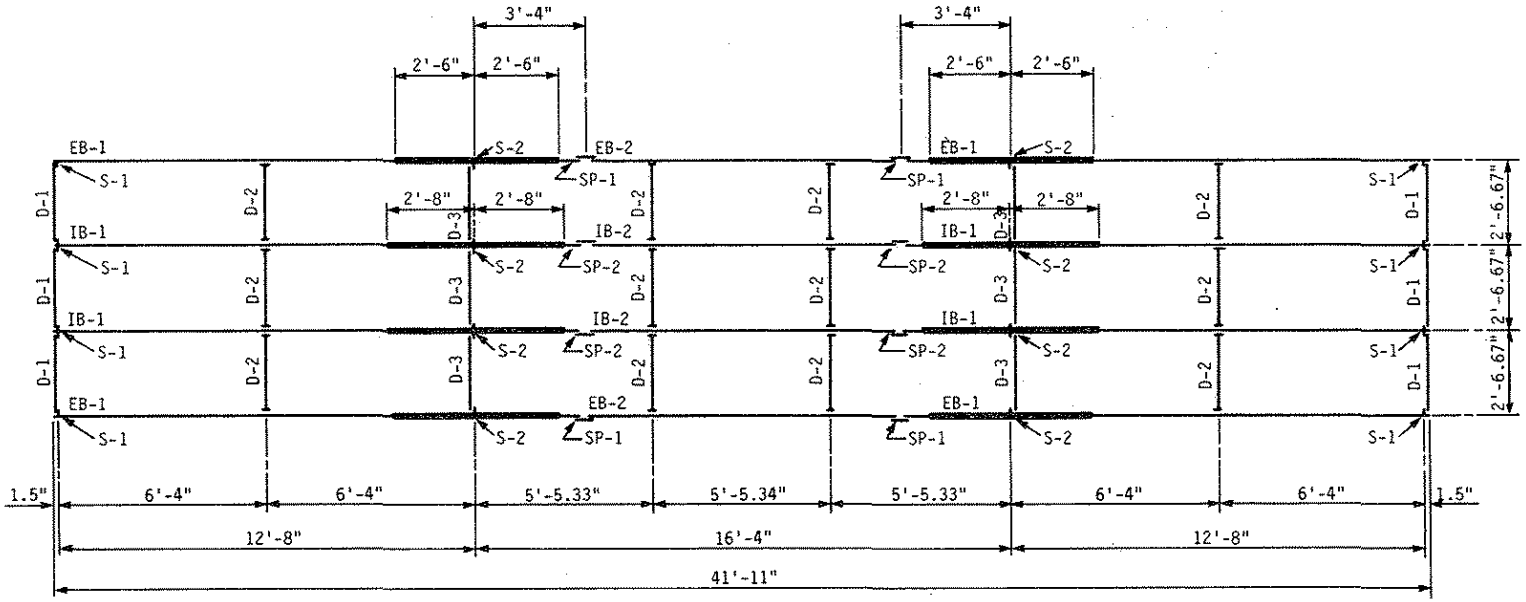

ALL STEEL SHALL HAVE A SPECIFIED YIELD POINT, Fy = 30 KSI TO 36 KSI

WELDING ELECTRODES SHALL BE COMPATIBLE WITH PARTS TO BE CONNECTED.

NOTE:
THERE IS A PLANNED 0.16" GAP BETWEEN BEAMS AT SP-1 & SP-2.

Fig. A.1. Framing plan.

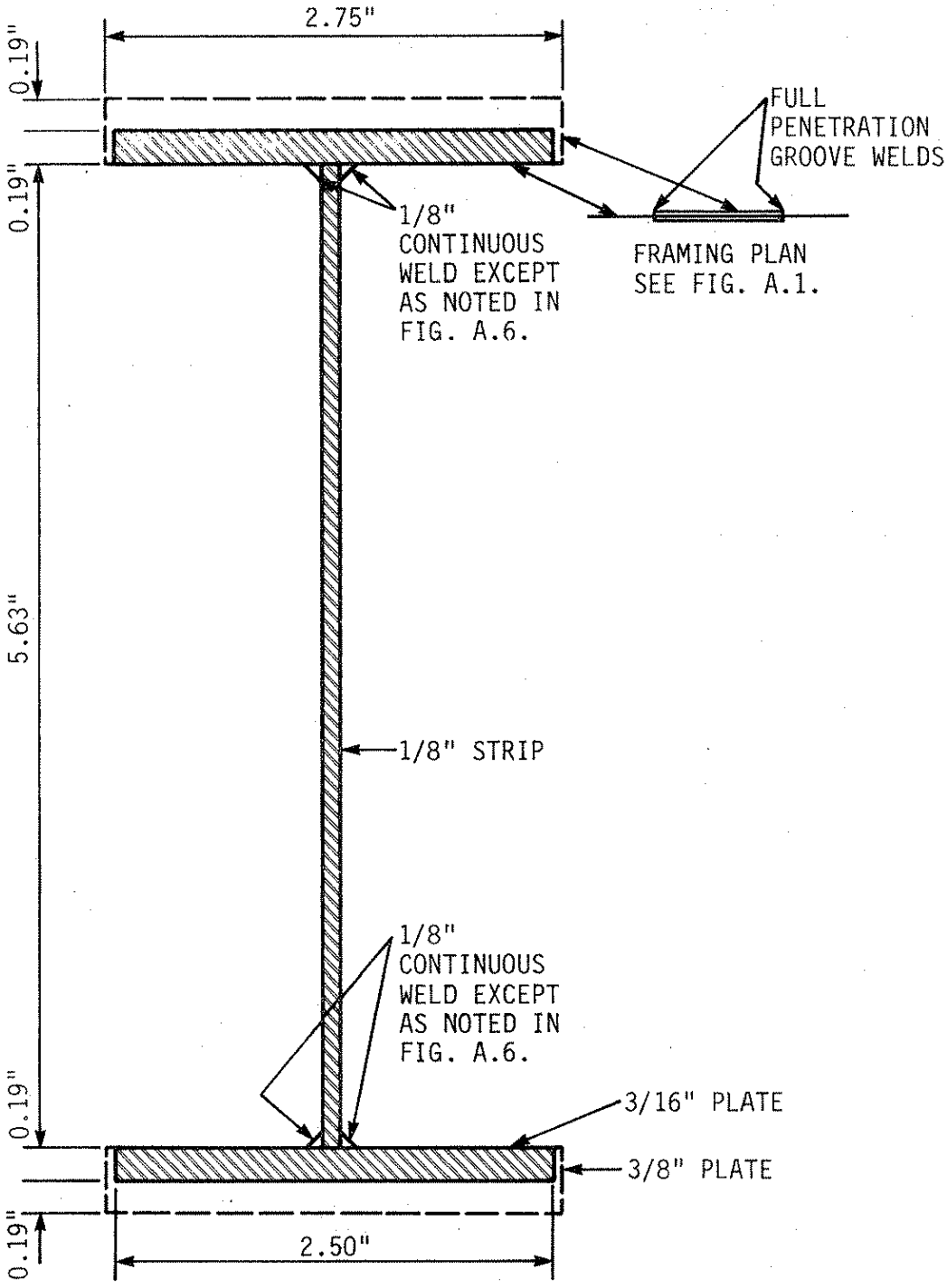

NOTE: 4 EB-1 REQUIRED, 2 EB-2 REQUIRED

Fig. A.2. Exterior beam: EB-1, EB-2.

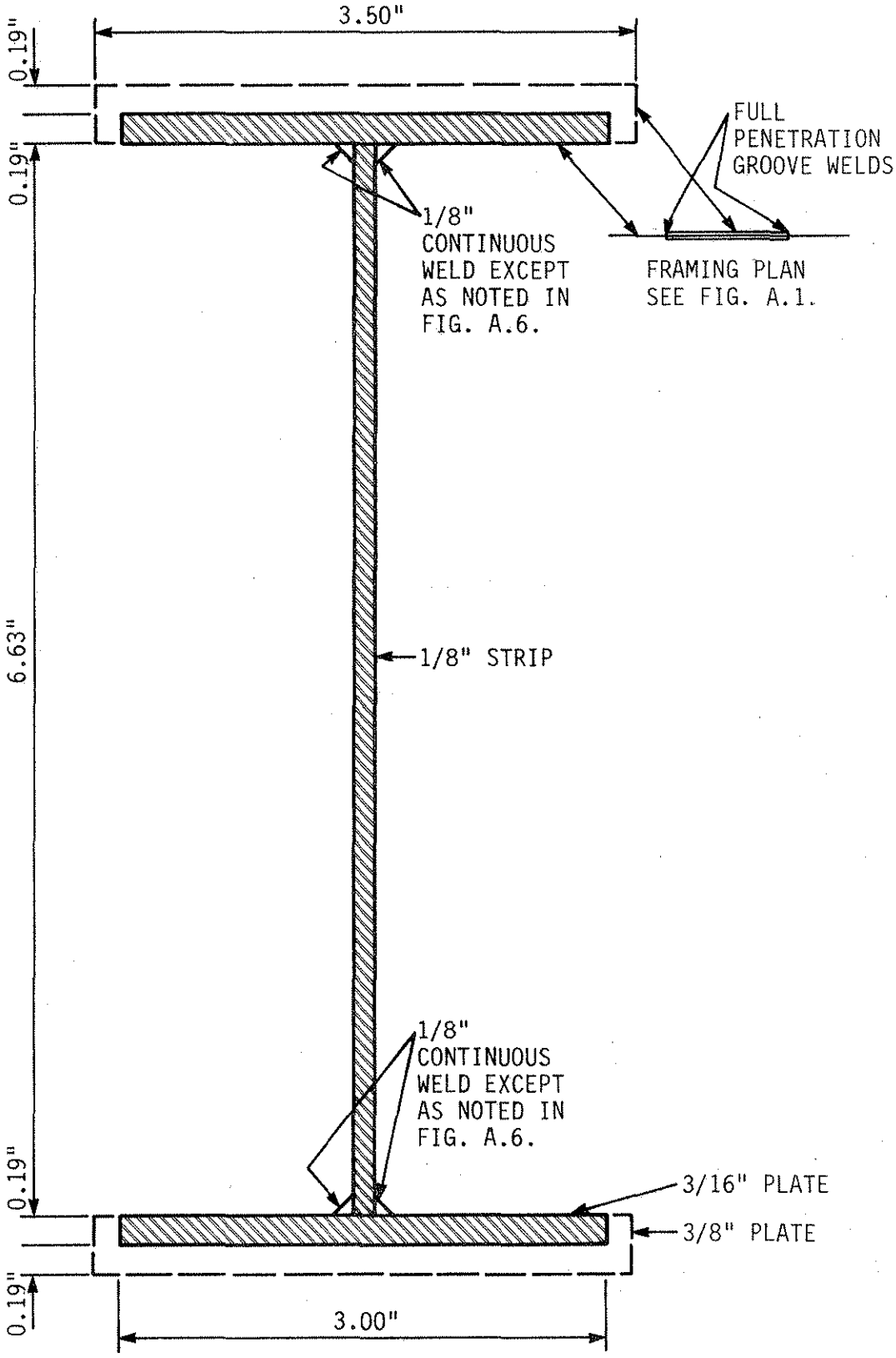

NOTE: 4 IB-1 REQUIRED, 2 IB-2 REQUIRED

Fig. A.3. Interior beam: IB-1, IB-2.

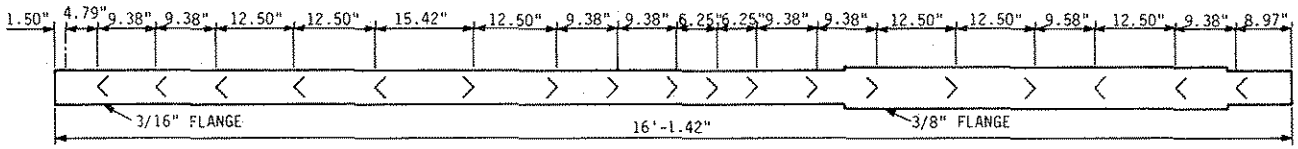

A. EB-1 PLAN

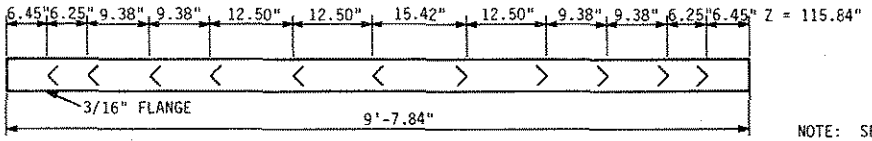

B. EB-2 AND IB-2 PLAN

NOTE: SEVERAL SHEAR LUGS WERE OMITTED, ALTERED, OR MOVED TO CLEAR 1" BAR TABS, FLANGE SPLICES OR BEAM SPLICES.

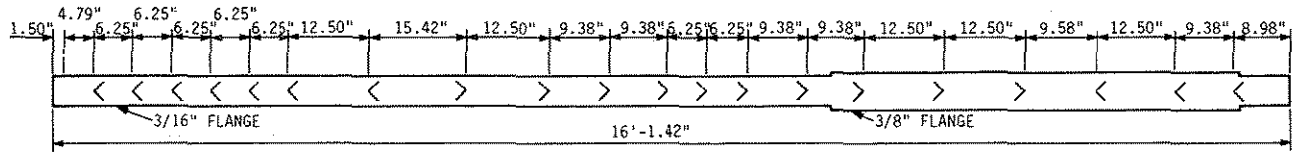

C. IB-1 PLAN

Fig. A.4. Shear lug plan.

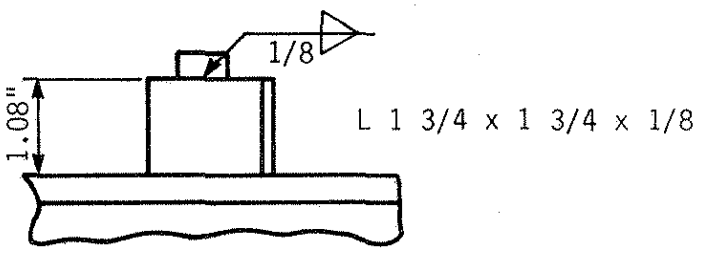

A. ELEVATION

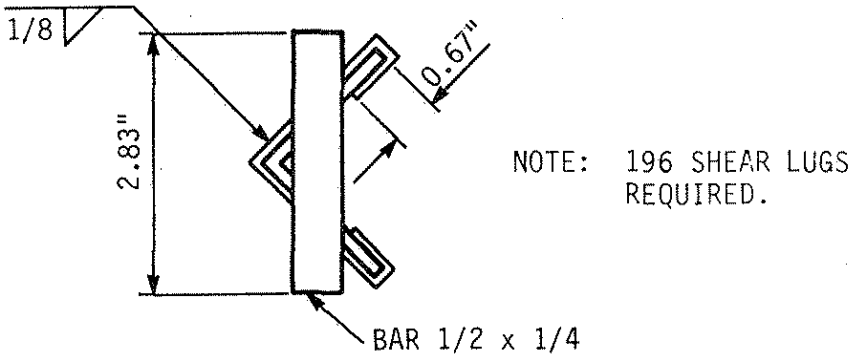

B. PLAN

Fig. A.5. Shear lug details.

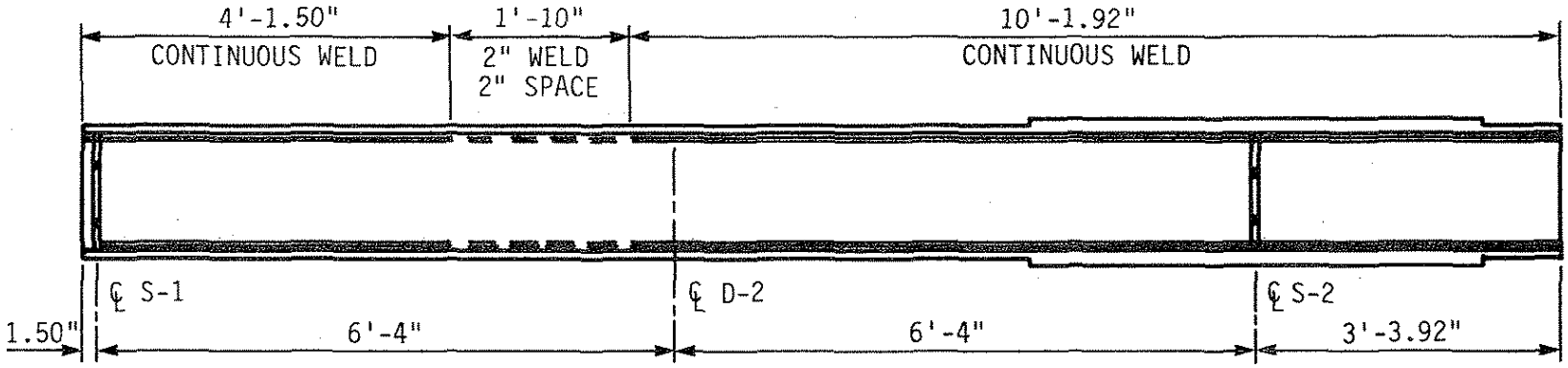

a. EB-1 AND IB-1 LAYOUT

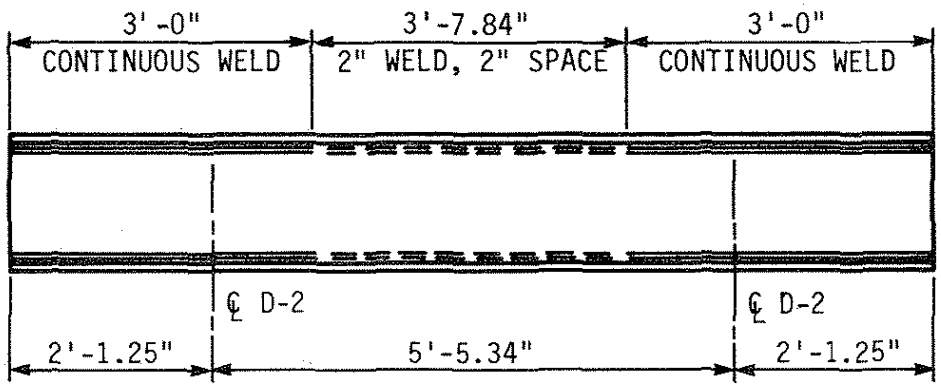

b. EB-2 AND IB-2 LAYOUT

Fig. A.6. Weld and stiffener layout.

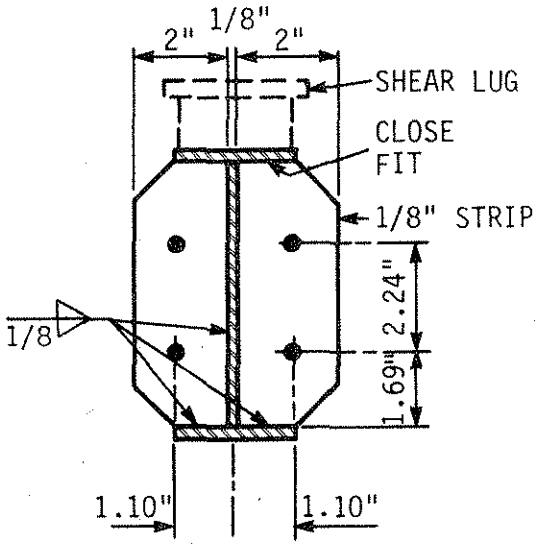

a. STIFFENER S-1

NOTE: 8 S-1 STIFFENERS REQUIRED

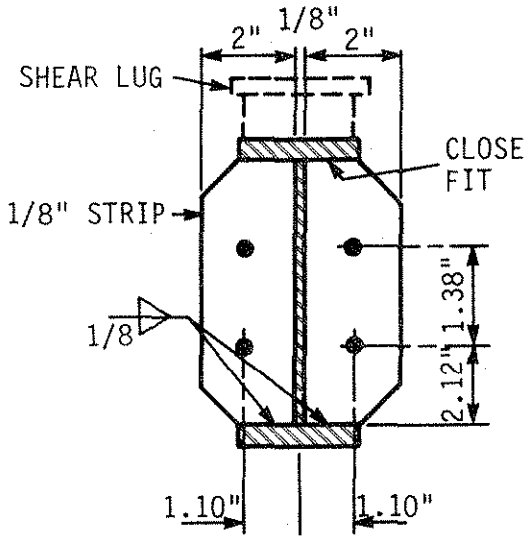

b. STIFFENER S-2

NOTE: 8 S-2 STIFFENERS REQUIRED

NOTE: ALL HOLES SHALL BE 0.56" DIA.

Fig. A.7. Stiffener details.

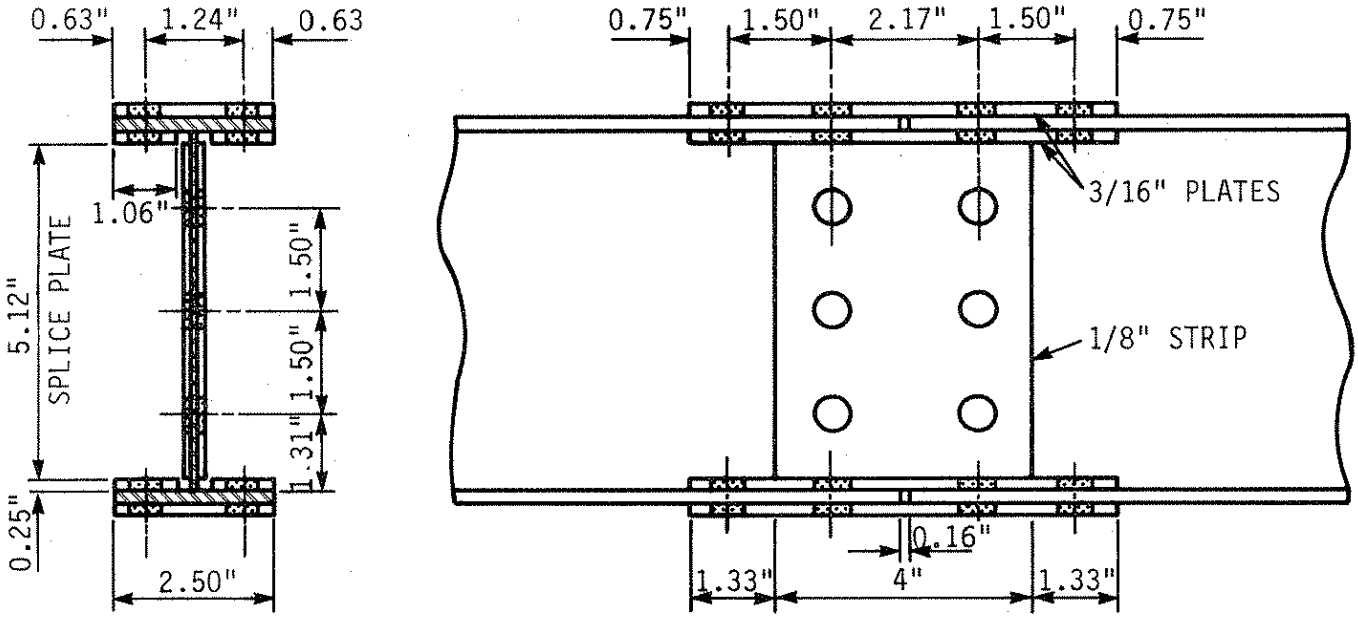

a. SPLICE SP-1: EB-1 TO EB-2
NOTE: 4 SP-1 SPLICES REQUIRED

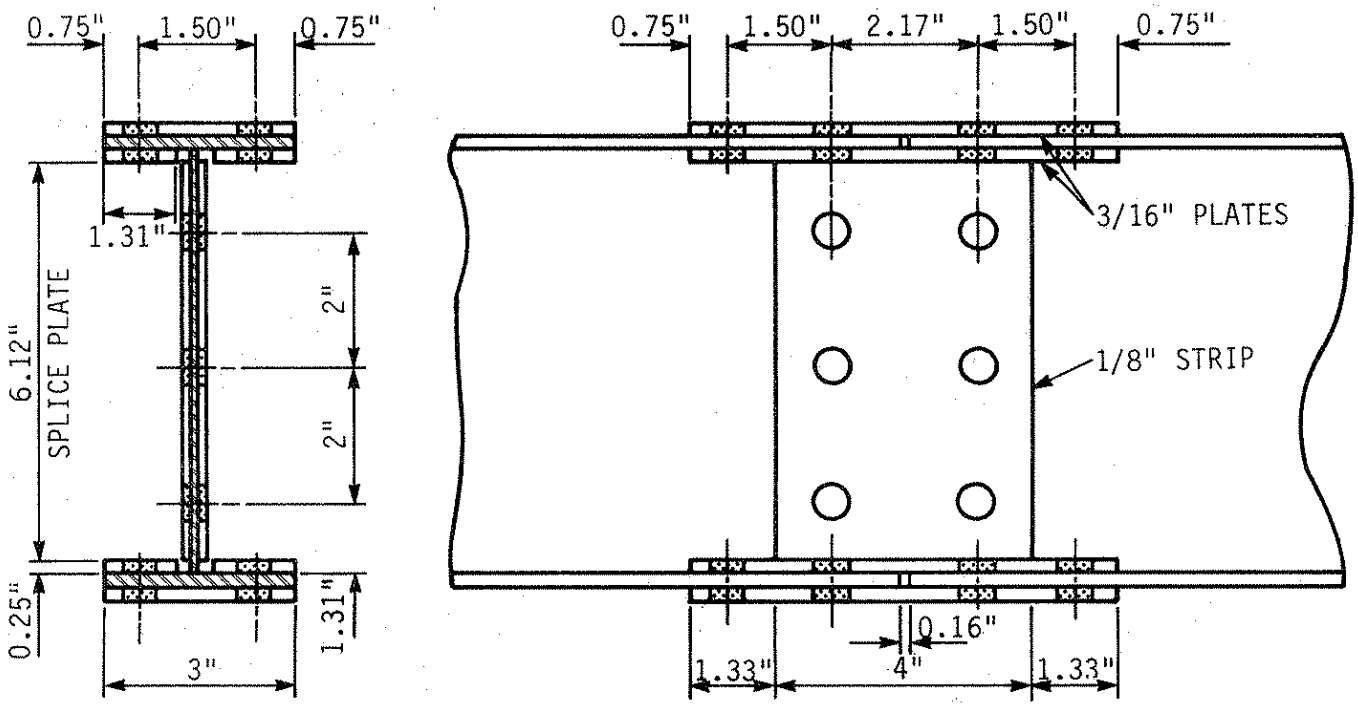

b. SPLICE SP-1: IB-1 TO IB-2
NOTE: 4 SP-2 SPLICES REQUIRED

Fig. A.8. Splice details.

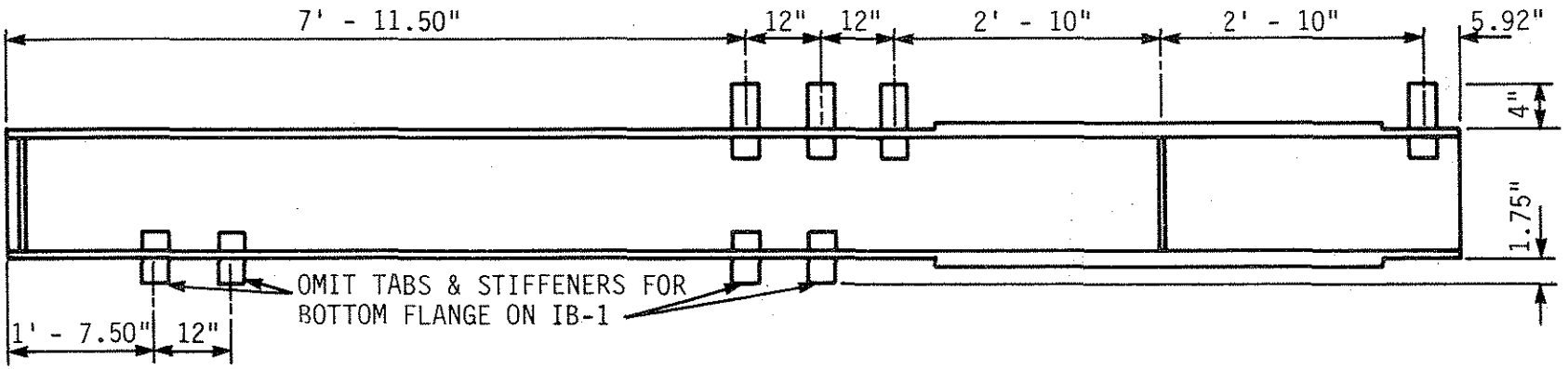

a. EB-1 AND IB-1 LAYOUT

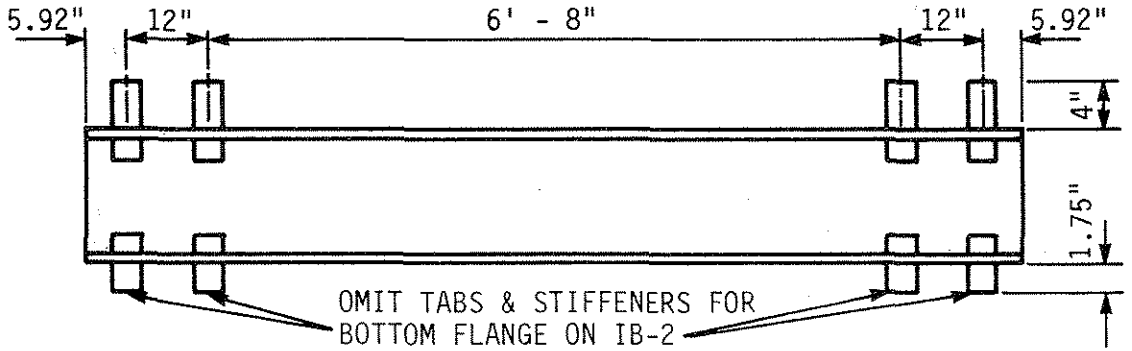

b. EB-2 AND IB-2 LAYOUT

Fig. A.9. Tab layout.

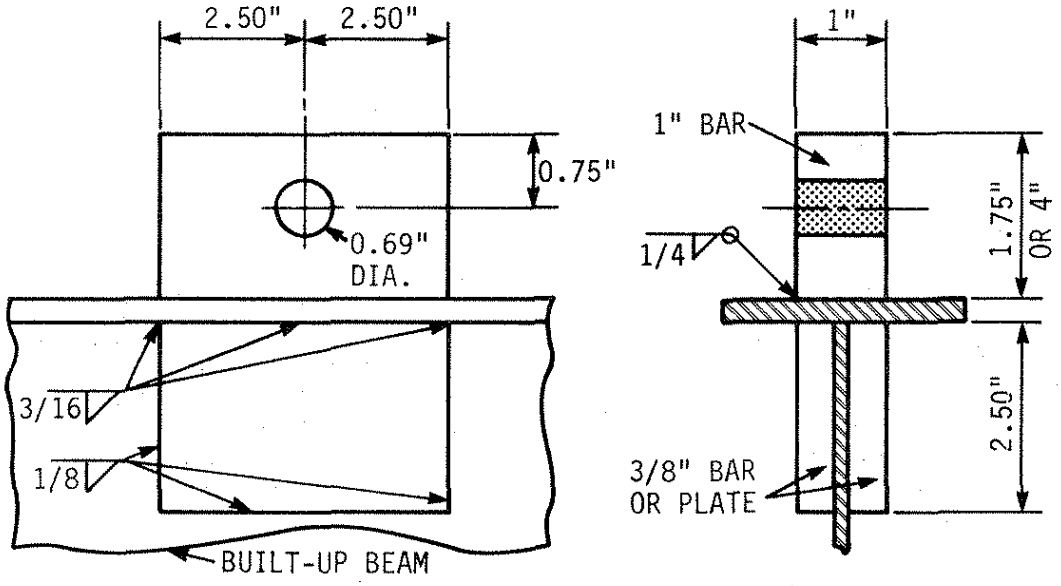

a. SIDE ELEVATION

b. END ELEVATION

NOTE: 24-1.75" HEIGHT TABS, 48 STIFFENERS REQUIRED
48-4" HEIGHT TABS, 96 STIFFENERES REQUIRED

NOTE: ALL WELDS SHOWN ON THIS SHEET SHALL BE MADE WITH E70XX ELECTRODES.

Fig. A.10. Tab details.

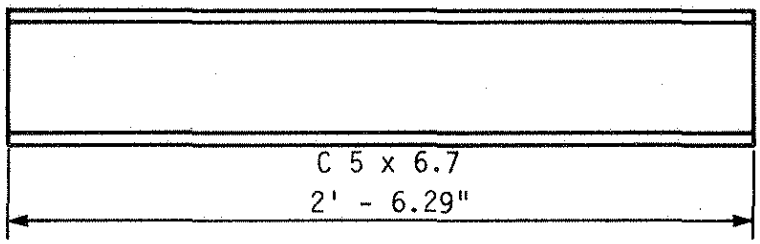

a. ABUTMENT DIAPHRAGM: D-1

NOTE: 6 D-1 DIAPHRAGMS REQUIRED

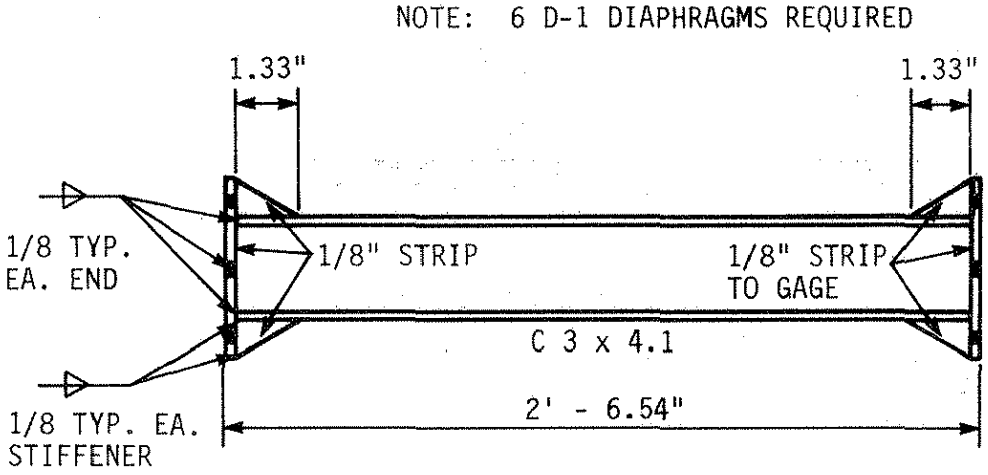

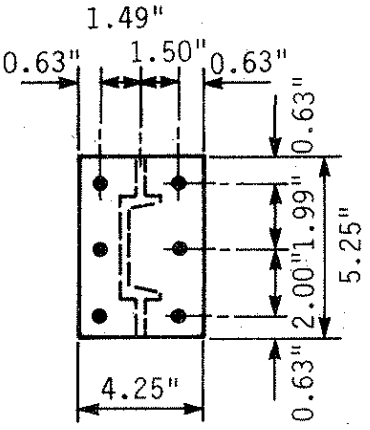

b. INTERMEDIATE DIAPHRAGM: D-2

NOTE: 12 D-2 DIAPHRAGMS REQUIRED

C 3 x 4.1 CENTERED ON END PLATE

NOTE: ALL HOLES SHALL BE 0.56" DIA.

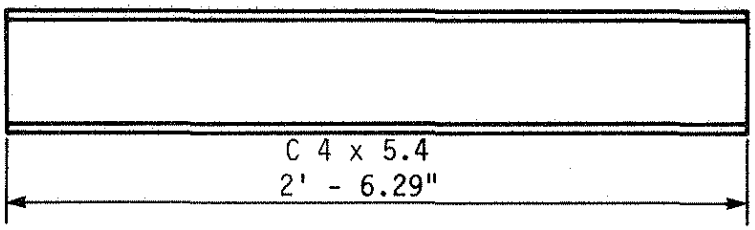

c. PIER DIAPHRAGM: D-3

NOTE: 6 D-2 DIAPHRAGMS REQUIRED

Fig. A.11. Diaphragms.

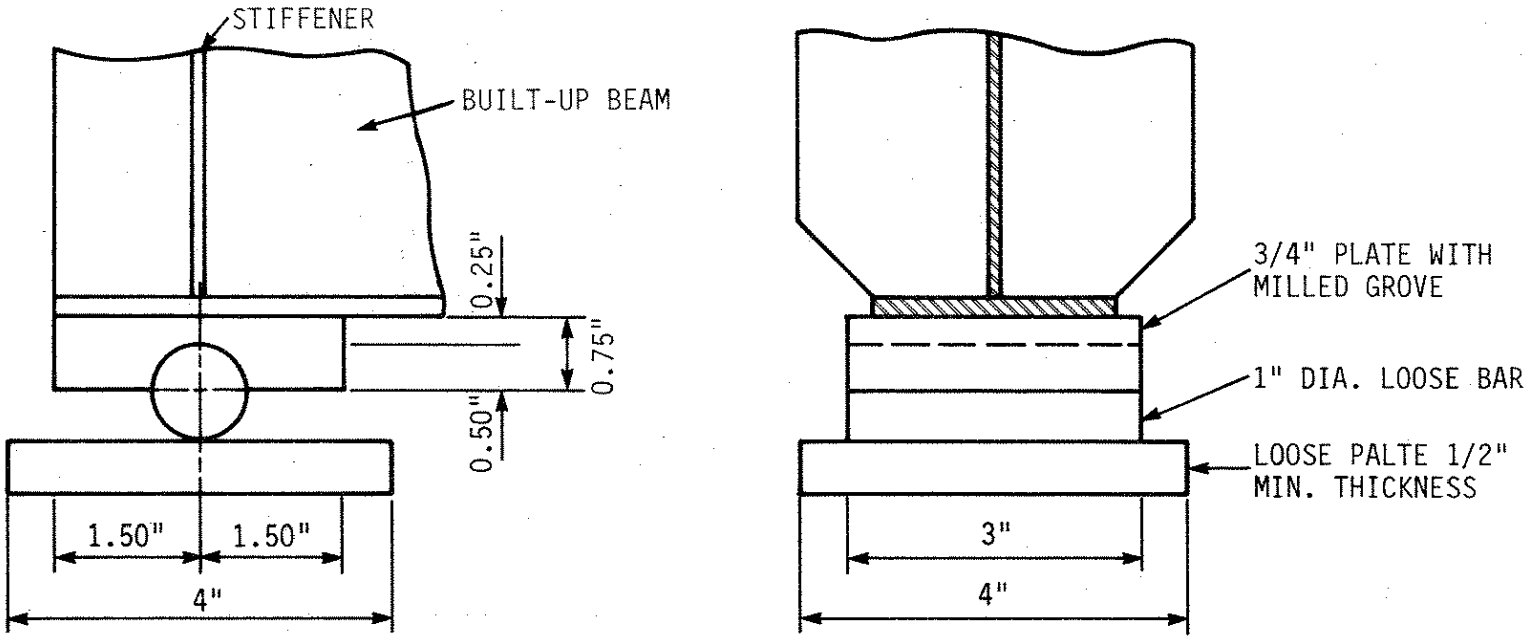

a. SIDE ELEVATION

b. END ELEVATION

NOTE: 16 BEARINGS REQUIRED

NOTE: WELD GROOVED PLATES TO BOTTOMS OF EB-1 & IB-1. CENTER EACH PLATE ON A STIFFENER AND USE MIN. 3" OF 1/8" FILLET WELD.

Fig. A.12. Bearing details.

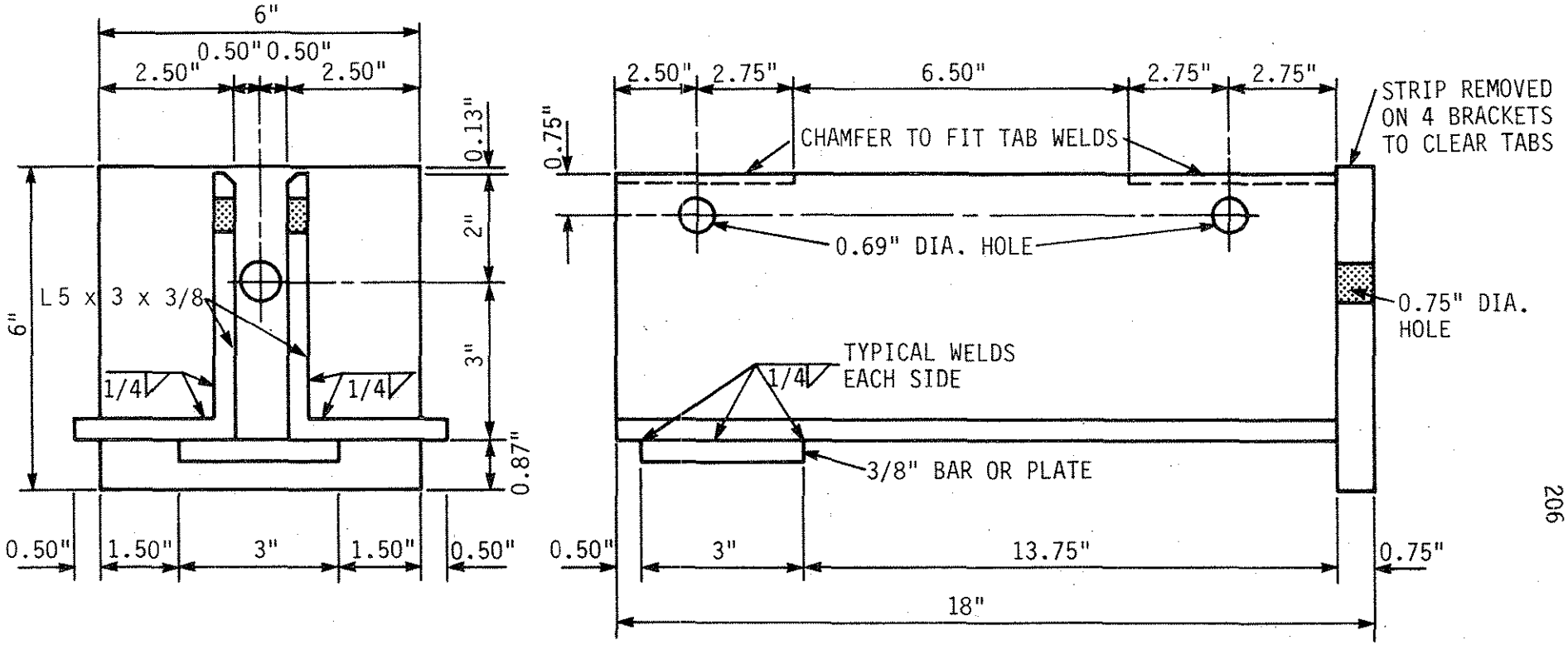

NOTE: 16 BRACKETS REQUIRED

Fig. A.13. Bracket details.

APPENDIX B: PLANS AND DETAILS FOR THE FULL-SCALE NEGATIVE MOMENT REGION MOCKUP

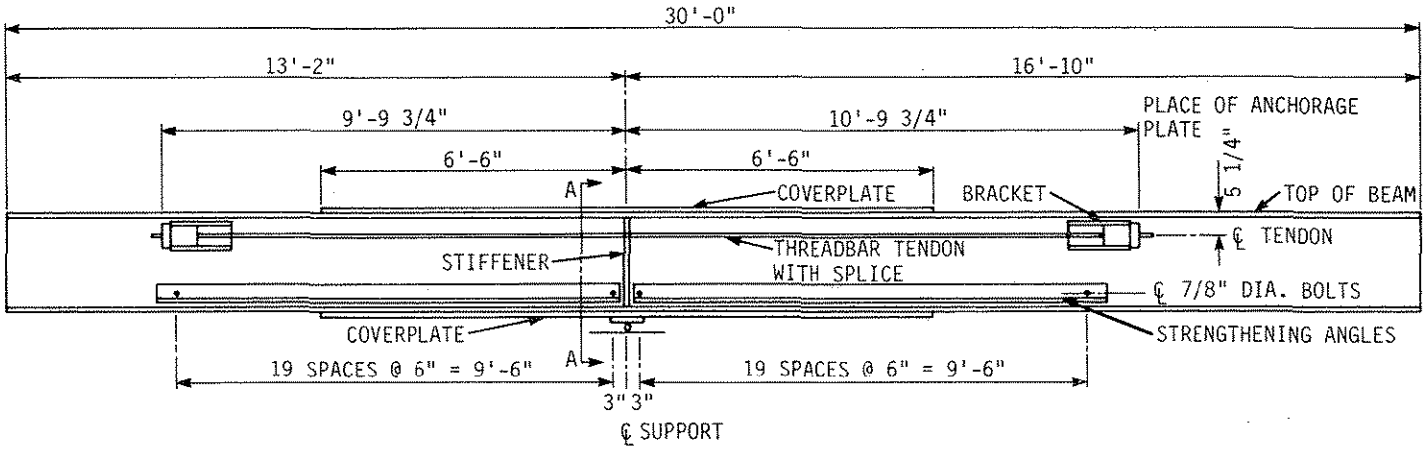

a. THREADBAR TENDON

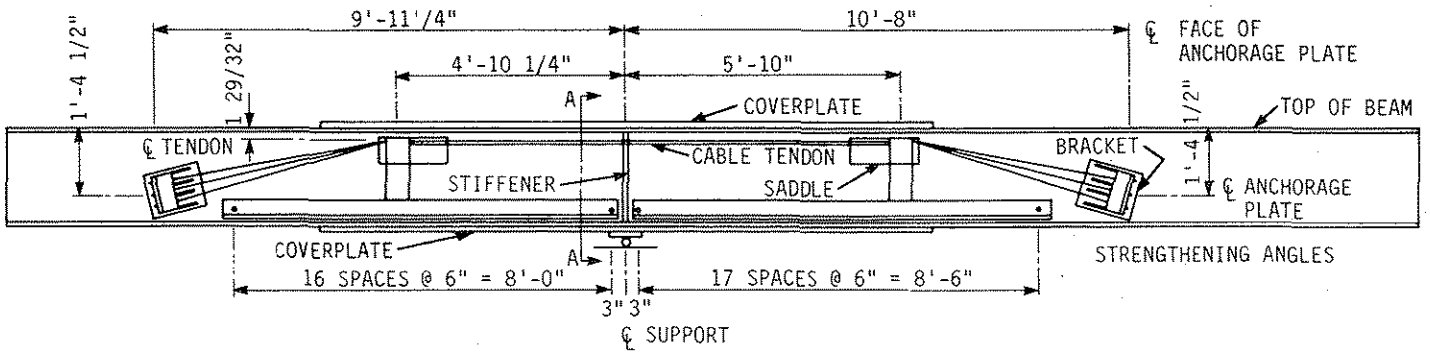

b. CABLE TENDONS

Fig. B.1. Steel beam layout elevations.

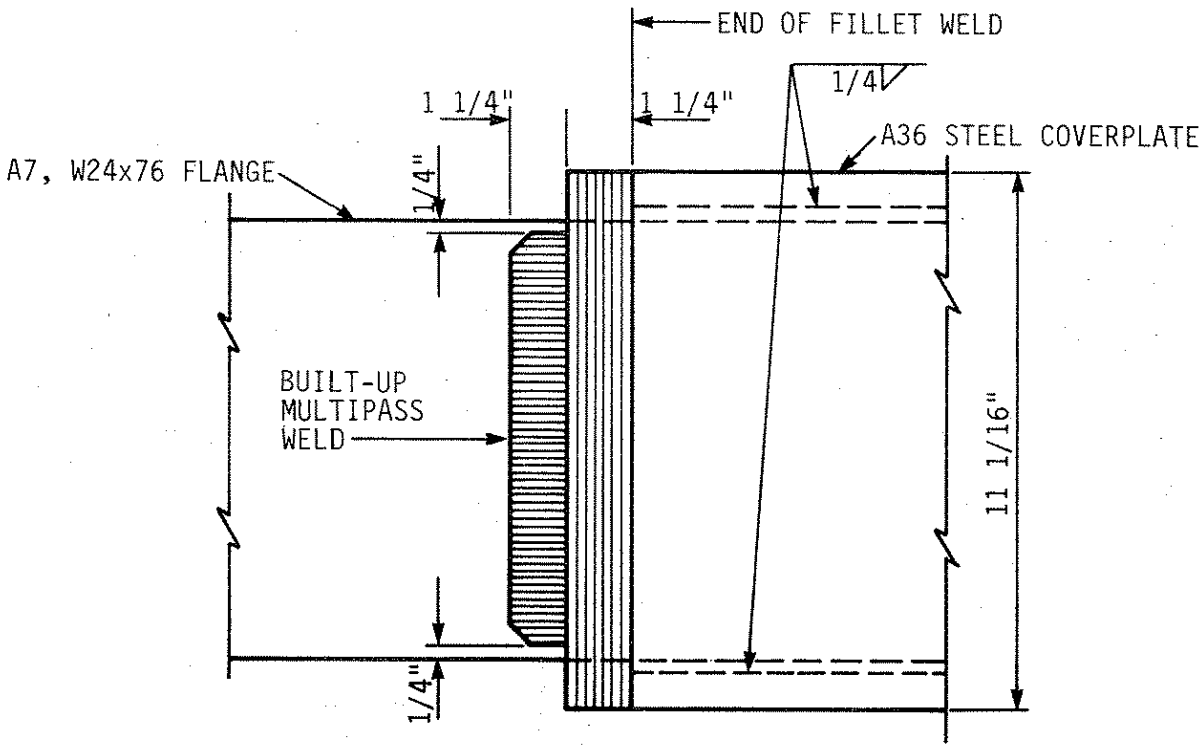

a. END PLAN

NOTE: ELECTRODES ARE
ER 70S-3 (WIRE)

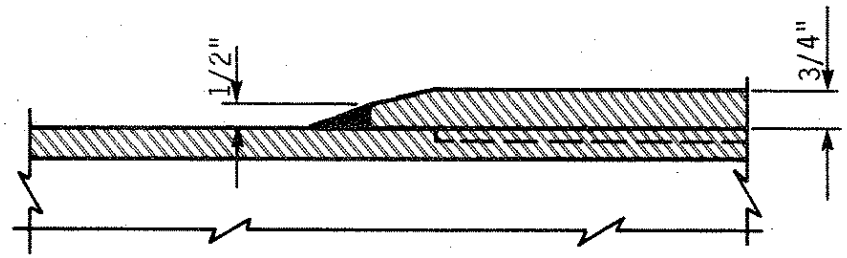

b. END SECTION

Fig. B.2. Coverplates.

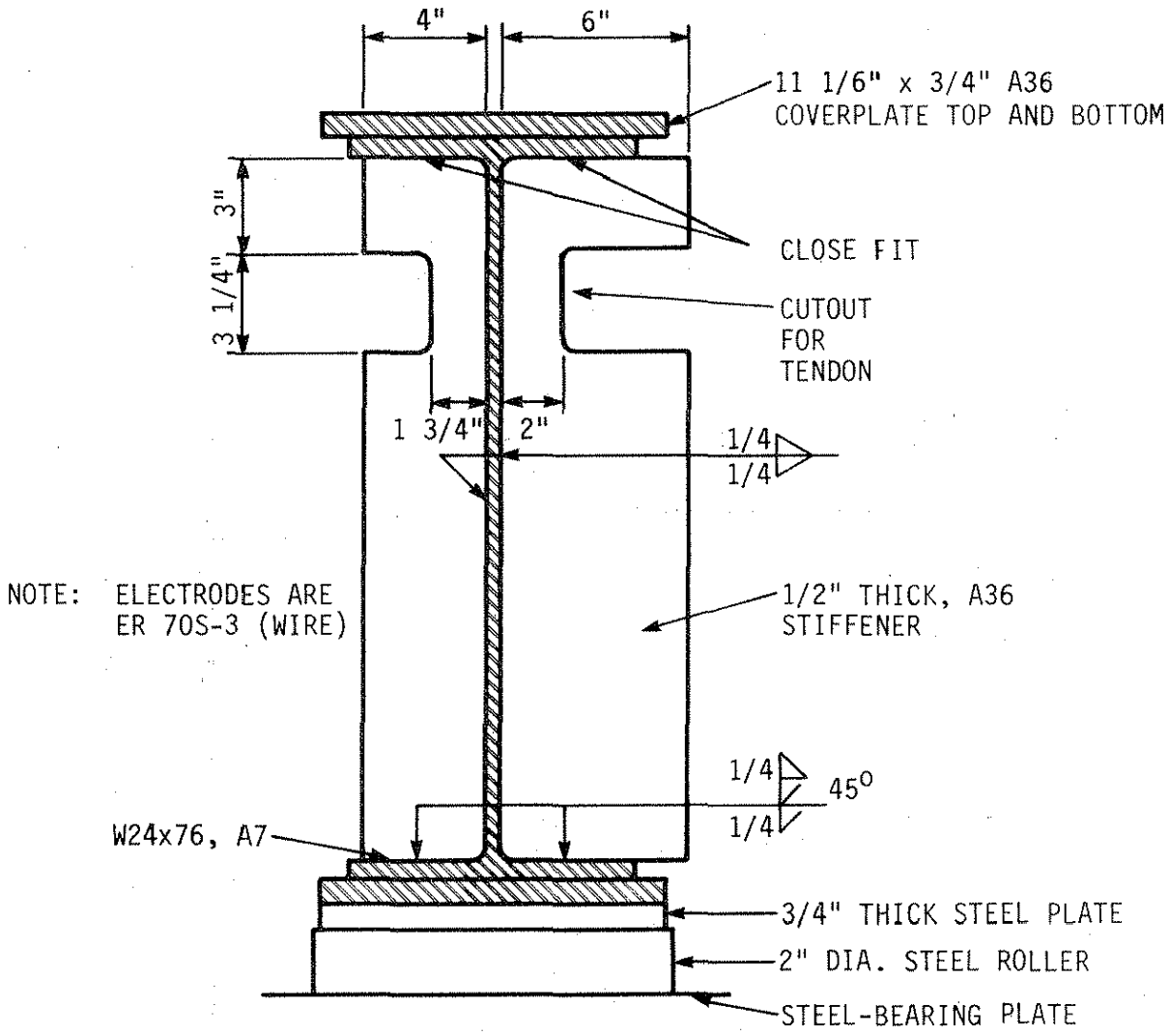

Fig. B.3. Bearing stiffeners, Section A-A.

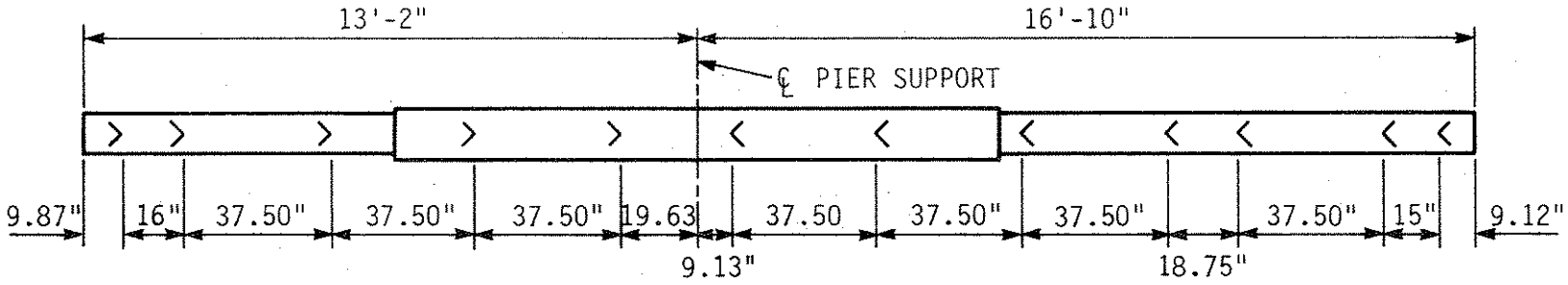

a. LAYOUT PLAN

NOTE: ELECTRODES FOR ANGLE-BAR FILLETS ARE E 7014
ELECTRODES FOR LUG-BEAM FILLETS ARE ER 70S-3 (WIRE)

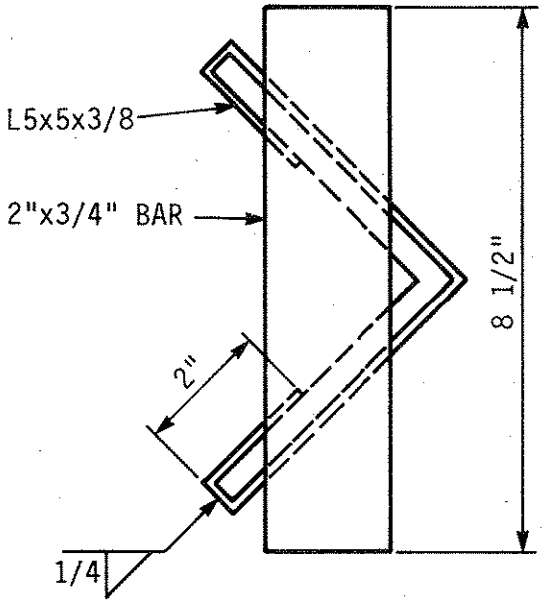

b. SHEAR LUG PLAN

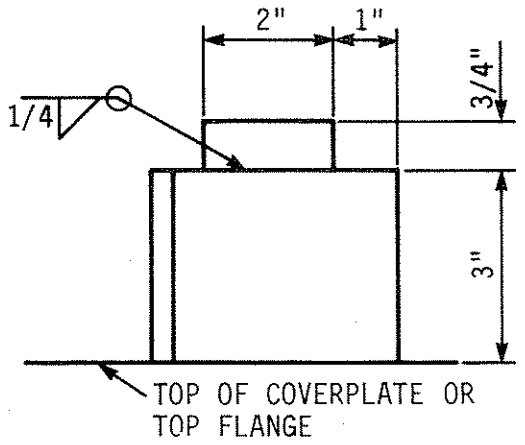

c. SHEAR LUG ELEVATION

Fig. B.4. Shear lugs.

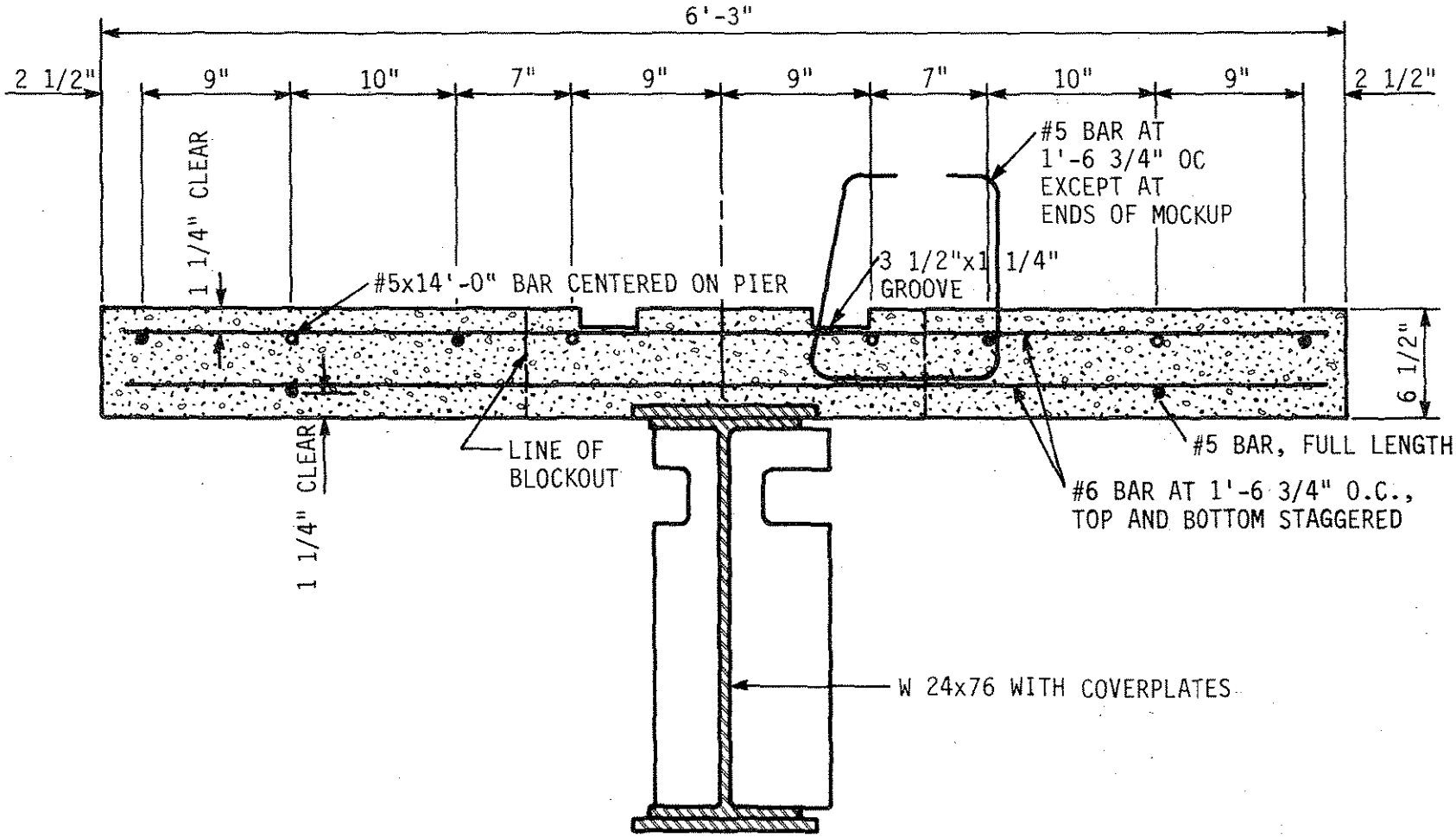

Fig. B.5. Composite beam, Section B-B. (see Fig. B.6.)

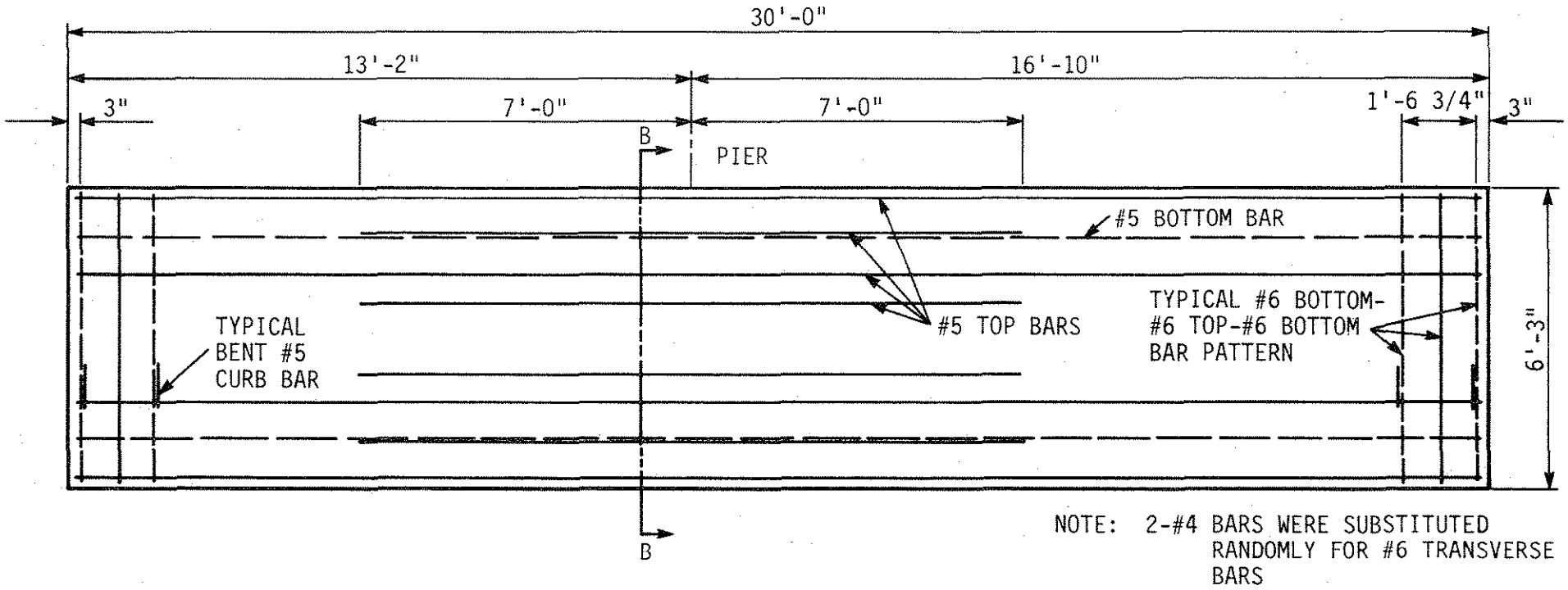

Fig. B.6. Deck-reinforcing plan.

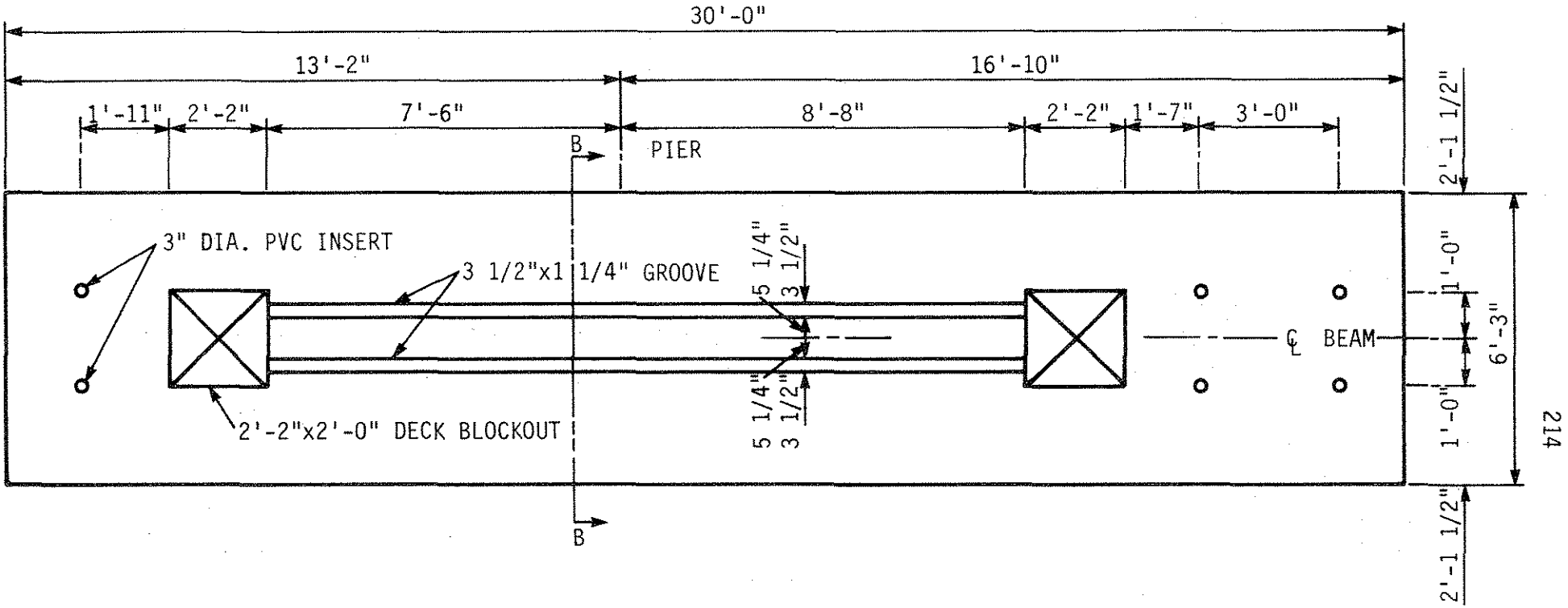

Fig. B.7. Deck blockout and insert plan.

NOTE: ALL ELECTRODES ARE E70XX.
ALL BOLTS ARE A325, 7/8" DIA.

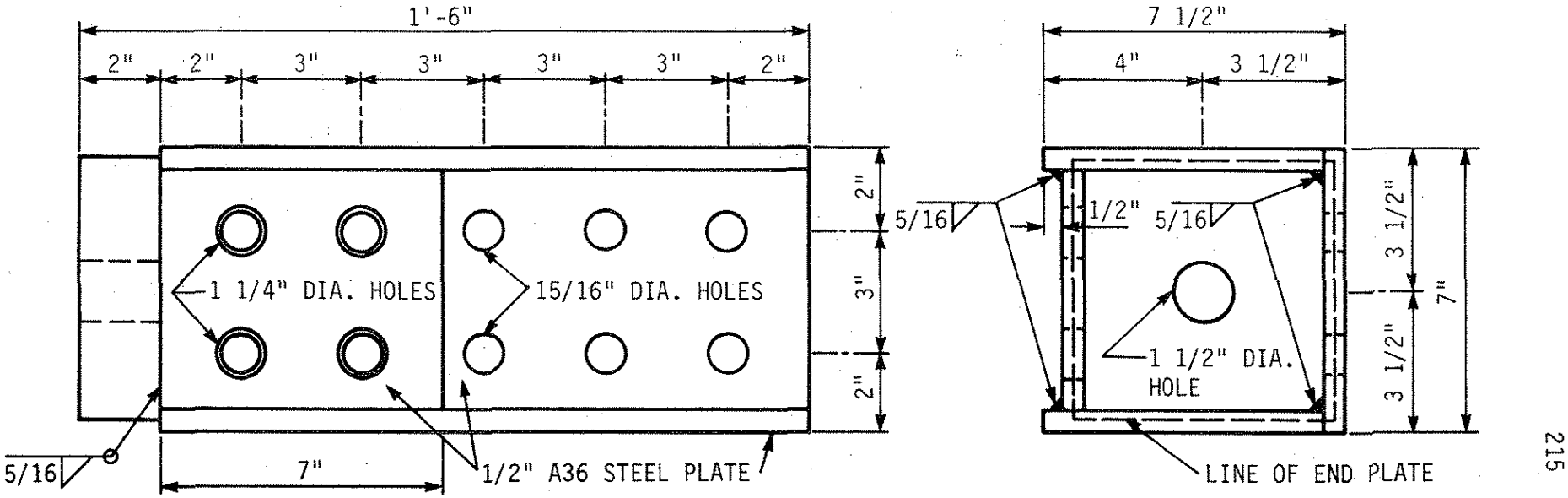

Fig. B.8. Bracket for threadbar tendon.

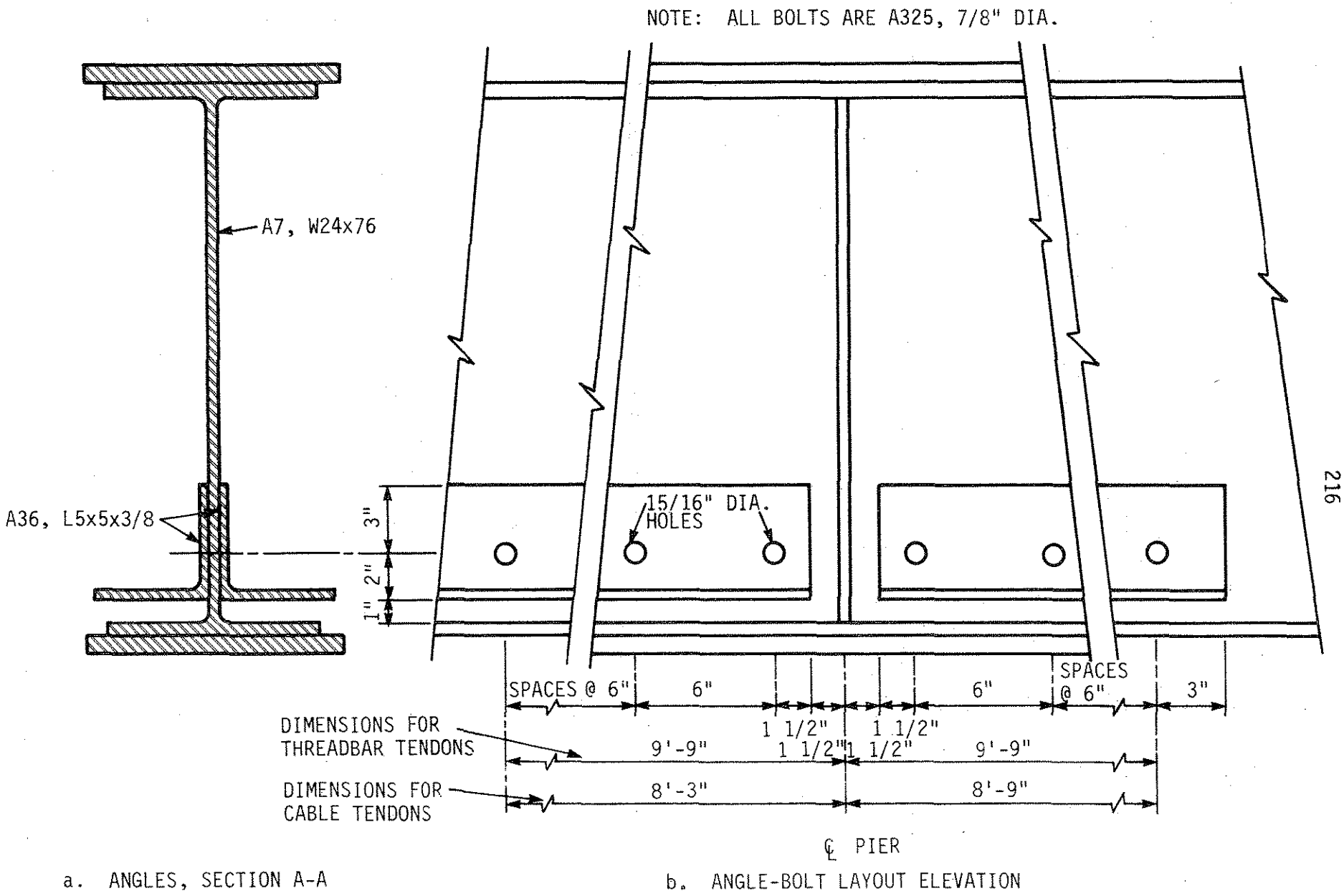

Fig. B.9. Bottom flange strengthening angles.

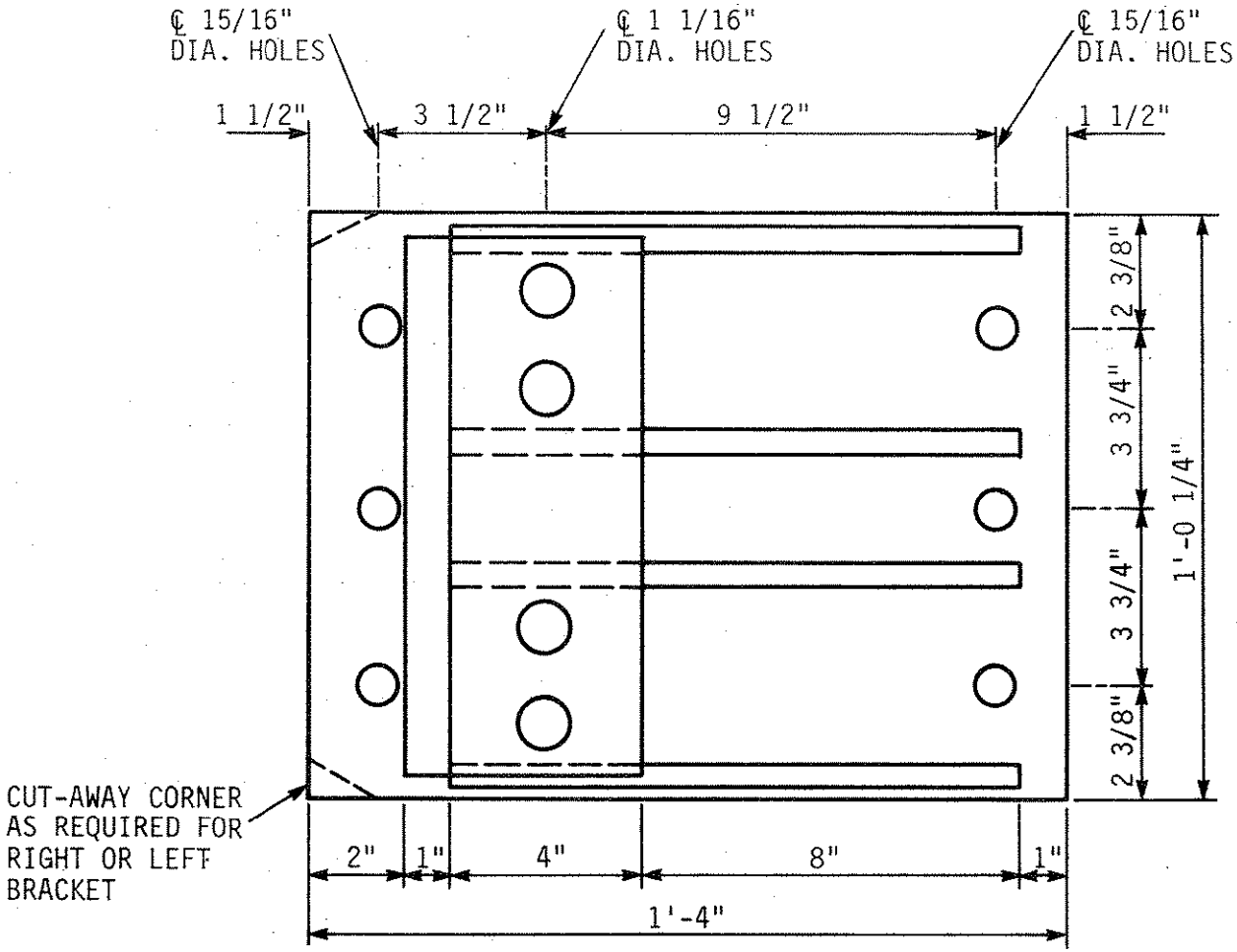

a. SIDE ELEVATION

Fig. B.10. Bracket for cable tendons.

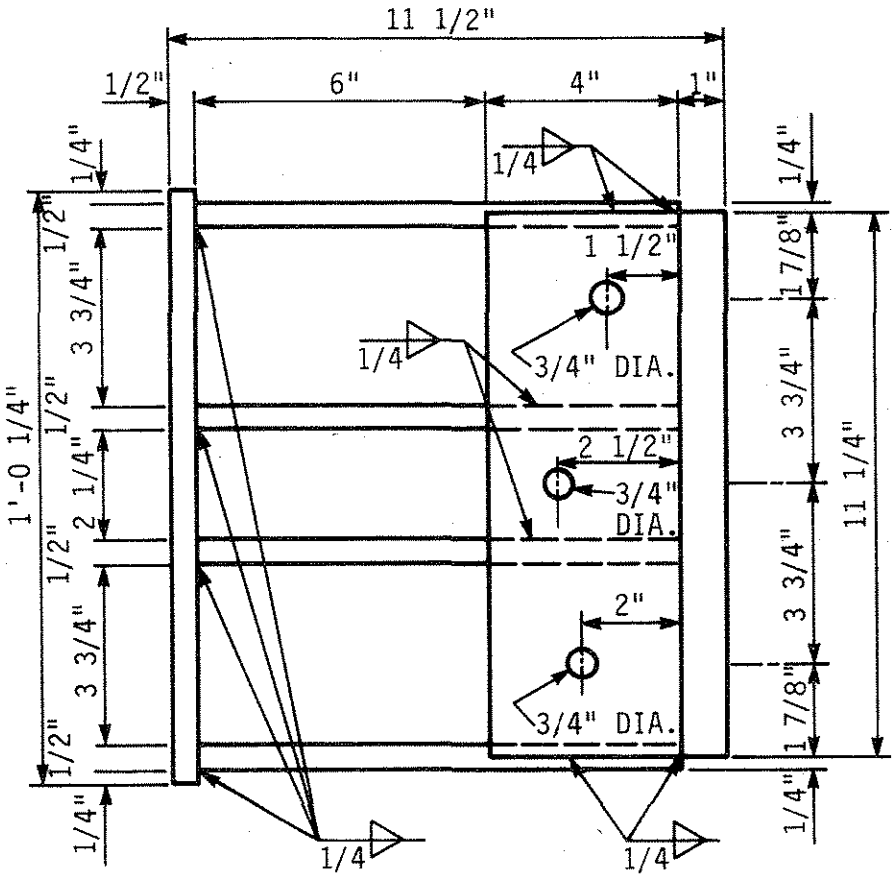

b. ANCHORAGE END ELEVATION

NOTE: ELECTRODES ARE E70XX.

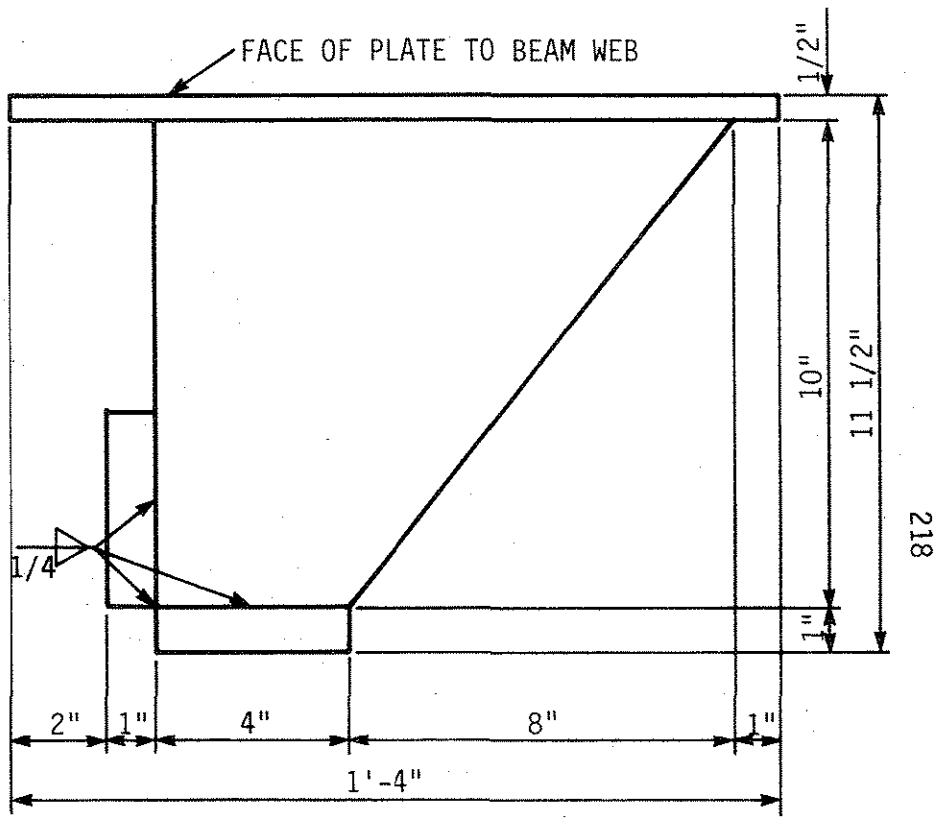

c. TOP ELEVATION

Fig. B.10. continued

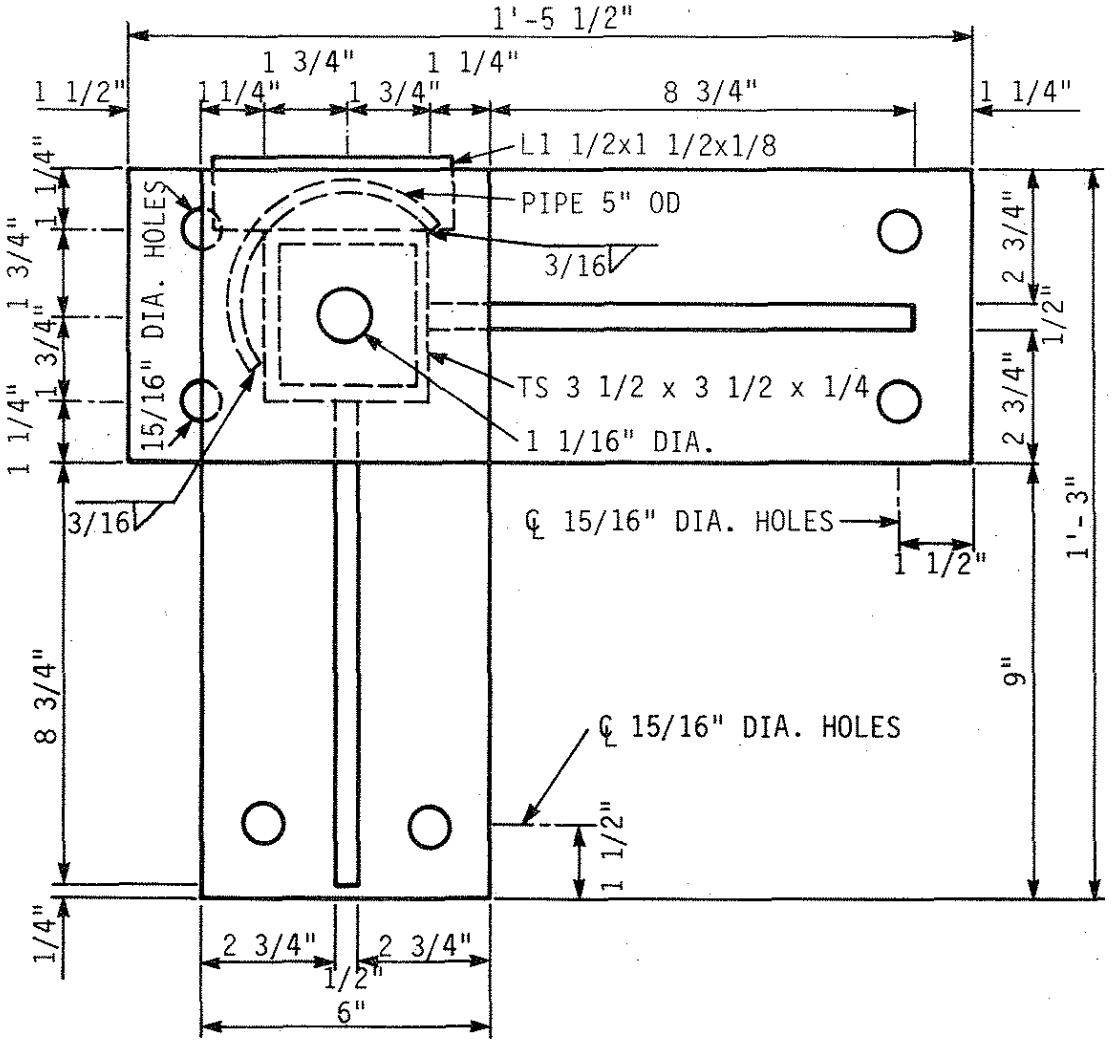

a. SIDE ELEVATION

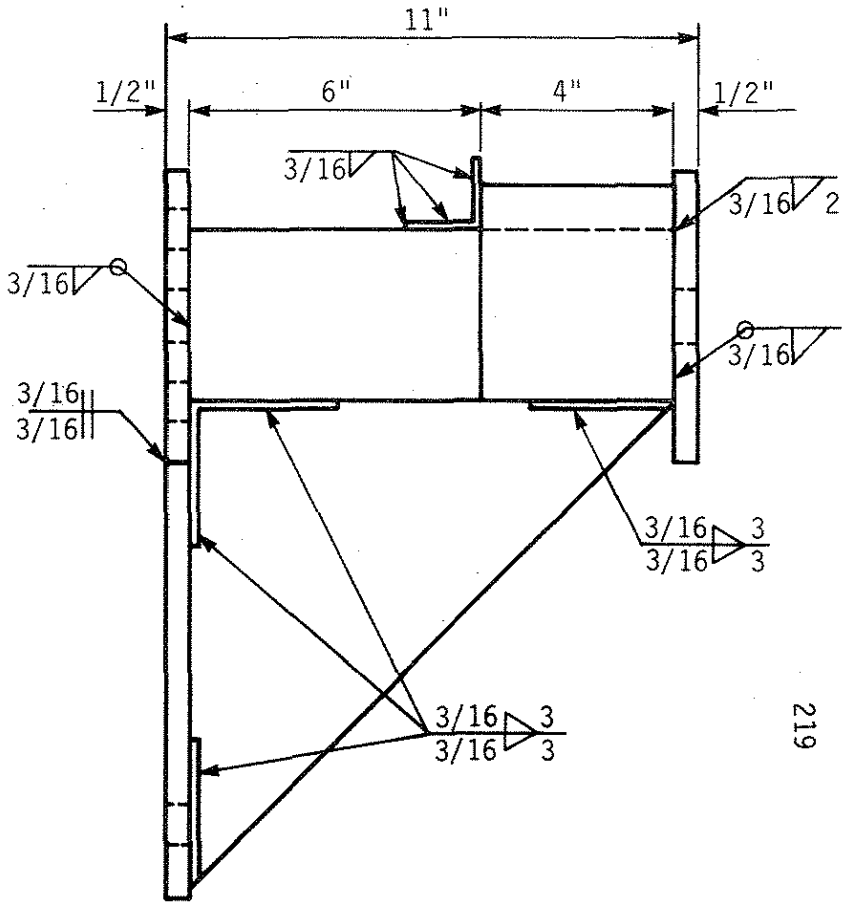

NOTE: ELECTRODES ARE E7014

b. END ELEVATION

Fig. B.11. Saddle for cable tendons.

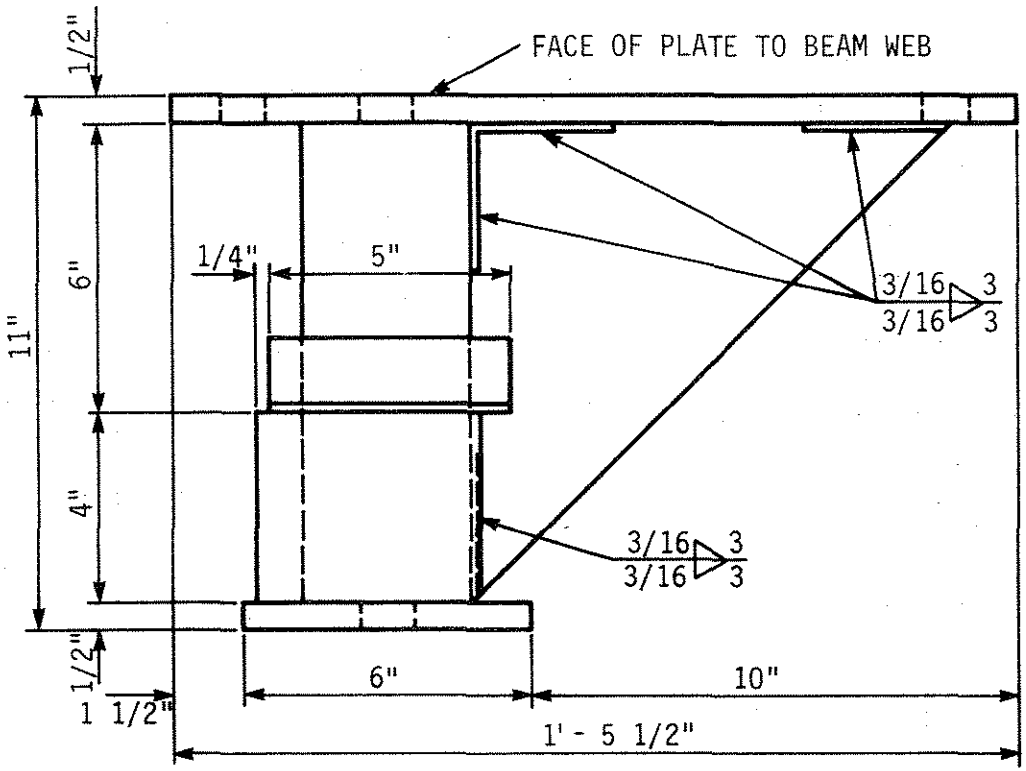

c. TOP ELEVATION

Fig. B.11. continued